Newcastle University

Mechanical Interactions between Bacterial Cells and Hydrogels: An Experimental and Modelling Approach

A thesis submitted to the Faculty of Science, Agriculture and Engineering for the Degree of

Doctor of Philosophy

by

Nehir Kandemir

School of Mechanical and Systems Engineering

Newcastle upon Tyne

October, 2018

To my dear family and beloved friends who supported me on this journey

Abstract

There is an increasing demand for medical implants and prosthetic devices due to increased life expectancy. It is important to understand how microorganisms affect the mechanical properties of hydrogels since they can get severely affected by bacteria associated infections which may lead to complete implant removal.

Bacterial adhesion on surfaces has been a widely investigated subject in many areas including biomaterial associated infections since it is considered the starting point for colonisation and biofilm formation. It has been shown that mammalian cell structure and function can be adjusted by altering the mechanical properties, such as stiffness, of their 3D microenvironment. The effect of stiffness on cell adhesion and cell function for eukaryotic cells is investigated in many studies however little work is done for bacteria for which similar interaction may happen.

This study focused on demonstrating how the encapsulated bacterial cells (*Escherichia coli* and *Staphylococcus epidermidis*) and the nutrients supplied to the hydrogels from the culture media alter their overall mechanical properties, using various characterisation techniques.

In the first part of this work, stress relaxation tests were used to reveal the mechanical properties of hydrogel-bacterial cell constructs. It was shown that the type of nutrients has an effect on the mechanical properties of the hydrogels. Similar test conditions were modelled for inert particles using finite element analysis (FEA) to show the effect of encapsulated bacterial cells.

Rheological tests, which represented a different type of loading, were also adopted for determination of mechanical properties of hydrogel-bacterial cell constructs where the results exhibited a different behaviour.

This research overall has revealed a complicated interaction mechanism between hydrogels, nutrients supplied and bacterial cells, depending on the loading type. Therefore, it is important to take into consideration the effects of media and the characterisation technique employed for the mechanical

characterisation of hydrogels and their interactions with the embedded bacterial cells.

Acknowledgements

Throughout my PhD, I have had the opportunity to meet and work with several wonderful people who so generously contributed to the work presented in this thesis in many different ways, to only some of whom it is possible to give particular mention here.

My deepest appreciations go to my supervisors Dr Jinju Chen, Prof Waldemar Vollmer and Dr Nicholas Jakubovics for sharing their invaluable knowledge, expertise and guidance. Their encouragement and support was extremely valuable especially at the more difficult times and helped me grow as an independent researcher.

I want to specifically thank Dr Saikat Jana for the exceptionally inspiring and constructive discussions, advice, help and availability. I would also like to thank Dr Katherina Peters who helped me immensely to survive in a microbiology lab.

A tremendous thank you goes to *all my friends* spread all over the world. Their support and faith in me was simply invaluable. Special recognition goes to Burla, Hare and Deniz who have always been there, wherever and whenever I needed them.

Heartfelt thanks to the Grand Hotel people who have a special place in my heart and our tiny Stephenson Building gang of Subash, Pavlos and Fatma who made my time here in Newcastle much more enjoyable.

I would like to especially thank Chinedum, who has been next to me even when he was miles away. His love, endless support and encouragement at every step, specifically during the final stages of this PhD, is much appreciated. I could not have made it without him.

Above all I would like to thank my family, especially my Mum and Dad and my sister, for their never ending support on every decision I made, the motivation to keep going every single day and everything they provided to fulfil my dreams.

Contents

List of Tables

List of Figures

Nomenclature

A	Burger's model parameter
B	Bulk modulus
B_C	Composite bulk modulus
E	Elastic modulus (Young's modulus)
E_∞	Equilibrium (relaxation) elastic modulus
E_0	Instantaneous elastic modulus
E_C	Composite elastic modulus
F	Force
G	Shear modulus
G^*	Complex shear modulus
G'	Storage modulus (elastic shear modulus)
G''	Loss modulus (viscous shear modulus)
G_C	Composite shear modulus
H	Coupling parameter
I	Identity tensor
$J(t)$	Creep compliance
L^e	Equivalent stiffness
L^m	Matrix stiffness
M	Coupling parameter
$\boldsymbol{P}$	Linear differential operator
P_0	Instantaneous force
P_∞	Equilibrium force
$p_{1,2}$	Burger's model parameter
$\boldsymbol{Q}$	Linear differential operator
$q_{1,2}$	Burger's model parameter
R_n	Radius
$r_{1,2}$	Burger's model parameter
t	Time
t_R	Retardation time
V	Volume fraction
γ	Shear strain

γ_0	Initial shear strain amplitude
$\dot{\gamma}$	Shear strain rate
δ	Phase angle
ε	Strain
ε_0	Initial applied strain
ε_T	True strain
$\dot{\varepsilon}$	Strain rate
ε^0	Strain tensor
η	Viscosity
η^*	Complex shear viscosity
ν	Poisson's ratio
σ	Stress
σ_0	Initial applied stress
σ_s	Shear stress
$\dot{\sigma}$	Stress rate
σ^0	Stress tensor
τ	Normalised time
τ_R	Relaxation time
τ_{σ_0}	Stress removal time of Kelvin-Voigt model creep curve
τ_Y	Yield stress
ω	Oscillation frequency

List of Abbreviations

AFM	Atomic force microscope
ANOVA	Analysis of variance
CFU	Colony forming unit
CV	Crystal violet
CPD	Critical point drier
DMA	Dynamic mechanical analysis
ECM	Extracellular matrix
FEA	Finite element analysis
FEM	Finite element modelling

GFP	Green fluorescent protein
HRSEM	High resolution scanning electron microscopy
HV	High vacuum
LAOS	Large amplitude oscillatory shear
LB	Luria-Bertani
LPS	Lipopolysaccharide
LVER	Linear viscoelastic region
NB	Nutrient broth
OD	Optical density
PAA	Poly(acrylic acid)
PAAm	Polyacrylamide
PBS	Phosphate buffered saline
PEG	Poly(ethylene glycol)
PFS	Perfect focus system
PHEMA	Poly(hydroxyethyl methacrylate)
PMMA	Poly(methyl methacrylate)
PVA	Poly(vinyl alcohol)
SAOS	Small amplitude oscillatory shear
SEM	Scanning electron microscopy

1 Introduction

All living things interact with their external environment and are susceptible to changes when the environment changes. Many studies have been conducted on animal cells to establish how they are affected by changes in the extracellular matrix (*i.e.* the environment), either in terms of two-dimensional interactions with surfaces (Bausch *et al.*, 1998; Koh *et al.*, 2003; Yeung *et al.*, 2005; Shih *et al.*, 2011; Jiang *et al.*, 2015) or when cells are surrounded by an external 3D environment (Wang and Tarbell, 2000; Wozniak and Keely, 2005; Baker *et al.*, 2010; Baker and Chen, 2012; Chen *et al.*, 2012; Hur *et al.*, 2012; Edmondson *et al.*, 2014). The impact of these environments on cell metabolism, protein synthesis, cytoskeletal architecture, cell motility, gene expression and cell mechanical properties have been studied (Knight *et al.*, 2002; Chen *et al.*, 2012; Chen *et al.*, 2015; Hunt *et al.*, 2017).

Bacterial adhesion on surfaces has been widely investigated in many contexts including biomaterial associated infections, for example, since these interactions are considered to be the starting point for colonisation and biofilm formation (Absolom *et al.*, 1983; Harkes *et al.*, 1991; An and Friedman, 1998; Li and Logan, 2004; Cheng *et al.*, 2007; Garrett *et al.*, 2008; Guegan *et al.*, 2014). Interactions of bacteria with many different surfaces have been studied including hard surfaces such as metals (Li and Logan, 2004; Mansfeld, 2007), and different types of hydrogels (Corkhill *et al.*, 1989; Rasmussen and Østgaard, 2003) that are natural, synthetic or a combination of both. Due to their aqueous environment, controllable mechanical and chemical properties and porous structure, hydrogels are suitable environments to interact with bacterial cells (Hoffman, 2012; Tuson *et al.*, 2012a). The chemical (Katsikogianni and Missirlis, 2004; Tuson *et al.*, 2012b) and physical properties (Katsikogianni and Missirlis, 2004; Lichter *et al.*, 2008; Saha *et al.*, 2013; Song and Ren, 2014; Kolewe *et al.*, 2015) of hydrogels, and environmental factors (Katsikogianni and Missirlis, 2004; Wang *et al.*, 2013) have been shown to affect bacterial growth rate and their ability to adhere. However, there is a lack of studies on how bacterial cells may be affected by a 3D micromechanical environment (Eun *et al.*, 2010) such as when bacteria penetrate soft tissues to form localised or systemic

infections. There are several studies on embedding bacterial cells for 3D printing applications combining multiple types of bacterial cells to study cell-cell interactions (Connell *et al.*, 2013) and a controlled spatial distribution and concentration (Schaffner *et al.*, 2017) but the information on the mechanical interactions between the bacterial cells and hydrogels is limited.

There has been a higher demand for implants due to increased life expectancy and the use of hydrogels in biomedical applications such as in implants (*i.e.* hydrogel coated cochlear implants (Wrzeszcz *et al.*, 2015)) and indwelling medical devices (*e.g.* hydrogel coated venous catheters (Fischer *et al.*, 2015)) has increased. Although some of these inserted implants or medical devices coated with polymeric hydrogels showed no complications after insertion, a part of them can get severely affected by biofilm associated infections which can lead to complete implant removal. According to National Joint Registry's annual report in 2017, a total number of 890,681 hip replacement operations and 975,739 knee joint replacement operations were recorded between the years 2003-2016 where approximately 3% of the operations were subsequently revised for various reasons including infection of the implant (Shlomo *et al.*, 2017). In the United States, an estimation of more than 30,000,000 bladder catheters and 5,000,000 central venous catheters were inserted each year, where 10-30% of the former and 3-8% of the latter operations caused infections (Weinstein and Darouiche, 2001). The use of antibiotics to treat the infections can provide a short-term solution (Johnson *et al.*, 2006; Scharfenberger *et al.*, 2007; Hooton *et al.*, 2010; Romanò *et al.*, 2016) but it also increases the possibility of antibiotic resistance which is a current and emerging problem.

To tackle such problems, understanding the mechanical interactions between bacterial cells and hydrogels, and bacteria cell mechanics when they are encapsulated in a 3D micro-environment is of particular importance. These properties might help us design new materials or select the most appropriate materials based on their interactions with bacterial cells. In addition, bacteria encapsulated in hydrogels have been used as artificial biofilm models (Chen and Stewart, 1996; Stewart *et al.*, 2015; Pabst *et al.*, 2016), which could simulate some important physicochemical

characteristics of real biofilms and enable more reproducible results than the real biofilms.

Therefore, in this project it is proposed to investigate how physical (*i.e.* stiffness) and chemical (*i.e.* chemical composition of the growth environment) factors affect bacterial cell and hydrogel mechanical interactions and bacteria cell mechanics when they are encapsulated in a 3D micro-environment. A combined experimental, numerical and a theoretical approach is adopted to understand such interactions. This proposed project is important as it will help the further understanding of bacterial cell and material interactions which would have a great potential impact in various healthcare industries.

1.1 Aim and Objectives of the Project

This project's primary aim is to study bacterial cell and hydrogel interactions and how these may affect bacteria cell mechanics. More specifically, the objectives of the project include:

• To study the mechanical properties of hydrogels and the hydrogel construct with bacterial cells

• To study how the physical properties of a given hydrogel would affect bacterial cell - material interactions

• To study how bacterial cells' mechanical behaviour changes when encapsulated in hydrogels and the mechanism behind it

• To develop and apply computational models to enable the determination of viscoelastic mechanical properties of bacterial cell and hydrogel constructs

1.2 Thesis Structure

In order to achieve the project objectives, the dissertation is divided into eight chapters.

Chapter 1 provides an introduction to the project, including the main objectives developed to reach the aim as well as illustrating how this manuscript is organised.

A detailed literature review is given in **Chapter 2** about hydrogels and bacterial cells with the factors affecting bacterial adhesion on surfaces, bacterial growth on hydrogels and bacterial encapsulation in hydrogels. Mechanical characterisation techniques of hydrogels (including indentation, atomic force microscopy (AFM), rheology, stress relaxation and compression) are introduced and the mathematical models used to describe the behavioural phenomena are explained. In addition, details of various theoretical models used for composite stiffness are provided.

Chapter 3 summarises the general materials and methods used throughout the study.

Chapter 4 summarises the experimental findings from compression tests with stress relaxation. A viscoelastic model is used to determine hydrogel mechanical properties. The effect of physical (*i.e.* stiffness) and chemical (*i.e.* chemical composition of the growth environment) factors on the mechanical interactions between bacterial cells and hydrogels, and bacteria cell mechanics when they are encapsulated in a 3D micro-environment are explained.

In **Chapter 5**, finite element analysis is adopted to model compression response of agarose hydrogels and bacteria – agarose constructs with a similar setup used in the compression experiments, testing the effect of various parameters. Simulation results and experimental results are compared to several mathematical models that are used to calculate composite stiffness.

Chapter 6 presents the experimental findings from rheological characterisation of agarose hydrogels and bacterial cell – hydrogel constructs. Rheological responses are characterised in terms of different variables. In this chapter, mechanical interactions between bacterial cells and hydrogels are investigated when they are exposed to shear forces, when similar variables are taken into account (stiffness and chemical composition of the growth environment).

Bacterial cell growth behaviour when they are encapsulated in hydrogels is shown in **Chapter 7**. This is done by imaging the elongation of the bacterial cells in agarose hydrogels made with various growth media. Also, the

elongation behaviour is modelled to gain more insights of the bacterial cell behaviour when they are encapsulated, testing the effect of various parameters.

In **Chapter 8**, the findings from all of the experiments and the modelling work are summarised and discussed. The overall conclusions of this study are mentioned in the light of the project aims and the future possible directions of this work are identified.

2 Literature Review

2.1 Classification of Bacteria

Bacterial cells can be divided into groups based on different criteria: cell structure, cell shape (most commonly cocci – spherical or bacilli – rod shaped), cellular metabolism or variety of cell components such as DNA, fatty acids, pigments and antigens. Gram staining is widely used in bacteriology to diagnose and classify the bacterial cells based on their cell wall into two groups, namely, Gram-positive bacteria and Gram-negative bacteria (Bartholomew and Mittwer, 1952; Brown and Hopps, 1973). *Staphylococcus epidermidis, Staphylococcus aureus* and *Bacillus subtilis* are examples of widely studied Gram-positive bacteria and *Escherichia coli, Neisseria gonorrhoeae* and *Pseudomonas aeruginosa* are examples of widely studied Gram-negative bacteria.

The cell wall of bacteria from either of the Gram-stained groups are made out of polymer peptidoglycan which provides the bacterial cells their shape and mechanical protection (Salton and Kim, 1996) however the cell wall thickness for these groups varies from each other (Huang *et al.*, 2008). Gram-positive bacteria usually have thick cell walls composed of many layers (Jasuja and Sehgal) while Gram-negative bacteria cell walls are generally 1-3 layers thick (Huang *et al.*, 2008). The schematic representation for cell wall structure of Gram-positive and Gram-negative bacteria is given at Figure 2.1.

Gram Negative

Outer membrane

Lipoprotein

Cytoplasm

Inclusion body

Nucleoid

Ribosome

Inner membrane

Cell wall

Capsule

Pili

Flagella

Gram Positive

Septum

Mesosome

Flagella

Gram negative cell envelope

Porin protein

LPS

Phospholipid

Outer membrane

Protein

Binding protein

Lipoprotein

Periplasmic space

Peptidoglycan

Phospolipid

Inner membrane

Protein

Cytoplasm

Thin cell wall

Gram positive cell envelope

Teichoic acids

Lipoteichoic acids

Thick cell wall

Figure 2.1. Cell wall structure of Gram-positive and Gram-negative bacteria (Salton and Kim, 1996)

Due to Gram-negative bacteria having a much thinner cell wall, they have an outer membrane which does not exist in Gram-positive bacteria. This outer membrane maintains proteins, phospholipids, and lipopolysaccharides (LPS) (Beveridge, 1999). LPS and phospholipid are the major components of the outer membrane contributing to the structural integrity of the bacteria in addition to the peptidoglycan layer and protects the bacteria against certain environmental changes including chemical intrusions and is vital for cell viability (Rietschel *et al*., 1994). The

comparison for Gram-positive and Gram negative bacterial cells based on their structure and function is given at Table 2.1.

Property of Bacteria	Gram Positive	Gram Negative
Gram reaction	Retain Crystal Violet (CV) dye and remain purple (Beveridge and Davies, 1983)	Decolourises and stains red/pink (Brown and Hopps, 1973)
Thickness of cell wall	30-100 nm (Silhavy et al., 2010)	5-10 nm (Salton and Kim, 1996)
Peptidoglycan layer	Thick (multi-layered) (Jasuja and Sehgal)	Thin (single layered) (Huang et al., 2008)
Lipopolysaccharide content	Absent	Present (Beveridge, 1999)
Periplasmic space	Absent (Salton and Kim, 1996)	Present (Salton and Kim, 1996)

Table 2.1 Differences between Gram-positive and Gram negative bacterial cells

2.2 Factors Affecting Bacterial Growth

Bacteria cell growth is affected by several factors. These factors can be grouped into two main categories that are nutritional requirements and environmental requirements. Although there are several generic requirements for the bacteria growth in media, different bacteria species grow best under the conditions similar to where they were extracted from (Morishita et al., 1981).

2.2.1 Nutritional requirements

Over the years, microbiologists characterised the bacteria growth characteristics and determined the most suitable growth media and environmental requirements for different types of bacterial cells (Atlas, 2010). The different types of growth media with different properties in terms of nutritional requirements can be listed as culture media, minimal media, enriched media, selective media and differential media, and they are used for different purposes as explained below.

Nutrient rich media are widely used growth media since they contain the constituents most bacterial cells require for growth that are: water, a carbon source (*i.e.* glucose), different types of minerals (*i.e.* salts), a source of proteins (*i.e.* yeast extract, beef extract) and nitrogen (which is necessary for the synthesis of amino acids and nucleic acids). This type of media where a source of proteins is used are also called an undefined media because the protein source may contain a wide range of compounds with unknown compositions. The defined medium (or synthetic medium) term is used when all the chemicals used in the media are known and therefore lacking the protein source from plants or animals.

Minimal media is used when the nutrients in the media are kept at a minimum for bacteria growth, containing water, a carbon source and different types of minerals. Enriched media is used to promote the growth of a certain organism by supplying the necessary nutrients where the specimen includes several organisms. Selective media and differential media are used to indicate organisms with different properties and favour their growth by a certain antibiotic, a specific nutrient or an indicator while preventing other organisms to grow. Selective media are sometimes used to maintain plasmids in laboratory strains. For example, ampicillin may be included in *Escherichia coli* MG1061 pEGFP to maintain the plasmid and enable expression of the *gfp* gene encoding the green fluorescent protein. Without the plasmid, *E. coli* MG1061 cannot grow in ampicillin. Another example for the selective media is given at Figure 2.2.
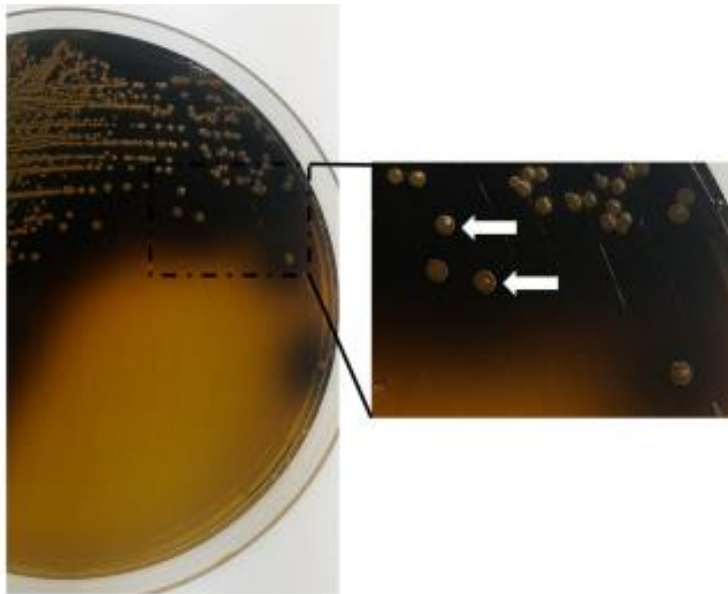
Figure 2.2. *Bacteroides fragilis* bacteria cultured on selective media (*Bacteroides fragilis* selective - BFS medium) after 48 h of anaerobic incubation at 35°C. After incubation, *B. fragilis* (indicated with white arrows) appears as large yellow colonies due to glucose fermentation with blackening of the surrounding medium (Ho *et al.*, 2017)

2.2.2 Environmental requirements

The factors affecting bacteria growth in terms of environmental requirements include temperature, pH level, oxygen level and osmotic pressure of the environment.

It has been recognised long before that temperature plays an important role on the growth rate of microbial populations (Ratkowsky *et al.*, 1982). Bacterial cells have an optimum growth temperature but can grow within a range of temperatures. Growth does not take place below the minimum temperature or above the maximum temperature of this range. Bacterial cells can be classified into three groups based on their growth temperature, namely: thermophilic bacteria, psychrophilic bacteria and mesophilic bacteria (Ingraham, 1958). Thermophilic bacteria, which are found in soil and in volcanic habitats, are thermally stable at high temperatures and their optimum growth temperature is about 60°C (Zeikus, 1979; Brock and Finley, 1985). The optimum growth temperature for psychrophilic bacteria, which can proliferate at environments with low temperatures such as deep sea and polar regions, is generally documented as 15°C (Morita, 1975; D'Amico *et al.*, 2006). Bacterial cells that are categorised as mesophilic have an

optimum growth temperature ranging from room temperature (~20°C) to about 45°C (Joanne *et al.*, 2008). Normal human microbiota and pathogens are mesophilic bacteria which can grow at the physiological temperature of 37°C.

The pH level of the environment is another factor affecting bacteria growth since it affects the bacterial protein synthesis. Like the case of temperature, different bacterial cells can survive and grow at different pH levels. The bacterial cells can be grouped as acidophilic bacteria, alkaliphilic bacteria and neutrophilic bacteria. *Thiobaciiius* strains, which are corrosive due to the sulfuric acid that they produce, are examples of acidophilic bacterial cells and they can survive $pH \leq 3$ (Harrison Jr, 1984). Alkaliphilic bacteria, such as *Bacillus* strains, grow well at pH 9 or above and they are used in applications to remove H_2S in petrochemical industries (Preiss *et al.*, 2015). However, most neutrophilic bacteria, including *E. coli* and *Staphylococcus* strains, maintain a near neutral pH (Russell and Dombrowski, 1980).

Based on their oxygen need, bacteria can be classified into three groups: obligate aerobic bacteria, obligate anaerobic bacteria and facultative anaerobic bacteria. Obligate aerobic bacteria such as *Mycobacterium tuberculosis* require an oxygenated environment to survive and grow whereas obligate anaerobic bacteria such as *Clostridium tetani* do not require an environment with oxygen (Hogg, 2013). However, most bacteria species are facultative anaerobes meaning that they behave as aerobic bacteria at oxygenated environments and switch to anaerobic respiration in the absence of oxygen. *Staphylococcus* species, *Streptococcus* species and *E. coli* are facultative anaerobes (Hogg, 2013).

Bacterial cells respond to changes in external osmotic pressure by increasing or decreasing solutes such as ions (*i.e.* K^+) and organic molecules to avoid disturbing cellular functions (Wood, 2015). This exchange of solutes creates turgor pressure which provides the force for cell expansion during cell growth (Csonka, 1989). Therefore, environments with different osmotic challenges can have different effects on bacteria growth. For example, *E. coli* cells can adapt in a wide range of osmolarities and their osmotic stress response is well characterised (Record Jr *et al.*, 1998; Wood, 2015).

Although these environmental requirements affect the bacteria growth individually, the combination of these factors can also vary the growth rate of the bacterial cells (Rosso *et al.*, 1995).

2.3 Growth of Bacterial Populations

The principle for bacterial cell population growth is based on cell division by binary fission (Rao, 1997). Cell propagation by binary fission, which can take from 20 minutes to 2 hours, follows a process as such: cells double in length, replicate the DNA and split into two at the correct time and location ensuring each daughter cell receives all the necessary complement of macromolecules, monomers, inorganic ions and nuclear material (Rao, 1997; Angert, 2005). The replication of DNA initiates when the cell mass to chromosome origin ratio reaches a specific critical value which is an integral multiple of the cell mass (Donachie, 1968). After these daughter cells reach that particular cell mass to chromosome origin ratio, they divide resulting in four cells, then those four cells divide resulting in eight cells and so on, leading to an exponential increase (2^n) in the total cell number. This type of increase takes place under ideal physicochemical conditions of that particular type of bacteria. The exponential increase does not continue indefinitely due to the nutrients within the growth medium becoming exhausted or harmful waste substances produced by cell metabolic activities.

Growth of bacteria in a liquid culture can be divided into four different phases, namely: lag phase, exponential phase (also known as log phase), stationary phase and death phase. These different phases are illustrated in Figure 2.3.
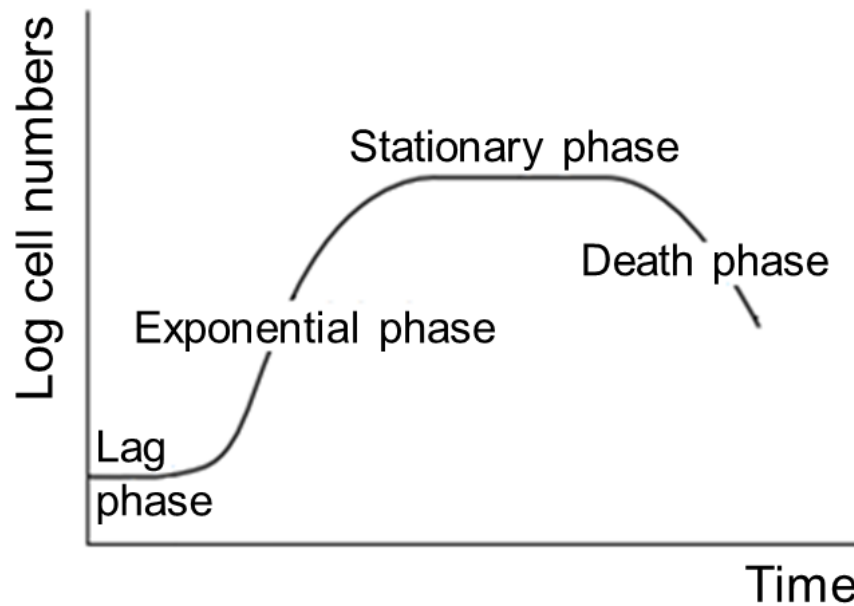
Figure 2.3. A typical microbial growth curve showing the different growth phases, adapted from (Hogg, 2013)

Lag phase: When bacterial cells are inoculated in a liquid growth medium, they require a period of time to adapt to their new environment. During this period, although the cells are metabolically active, they do not increase in number but synthesize necessary enzymes for their metabolism.

Exponential (log) phase: When the bacterial cells adapt to their new environment and synthesised the necessary enzymes to utilise the substrates, they start to divide regularly, resulting in an exponential increase.

Stationary phase: During this phase, the growth rate decreases and balances with the death rate so that the growth rate and the death rate of bacterial cells are equal and the overall number of bacterial cells does not increase. This behaviour is due to a growth limiting factor such as the exhaustion of an essential nutrient within the culture medium, production of an inhibitory toxic metabolic products or changes in pH (Monod, 1949; Kolter *et al.*, 1993).

Death phase: This phase is also known as decline phase where the bacterial cells die due to lack of nutrients and the amount of toxic metabolic products present in the growth medium.

2.4 Classification and Properties of Hydrogels

Hydrogels are hydrophilic polymer networks which can absorb up to thousands of times water compared to their dry weight (Hoffman, 2012). The ability to absorb such a large amount of water comes from the hydrophilic functional groups (monomers) which are attached to the polymeric base and the cross-links between network chains prevent the hydrogels from dissolving (Buwalda *et al.*, 2014; Ahmed, 2015). Hydrogels can be classified based on their different properties including source, polymeric composition, configuration, type of cross-linking, physical appearance and electrical charge (Ahmed, 2015) with each area affecting how the hydrogels are formed.

2.4.1 Types of hydrogels based on their source

Based on the source of the polymers, hydrogels can be classified in three different groups, namely: natural (biological) hydrogels, synthetic hydrogels and hybrid hydrogels (Peppas *et al.*, 2006). Hybrid hydrogels are formed by combining naturally derived and synthetic polymers.

Due to their biological origin, natural hydrogels are easily acquired from their sources. Agarose, agar and alginate are examples of widely used natural hydrogels extracted from plants whereas collagen and chitosan hydrogels are examples of widely used natural hydrogels extracted from animals. Agarose is a purified linear galactan hydrocolloid obtained from agar or agar-bearing marine algae having a linear polymer structure (see Fig. 2.4) consisting of alternating D-galactose and 3,6-anhydro-L-galactose units (Balgude *et al.*, 2001). Agarose gels are commonly used in tissue culturing (especially in cartilage repair) as they allow cells and tissues to grow in a three dimensional suspension and their stiffness values can be modifiable (Chen *et al.*, 2004; Zignego *et al.*, 2014). Agarose is considered a porous solid filled with liquid so it behaves as a biphasic gel with viscoelastic properties (Chen *et al.*, 2004).
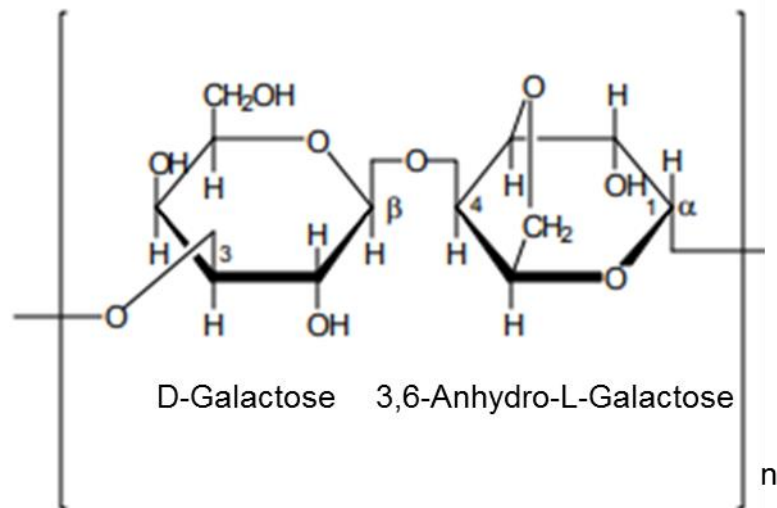
Figure 2.4. Polymer structure of agarose (Sigma-Aldrich)

Agar, which is obtained through bleaching and hot water extraction of agarocytes from red algae (Sigma-Aldrich), is the most commonly used polysaccharide complex as it is biocompatible, inert to bacterial degradation, keeps its gelled structure at the range of temperatures used for bacteria culturing and contains a considerable amount of bound water which hydrates cells that are in contact with the polymer (Tuson *et al.*, 2012b). However, agar is chemically variable which makes it difficult to characterise and reproduce its chemical and physical properties (Tuson *et al.*, 2012b). Agar is composed of ~70% agarose and 30% agaropectin (Ozel *et al.*, 2008). The polymer structure of agar is given in Figure 2.5.
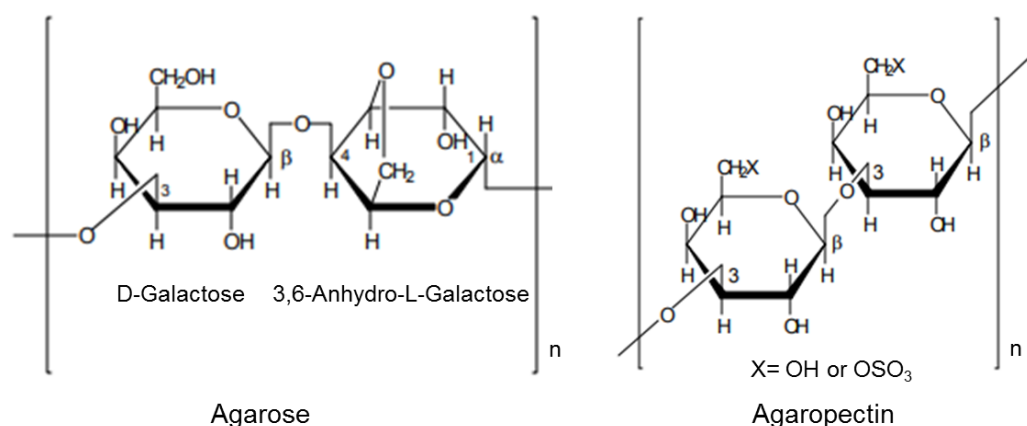
Figure 2.5. Polymer structure of agar (Sigma-Aldrich)

Alginate hydrogels are being used as scaffolds for tissue engineering and they can be used in many applications because of its controllable gelling, physical and chemical properties (Augst *et al.*, 2006). This organic macromolecule is the primary component of the cell walls of brown algae types, such as kelp. The monomeric composition of alginate hydrogels should be chosen carefully as it affects the gelling properties (Martinsen *et al.*, 1989). Mechanical properties of alginate hydrogels can be modified by varying cross-linking density and cross-linking molecules (Lee *et al.*, 2000).

Collagen type I is usually extracted from an animal source (such as rat tail, porcine skin and bovine skin) and is commonly used as a tissue culture matrix for skin, ligament, cartilage, tendon and bone (Hesse *et al.*, 2010; Antoine *et al.*, 2014). Chitosan which is derived from chitin (commonly found in invertebrates) is commonly preferred due to its bio-adhesive properties related to its positive charge and its selective release mechanism for drug delivery (Bhattarai *et al.*, 2010; Croisier and Jérôme, 2013).

In synthetic hydrogels, the polymeric networks are synthesised by chemical methods (*e.g.* polymerisation). Due to this controlled synthesis, hydrogel properties such as mechanical strength, electrical charge, biodegradation rate can be controlled easily allowing the hydrogels to have desired characteristics (Peppas *et al.*, 2006; Chai *et al.*, 2017). Poly(hydroxyethyl methacrylate) (PHEMA), poly(ethylene glycol) (PEG), poly(vinyl alcohol) (PVA), Poly(methyl methacrylate) (PMMA), Poly(acrylic acid) (PAA) and Polyacrylamide (PAAm) are examples of synthetic hydrogels.

Hybrid hydrogels can be assembled by combining natural and synthetic polymers to attain desirable characteristics from both types of hydrogels. For instance, PVA hydrogels can be modified with collagen and fibronectin where the combination favours from both the tough hydrogel characteristics obtained by crystallisation of PVA at low temperatures and the adhesive characteristics of collagen and fibronectin (Kobayashi and Ikada, 1991).

2.4.2 Types of hydrogels based on gelation mechanisms

Hydrogels can also be classified based on the type of cross-linking/gelation mechanisms between the polymer chains, that are physical cross-linking and chemical cross-linking. Physical cross-linking, which is a reversible

cross-linking, involve entangled chains, hydrogen bonding, hydrophobic interactions and crystallite formation (Maitra and Shukla, 2014). Although homogeneity of the gel can be obtained by this type of cross-linking, due to the random occurrence of the polymer loops it is not easily controlled (Sakai *et al.*, 2008). Chemical cross-linking is obtained by covalent cross-linking of polymers and they are permanent (Hoffman, 2012). The gelation mechanisms of physical and chemical gels are summarised at Fig. 2.6 with examples from each group. The schematic given at Fig. 2.7 illustrates the methods for transforming a hydrophobic polymer into a physical or a chemical hydrogel. As can be seen from this schematic, the structure of the physical hydrogel which can be obtained by hydrophobic interactions involves the entangled polymer chains while the structure of the chemical hydrogel which can be obtained by chemical cross-linking involves covalent bonding of the chains.

Radical polymerisation, high energy radiation and reaction between functional groups are some of the ways to obtain chemical cross-linking (Buwalda *et al.*, 2014). These ways are shown in Figure 2.8.
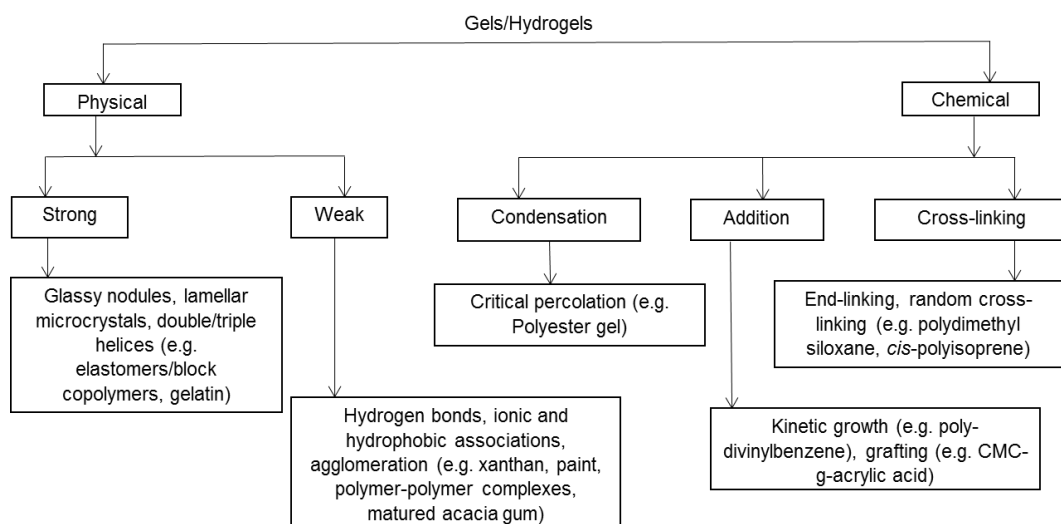
Figure 2.6. Classification of gelation mechanisms (Gulrez *et al.*, 2011)
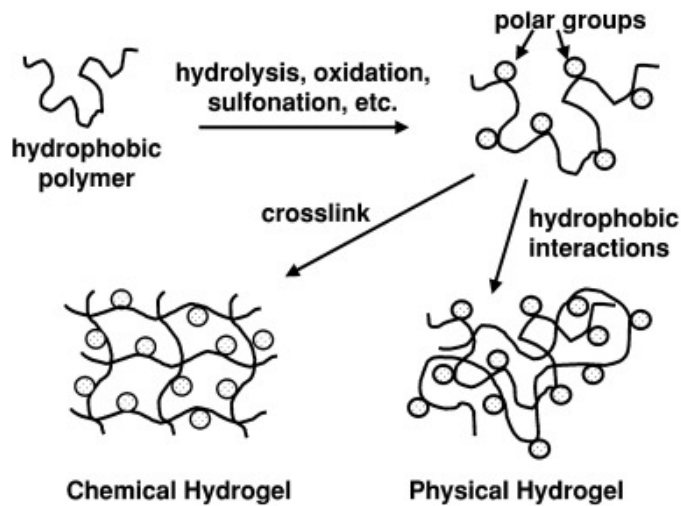
Figure 2.7. Methods for transforming a hydrophobic polymer into a physical or a chemical hydrogel (Hoffman, 2012)
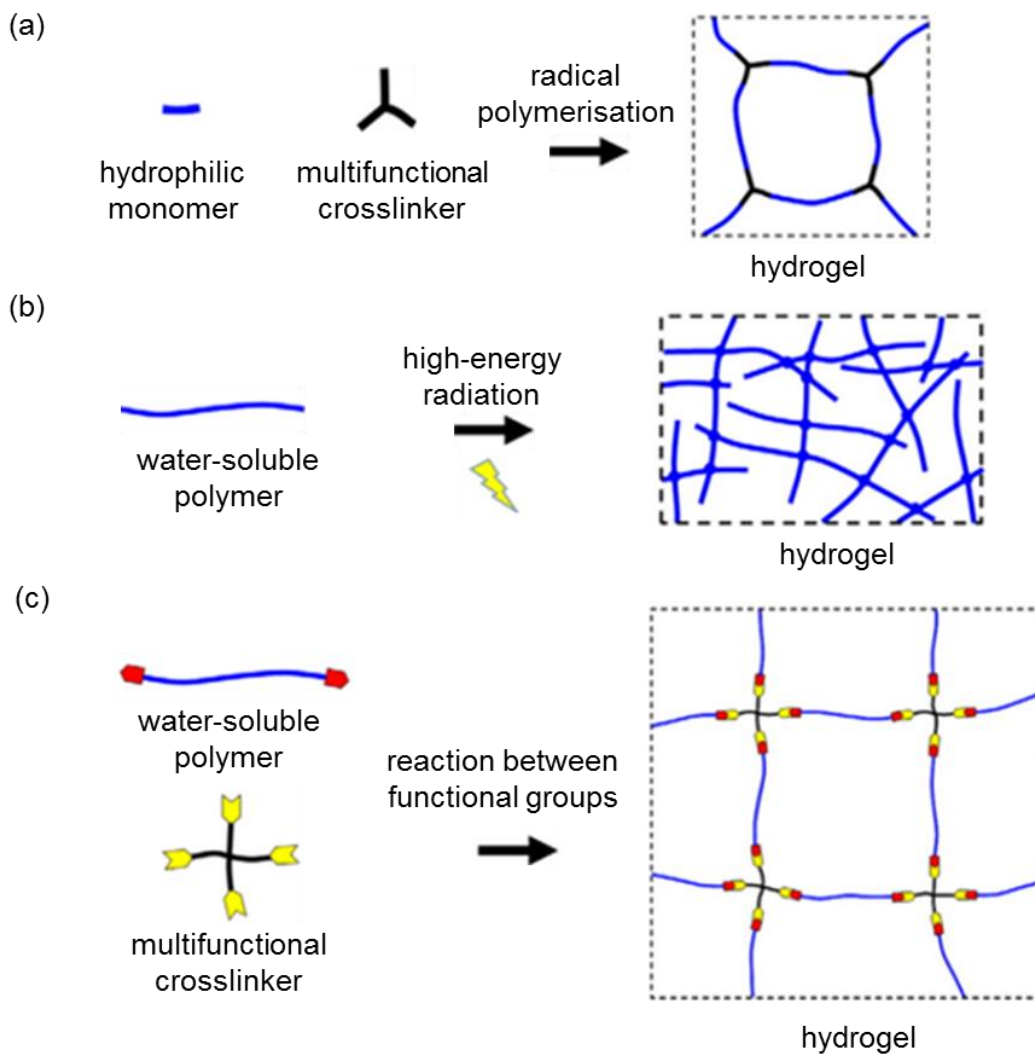
Figure 2.8. (a) Radical polymerization of water-soluble monomers with multifunctional crosslinker, (b) Crosslinking of water-soluble polymers by high energy radiation, (c) Crosslinking water-soluble polymers between functional groups (adapted from (Buwalda *et al.*, 2014))

2.5 Hydrogels as Culture Media

Due to their unique properties such as their high water content, porous structure, biocompatibility, flexibility and tuneable mechanical strength, hydrogels have been used in biomedical applications including wound dressings, dental materials, tissue engineering implants/scaffolds, pharmaceutical, ophthalmic and drug delivery applications (Gulrez *et al.*, 2011; Hoffman, 2012; Caló and Khutoryanskiy, 2015). These properties make hydrogels suitable mediums as tissue culturing environments for both eukaryotic and prokaryotic cells (Tuson *et al.*, 2012b; Ahearne, 2014).

There have been many studies on the interactions between mammalian cells and hydrogels as their synthetic extracellular matrix (ECM) for cell immobilisation and cell transplantation (Jen *et al.*, 1996; Kong *et al.*, 2003; Hu *et al.*, 2009). It has been shown that in addition to providing a suitable environment for cell immobilisation in 2D for studies *in vitro*, hydrogels are also suitable for encapsulation of the mammalian cells in a 3D environment (Lim and Sun, 1980; Tibbitt and Anseth, 2009; Mao *et al.*, 2017). For mammalian cells, the transition of the environment from 2D to 3D is based on several limitations of the former. These limitations include the cells being exposed to environments having very different properties (such as when one side of the cells is in contact with the flask bottom while the other is exposed to the liquid medium) and the cell-cell connections only taking place at the periphery (Ruedinger *et al.*, 2015) which does not reflect the *in vivo* conditions. The mammalian cells are encapsulated in 3D environment in different ways including 3D printing (Xu *et al.*, 2005; Kang *et al.*, 2016), electro-spraying (Zhao *et al.*, 2014; Lu *et al.*, 2015) and electrospinning (Townsend-Nicholson and Jayasinghe, 2006; Zussman, 2011), where the viability of the cells are maintained.

Similar to the studies on mammalian cells, bacterial adhesion on hydrogels has also been widely investigated since it is considered the starting point of biofilm formation which can lead to chronic infections (Harkes *et al.*, 1991; Gu and Ren, 2014; Guegan *et al.*, 2014; Kolewe *et al.*, 2017). The studies on the adhesion of bacteria on surfaces involve 2D environments which has similar limitations as listed for mammalian cells. Also, growing bacterial cells on 2D hydrogel surfaces can have other drawbacks such as the requirement

of large quantities of chemicals on hydrogel surfaces and the need for frequent screening (Eun *et al.*, 2010). So, in addition to growing bacterial cells on hydrogel surfaces, they can also be encapsulated in hydrogels generating a 3D medium for growth. This provides improved catalytic activity and stability of bacterial cells and also protects microorganisms from mechanical degradation (Gutiérrez *et al.*, 2007). Encapsulation of bacterial cells can be done by techniques including 3D printing (Connell *et al.*, 2013; Schaffner *et al.*, 2017), electro-spraying (Pitigraisorn *et al.*, 2017), electrospinning (Salalha *et al.*, 2006) and simply by mixing (Tuson *et al.*, 2012a). Samples having different shapes can be obtained from different techniques, *i.e.* micro-droplets can be obtained from electro-spraying and nanofibers can be obtained from electrospinning. Figure 2.9 shows scanning electron microscopy (SEM) and high resolution scanning electron microscopy (HRSEM) images of encapsulated bacterial cells by electro-spraying and electrospinning techniques. When the hydrogel and the bacterial cells are mixed together, the mixture can also be moulded to produce samples having required dimensions for different testing methods.
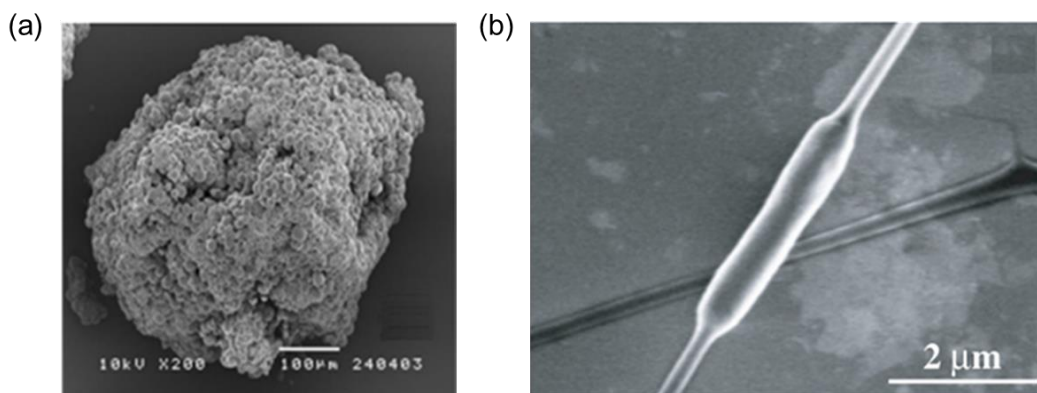
Figure 2.9. (a) SEM image showing multi-layered alginate capsules containing *L. acidophilus* (Pitigraisorn *et al.*, 2017), (b) HRSEM image of an *E. coli* cell embedded in an electrospun PVA nanofiber (Salalha *et al.*, 2006)

2.6 Measurement of Mechanical Properties of Hydrogels

In general, materials are considered to have either elastic behaviour which indicates a recovery of size and shape when the applied forces or deformations are removed storing energy (Sokolnikoff, 1956) or viscous behaviour which indicates a dissipation of energy (Christensen, 2012b). After the development and utilisation of polymeric materials, the concept of

viscoelasticity has been developed since such materials demonstrate both elastic and viscous characteristics under defined conditions (Christensen, 2012a).

Hydrogels have the ability to exhibit large changes in volume with an external stimuli and this volume change can be in the form of swelling or a transition between sol and gel phase (Holback *et al.*, 2011). When the polymer network is in contact with a fluid (such as aqueous solutions), it starts to swell because of the thermodynamic compatibility of the polymer chains and water, until the retractive force from the polymer network cross-links and the swelling force balance (Peppas *et al.*, 2000). This equilibrium depends on the level of cross-links within the hydrogel network which affects the area of diffusion (Peppas *et al.*, 2000). The water content of the hydrogels has an effect on stiffness, as the water content of the hydrogel increases, the stiffness of the hydrogel decreases (Ronken *et al.*, 2013; Li *et al.*, 2014). Therefore, the higher cross-link density within a polymer network reduces the amount of water absorbed while increasing the overall stiffness of the hydrogel.

Understanding the mechanical properties of hydrogels is crucial as they reveal information about their structure and behaviour. For instance, stiffness of hydrogels is one of the important factors affecting bacterial adhesion (Guegan *et al.*, 2014), so it should be determined thoroughly. Similar to most polymers, hydrogels show time dependent mechanical behaviour due to their viscoelastic nature (Oyen, 2014). There are several methods to determine the mechanical properties of hydrogels. These methods can be grouped depending on various characteristics such as the extent of the measurement (*i.e.* if they measure bulk properties or local properties of the materials) and the scope of the characterisation (*i.e.* if the characterisation is in time or frequency domain). Nano-indentation, rheology and compression are several testing techniques commonly used to measure hydrogel mechanical properties.

2.6.1 Nano-indentation techniques

Nano-indentation techniques, which are also known as depth sensing indentation techniques, enable probing the surface mechanical properties of materials at microscale or nanoscale. The general working principle of

these techniques is as follows: the material is indented to be deformed with a probe of known geometry, based on the indenter position with respect to the sample, deformation can be calculated as a function of the applied force and a continuum elastic theory is applied to the force and displacement data to determine the local mechanical properties of the material (Griepentrog *et al.*, 2013; Oyen, 2014). The general concept of the indentation technique is given in Figure 2.10.
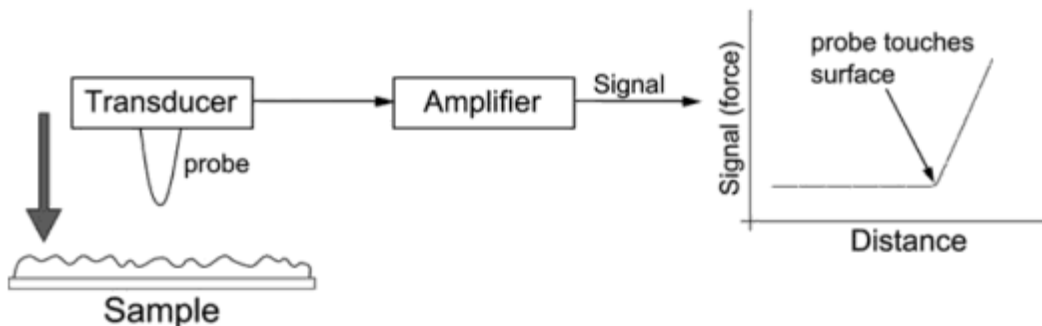
Figure 2.10. Working principle of indentation techniques (Eaton and West, 2010)

As the name suggests, the measured area of the samples is at a small scale, which can be only a few square micrometres or nanometres. There are different approaches to take in terms of testing instrumentation. In general, it can be divided into nano-indenter apparatus and atomic force microscope (AFM). The main difference between the two of them is the physical principle controlling the transducer: nano-indenters use speaker coils or capacitance gauges to directly actuate the indenter probe into the sample while AFMs actuate the tip indirectly via a calibrated cantilever (Oyen, 2014).

As discussed in (Portoles and Cumpson, 2013), the nano-indenter apparatus allows a better control of the indentation force and displacement, and AFM offers the unique advantages of applying very small indentation forces (below 100 pN) but the accurate calibration of the equipment is not easy. As documented in (Chen, 2014a), both quasi-static loading and dynamic loading can be performed in nano-indenter apparatus (Chen *et al.*, 2010b) and AFM (Mahaffy *et al.*, 2004). This indentation process generates a force-displacement curve (see Fig. 2.11 for an example) which enables measurement of viscoelastic properties such as storage modulus and loss

modulus which are related to instantaneous modulus, equilibrium modulus and viscosity (Kurland *et al.*, 2012).
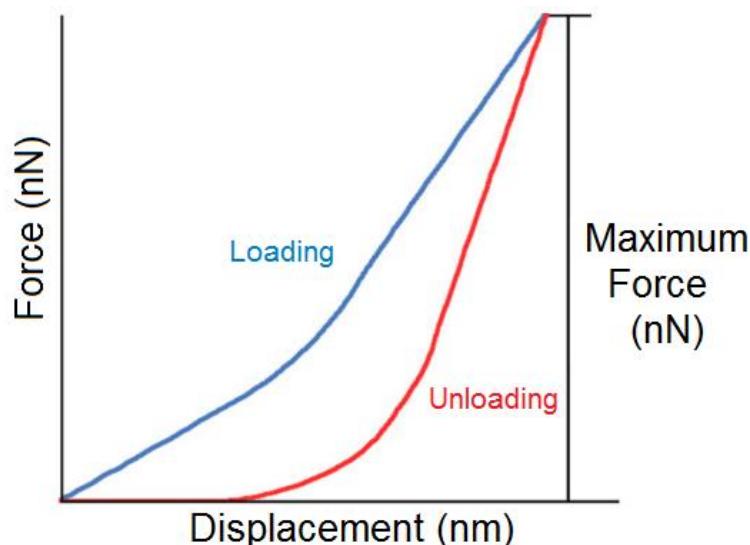
Figure 2.11. A typical force-displacement curve consisting of loading and unloading components that can be used to determine mechanical properties of a sample (adapted from (Kurland *et al.*, 2012))

2.6.2 Rotational rheology

Rheology studies flow and deformation of materials under applied forces (Cowie and Arrighi, 2007). The rheological behaviour of polymers includes ideal elastic behaviour and mechanical properties of elastic solids, irreversible flow of viscous liquids and time dependent behaviour of viscoelastic materials (Cowie and Arrighi, 2007; Chen *et al.*, 2010a). When the rheometer is operated in an oscillating mode, the viscoelastic parameters such as storage modulus, loss modulus and phase angles can be determined. In addition, creep test, and stress relaxation test can be carried out using rheometers (Chen, 2014b) to assess instantaneous modulus, equilibrium modulus and viscosity. Unlike AFM and nano-indentation techniques, rheology is used to measure bulk properties of materials.

Viscoelastic properties of hydrogels when deformed under periodic oscillation are provided by dynamic mechanical analysis (DMA) where the material is subjected to a sinusoidal shear strain (or shear stress) (Barbucci, 2009) through,

$$\gamma = \gamma_0 \sin(\omega t) \tag{1}$$

where γ_0 is shear strain amplitude, ω is the oscillation frequency and t is time. The mechanical response as the shear stress (σ_s) of the viscoelastic material is between an ideal pure elastic solid which is in phase with the deformation and an ideal pure viscous fluid which is 90° out of phase with the deformation which is expressed as,

$$\sigma_s = G^*(\omega)\gamma_0 \sin(\omega t + \delta) \tag{2}$$

$$\sigma_s = G^*(\omega)\gamma_0 \sin(\omega t)\cos(\delta) + G^*(\omega)\gamma_0 \cos(\omega t)\sin(\delta) \tag{3}$$

When $G'(\omega) = G^* \cos(\delta)$ and $G''(\omega) = G^* \sin(\delta)$ definitions are made and substituted in Eq.2,

$$\sigma_s = G'(\omega)\gamma_0 \sin(\omega t) + G''(\omega)\gamma_0 \cos(\omega t) \tag{4}$$

is obtained. G' is called the storage modulus and G'' is called the loss modulus. The storage modulus (also called elastic modulus) give information about the elastic behaviour of the sample which can be also explained as the energy stored in the material during deformation. The loss modulus (also called viscous modulus) give information about the viscous behaviour of the sample which can be also explained as the energy dissipated as heat (Barbucci, 2009).

The complex shear modulus, which can be defined as the resistance of a material to deformation, is defined by storage and loss modulus through,

$$G^* = G' + iG'' \tag{5}$$

The ratio between viscous modulus and storage modulus is expressed by loss tangent which is a measure of the energy lost to energy stored in the cyclic deformation,

$$tan\delta = \frac{G''}{G'} \tag{6}$$

where δ is the phase angle. Using the information from the shear moduli of the materials, one can decide on the material structure.

In general, mechanical behaviour of fluid-like materials can be divided into four groups including Newtonian fluid, shear thickening (also called dilatant), shear thinning, and Bingham plastic (also known as the yield plastic which is among yield stress fluids) (Wilson; Barnes *et al.*, 1989). For liquids having

Newtonian behaviour (which is described by using Eq.7), viscosity is independent of shear rate and it is constant with respect to shear time and stress (Barnes *et al.*, 1989),

$$\sigma = \eta\dot{\gamma} \tag{7}$$

where η is the viscosity and $\dot{\gamma}$ is the shear rate. Water and milk are examples of Newtonian liquids.

Shear thickening indicates an increase in viscosity with increasing shear strain rate while shear thinning indicates a decrease in viscosity with increasing shear strain rate (Barnes *et al.*, 1989). Corn starch is a good example for a shear thickening material and gels are shear thinning materials. Both shear thinning and shear thickening can be explained using the concept of the dissociation of the transient, associative cross-linkers and polymer chains (Xu *et al.*, 2011). For shear thinning behaviour, with the increasing shear strain rate, the polymer chains and cross-linkers disentangle and reform themselves such that their viscosity is smaller compared to their initial viscosity and for shear thickening materials they reform themselves in a way that they have a higher viscosity compared to the initial viscosity value. Figure 2.12 shows the change in shear stress and viscosity with the increasing shear rate for Newtonian fluid, shear thickening and shear thinning fluid.
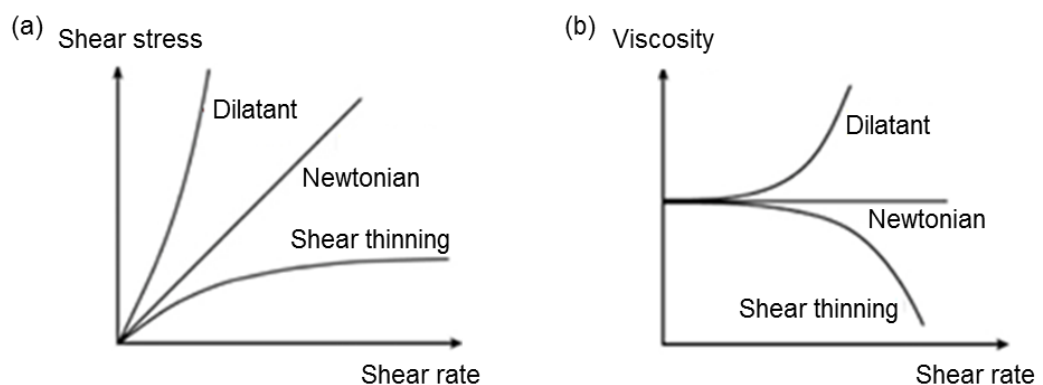
Figure 2.12. The change in shear stress (a) and viscosity (b) with the increasing shear rate for Newtonian fluid, shear thickening (dilatant) and shear thinning fluid (Brockel *et al.*, 2013)

A yield stress fluid behaves like a solid under a critical stress value (i.e. yield stress) and like a viscous liquid when this yield stress value is exceeded.

For Bingham plastic, which is a special type of a yield stress fluid, the shear stress above the yield point is linearly proportional to the shear rate, therefore if the yield stress approaches to zero, the Bingham plastic can be treated as a Newtonian fluid (Liu, 2004). Mayonnaise and toothpaste can be given as examples for Bingham plastic. The dependence of shear stress on shear rate for Bingham plastic is given in Figure 2.13 where τ_Y indicates the yield stress.
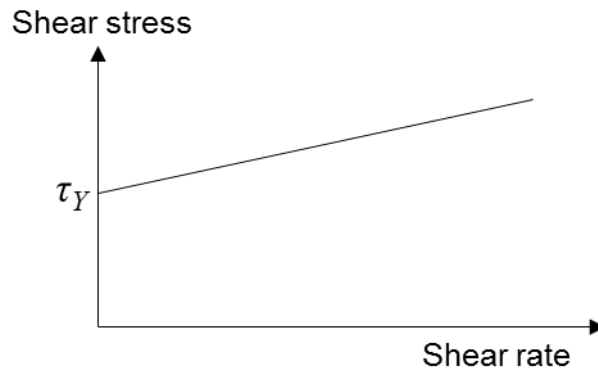
Figure 2.13. The dependence of shear stress on shear rate for Bingham plastic (adapted from (Liu, 2004))

2.6.2.1 Creep and stress relaxation tests

Creep and stress relaxation tests give information about mechanical properties of viscoelastic materials, such as polymers. The viscoelastic behaviour is reflected by the time dependent mechanical response of the material during loading. Therefore, the polymer behaves differently when subjected to short term or long term loads. The viscoelastic behaviour can be linear or nonlinear based on the size and the duration of the deformation, for example, if the deformation on the material is small and the relationship between strain and stress is linear, it is considered as linear viscoelastic, on the other hand, when the deformation is large nonlinear viscoelasticity is considered (White, 1990; McCrum *et al.*, 1997; Osswald, 2015).

Creep is a thermally activated process and takes place at high temperatures for metals and ceramics, however polymer materials can show creep behaviour even at room temperature (Chawla and Meyers, 1999). For a creep test, a constant stress, σ_0, is applied to the material and the strain response is measured as a function of time. A typical creep curve is given in Figure 2.14.
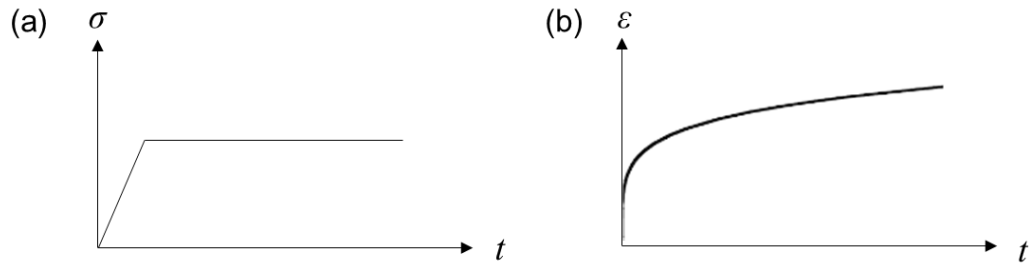
Figure 2.14. Creep curve of materials under a constant stress: (a) applied stress versus time, (b) the resultant curve for strain versus time

Like in the case of temperature, creep behaviour of polymers is different than that of metals and ceramics. Since these materials are viscoelastic, the deformation is reversible, which means that they can nearly return to their original dimensions in time after the load is removed (François *et al.*, 1998; Bowman, 2004; Hosford, 2010).

In creep, for a linear material the strain is represented as,

$$\varepsilon(t) = \sigma_0 J(t) \tag{8}$$

where $J(t)$ is the creep compliance defined as the creep strain per applied stress (Findley *et al.*, 1989; McCrum *et al.*, 1997; Lakes and Lakes, 2009). Similar to elastic modulus, creep compliance is also a material property.

Stress relaxation is a time dependent response of a material to elastic straining (Bowman, 2004). In a stress relaxation test, the test specimen is suddenly deformed by a fixed amount, ε_0, and the stress required to hold that amount of deformation is recorded over time which will then be used to interpret the viscoelastic behaviour of the material. A typical stress relaxation curve is given in Figure 2.15.
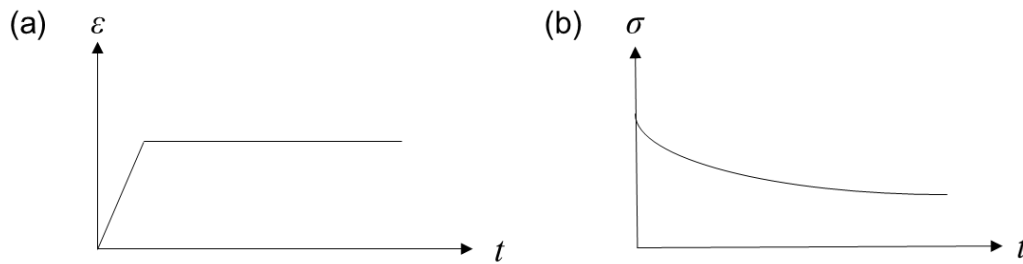
Figure 2.15. Stress relaxation curve of materials under a constant strain: (a) applied strain versus time, (b) the resultant curve for stress versus time

In linear viscoelasticity, the stress relaxation modulus is defined as the ratio of the stress to the applied strain at a given time, t.

$$E(t) = \frac{\sigma(t)}{\varepsilon_0} \tag{9}$$

Here, ε_0 is the applied strain and $\sigma(t)$ is the stress being measured at a given time. When a constant strain is applied to a viscoelastic sample, the force (or stress) necessary to maintain that strain is not constant but decreases with time, this behaviour is called stress relaxation (Spetz, 1999).

Mechanical models to predict creep and stress relaxation behaviour of materials are explained in detail at Section 2.7.

2.6.3 Compression tests

Universal test frame is the most commonly used characterisation technique for determination of mechanical properties of materials which can perform a wide variety of uniaxial experimental tests including tensile and compression tests. They are built in various sizes and having load cells of different capabilities so that they can be used to test a wide variety of samples, from large civil engineering components to soft biological materials and biomedical components including hydrogels (Oyen, 2014).

Compression tests are performed to observe material behaviour under a compressive load. During compression tests, the test specimen is compressed and the deformation against applied force is recorded, a typical curve obtained from an unconfined compression loading is given in Figure 2.16. This test is used to determine several material mechanical properties such as elastic limit, proportional limit, yield point, yield strength and compressive strength (Kuhn and Medlin, 2000; Hanke, 2001). Within the elastic limit, the stress and strain is linearly proportional so when the applied

28

strain is known, using the corresponding stress the elastic property of the material can be calculated. The compression test protocols can be user-defined. For example, a fast loading segment followed by a prolonged stress relaxation or creep segments have been often employed to study the viscoelastic properties of hydrogels (Mauck *et al.*, 2000; Stammen *et al.*, 2001; Zhao *et al.*, 2010). The viscoelastic properties of hydrogels can also be determined during the compression segment only, provided that the ramping rate is relatively small, in this case, the Boltzmann integral operator should be applied (Chen *et al.*, 2014).
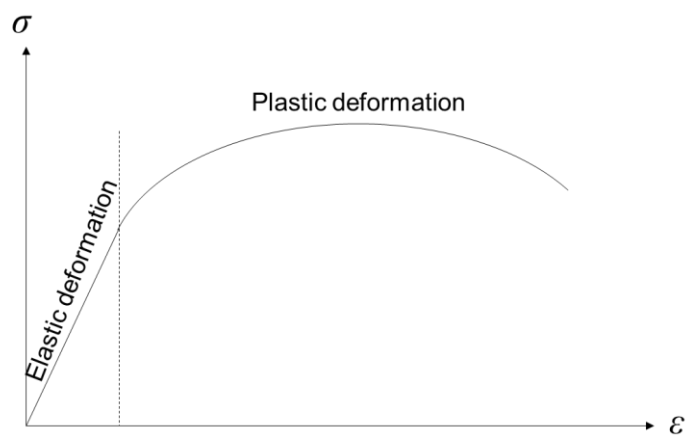
Figure 2.16. A typical stress – strain curve for a representative elastic-plastic material obtained from an unconfined compression loading

For viscoelastic materials, a typical stress and strain curve obtained from compression tests is given in Figure 2.17 which involves an immediate elastic response, strain softening behaviour and strain stiffening behaviour (Tamplenizza *et al.*, 2015; Gasik *et al.*, 2017).
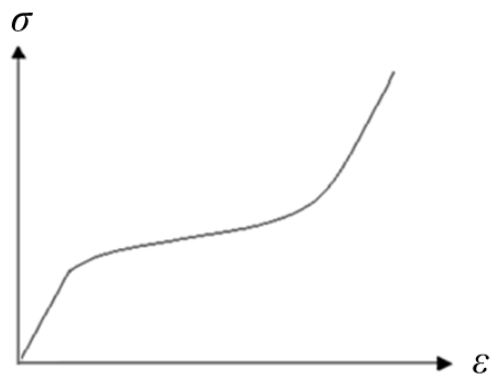
Figure 2.17. Stress – strain curve for a representative viscoelastic material obtained from an unconfined compression loading

2.7 Mechanical Models for Viscoelastic Response of Hydrogels

In the literature, there are several mechanical models to represent the viscoelastic response of hydrogels. These models use linear elastic springs (mimicking elastic response) and linear viscous dash-pots (mimicking viscous response) connected in various ways and in various numbers to determine their stress and strain behaviour. In this section, different mechanical models for viscoelastic response are explained.

2.7.1 Linear elastic spring and linear viscous dash-pot

A linear elastic spring is used to model the elastic behaviour of materials. The material is subjected to an instantaneous elastic strain upon loading and maintains the strain as long as the strain is applied and goes back to its original shape upon removal of the load. Linear elastic springs follow Hooke's law (Eq. 10), *i.e.* the strain, ε, is proportional to the applied stress, σ.

$$\sigma = E\varepsilon \tag{10}$$

Here E represents the elastic modulus (Young's modulus) of the material. In Figure 2.18, a linear elastic spring is represented and the stress strain behaviour of a linear elastic spring is shown.
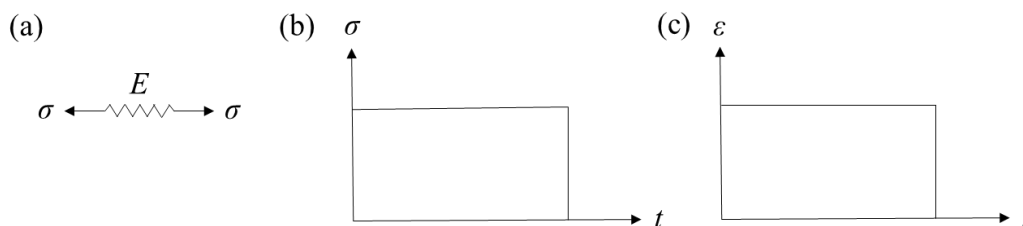
Figure 2.18. (a) A linear elastic spring. (b) Stress behaviour of the linear elastic spring. (c) Strain behaviour of the linear elastic spring

A linear viscous dash-pot is used to model the viscous behaviour of materials and responds with a strain rate proportional to stress, obeying Newton's law of viscosity (Eq. 11).

$$\sigma = \eta\dot{\varepsilon} \tag{11}$$

where η is the viscosity of the material and $\dot{\varepsilon}$ is the strain rate. Upon a suddenly applied stress (σ_0), when the initial strain is neglected, the strain can be found by integrating Eq. 12.

$$\varepsilon = \frac{\sigma_0}{\eta} t \tag{12}$$

The material is subjected to an instantaneous stress, the developed strain is permanent. In Figure 2.19, a linear viscous dash-pot is represented and the stress strain behaviour of a linear viscous dash-pot is shown.
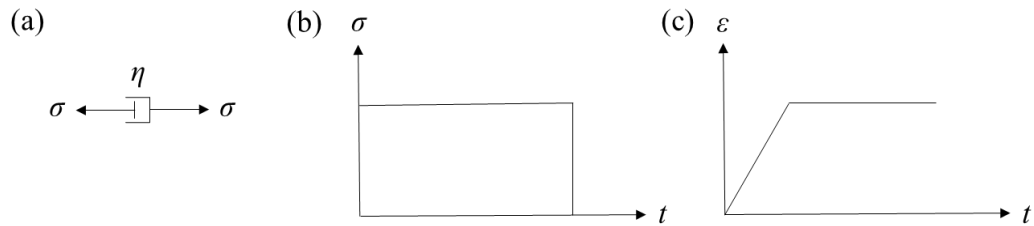
Figure 2.19. (a) A linear viscous dash-pot. (b) Stress behaviour of the linear viscous dash-pot. (c) Strain behaviour of the linear viscous dash-pot

2.7.2 Maxwell model

Maxwell model is a two element model consisting of a spring and a dashpot connected in series, as illustrated in Figure 2.20. Due to the equilibrium, the applied stress is the same for both elements and the resulting strain can be divided into spring and dashpot.
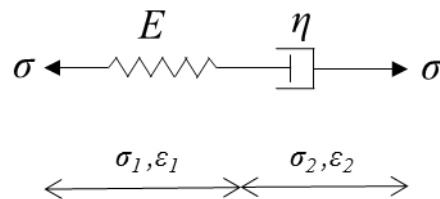
Figure 2.20. A Maxwell element consisting of a spring and a dashpot connected in series. σ_1 and ε_1 are the stress and strain for the spring, σ_2 and ε_2 are the stress and strain for the dash-pot

$$\sigma = \sigma_1 = \sigma_2 \tag{13}$$

$$\varepsilon = \varepsilon_1 + \varepsilon_2, \quad \varepsilon_1 = \frac{1}{E}\sigma \text{ and } \dot{\varepsilon}_2 = \frac{1}{\eta}\sigma \tag{14}$$

31

The constitutive equation of the Maxwell model (given below) is obtained by using equations given at Eq.14.

$$\sigma + \frac{\eta}{E}\dot{\sigma} = \eta\dot{\varepsilon} \qquad (15)$$

When a constant stress is applied (σ_0), the spring stretches immediately, making the initial strain determined by the spring, and the dashpot will take time to react. A similar case takes place for when the stress is removed. Maxwell model cannot be used to predict the behaviour of the material under constant stress (creep) accurately, since the model predicts that the strain increases linearly with time (elastic response) and when the stress is removed there is no inelastic recovery, *i.e.* there is an elastic response under constant stress and a permanent strain when the stress is removed (see Figure 2.21). However, most polymers show the opposite behaviour where the strain decreases with time (Findley *et al.*, 1989; Rodriguez *et al.*, 2014).
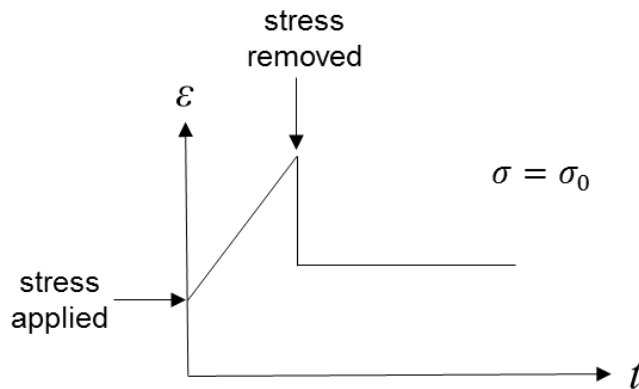
Figure 2.21. Creep response of Maxwell model under constant stress

This model predicts the stress relaxation behaviour more accurately during when a constant strain is applied (where $\dot{\varepsilon} = 0$). Under this circumstance, the constitutive equation of the Maxwell model can be written as;

$$\frac{\sigma}{\eta} + \frac{1}{E}\dot{\sigma} = 0 \qquad (16)$$

Eq. 16 can be integrated to get the following equation;

$$\sigma = \sigma_0 \exp(-\frac{E\,t}{\eta}) \qquad (17)$$

where η/E is the relaxation time (τ_R). Eq. 17 can be rewritten to obtain the stress relaxation equation for Maxwell model where stress decreases exponentially with time (Fig. 2.22).

$$\sigma = \sigma_0 \exp(-\frac{t}{\tau_R}) \tag{18}$$
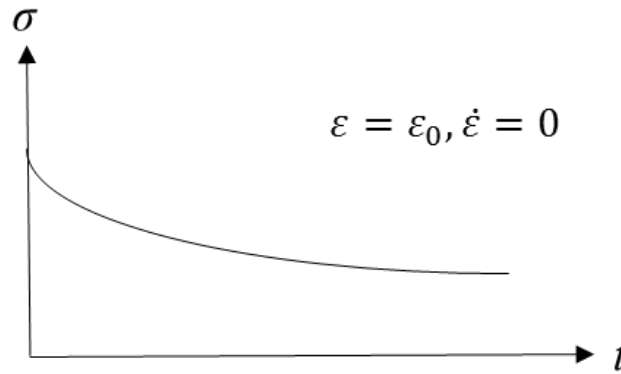
Figure 2.22. Stress relaxation response of Maxwell model under constant strain

2.7.3 Kelvin-Voigt model

Kelvin-Voigt model is a two element model consisting of a spring and a dashpot connected in parallel, as illustrated in Figure 2.23. In this model, bending is neglected, so that the strain experienced by the spring and the dash-pot is the same.
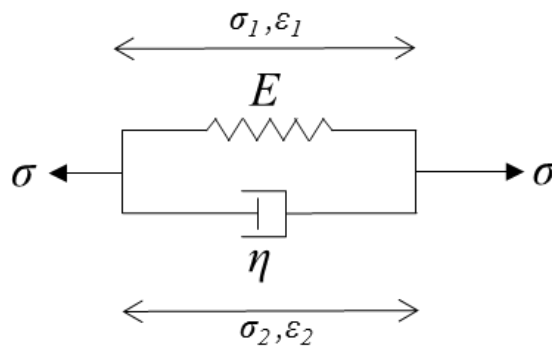
Figure 2.23. A Kelvin-Voigt element consisting of a spring and a dashpot connected in parallel. σ_1 and ε_1 are the stress and strain for the spring, σ_2 and ε_2 are the stress and strain for the dash-pot

$$\varepsilon = \varepsilon_1 = \varepsilon_2 \tag{19}$$

$$\sigma = \sigma_1 + \sigma_2, \quad \varepsilon = \frac{1}{E}\sigma_1 \text{ and } \dot{\varepsilon} = \frac{1}{\eta}\sigma_2 \tag{20}$$

33

The constitutive equation of the Kelvin-Voigt model (given below) is obtained by using equations given at Eq.20.

$$\sigma = E\varepsilon + \eta\dot{\varepsilon} \tag{21}$$

When a constant stress is applied (σ_0), the spring tries to stretch however its movement is restrained by the dash-pot which initially takes up the stress. This makes the creep curve to start with an initial slope of σ_0/η. The dash-pot transfers some of the strain to the spring which changes the slope to σ_2/η, with σ_2 decreasing continually. When $\sigma_2 = 0$, the spring experiences all of the applied stress, resulting the maximum strain to be σ_0/E. Under these circumstances, the constitutive equation of the Kelvin-Voigt model for the loading part of the creep curve can be written as;

$$\varepsilon = \frac{\sigma_0}{E}(1 - \exp(-\frac{E}{\eta}t)) \tag{22}$$

where η/E is the retardation time (t_R) which is the time for the creep strain to accumulate. When the stress is removed at a time $t = \tau_{\sigma_0}$, the spring tries to contract however its movement is again restrained by the dash-pot. The spring eventually moves the dash-pot back to its initial position resulting in full recovery (Kelly, 2013). After the stress is removed, the constitutive equation of the Kelvin-Voigt model for the unloading part of the creep curve can be written as;

$$\varepsilon = \frac{\sigma_0}{E}\exp\left(-\frac{E}{\eta}t\right)\left(\exp\left(\frac{E}{\eta}\tau_{\sigma_0}\right) - 1\right), \text{t} > \tau_{\sigma_0} \tag{23}$$

There is a transient creep and anelastic recovery, but instantaneous or permanent strain do not occur (Chawla and Meyers, 1999; Kelly, 2013), so this model predicts the creep behaviour accurately.
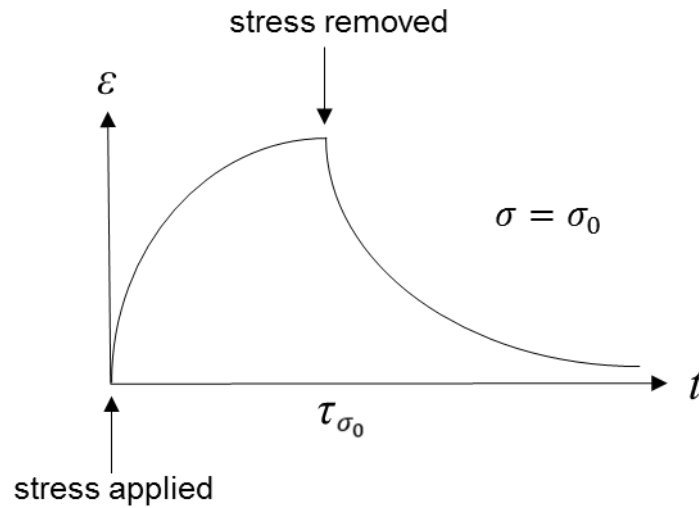
Figure 2.24. Creep response of Kelvin-Voigt model under constant stress

During a stress relaxation test, since the strain is constant, the constitutive equation of the Kelvin-Voigt model can be rewritten as;

$$\sigma = E\varepsilon_0 \tag{24}$$

Eq. 24 indicates that the spring is the only element being affected by the stress and, stress relaxation does not take place when the applied strain is removed. Therefore, Kelvin-Voigt model cannot accurately predict stress relaxation behaviour.

2.7.4   Three-element models (Zener Models)

As discussed above, Maxwell model and Kelvin-Voigt model are the simple two-element models to predict viscoelastic behaviour, however both of those models have several limitations. To overcome such limitations, three element models, which are also referred as Zener models, are introduced. These models are obtained by using a spring connected in series or parallel with either Maxwell or Kelvin-Voigt models to predict solid-like behaviour (Fig. 2.25a and 2.25b) or by using a dash-pot connected in series or parallel with either Maxwell or Kelvin-Voigt models to predict fluid-like behaviour (Fig. 2.25c and 2.25d) (Schiessel *et al.*, 1995; Mainardi and Spada, 2011).
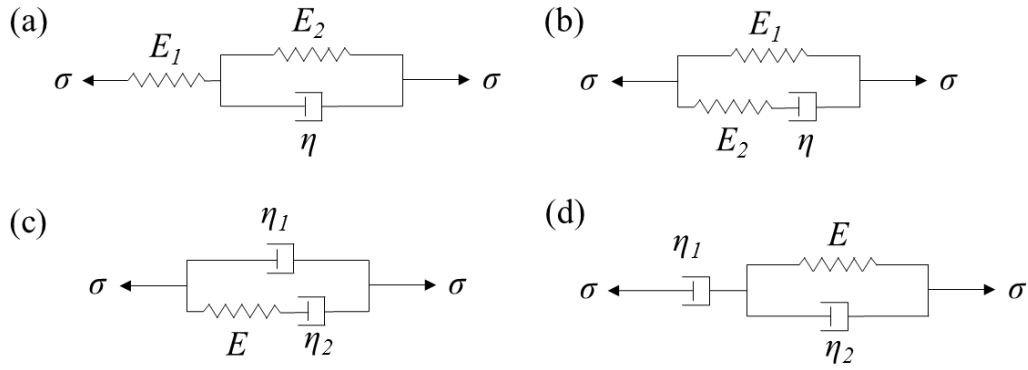
Figure 2.25. Three element models. (a) A spring connected in series with Kelvin-Voigt model, (b) a spring connected in parallel with Maxwell model, (c) a dash-pot connected in parallel with Maxwell model and (d) a dash-pot connected in series with Kelvin-Voigt model

The constitutive equations for the models shown in Figure 2.25 are given below (Kelly, 2013). The equation order is the same as the models given in Figure 2.25.

$$\sigma + \frac{\eta}{E_1+E_2}\dot{\sigma} = \frac{E_1E_2}{E_1+E_2}\varepsilon + \frac{\eta E_1}{E_1+E_2}\dot{\varepsilon} \tag{25}$$

$$\sigma + \frac{\eta}{E_2}\dot{\sigma} = E_1\varepsilon + \frac{\eta(E_1+E_2)}{E_2}\dot{\varepsilon} \tag{26}$$

$$\sigma + \frac{\eta_2}{E}\dot{\sigma} = (\eta_1 + \eta_2)\dot{\varepsilon} + \frac{\eta_1\eta_2}{E}\ddot{\varepsilon} \tag{27}$$

$$\sigma + \frac{\eta_1+\eta_2}{E}\dot{\sigma} = \eta_1\dot{\varepsilon} + \frac{\eta_1\eta_2}{E}\ddot{\varepsilon} \tag{28}$$

The model responses can be determined by specifying a stress value and solving the differential equation for strain or by specifying a strain value and solving the differential equation for stress depending on either creep or stress relaxation behaviour. Although these models are more accurate compared to Maxwell and Kelvin-Voigt models in terms of fitting the experimental data over the full range due to having more elements, the numerical strain prediction under specific loading conditions can be inaccurate (Roylance, 2001).

2.7.5 Burger's model

Burger's model consists of a Maxwell model and a Kelvin-Voigt model connected in series (Fig. 2.26). By doing so, the relaxation and the retardation can be analysed using the same model (Malkin and Isayev,

2017). When a stress is applied, the total strain of the model is the sum of the strain in each element.
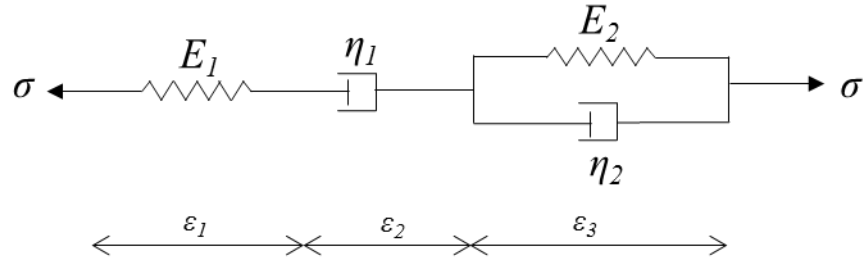
Figure 2.26. Schematic representation of Burger's model consisting of a Maxwell and a Kelvin-Voigt element connected in series

$$\varepsilon = \varepsilon_1 + \varepsilon_2 + \varepsilon_3 \ , \ \varepsilon_1 = \frac{\sigma}{E_1} \ , \ \dot{\varepsilon}_2 = \frac{\sigma}{\eta_1} \ , \ \dot{\varepsilon}_3 + \frac{E_2}{\eta_2}\varepsilon_3 = \frac{\sigma}{\eta_2} \qquad (29)$$

The constitutive equation of the Burger's model (given below) is obtained by using equations given at Eq. 29.

$$\sigma + \left(\frac{\eta_1}{E_1} + \frac{\eta_1}{E_2} + \frac{\eta_2}{E_2}\right)\dot{\sigma} + \frac{\eta_1\eta_2}{E_1E_2}\ddot{\sigma} = \eta_1\dot{\varepsilon} + \frac{\eta_1\eta_2}{E_2}\ddot{\varepsilon} \qquad (30)$$

Under a constant stress, using the initial conditions, the creep behaviour of Burger's model is determined as;

$$\varepsilon(t) = \frac{\sigma_0}{E_1} + \frac{\sigma_0}{\eta_1}t + \frac{\sigma_0}{E_2}(1 - \exp(-\frac{E_2}{\eta_2}t)) \qquad (31)$$

Under a constant strain, stress response of Burger's model in the case of stress relaxation is given as follows;

$$\sigma(t) = \sigma_0[(q_1 - q_1r_1)exp(-r_1t) + (q_1 - q_2r_2)exp(-r_2t)] \qquad (32)$$

$$r_1 = \frac{p_1-A}{2p_2} \ ; \ r_2 = \frac{p_1+A}{2p_2} \ ; A = \sqrt{p_1^2 - 4p_2} \qquad (33)$$

$$p_1 = \frac{\eta_1}{E_1} + \frac{\eta_1}{E_2} + \frac{\eta_2}{E_2} \ ; \ p_2 = \frac{\eta_1\eta_2}{E_1E_2} \ ; \ q_1 = \eta_1 \ ; \ q_2 = \frac{\eta_1\eta_2}{E_2} \qquad (34)$$

In Equation 32, σ_0 was calculated using true strain and true area and the stress response is a function of Burger's model parameters: E_1, η_1, E_2 and η_2. The stress function was simplified visually by using the Burger's model parameter dependent coefficients, namely: $r_1, r_2, A, p_1, p_2, q_1$ and q_2, given at equations 33 and 34. Here, $E_1 \ and \ E_2$ are the linear spring constants (*i.e.* Young's modulus) representing the elastic response, and η_1 and η_2 are the linear dashpot constants representing the viscous response when a specific strain is applied.

2.7.6 Generalised models

Generalised models to predict the linear viscoelastic behaviour can be obtained by employing more elements (linear springs and dash-pots). These models can be in the form of generalised Maxwell model where N number of Maxwell elements are connected in parallel or a generalised Kelvin-Voigt model where N number of Kelvin-Voigt elements are connected in series (see Fig. 2.27). In both generalised models, the individual elements have different parameter values. When the isolated spring is detached fluid-type behaviour can be modelled and when the isolated dash-pot is detached an instantaneous response can be modelled (Park, 2001).
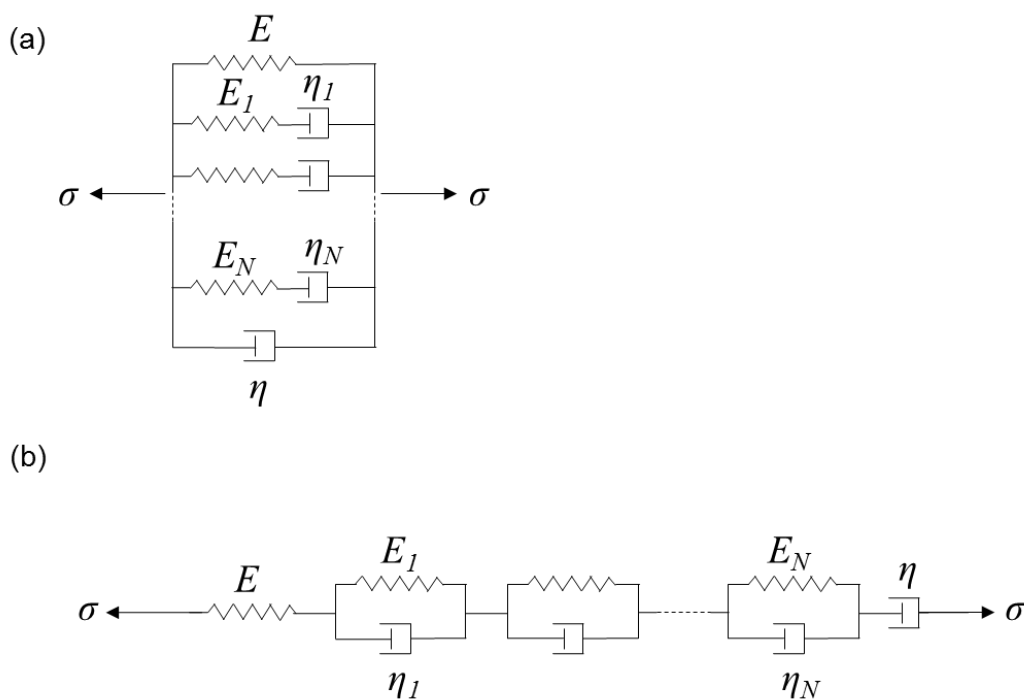
Figure 2.27. Generalised viscoelastic models (a) generalised Maxwell model, (b) generalised Kelvin-Voigt model

The increase in the number of elements that are used in the models increases the accuracy of the model. However, this also increases the number of material parameters to be determined which makes the differential equations to be solved to be more difficult due to the equations having a higher order.

The constitutive equation for the linear viscoelastic models can be written as (Makris *et al.*, 1993; Kelly, 2013);

$$\boldsymbol{P}\sigma = \boldsymbol{Q}\varepsilon \tag{35}$$

Here, **P** and **Q** are the linear differential operators:

$$\boldsymbol{P} = \sum_{i=0}^{n} p_i \frac{\partial^i}{\partial t^i} \quad , \quad \boldsymbol{Q} = \sum_{i=0}^{n} q_i \frac{\partial^i}{\partial t^i} \tag{36}$$

2.7.7 Prony series

Creep and recovery experiments are performed to determine the linear viscoelastic region. A suitable model complying the creep data is used and based on the agreement between the data and the model, the recovery strains are predicted and compared to the strains obtained during experiments. If they match, the linear superposition principle is applicable and the viscoelastic behaviour is linear. Under these circumstances, Prony series can be used to represent such data (Park and Schapery, 1999; Tzikang, 2000; Papanicolaou and Zaoutsos, 2011).

The Prony series equation for the shear relaxation is as follows;

$$E(t) = E_\infty + \sum_{i=1}^{n} E_i \exp\left(-\frac{t}{\tau_i}\right) \tag{37}$$

Here, E_∞ indicates the modulus when the material is completely relaxed and τ_i are the relaxation times. The instantaneous modulus, E_0, can be calculated using this model by;

$$E_0 = E_\infty + \sum_{i=1}^{n} E_i \tag{38}$$

2.7.8 Poroelastic model

Multiphasic poroelastic models are used to describe the time dependence of hydrated materials, such as hydrogels. This behaviour is due to the flow of a fluid through an elastic (or viscoelastic), porous solid (Chen, 2014a; Oyen, 2014). This model assumes that there is a linear relationship between stress and strain and the deformation is reversible.

The constitutive equation of poroelastic model for isotropic materials is as follows;

$$\varepsilon_{ij} = \frac{\sigma_{ij}}{2G} - \left(\frac{1}{6G} - \frac{1}{9B}\right)\delta_{ij}\sigma_{kk} + \frac{\delta_{ij}p}{3H} \quad , \quad \rho = \frac{\sigma_{kk}}{3H} + \frac{p}{M} \tag{39}$$

Here, B and G are bulk and shear modulus of the drained elastic solid, and parameters H and M represent the coupling between solid and fluid stress and strain.

This model can be applied to model the mechanical behaviour of hydrogels, since when a load is applied on the hydrogels the solvent in the hydrogel migrates (Hu *et al.*, 2010; Strange *et al.*, 2013). During stress relaxation, the following equation can be used;

$$\frac{P(t)-P(\infty)}{P(0)-P(\infty)} = g(\tau) \tag{40}$$

where $P(0)$ and $P(\infty)$ are the forces at $t = 0$ and $t = \infty$, respectively. The normalised time, τ, is a function of the contact radius, diffusivity and time. The parameters used in this model are physical constants directly related to the microstructure of the material, however the data analysis for this model is complicated.

2.8 Analytical Models for Calculating Composite Stiffness

Composite materials are made by combining two or more materials having different properties in a way that they do not dissolve or blend in each other to obtain a new material with its unique properties (Jones, 1998). In this sense, hydrogels with encapsulated cells or particles can be treated as composites providing the mentioned composite characteristics. In literature, there are several theoretical models to determine composite stiffness such as Voigt model, Reuss model, Hashin and Strikman model with upper and lower bounds, Mori-Tanaka model, self-consistent model and Bridging model. The details of these models are explained in this section.

2.8.1 Voigt model

The Voigt limit, also known as the rule of mixtures of composites, is regarded as an unexceedable upper limit for the stiffness of isotropic composite materials (Jones, 1998; Lakes and Drugan, 2002; Gay *et al.*, 2003; Zhu *et al.*, 2015). For an elastic composite having two phases, made of two different isotropic materials A and B with Young's moduli E_A and E_B, respectively, the Voigt limit for the Young's modulus of the composite is given as;

$$E_{C-Voigt} = E_A V_A + E_B V_B \tag{41}$$

where V_A and V_B are volume fractions of the two materials. Here, $V_A + V_B = 1$ equality should be attained. As can be seen from Equation 41, the Voigt model represents a simple linear variation of Young's modulus in the direction of fibres assuming each phase experiencing the same uniform strain (Watt and Peselnick, 1980; Lakes and Drugan, 2002).

2.8.2 Reuss model

Similarly, a lower limit for composite stiffness is also defined which is known as Reuss model again depending on the Young's moduli (E_A and E_B) and volume fraction (V_A and V_B) of the two phases. The Reuss model is given as;

$$E_{C-Reuss} = \frac{E_A E_B}{E_A V_B + E_B V_A} \tag{42}$$

As in the Voigt model, $V_A + V_B = 1$ equality should be attained for Reuss model as well. On the other hand, the effective elastic modulus calculated by the Reuss model focuses on the Young's modulus in the direction transverse to the fibres, assuming each phase experiencing uniform stress (Watt and Peselnick, 1980; Lakes and Drugan, 2002).

2.8.3 Hashin and Shtrikman model with upper and lower bounds

Hashin and Shtrikman (HS) developed principles having tighter bounds than the Voigt and Reuss bounds by focusing on the macroscopically isotropic composites (Watt and Peselnick, 1980; Lakes and Drugan, 2002). The shear and bulk HS bounds are given below respectively at Equations 43 and 44. HS shear moduli and bulk moduli equations given below refer to the HS upper bounds. To obtain HS lower bounds, the indices (1 and 2) were reversed.

$$G_{C-HS} = G_2 + \frac{V_1}{\frac{1}{G_1 - G_2} + 6(B_2 + 2G_2)V_2 / [5(3B_2 + 4G_2)G_2]} \tag{43}$$

$$B_{C-HS} = B_2 + \frac{V_1(B_1 - B_2)(3B_2 + 4G_2)}{(3B_2 + 4G_2) + 3(B_1 - B_2)V_2} \tag{44}$$

Here, 1 and 2 refer to the matrix (or gel) and particle (or cell), respectively. G and B refer to shear modulus and bulk modulus respectively and they can be calculated using Eq.45.

$$G = \frac{E}{2(1+v)} \quad , B = \frac{E}{3(1-2v)} \tag{45}$$

Different from Voigt and Reuss bounds, HS bounds depend on the Poisson's ratio of the two phases in addition to their elastic moduli and volume fractions. The plot given below shows how the shear modulus changes with volume fraction for all of the models mentioned. The stiffness values used to generate this plot are 100 GPa and 10 GPa for the stiff phase and the soft phase, respectively, and the Poisson's ratio for both phases are taken as 0.3.
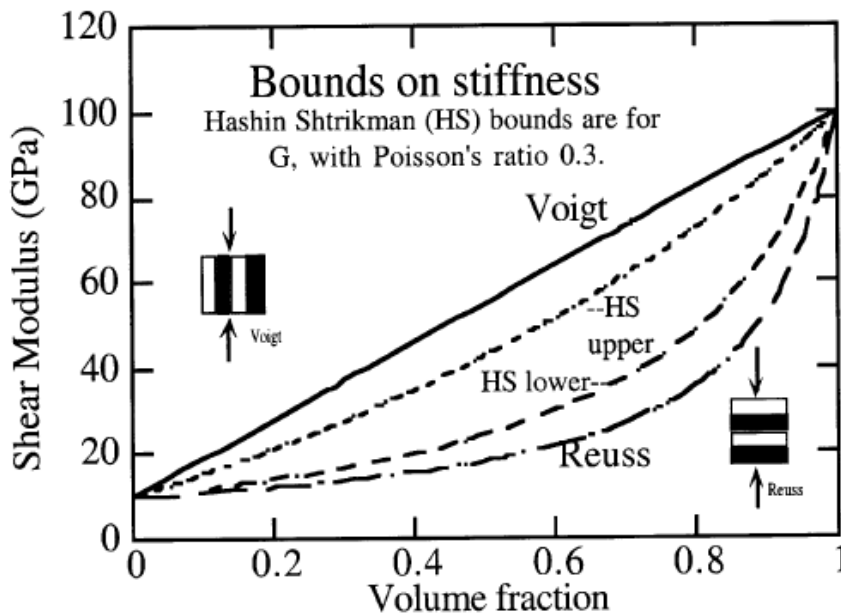
Figure 2.28. Representation of the theoretical model bounds for composite stiffness (Lakes and Drugan, 2002)

The bounding theorems, which assume positive definiteness of the strain energy density, state that no composite can be stiffer than the Voigt bound (Paul, 1959) and no macroscopically isotropic composite can be stiffer than the HS upper bound (Hashin, 1962; Hashin and Shtrikman, 1963). So these bounds can be used when each phase of the composite has a positive stiffness.

2.8.4 Self-consistent model

The self-consistent model is used to predict the elastic properties of composite materials reinforced by isotropic spherical particulates and of short fibre composites (Hill, 1965; Younes *et al.*, 2012). The self-consistent method follows an iterative method to find matrix stiffness. In this method, the fibres (which represent the inclusions) are assumed to be surrounded by an isotropic matrix which makes this model to be similar to the Eshelby's

equivalent inclusion theory (Eshelby, 1957). In addition, the inclusions are considered to be embedded in a homogeneous medium having a stiffness as calculated at the first iteration. The representation of the self-consistent model is given in Figure 2.29.
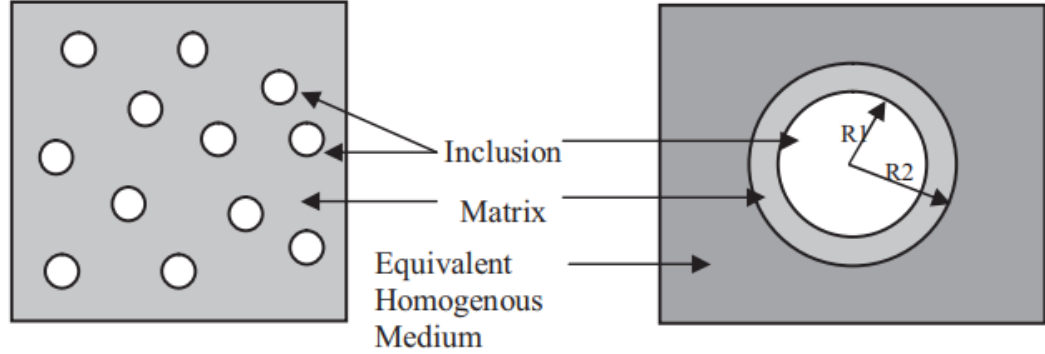
Figure 2.29. A representative volume showing the composite of polymers and inclusions for self-consistent model (Alam and Hammoum, 2015)

For a composite structure having *n* number of phases, the effective bulk modulus and shear modulus are calculated as follows;

$$B = B_n + \frac{R_{n-1}^3/R_n^3}{(1)/(B_{n-1}-B_n)+((3(R_n^3-R_{n-1}^3))/R_n^3)1/(3B_n+4\mu_n)} \tag{46}$$

$$A_{SC}\left(\frac{\mu}{\mu_n}\right)^2 + B_{SC}\left(\frac{\mu}{\mu_n}\right) + C_{SC} = 0$$

(47)

and a concentric shell of inner and outer radii, respectively. A_{SC}, B_{SC} and C_{SC} are coefficients which depend on shear modulus, volumetric fraction and Poisson's ratio of each phase.

2.8.5 Mori-Tanaka model

Mori-Tanaka model, which is an inclusion model of inclusions embedded in a homogeneous medium, considers a non-dilute composite with spheroidal particles that allowed the matrix to bear a stress different from the loaded stress (Younes *et al.*, 2012; Li *et al.*, 2017). This model uses an analytical approach to determine the effective composite stiffness using homogenization techniques (Gong *et al.*, 2011). Similar to self-consistent model, this is done by Eshelby's equivalent inclusion theory. For an infinite composite material subjected to a uniform stress σ^0, the stress field can be described as,

$$\sigma^0 = L^e \varepsilon^0 \tag{48}$$

where σ^0 is the stress tensor, ε^0 is the strain tensor and L^e is the equivalent stiffness of the matrix. Using the Eshelby theory, the equivalent stiffness can be found in an explicit form as,

$$L^e = L^m (I + VA)^{-1} \tag{49}$$

where L^m is the matrix stiffness, I is the identity tensor, V is the volume fraction and A is strain concentration tensor.

The Mori-Tanaka model has several limitations due to the model being suitable only for composites with low volume fraction of inclusions and the assumption of homogeneous microstructure (Gong *et al.*, 2011).

2.9 Hydrogel mechanical properties affecting bacteria physiology

In this chapter, it was explained that hydrogels can be used as culture mediums for bacterial cells and that bacterial cell physiology is affected by the environment. Therefore, hydrogel mechanical properties (*i.e.* stiffness) would also have an effect on bacterial physiology, including their adhesion, motility and growth behaviour.

Bacterial cells can regulate their behaviour based on their mechanosensors even at single cell level (Persat *et al.*, 2015; Even *et al.*, 2017), which can affect their adhesion to different surfaces (Ellison and Brun, 2015; Harapanahalli *et al.*, 2015). In addition to the surface sensing property of bacterial cells, it has been shown in many studies that hydrogel stiffness plays a role in adhesion (Lichter *et al.*, 2008; Guegan *et al.*, 2014; Song and Ren, 2014; Kolewe *et al.*, 2015; Persat *et al.*, 2015; Kolewe *et al.*, 2017; Song *et al.*, 2017). These studies have reported an opposite behaviour of bacterial cell adhesion, either suggesting that softer hydrogels promote a stronger adhesion or stiffer hydrogels promote a stronger adhesion. For these differences, it should be taken into account that other factors (such as chemical composition, source of hydrogels etc.) could be contributing to the adhesion as well.

In addition to adhesion, hydrogel stiffness also affects migration of bacteria (Copeland and Weibel, 2009; Guegan *et al.*, 2014). For instance, agar gels

having a concentration of less than 0.4% allow the bacterial cells to penetrate into the polymer network and swim whereas gels having a concentration above 2% do not allow swarming motility (Copeland and Weibel, 2009).

While both adhesion and motility studies have been carried out at 2D, bacterial growth has been considered both in 2D and 3D. Regarding bacterial growth on hydrogel surfaces, conflicting results have been reported (Saha *et al.*, 2013; Kolewe *et al.*, 2015). Similar to the results from adhesion, this is also related to additional factors. In 3D, bacterial growth (in terms of elongation) has been reported to decrease with increasing hydrogel stiffness (Tuson *et al.*, 2012a).

3 General Materials and Methods

In this chapter, the materials used in the experiments were listed and the methods that were used throughout the study were explained in detail. The materials and methods specific to different testing techniques are given in the relevant results sections.

3.1 Materials

3.1.1 Gelling agents: agar and agarose powders

Agar powder (VWR International, Lutterworth, Leicestershire, UK) was used for preparing gels for bacteria growth on surfaces. This powder is routinely used in microbiology laboratories to prepare gels for bacteria growth.

The type of agarose used in this study was low gelling 2-hydroxyethyl agarose type VII-A (Sigma-Aldrich, Gillingham, Dorset, UK). This type of agarose powder was selected due to its lower gelation temperature which enabled a longer working time at a liquid state for encapsulation applications. Since bacterial cells were involved in the study which cannot survive at high temperatures, it was advantageous to have this low temperature gelling property. The gelation point of this type of agarose is specified as $26^{\circ}C \pm 2^{\circ}C$.

3.1.2 Growth media and buffers

Luria-Bertani (LB) broth medium, nutrient broth (NB) medium and phosphate buffered saline (PBS) buffer were used in the study. *Escherichia coli* was routinely cultured in LB broth medium and *Staphylococcus epidermidis* was routinely cultured in NB medium.

LB medium consists of tryptone which is a collection of peptides obtained by digestion of casein by the protease enzyme trypsin (1% w/v), yeast extract (0.5% w/v) and NaCl (1% w/v). Due to the amount of NaCl used, it is also referred as high salt LB medium. When required, modified versions of LB growth medium were prepared by omitting one reagent, either yeast extract for 'LB-no yeast extract' or tryptone for 'LB-no tryptone'. NB medium consists of peptone which is a collection of amino acid monomers from animal meat digestion (1% w/v), 'Lab-Lemco powder' which is refined meat extract (1% w/v) and NaCl (0.5% w/v). This medium was prepared from a commercially available mixture (Oxoid CM0067 Nutrient Broth No.2). PBS

buffer consists of KH_2PO_4 (0.1440% w/v), NaCl (9% w/v) and Na_2HPO_4 (0.7950% w/v) without the addition of calcium and magnesium. The buffer was diluted from a commercially available 10X stock solution (Lonza, 17-517Q). The pH of these media (including the modified versions of LB) and the buffer was adjusted to 7.5 ± 0.2 and they were autoclaved at 121°C and a pressure of 1.2 bar for 15 min. They were used for the preparation of hydrogels.

3.1.3 Bacterial strains

E. coli BW25113 cells (Baba *et al.*, 2006) and *E. coli* MC1061 pEGFP cells (Casadaban and Cohen, 1980) which expresses green fluorescent protein (GFP) were used as the representatives of Gram negative bacteria (plasmid kindly provided by Jörg Götz, University of Tübingen, Germany). *Staphylococcus epidermidis* FH30 strain was isolated from a case of chronic rhinosinusitis (Shields *et al.*, 2013) and used as the representative of Gram positive bacteria. Bacterial stock suspensions were kept at -80°C and the working cultures were obtained from single colonies on fresh agar plates prepared with the suitable growth media. For the *E. coli* BW25113 and *S. epidermidis* FH30 overnight cultures, 20 ml of previously autoclaved growth media were inoculated with a single colony from a fresh plate and shaken at 37°C, 180 rpm. Baffled Erlenmeyer flasks were chosen as suitable culture flasks which were useful to increase oxygenation of the media, complementing the growth. For the selection of *E. coli* MC1061 pEGFP containing GFP plasmid, 100 µg/mL ampicillin was included in the growth media. After 16 h, cells were in stationary phase ($OD_{600} \approx$ 1.7-1.8). The optical density (OD) measurements were taken using a spectrophotometer (Biochrom Libra 22 UV/Vis Spectrophotometer, Biochrom Libra Instruments, Cambridge, UK) which measures the absorbance of light at a particular wavelength (Sutton, 2006) in this case 600 nm which is indicated by OD_{600}. Total viable counts revealed that these cultures contained ~ 1.3×10^{11} cfu/ml.

3.2 Methods

This study involved various preparation and testing techniques. Methods for preparation of samples that were used throughout the experiments included encapsulation of bacterial cells in various hydrogels for mechanical tests.

The methods used to show bacteria viability after mechanical tests are also described in this section.

3.2.1 Bacteria growth on the hydrogel surface

For the first step of bacterial cell culturing on the surface of hydrogel experiments, *E. coli* cells were grown on 1% and 5% agar and agarose hydrogels. The bacterial strain used for the experiments was *E. coli* wild-type strain BW25113.

Agar plates were prepared with high salt LB medium. The gel solution was poured into petri dishes (60 mm x 15 mm) close to the Bunsen burner to minimise contamination. There should be no vaporisation in the poured plates for a better visualisation of the bacterial cells when they were plated. Also, avoiding vaporisation was important so that the bacterial cells were not affected by the water droplets when growing on the surface. Therefore, after the agar gel solidified, the plates were kept close to the Bunsen burner with the lids partially open until all the vapour on the lids disappeared.

Because the bacteria solution had a very high number of bacterial cells after reaching a certain OD value which was taken at the growth phase, they could not be counted unless dilution series were made. For this reason, dilution series from 10^{-1} to 10^{-8} were made and spread on the plates along with the spread of undiluted suspension. After keeping these plates in the 37°C incubator overnight, the number of colonies were counted (from the diluted spreads) and the CFU (colony forming unit) value of the main bacteria solution was calculated. For the calculation, at least three consecutive dilution series were used and the average of these three plates was taken to determine the number of the bacterial cells in the original solution.

3.2.2 Preparation of hydrogels and encapsulation of bacterial cells

For all the mechanical testing experiments, agarose hydrogels were prepared as described below. Based on the required concentration of the hydrogel, the corresponding amount by weight was added to the growth media or buffer and the mixture was placed in an autoclave. There were two advantages of using the autoclave for gel preparation: in the autoclave the

solution was heated up to 121°C at a high pressure (1.2 bar) so the agarose powder dissolved completely to form a homogeneous gel solution and after the autoclaving process the gel to be used was sterile which was important especially for the encapsulation process. The gels to be used for the encapsulation process were prepared the same way but before the addition of bacterial cells, the gel solution was cooled down to ~35°C. The sterile agarose gel or the encapsulation solution was injected into a 120×100×3 mm PMMA mould (Figure 3.1a), which was designed and manufactured to hold 8 individual cylindrical samples, and placed tightly on a glass slide having the same dimensions. During the injection process, bubbles on the surface must be avoided and the mould should not be overfilled to obtain flat and smooth surfaces and to maintain a uniform thickness of the samples. After the injected solution solidified completely (~30 min), the mould and the glass slide were separated and the gels were collected inside a sterile container filled with the corresponding liquid medium or buffer to avoid drying of the samples. The fabricated hydrogel is shown in Figure 3.1b. The schematic representation of the encapsulation process is given in Figure 3.2. The samples were kept in the liquid medium or buffer at 4°C for 3 h prior to any mechanical testing so that they could reach a fully hydrated state. The diameter of the fully hydrated hydrogel samples were 20 mm and the thickness of the hydrogels were 3 mm.

(a)   (b)
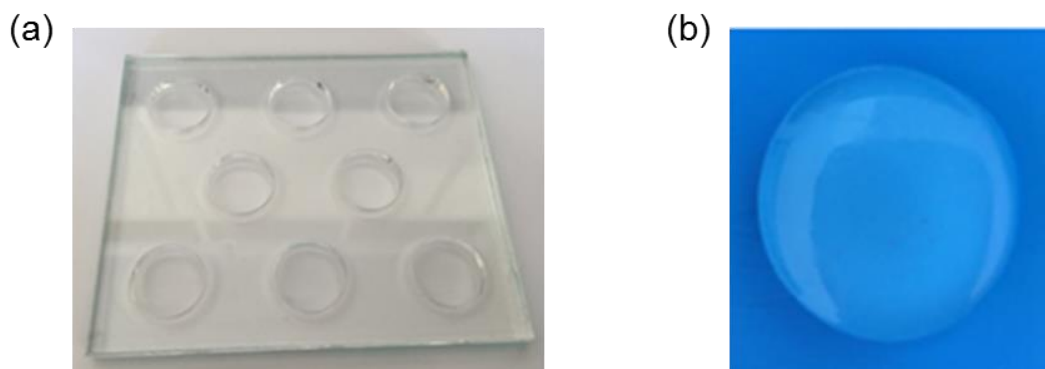
Figure 3.1 (a) PMMA mold used in fabrication of agarose hydrogels, (b) Agarose hydrogel fabricated using the PMMA mould having a diameter of 20 mm and a thickness of 3 mm
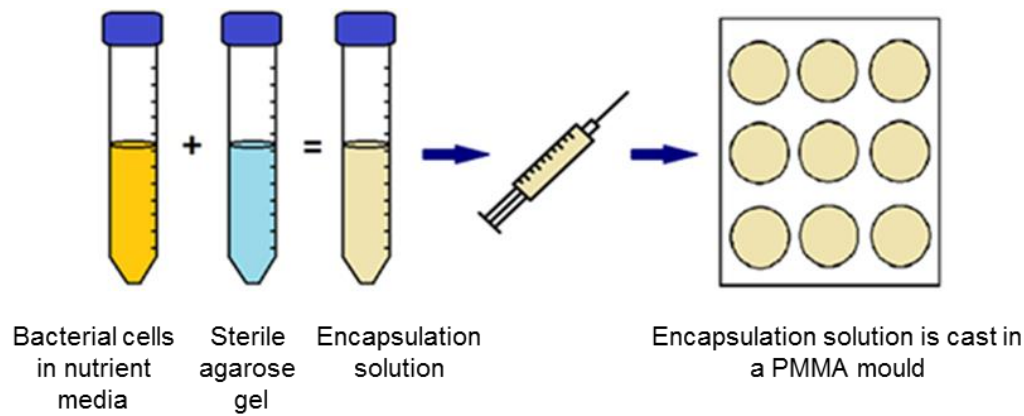
Figure 3.2. Schematic representation of encapsulation process of bacterial cells

3.2.3 Determining the melting temperature of agarose

From the material properties supplied from the manufacturer, melting point of the low gelling agarose type VII-A is specified as ≤ 65 °C for 1.5% gel. In the experiments, gel concentrations of 1%, 2%, 3%, 4% and 5% were intended to be used. This characterisation of the melting temperature was important for demonstrating the viability of the bacterial cells after they were encapsulated and also after various mechanical tests were applied on the samples. The melting points of different concentration hydrogels were determined using different techniques and different volumes of hydrogels. The reason for using different techniques was to determine the most suitable way to melt the hydrogels and the reason for using different volumes was to determine if the volume of the samples would make a difference in the melting behaviour. Based on the acquired melting temperatures, the appropriate concentration to be used in the mechanical tests was determined.

3.2.3.1 Determining the melting temperature using the PCR machine

In order to find the melting temperature of different percentage agarose gels, they were placed in small plastic tubes (100 µl) and placed in a PCR (polymerase chain reaction) machine (Applied Biosystems 2720 Thermal Cycler, Thermo Fisher Scientific, UK) for a temperature controlled experiment. The agarose gels (1%-8%) were prepared a day before so they were at room temperature and therefore completely solid at the beginning of the experiment. Because they were solid, the first experiment involved

raising the temperature. The temperature range was 30°C – 50°C, the heating rate was 1°C/sec and the temperature was held for 10 min for all tested temperatures. The higher temperature level of the range was selected as 50°C since it is the highest temperature the bacterial cells can tolerate. A second experiment was carried out by decreasing the temperature from 95°C for 100 µl samples where all percentage gels were liquid-like to the lower value of the target temperature range. During this experiment, the temperature was not decreased directly to the range to avoid sudden solidification.

3.2.3.2 Determining the melting temperature from stock solutions

Stock solutions of 5 ml for each percentage agarose were prepared in test tubes and they were autoclaved. When they were kept at room temperature, they completely solidified. In order to identify the melting point of the solutions, they were placed in a 1L beaker filled with water to the level of 800 mL which corresponded to a level above the gel volumes inside the tubes, working as a water bath for equal distribution of the temperature. The beaker was placed on a hot plate and a thermometer was placed in the beaker making sure that it was not touching the plate so it measured the temperature of the water bath. A glass plate was placed on the beaker to avoid evaporation allowing the water level within the beaker to stay constant. The initial temperature of the water bath was measured as 10°C for each trial and the observations regarding the gel phases were taken after the temperature of the water bath reached 30°C (similar to the melting temperature observations from PCR machine. The gel phase observations were recorded at a temperature range of 30°C – 50°C.

3.2.3.3 Determining the melting temperature using rheometer

The melting temperature of the agarose hydrogels was also determined using a rheometer (Kinexus pro+, Malvern Instruments, Malvern, UK). For this experiment, 1-3% agarose gels were used. A single frequency strain controlled temperature ramp test was used to determine the melting temperature. The test properties are summarised below.

Start Temperature (°C)   :   20
End Temperature (°C)   :   90
Ramp rate (°C/min)   :   5
Final Temperature (°C)   :   90
Frequency (Hz)   :   0.1
Shear Strain (%)   :   1
Sampling Interval (sec)   :   2

3.2.4 Encapsulated bacterial cells for viability check by plating technique

For the encapsulation of the bacterial cells in hydrogels experiments, 1-5% agarose gels were used. 10 ml of each concentration of agarose gel was prepared with LB medium using an autoclave for sterilisation. After the autoclave process, the hydrogel solutions were kept at 50°C in a water bath to avoid solidification before the encapsulation of bacteria and they were removed from the water bath just before the addition of 200 µl of overnight bacteria solution. After the addition of the bacterial cells inside agarose, they were vortexed to obtain a homogeneous solution. Each homogeneous solution was divided into 1 ml aliquots in test tube which were then left at room temperature to solidify.

At time 0, one of the tubes was heated to 37°C and 9 ml of LB medium was added to complete the solution to 10 ml. This diluted solution was placed in 50°C water bath for the agarose to completely melt. After the solution was completely liquid, a dilution series up to 10^{-8} were obtained and plated on LB agar plates. The time intervals were taken as 0 min (as soon as the first dilution series were obtained), 120 min and 240 min. A dilution series up to 10^{-10} for the overnight culture were also plated on the LB agar plates to calculate the bacterial cell density of the overnight culture. All the plated LB plates were kept at 37°C incubator room overnight for the colonies to grow for colony count.

To avoid pipetting errors, three agar plates were used for each time interval and an average value was used for colony forming units.

The results for the viability of encapsulated bacterial cells by plating technique are summarised in Appendix A.

3.2.5 Encapsulated bacterial cells for viability check by imaging

To check the cell viability, the hydrogels with encapsulated bacterial cells were imaged. For imaging, the encapsulated bacteria were stained with fluorescent dyes using the LIVE/DEAD® BacLight™ Bacterial Viability Kit (Thermo Fisher Scientific, Loughborough, UK). The used kit monitors the viability of bacteria based on their membrane integrity. Bacterial cells with a damaged membrane are considered dead or dying and they appear red under the microscope when imaged. On the other hand, bacterial cells with intact and undamaged membrane will stain green which indicates live.

The LIVE/DEAD BacLight Bacterial Viability Kits involve mixtures of SYTO® 9 which is the green fluorescent nucleic acid stain and propidium iodide which is the red fluorescent nucleic acid stain. These stains are different from each other in terms of their spectral characteristics and their ability to penetrate healthy bacterial cells. When the SYTO 9 stain is used alone, it generally labels all bacteria present regardless of the condition of the membrane, however, propidium iodide penetrates only bacteria with damaged membranes, causing a reduction in the SYTO 9 stain fluorescence when both dyes are present. Therefore, using the appropriate mixture of the two stains, bacteria with intact cell membranes stain fluorescent green, whereas bacteria with damaged membranes stain fluorescent red. The optimum excitation/emission for SYTO 9 stain and propidium iodide are 480/500 nm and 490/635 nm, respectively.

The mentioned dyes are sensitive to light, so the containers with hydrogels are wrapped completely with foil to avoid contact with light. After this step, the dyes were added to the containers of encapsulated hydrogels filled with 5 ml of PBS medium at the specified amounts at the kit (3 µl of the dye mixture for each ml) and mixed thoroughly. They were incubated at room temperature for 45 minutes in the dark (provided by the foil) and observed with a confocal microscope. This technique was to used image 1% agarose hydrogels with encapsulated *E. coli* BW25113 and *S. epidermidis* FH30 cells at 1% and 3% volume fraction.

The results for the viability of encapsulated bacterial cells by imaging are summarised in Appendix A.

4 Compression Responses of Agarose Gels and Bacterial Cell-Hydrogel Constructs

4.1 Introduction

Compression tests are widely used to determine the compressive mechanical properties for a very broad range of materials including metals and composites to soft biological tissues and hydrogels (Miller, 2005; Cloyd *et al.*, 2007; Oyen, 2014). These tests are commonly used due to wide accessibility, ease of use and a wide range of measuring capability based on the material being tested. Generally, compression tests are performed using a universal testing machine to determine the compressive strength of the material. Typically, a force vs displacement curve is obtained as a result of a compression test (which is then transferred into stress vs strain curve), where the tested specimen is deformed until failure while the applied force and the deformation of the material are being recorded (Boresi *et al.*, 1993). Using the same apparatus, time dependent mechanical behaviour of viscoelastic materials can be determined as well, including creep or stress relaxation behaviour. Either the applied stress is kept constant and the strain response is measured as a function of time (which indicates creep) or the applied strain is kept constant and the stress response is measured as a function of time (which indicates stress relaxation).

In this chapter, compression responses of agarose hydrogels will be characterised using Burger's model which can be applied for viscoelastic materials (details about this model are explained at Chapter 2, Section 2.7.5) and Hooke's law which represents the elastic response. Also, the effect of physical (*i.e.* stiffness) and chemical (*i.e.* chemical composition of the growth environment) factors on the mechanical interactions between bacterial cells and hydrogels, and bacteria cell mechanics when they are encapsulated in a 3D micro-environment will be explained.

4.2 Methods

4.2.1 Sample preparation

The bacterial strains used for compression tests were *E. coli* BW25113 and *S. epidermidis* FH30 and they were grown as explained in Section 3.1.3. Agarose hydrogels at different concentrations were prepared and

autoclaved at 121ºC, 1.2 bar and cooled to ~ 35ºC. The volume of cells was estimated to occupy approximately 1% of the total volume of hydrogel. This was done by centrifuging the overnight culture of both bacterial cells at 4,000 rpm for 10 min at 10ºC to obtain a cell pellet. For instance, if the total volume of the hydrogel to be used for encapsulation was 15 ml, the overall bacteria pellet volume after centrifugation was 0.15 ml to provide an aimed volume fraction of 1%. After centrifugation, the supernatant was removed completely and the bacterial cells were suspended in 50 µl of the same growth medium or buffer as used for the hydrogel. The bacterial cell pellet was added to the sterile hydrogel solution and mixed until the encapsulation solution was homogenous. While preparing the sterile agarose hydrogels to be used for encapsulation, the addition of the cell pellet and the 50 µl of liquid medium/buffer were also taken into account so that the overall hydrogel concentration was kept at 1%. The hydrogels to be tested and the encapsulation process were prepared as explained in Section 3.2.2.

4.2.2 Compression tests with stress relaxation

Compression tests with stress relaxation were carried out at room temperature using the EZ test machine (EZ-SX, Shimadzu, Japan, shown in Figure 4.1) to determine the mechanical properties of hydrogels with and without encapsulation. They were applied to agarose hydrogels made with LB, LB-no yeast extract, LB-no tryptone, NB and PBS at various concentrations. The hydrogels were kept in the corresponding liquid media or the buffer prior to testing for 3 hours to obtain full hydration. In the tests, 0.5%, 2% and 5% strain values were used. These values were chosen since they were small strain values (*i.e.* the test samples were not harmed macroscopically after the compression tests) and there was a 10-fold difference between the lowest and the highest strain value which enabled a broad response range. In these tests, the strain value was fixed at a certain value (*i.e.* 0.5%, 2% and 5%) and the changing force values in time were recorded. A 0.05 N of pre-load was applied to the samples to determine the surface and to make sure that the stress relaxation test starts when the circular plate connected to the load cell was in contact with the hydrogel surface completely. The displacement rate for all tested strains was 0.01 mm/s. For different materials tested, at least 5 trials were carried out for

each measurement. For the measurements with bacterial cells, different sets of samples were prepared and tested as 3 independent experiments.

For the accuracy of the applied strain and the measurement of the force response, a 20 N load cell was used which is very sensitive and can measure very small changes.

Figure 4.1. Stress relaxation test setup

Since hydrogels are viscoelastic materials, they can take their original shapes in time after the strain is removed, given that the applied strain is within the linear viscoelastic region (LVER). To avoid any plastic deformation of the hydrogel samples which can change their structure and therefore the interaction between the bacterial cells and the agarose hydrogel, the specified fixed strain values were held on the hydrogel samples for 30 mins and the force values to keep the strain were recorded over the test time where the samples showed relaxation behaviour.

4.2.3 Finding the mechanical properties of hydrogels without encapsulation

For stress relaxation tests, the Burger's model (Equations 32-34 in Section 2.7.5), which consists of a Maxwell element (a linear spring and a linear viscous dashpot connected in series) and a Kelvin-Voigt element (a linear spring and a linear viscous dashpot connected in parallel), was applied to

determine instantaneous Young's moduli of the hydrogel samples made with different growth media or buffer ($E_{gel.0}$). The area and the strain employed in the model were taken as true area and true strain. For stress relaxation, the true strain was calculated as $\varepsilon_T = -\ln(1 - \varepsilon)$, where ε_T is the true strain and ε is the applied strain. True area was calculated based on the applied strain.

In addition to Burger's model, Hooke's law (*i.e.* $\sigma = E\varepsilon$) was also applied to the loading curve to calculate instantaneous Young's moduli of the hydrogel samples made with different growth media or buffer ($E_{gel.0}$). To calculate $E_{gel.0}$, true strain and true area values were used. For gels with encapsulation, the instantaneous Young's moduli values were normalised by dividing the $E_{gel.0}$ value by the corresponding gel made with the same media but without encapsulation. The relationship between the stiffness of hydrogels with and without encapsulation were obtained by using the following equation.

$$E_{construct,0} = \frac{F_{construct}}{F_{gel}} E_{gel,0} \qquad (50)$$

4.2.4 Imaging the Structure of Hydrogels

4.2.4.1 Sample preparation prior to imaging

To image the structure of the hydrogels, Tescan Vega 3LMU scanning electron microscopy (SEM) fitted with a Bruker XFlash® 6 | 30 detector (Tescan-UK, Cambridge, UK) was used. Prior to imaging with SEM, the water content of the hydrogel samples needed to be dehydrated without inducing structure collapse. For this reason, a Leica Automated Critical Point Drier (CPD) EM CPD300 (Leica Microsystems, Milton Keynes, UK) was used to dry the hydrogels.

Supercritical drying is a process to remove liquid from hydrated samples in a controlled way (Tsotsas and Mujumdar, 2011). In order to assure the most ideal preservation of the surface topography of tissues, specimens should be completely dry before placing into the vacuum chamber of the scanning electron microscope.

When a pure liquid and its vapour are heated in a closed pressure chamber, the surface tension becomes zero at their interface at the critical temperature (T_C is indicated in Figure 4.2) since only gaseous phase can exist at high temperatures. For the case of biological samples which consist of water and a non-volatile material (such as agarose), when the temperature of the chamber is increased above the T_C of water, the liquid water would be replaced by its gaseous form. Since water has a high T_C of 647 K, direct CPD of the biological sample is not possible. Therefore, the water phase is firstly replaced by liquid CO_2 which is an inert liquid having a T_C of 304.25 K. However, liquid CO_2 is not completely miscible with water which can create a liquid – liquid interface which should be prevented. Therefore, the an intermediate liquid such as ethanol which is miscible with both water and liquid CO_2 should be used. So in CPD, first of all ethanol is replaced by liquid CO_2 in the pressure chamber, the temperature is increased above the T_C of CO_2 and the gaseous CO_2 is let out isothermally resulting in the pressure of the chamber to fall back to atmospheric pressure. After several cycles of this procedure, the biological samples would be critical point dried. (Hall *et al.*, 1978; Bray, 2000)
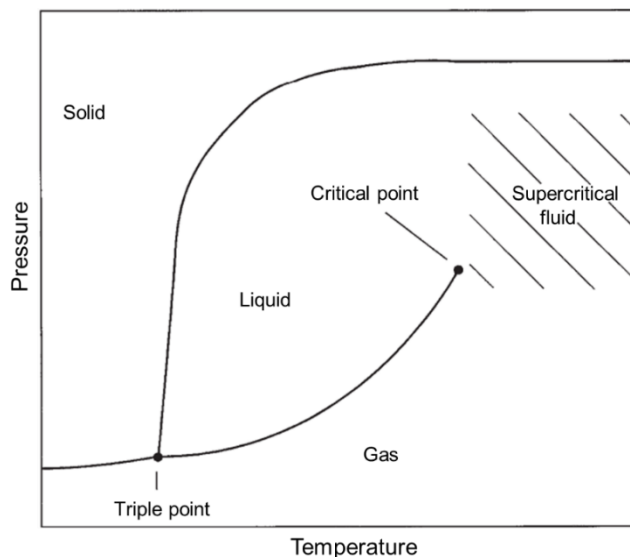
Figure 4.2. Phase diagram of a substance (Bray, 2000)

There were several steps to follow before the samples were critical point dried. These steps included fixation of bacterial cells and dehydration of the hydrogel sample. For fixing the bacterial cells, the samples were left in 2% glutaraldehyde in Sorenson's phosphate buffer overnight. After this step,

the samples were rinsed in Sorenson's phosphate buffer for 15 minutes and the rinsing step was repeated twice. Since the SEM imaging was done to hydrogels without encapsulation, the fixation step was omitted. At the dehydration step, the samples were subjected to ethanol series for different time intervals. The samples were kept at 25%, 50% and 75% ethanol respectively at each concentration of ethanol for 30 minutes followed by keeping them in 100% ethanol for one hour, which was repeated twice. After dehydrating the hydrogel samples, they were transferred to the chamber of the critical point drier which was then completely filled with 100% ethanol. The hydrogels were then critical point dried by fully automated Leica EM CPD300 Critical Point Dryer where the complete drying process took approximately 200 min. The cycles were carried out at their slowest setting to protect the hydrogel structure. The comparison of a hydrated and a critical point dried hydrogel is shown in Figure 4.3.

Figure 4.3. A hydrated (left) and a critical point dried hydrogel (right)

4.2.4.2 Scanning electron microscopy (SEM)

A SEM is a type of electron microscope presenting the sample surfaces with a focused electron beam where the electrons are accelerated through a voltage difference between cathode and anode (Reimer, 1998). The electron current deflected due to the object are collected by the electron detectors and amplified, which then creates the picture of the scanned surface on the cathode ray tube (Smith and Oatley, 1955).

After the hydrogels were critical point dried, based on the type of the SEM, they may need a coating which can be gold or platinum. For the SEM used in this study (Tescan Vega 3LMU), the hydrogels samples were coated in gold and images were taken at 50,000x at HV (high vacuum) of 15kV. The imaged hydrogels were 1% agarose hydrogels made with LB, PBS and NB.

4.2.5 Statistical analysis

Analysis of Variance (ANOVA) with Tukey's post hoc test was applied to determine the statistical differences between hydrogels with and without encapsulation and of gels made with different growth media or buffer for the data acquired from the compression tests with stress relaxation. The significance level (α) was taken as 0.05. The statistical analysis was carried out using Minitab 17.1.0.

4.3   Results and Discussion

4.3.1 Stiffness of 1% agarose hydrogels without encapsulation at various strain values

Agarose hydrogels were chosen as the matrix material due to their biocompatibility, inertness, gelling behaviour and the large content of water which favours bacterial cell hydration. In addition, previous work has demonstrated that agarose as a matrix polysaccharide was appropriate to simulate the extracellular polymeric matrix (Strathmann *et al.*, 2000). The stiffness of 1% agarose gels made with phosphate buffered saline (PBS), bacterial culture media (Luria-Bertani Broth (LB)) or distilled water has been reported in several studies (Normand *et al.*, 2000; Ahearne *et al.*, 2005; Tuson *et al.*, 2012a; Guegan *et al.*, 2014). These values were obtained from different mechanical tests, including simple tensile or compression tests, rheological characterisation or atomic force microscopy (AFM), and the range of the reported values varied between 14 kPa – 60 kPa. In addition to different constituents used and the various testing techniques, mechanical properties of agarose hydrogels also depended on the preparation protocols (Normand *et al.*, 2000).

The stress relaxation curves for gels without bacterial cells are given in Figure 4.4. Based on the results, PBS gels were the stiffest for all tested strains. As can be seen from the force-time curves, the hydrogels did not show the same relaxation behaviour when different strain values were applied. At 0.5% strain, the hydrogels did not reach a complete equilibrium however when the applied strain was increased from 0.5% to 5%, the hydrogels showed a more clear relaxation behaviour after 30 min. To avoid differences between the various responses of relaxation behaviour, the elastic response (*i.e.* instantaneous response) of the hydrogels were taken

into account. This corresponds to the initial force value applied on the gel to reach the specified strain, *i.e.* the maximum force value applied on the hydrogel. The statistical differences between hydrogels made with different growth media or buffer are summarised in Table 4.1. The comparisons were made based on the maximum force applied on the hydrogels to reach the strain value for the first time.
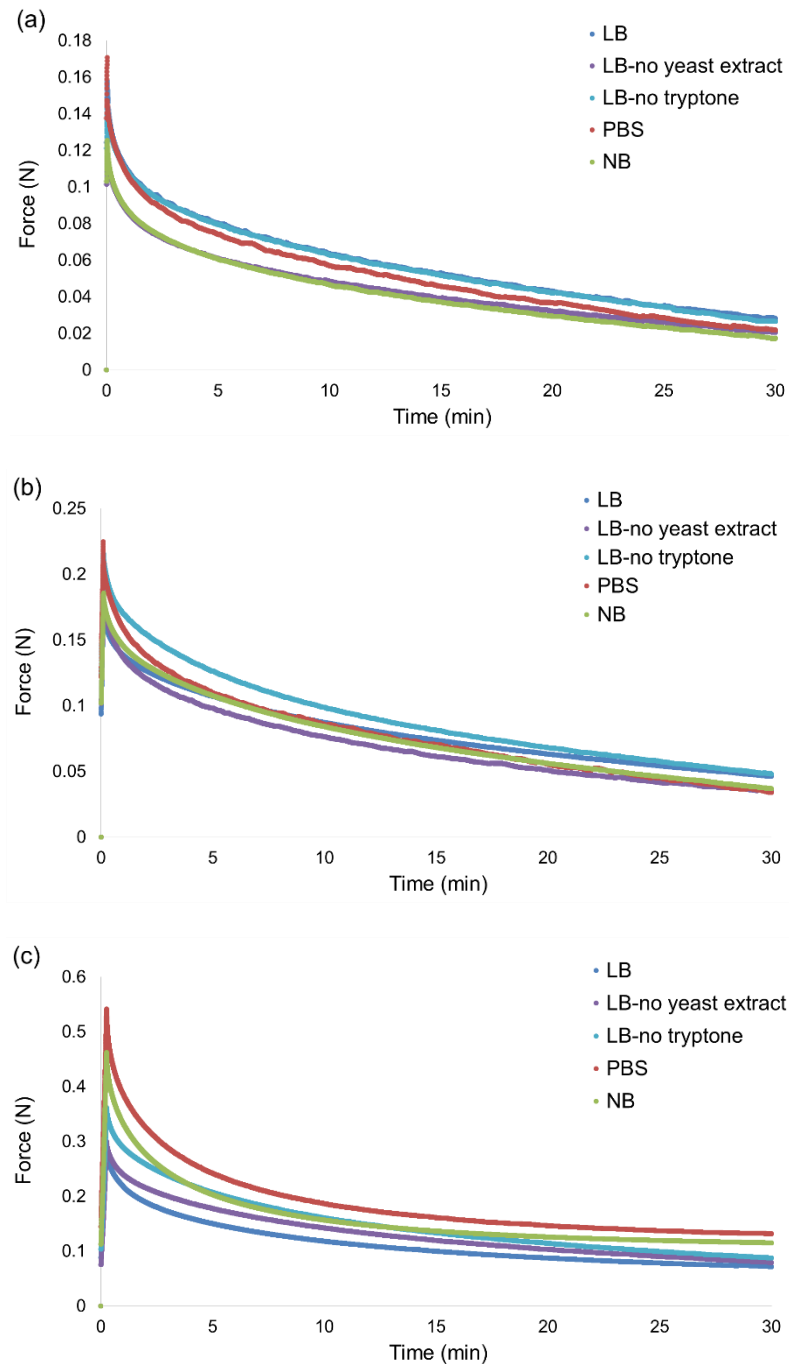
Figure 4.4. Force-time curves for hydrogels without encapsulation at (a) 0.5% strain, (b) 2% strain and (c) 5% strain. The plotted force curves represent the average force curves value from all tested samples and error bars were removed for better visualisation

	PBS	NB	LB-no yeast extract	LB-no tryptone
0.5% strain				
LB	0.032 (*)	0.251	0.554	0.007 (**)
PBS		0.044 (*)	0.041 (*)	0.548
NB			0.597	0.006 (**)
LB-no yeast extract				0.008 (**)
2% strain				
LB	0.040 (*)	0.723	0.900	0.059
PBS		0.219	0.019 (*)	0.698
NB			0.530	0.118
LB-no yeast extract				0.005 (**)
5% strain				
LB	0.002 (**)	0.011 (*)	0.703	0.012 (*)
PBS		0.275	0.001 (**)	0.004 (**)
NB			0.007 (**)	0.052
LB-no yeast extract				0.009 (**)

Table 4.1. *p* values obtained from Tukey's post hoc test for hydrogels without encapsulation. Here (*) indicates $p < 0.05$ and (**) indicates $p < 0.01$. The comparisons were made based on the maximum force applied on the hydrogels to reach the strain value

The curves shown in Figure 4.4 consisted of two parts: loading period and relaxation period. Due to a fast loading rate, the gels were considered to stay in elastic region and therefore the measured force values to change linearly with time. To show the linear trend in loading, the curves were studied in two parts as well. The loading curves for all tested hydrogels without encapsulation at 0.5%, 2% and 5% strain values were shown in Figure 4.5. For all gels, a linear line was fitted and the R^2 values for the fits were determined which showed $R^2 = 0.99$ at all tested strain values.
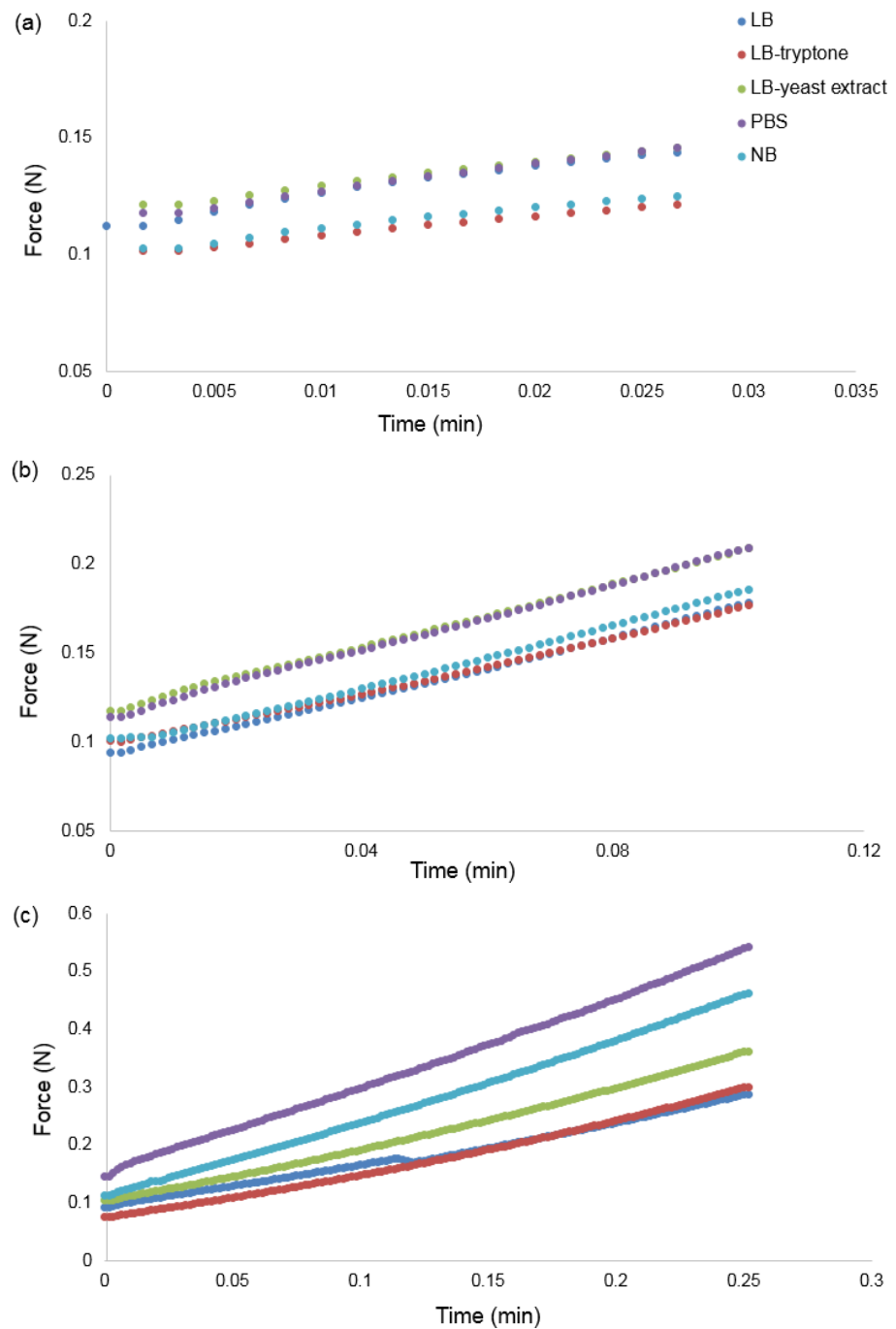
Figure 4.5. Loading curves of hydrogels without encapsulation at (a) 0.5% strain, (b) 2% strain and (c) 5% strain. The plotted force curves represent the change in average force with time to reach the specific strain value. Error bars were removed for better visualisation

It has been shown that hydrogels with different types of cross-linking (either ionic or covalent) show different relaxation behaviour which can affect the relaxation time (Zhao *et al.*, 2010). For certain types of agarose hydrogels tested at 25°C, the relaxation time can be up to 4 hours (Watase and Arakawa, 1968; Watase and Nishinari, 1980). Other studies have shown that the relaxation time can be between ~10 min - 45 min (Fitzgerald *et al.*,

2015; Chaudhuri *et al.*, 2016). In this work, the relaxation time was kept at 30 min. This choice of relaxation time reduced the variability between the samples. Also, for the materials exhibiting linear viscoelastic behaviour at given test protocol, it was not necessary to wait for the materials to be completely relaxed to determine the viscoelastic properties.

Measuring the stiffness of hydrogels infused with different growth media or buffer without bacterial encapsulation provided the basis of the measurements as the stiffness values measured were compared to the stiffness of gels with encapsulation. The hydrogels, that are viscoelastic substrates exhibiting stress relaxation (Chaudhuri *et al.*, 2015), were firstly modelled using Burger's model which represents a quantitative model of polymeric material behaviour (Malkin and Isayev, 2017). As an example, Burger's model fit for 1% LB gels when the applied strain was 0.5% is presented in Figure 4.6 and the Burger's model fit for the other gels are presented in Appendix B. The curve fitting was carried out using MATLAB function `lsqcurvefit` to the relaxation curves. From the Burger's model fit, instantaneous Young's moduli of 1% agarose hydrogels without encapsulation were obtained (Table 4.2). These Young's modulus values were determined based on the best fit of the model on the force data from the relaxation part after the samples were compressed to the specified strain and only instantaneous elasticity was considered. The element of Burger's model responsible for the initial elastic response is the spring of the Maxwell element (see Figure 2.26). Therefore, this spring coefficient obtained from the model fit was used as the instantaneous stiffness of the hydrogel. For all tested strains, 1% agarose gels made with PBS were substantially stiffer than the gels made with growth media, suggesting that the medium used to form the hydrogel affects the stiffness of the gel. When the stiffness of the gels made with buffer and culture media (*i.e.* LB and NB) were compared at 0.5% strain, PBS gels were stiffest, followed by gels made with LB and then those made with NB. These were all stiffer than gels made with NB at 2% and 5% strains, which in turn were stiffer than gels made with LB at these strains. For all applied strains, PBS gels were significantly stiffer than LB gels ($p < 0.05$ for 0.5% and 2% applied strain and $p < 0.01$ for 5% applied strain). Also at 0.5% applied strain, PBS gels

were significantly stiffer than NB gels ($p < 0.05$) but there were no significant differences observed between PBS and NB gels when the strain was increased to 2% and 5%. At lower strains (0.5% and 2%), there were no statistically significant differences between the stiffness of gels made with LB or NB. By contrast, at 5% strain, gels containing NB were significantly stiffer than those containing LB ($p < 0.01$).
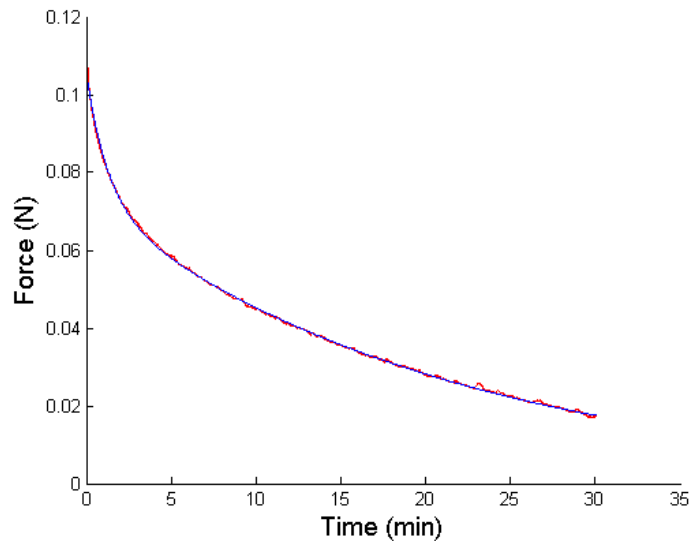
Figure 4.6. Burger's model fit for 1% LB hydrogels without encapsulation when the applied strain was 0.5%

Applied strain (%)	Buffer or media	$E_{gel.0}$ (kPa)
0.5	PBS	88.3 ± 11.4
	NB	71.4 ± 6.6
	LB	80.8 ± 10.2
	LB-no yeast extract	71.2 ± 6.7
	LB-no tryptone	85.7 ± 9.0
2	PBS	31.5 ± 3.7
	NB	26.9 ± 3.8
	LB	25.2 ± 4.1
	LB-no yeast extract	26.5 ± 2.6
	LB-no tryptone	30.7 ± 2.9
5	PBS	28.5 ± 5.5
	NB	24.7 ± 5.5
	LB	15.7 ± 2.4
	LB-no yeast extract	16.5 ± 2.1
	LB-no tryptone	19.8 ± 1.6

Table 4.2. Instantaneous Young's moduli of 1% agarose hydrogels without encapsulation obtained from Burger's model (Data represented as mean ± standard deviation, $n \geq 5$)

A strain dependent behaviour of stiffness was observed for the tested hydrogels (see Table 4.2). For instance, the apparent stiffness of LB gels decreased with the increasing applied strain, *i.e.* the stiffness of the gel was obtained as 80.8 kPa, 25.5 kPa and 15.7 kPa when the applied strain was increased from 0.5% to 2% and 5% respectively. As reported previously (Moran and Knauss, 1992; Van Breemen *et al.*, 2012; Rose *et al.*, 2013), several polymers have shown strain softening effect similar to the classical model of rubber elasticity, where the apparent stiffness of the material decreases with the increasing applied strain (where area indicated with I represents the immediate elastic response, the area indicated with II shows strain softening behaviour and area indicated with III shows strain stiffening behaviour, as shown in Figure 4.7). At the tested strain range, 1% agarose hydrogels presented strain softening behaviour. As shown previously, if the applied strain was increased further ($> 10\%$), the behaviour changed to strain stiffening behaviour due to the material not being in the linear regime (Moreno-Arotzena *et al.*, 2015).
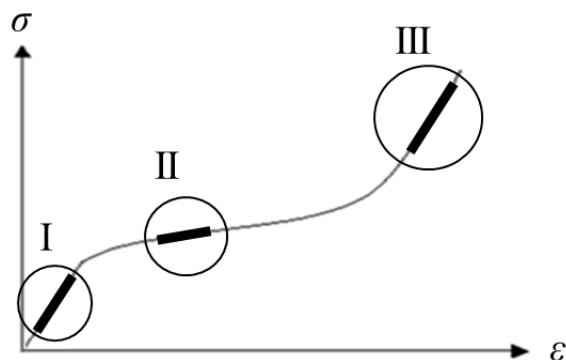
Figure 4.7. Strain dependent effect showing strain softening and stiffening behaviour

Usually, relaxation behaviour can be captured by different viscoelastic models (Chen *et al.*, 2012; Shapiro and Oyen, 2014). The viscoelastic models (e.g. Prony series model and Burger's model) were adopted for curve fitting, however, they failed to accurately capture the relaxation curves in this study. They only predicted the equilibrium modulus well. Although there are other more complicated models available (Chen, 2014a), it makes the data interpretation challenging. When the loading time is much shorter compared to the relaxation characteristic time constant, the Hooke's law was a reasonable approximation at the given strains in this study. In such

case, the instantaneous Young's modulus can be obtained either from the loading curve or the relaxation curve which should give similar results given the assumptions. The stiffness values of 1% hydrogels without encapsulation were also calculated by Hooke's law and instantaneous Young's moduli values were obtained (Table 4.3). These Young's modulus values were determined based on maximum force applied when the hydrogels were compressed to the specified strain and instantaneous elasticity was considered. For all tested strains, 1% agarose gels made with PBS were substantially stiffer than the gels made with growth media, suggesting that the medium used to form the hydrogel affects the stiffness of the gel. When the stiffness of the gels made with buffer and culture media (*i.e.* LB and NB) were compared, PBS gels were stiffest, followed by gels made with NB and then those made with LB. For all applied strains, PBS gels were significantly stiffer than LB gels ($p < 0.05$ for 0.5% and 2% applied strain and $p < 0.01$ for 5% applied strain) but there were no significant differences observed between PBS and NB gels. At lower strains (0.5% and 2%), there were no statistically significant differences between the stiffness of gels made with LB or NB. By contrast, at 5% strain, gels containing NB were significantly stiffer than those containing LB ($p < 0.01$).

Applied strain (%)	Buffer or media	$E_{gel.0}$ (kPa)
0.5	PBS	89.9 ± 9.2
	NB	79.8 ± 7.3
	LB	74.2 ± 11.0
	LB-no yeast extract	77.6 ± 7.8
	LB-no tryptone	88.8 ± 4.5
2	PBS	32.3 ± 3.9
	NB	28.7 ± 4.8
	LB	24.8 ± 2.0
	LB-no yeast extract	27.6 ± 2.0
	LB-no tryptone	31.7 ± 2.7
5	PBS	31.9 ± 6.5
	NB	27.2 ± 6.2
	LB	17.1 ± 2.9
	LB-no yeast extract	16.9 ± 1.2
	LB-no tryptone	21.3 ± 1.6

Table 4.3. Instantaneous Young's moduli of 1% agarose hydrogels without encapsulation obtained from Hooke's law

As expected, a strain dependent behaviour of stiffness was observed for the tested hydrogels similar to the behaviour obtained from Burger's model. For instance, the apparent stiffness of LB gels decreased with the increasing applied strain, *i.e.* the stiffness of the gel was obtained as 74.2 kPa, 24.8 kPa and 17.1 kPa when the applied strain was increased from 0.5% to 2% and 5% respectively. When PBS, NB and LB gels were considered separately (e.g. stiffness values of PBS gels at strains 0.5%, 2% and 5%), there was a significant decrease ($p < 0.01$) in stiffness values when the applied strain was changed from 0.5% to 2%, however there were no significant differences ($p > 0.05$) when the stiffness values obtained for 2% and 5% strains were compared. For all the hydrogels characterised here, the stiffness drop from 0.5 to 5% could be due to the collapse of the porous structure of the hydrogels, as observed in many other porous materials (Lu *et al.*, 2008; Shen *et al.*, 2008; Wu *et al.*, 2014).

4.3.2 Stiffness of 1% hydrogels with encapsulated bacterial cells at various strain values

Having measured the stiffness of hydrogels alone, the next step was to assess whether the encapsulation of bacteria in the gels led to any measurable changes in the stiffness. Therefore, *E. coli* or *S. epidermidis* were encapsulated at a concentration equivalent to 1% of the total hydrogel volume. The stiffness values of the gels with encapsulated bacterial cells were characterised and the obtained stiffness values were normalised by the corresponding gel without encapsulation. The stiffness values of gels with encapsulated bacterial cells are given in Table 4.4. 1% LB gels with encapsulated *E. coli* and *S. epidermidis* cells were stiffer than 1% LB gels without bacteria. Interestingly, for the 1% gels made with PBS and NB, such an increase in stiffness was not observed and they showed similar stiffness values as the gels without bacteria (Fig. 4.8 a-c). The significantly higher stiffness of LB gels with encapsulated bacteria compared with LB gels without bacteria could be attributed to the interactions between the bacterial cells and the media used to prepare the hydrogel.

Applied strain (%)	Buffer or media	$E_{gel.0}$ (kPa) (*E. coli* encapsulation)	$E_{gel.0}$ (kPa) (*S. epidermidis* encapsulation)
0.5	PBS	81.0 ± 8.5	95.3 ± 8.4
	NB	74.6 ± 3.6	79.3 ± 10.2
	LB	91.2 ± 10.8	105.1 ± 11.6
	LB-no yeast extract	95.8 ± 9.4	95.0 ± 7.9
	LB-no tryptone	83.5 ± 3.6	89.7 ± 6.7
2	PBS	31.2 ± 2.4	30.4 ± 2.1
	NB	32.4 ± 3.6	30.8 ± 1.1
	LB	30.3 ± 2.7	30.6 ± 2.5
	LB-no yeast extract	34.6 ± 1.6	32.9 ± 3.2
	LB-no tryptone	30.8 ± 3.5	28.7 ± 2.2
5	PBS	28.6 ± 5.0	28.6 ± 2.5
	NB	29.6 ± 3.6	23.7 ± 2.6
	LB	31.7 ± 4.6	34.8 ± 4.3
	LB-no yeast extract	24.9 ± 2.5	25.5 ± 1.8
	LB-no tryptone	23.0 ± 1.7	22.5 ± 1.7

Table 4.4. Instantaneous Young's moduli of 1% agarose hydrogels with encapsulation obtained from Hooke's law (Data represented as mean ± standard deviation, $n \geq 5$ for each independent experiment ($n_{ie} = 3$))

To investigate this further, experiments were performed to determine which constituent of LB medium, tryptone or yeast extract, was causing this increase in stiffness. Different media were prepared in which either constituent was omitted, for LB-no yeast extract gels yeast extract was omitted and for LB-no tryptone gels tryptone was omitted. The salt content was not changed since NaCl was present also in NB and PBS, and therefore could not be solely responsible for the observed differences in hydrogel stiffness between agarose formulations. The stiffness of these gels with and without bacteria was calculated and normalised. Only LB-no yeast extract gels with bacteria showed significant increases in normalised stiffness when bacterial cells were encapsulated. This discrepancy could indicate that the change in stiffness observed in the LB-no yeast extract gels could be due to a change in bacterial surface properties affecting the interactions with the peptides present in tryptone (Fig. 4.8 a-c). Both types of bacterial cells (*E. coli* – rod shaped and *S. epidermidis* – spherical shaped) behaved in a similar pattern suggesting that different bacteria interact similarly with the media and the applied mechanical stimuli.
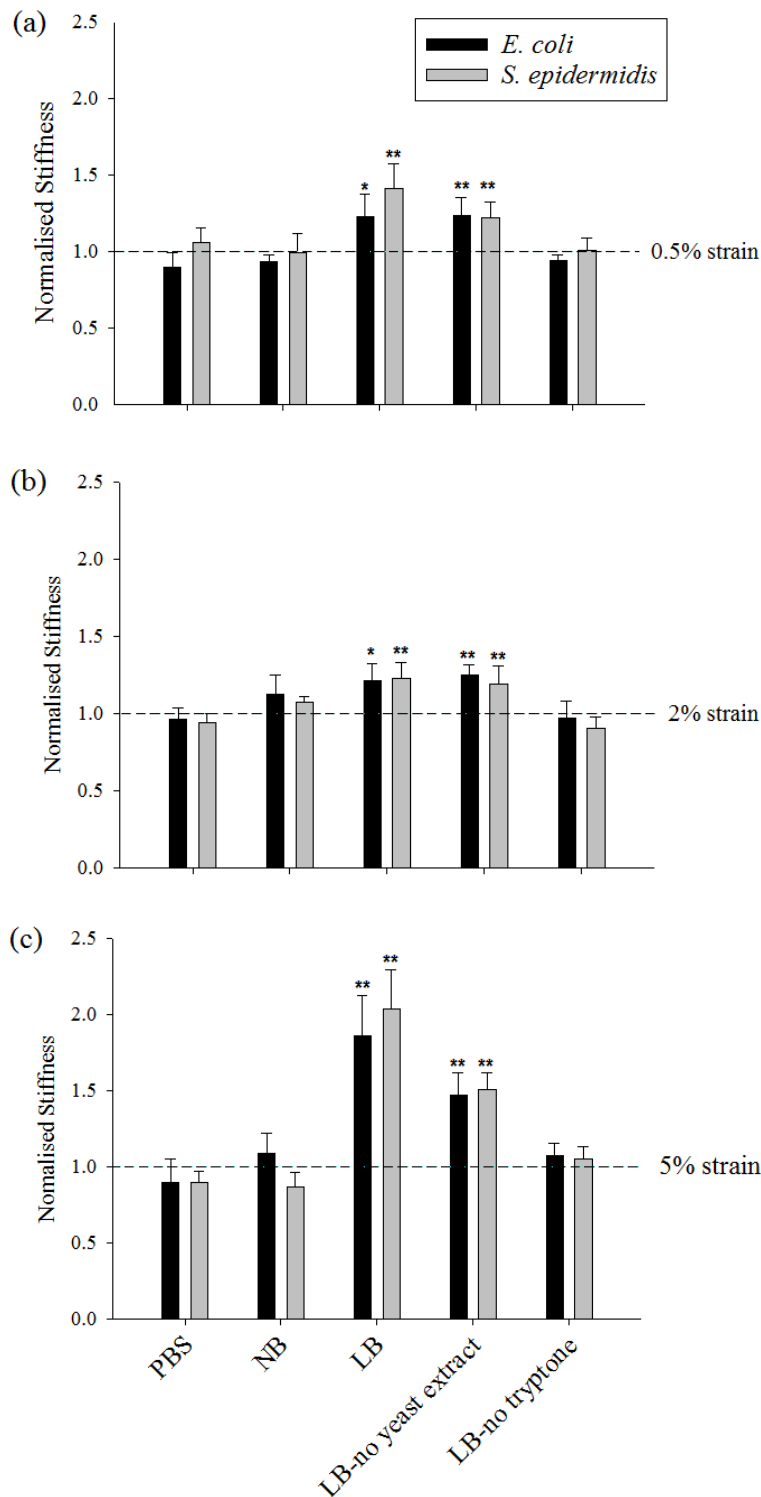
Figure 4.8. Normalised stiffness values of different LB-based, PBS and NB hydrogels, when (a) 0.5% strain, (b) 2% strain and (c) 5% strain were applied (the bars represent the gels with bacteria, the dashed line shows the normalised value for gels without encapsulation and error bars represent standard deviation). This normalisation represents the fold change in the stiffness in hydrogels containing encapsulated cells compared with those without cells. The symbols on plots * and ** indicate $p \leq 0.05$ and $p \leq 0.01$ respectively between the gels made with the same liquid media/buffer with and without encapsulation of bacterial cells, determined from 3 independent experiments

The effect of LB medium was further investigated by using the supernatant of the overnight culture where *E. coli* BW25113 cells were grown. To prepare the hydrogels, the overnight culture was centrifuged at 4,000 rpm for 10 min at 10ºC and 1% agarose hydrogels were made using the resulting supernatant LB, using the same procedures explained in Chapter 3. Since the supernatant of the overnight culture was used, the amount and/or type of nutrients within the resulting liquid medium was less compared to the freshly prepared LB medium. It is possibly because the bacterial cells use those nutrients to grow and reach the stationary phase. *E. coli* BW25113 cells were encapsulated in the hydrogels as explained in Chapter 3 and the compression tests with stress relaxation were applied using the same techniques described previously.

The stiffness of the 1% agarose hydrogels made with the supernatant without encapsulation was found as 86.6 ± 11.1 kPa from Burger's model and 92.4 ± 11.8 kPa from Hooke's law. When the stiffness values of LB supernatant gels were compared to the stiffness of the hydrogels made with fresh LB medium which were obtained from Burger's model, no statistically significant differences were observed ($p = 0.45$) and for the results obtained from Hooke's law a borderline statistical difference was observed between these gels ($p = 0.040$). From the previous tests, it was determined that both *E. coli* BW25113 and *S. epidermidis* FH30 cells had similar effect on the overall stiffness difference, therefore the experiments involving supernatant LB were only carried out for *E coli* BW25113 cells.

The Young's modulus of the construct (hydrogel and bacterial cell) was normalised by the Young's modulus of the gel and the results are presented in Figure 4.9. For comparison, LB gels and LB supernatant gels with encapsulated bacterial cells were presented together.
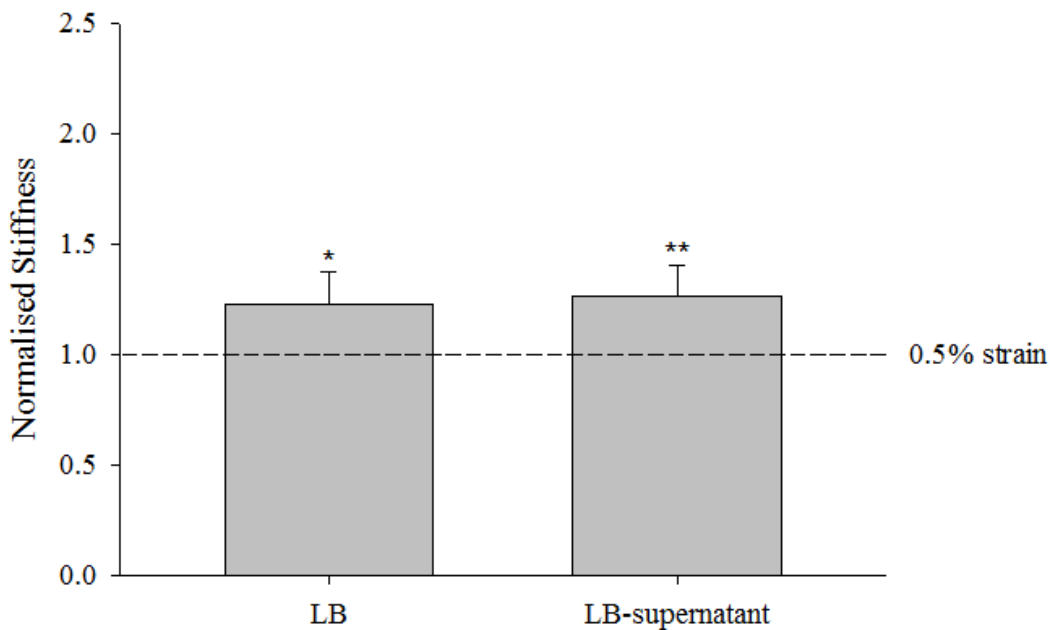
Figure 4.9. Normalised stiffness values of different LB-based, hydrogels, when 0.5% strain, was applied (the bars represent the gels with *E. coli* cells, the dashed line shows the normalised value for gels without encapsulation and error bars represent standard deviation). The symbols on plots * and ** indicate $p \leq 0.05$ and $p \leq 0.01$ respectively between the gels made with the same liquid media with and without encapsulation of bacterial cells, determined from 3 independent experiments

The results from the experiments involving supernatant LB revealed that both fresh LB and supernatant LB gels with encapsulation were significantly different than the gels without bacterial cells. The statistical difference for fresh LB gels was $p = 0.013$ and the statistical difference for supernatant LB gels was $p = 0.010$. This statistical difference was only a border-line difference so they were considered as similar cases. Another reason for considering these results as similar was, the content of supernatant LB was not as defined as the fresh LB media or the other LB-based media that were prepared in the study (*i.e.* LB-no yeast extract which contained tryptone and NaCl only and LB-no tryptone which contained yeast extract and NaCl only). Within the used media, a part of both of the ingredients could still be present however the overall amount was obscure and could change from culture to culture. Therefore, to avoid further variability, these experiments were not repeated for higher strain values (2% and 5%).

Previous studies have shown that, bacterial cells can adhere to soft surfaces more easily than to harder surfaces (Saha *et al.*, 2013; Song and Ren, 2014). This is in agreement with our observations showing that

bacterial cells interact differently with the 1% LB and LB-no yeast extract hydrogels, which were softer than the other hydrogels tested before encapsulation. Previously, it has been shown that mechanical properties of agarose gels were affected by the presence and amount of sugars (such as glucose and sucrose), urea and guanidine hydrochloride (Watase *et al.*, 1990; Deszczynski *et al.*, 2003). Although the peptide-based tryptone has an unclear chemical composition, the different peptides within tryptone could be affecting agarose gel mechanical properties in a similar manner.

It is likely that the pores of the agarose polymer and the bacterial cells interact causing the pores to be compressed and change the structure of the hydrogel (Fig. 4.10a), resulting in differences in the overall stiffness. A significant increase in hydrogel stiffness is usually caused by chemically induced cross-linkers of polymer chains that form the hydrogel network (Miyoshi *et al.*, 1996). The particle reinforced hydrogels were also observed elsewhere. For example, it was observed that bioactive glass particles can increase the stiffness of the polysaccharide gellan gum hydrogel by ~ 100 times at 2% concentration of particles (Gasik *et al.*, 2017). Such a huge stiffening effect cannot be accounted by composite theory but crosslinking the loose polymer chains by the particles. In this study, a similar principle may apply where bacterial cells crosslink the loose polymer chains. Also, it has also been demonstrated that the stiffness of material can affect the biological activities of bacterial cells when these cells are seeded on the material surface (Saha *et al.*, 2013; Song *et al.*, 2017) and such an effect can take place when bacterial cells are encapsulated inside hydrogels as well. It can also be speculated that, this behaviour might be due to changes in the structure of the gel caused by molecules secreted by cells. These molecules combined with the bacterial cells potentially could cause differences in stiffness when interacting with different media, as illustrated in Figure 4.10b-4.10d.

(a)

agarose polymer chain   molecule secreted by bacterial cells

bacterial cell

(b)   (c)   (d)

Stiffness gradient

1) Agarose polymer chains   2) Molecules secreted   3) Bacterial cells and molecules
by bacterial cells   secreted by bacterial cells
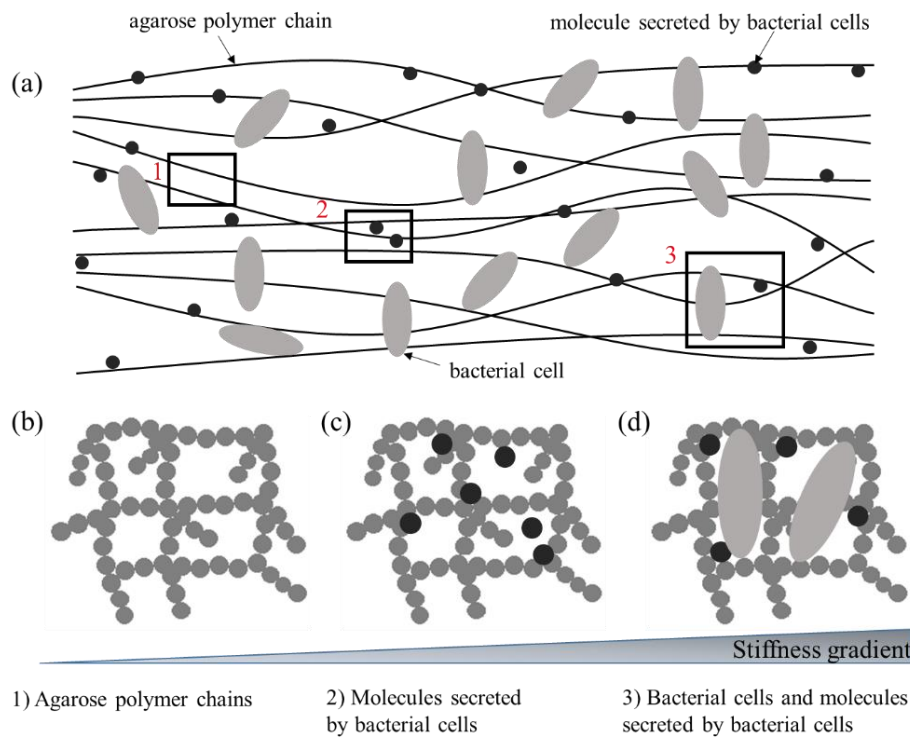
Figure 4.10. (a) Model showing possible alteration of the gel structure by molecules secreted by bacteria. These might interact with the agarose polymer to increase the crosslinking of individual chains (b) Structure of agarose gel where no secreted molecules or bacterial cells are present (section 1). (c) Structure of agarose gel when there are only molecules secreted by the bacterial cells (section 2). Compared to the gel structure without any other particles, the molecules secreted by bacterial cells crosslink some of the agarose polymer chains resulting in an increase in stiffness. (d) Structure of agarose gel when both bacterial cells and molecules secreted by bacterial cells are present (section 3). Due to the size difference between the secreted molecules and bacterial cells, it is proposed that the agarose polymer chains further crosslink resulting in an increase the overall stiffness of the hydrogel, when interacting with different media. The increase in stiffness is indicated by the stiffness gradient

4.3.3 Imaging of 1% agarose hydrogels without encapsulation with scanning electron microscopy (SEM)

The structure of 1% hydrogels that were made with LB, NB and PBS were imaged using scanning electron microscopy (SEM) to find out about the differences in the structure of the hydrogels. When the images of hydrogels without encapsulation were compared, the structure of the gels with different media appeared different from each other, therefore the structure of all the three different gels varied from gel to gel. Two images were taken from different areas of the samples to ensure that the structure was similar throughout the entire gel and they are shown at Fig 4.11-4.13.

74
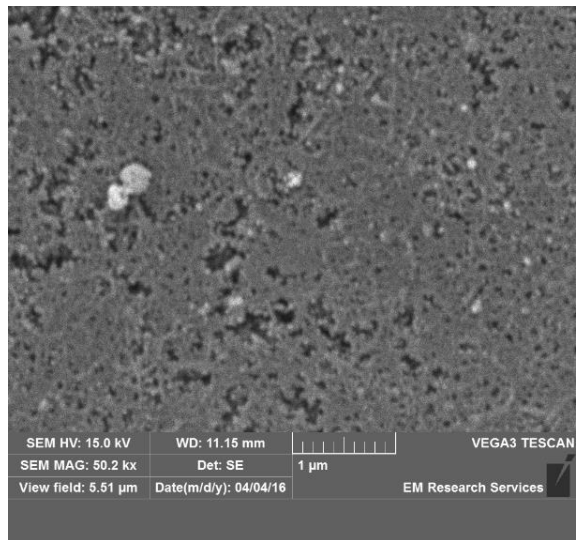
Figure 4.11. SEM images taken for 1% agarose hydrogels with LB medium
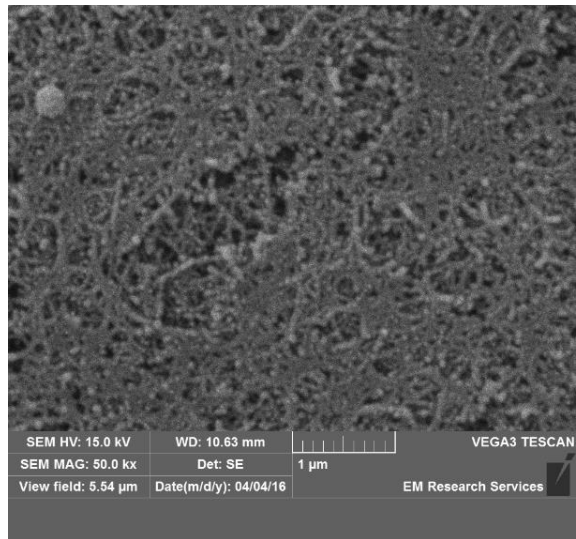
Figure 4.12. SEM images taken for 1% agarose hydrogels with NB medium
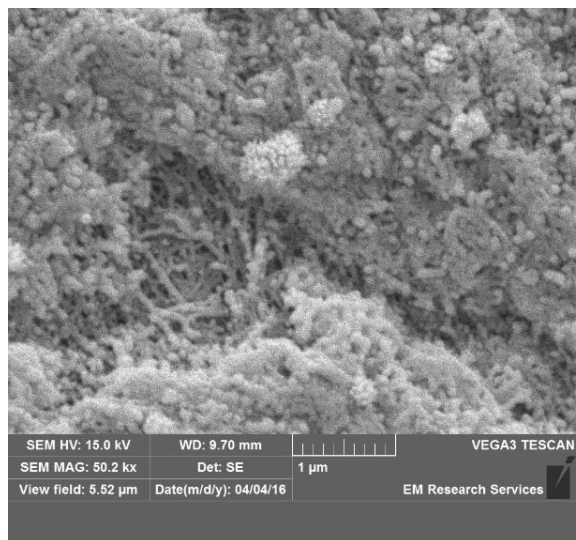
Figure 4.13. SEM images taken for 1% agarose hydrogels with PBS medium

For all of the imaged 1% gels, a more porous structure was expected however the images revealed a more compact structure. Even if it is a vague interpretation, the structure of NB and PBS were more alike compared to the structure of LB, which may explain the differences in the results obtained from the experiments.

In the methods section, it was explained that the hydrogels went through a dehydration process, critical point drying and then gold plating to be imaged by SEM. Therefore, they may alter their internal structure and these images may not be reflecting the true structure of a fully hydrated hydrogel. As documented in literature, different sample preparation techniques for SEM can result in different surface and bulk morphologies, where critical point drying could result in hydrogel structure to collapse to reveal a dense fibrous structure (Trieu and Qutubuddin, 1994; Zhang and Peppas, 2002).

4.3.4 Stiffness of critical point dried 1% agarose hydrogels without encapsulation

To check if the critical point drying affected the mechanical properties of hydrogels, a similar procedure was applied to the critical point dried gels. Here, only 5% strain was tested. Stiffness of the critical point dried hydrogels were determined by applying the Burger's model and Hooke's law to the stress relaxation test and the instantaneous elastic modulus of the gels are presented in Table 4.5. When the stiffness of critical point dried hydrogels were compared to the hydrated hydrogels of the same media/buffer, it was found that LB and NB critical point dried gels were significantly different than the hydrated gels of the same media with p values of $p = 0.001$ and $p = 0.008$, respectively. However, when critical point dried PBS gels were compared to hydrated PBS hydrogels, such a statistical significant difference was not observed ($p = 0.56$). The statistical differences between critical point dried hydrogels made with different growth media or buffer are summarised in Table 4.6. It is evident that the dehydrated gel made with PBS appears to be softer that the other two counterparts. Such findings agree with what was observed in the differences of SEM images (Fig. 4.11 - 4.13).

Applied strain (%)	Buffer or media	$E_{gel.0}$ (kPa) (Burger's model)	$E_{gel.0}$ (kPa) (Hooke's law)
	PBS	31.1 ± 8.0	56.3 ± 9.9
5%	NB	63.0 ± 23.9	69.2 ± 25.8
	LB	73.2 ± 18.4	81.6 ± 20.7

Table 4.5. Instantaneous Young's moduli of critical point dried 1% agarose hydrogels without encapsulation obtained from Burger's model and Hooke's law (Data represented as mean ± standard deviation, $n \geq 5$)

	Burger's model			Hooke's law	
	PBS	NB		PBS	NB
LB	0.004 (**)	0.47	LB	0.12	0.58
PBS		0.03 (*)	PBS		0.53

Table 4.6. *p* values obtained from Tukey's post hoc test for critical point dried hydrogels without encapsulation. Here (*) indicates $p < 0.05$ and (**) indicates $p < 0.01$. The comparisons were made based on the instantaneous Young's moduli determined from Burger's model and Hooke's law

During the stress relaxation texts, it was noticed that the critical point dried hydrogels made with growth media appear to be more adhesive, which can be due to their organic content. This may be the reason why there were significant differences between critical point dried and hydrated gels for LB and NB media.

4.3.5 Stiffness of higher concentration agarose hydrogels without encapsulation at 5% strain

Previously, it was shown that for certain growth media the stiffness of 1% agarose hydrogels was altered when bacterial cells were encapsulated in them. To examine the effect of the stiffness on hydrogel and bacterial cell interactions, higher concentration hydrogels (2% and 3%) were also tested. When 1% agarose hydrogels with and without encapsulation were compared, the highest fold change was observed when the applied strain was 5% which was approximately 2-fold for both of the encapsulated bacterial cells (*E. coli* BW25113 and *S. epidermidis* FH30).

Also, it was expected that the stiffness of the higher concentration hydrogels would be higher compared to the lower concentration hydrogels, so using 5% strain to detect the changes would avail. Therefore, only 5% strain was

considered for higher concentration hydrogels. Before the analysis of the effect of encapsulation, the stiffness values of higher concentration hydrogels without bacterial cells were determined.

Stress relaxation tests were applied to 2% and 3% agarose hydrogels made with LB, NB and PBS. The hydrogels were kept in the corresponding liquid media or the buffer prior to testing for 3 hours to obtain full hydration. Stress relaxation tests were carried out for 30 minutes to reach equilibrium. The strain value was fixed at 5% and the changing force values in time were recorded.

The stress relaxation curves for different concentration gels without bacterial cells at 5% strain are given in Figure 4.14. Based on the results, PBS gels appeared to be the stiffest for both concentrations, however there were no significant differences among different hydrogels. As can be seen from the force-time curves (Figure 4.14), the hydrogels showed similar relaxation behaviour where they appeared to reach a plateau over time and their loading curves also showed a linear trend. Similar to 1% gels, to avoid the differences between the various responses of relaxation behaviour, the elastic responses of the hydrogels were taken into account (the initial force value applied on the gel to reach the specified strain).

Statistical differences between hydrogels made with different growth media or buffer are summarised in Table 4.7. The comparisons were made based on the maximum force applied on the hydrogels to reach the strain value for the first time.
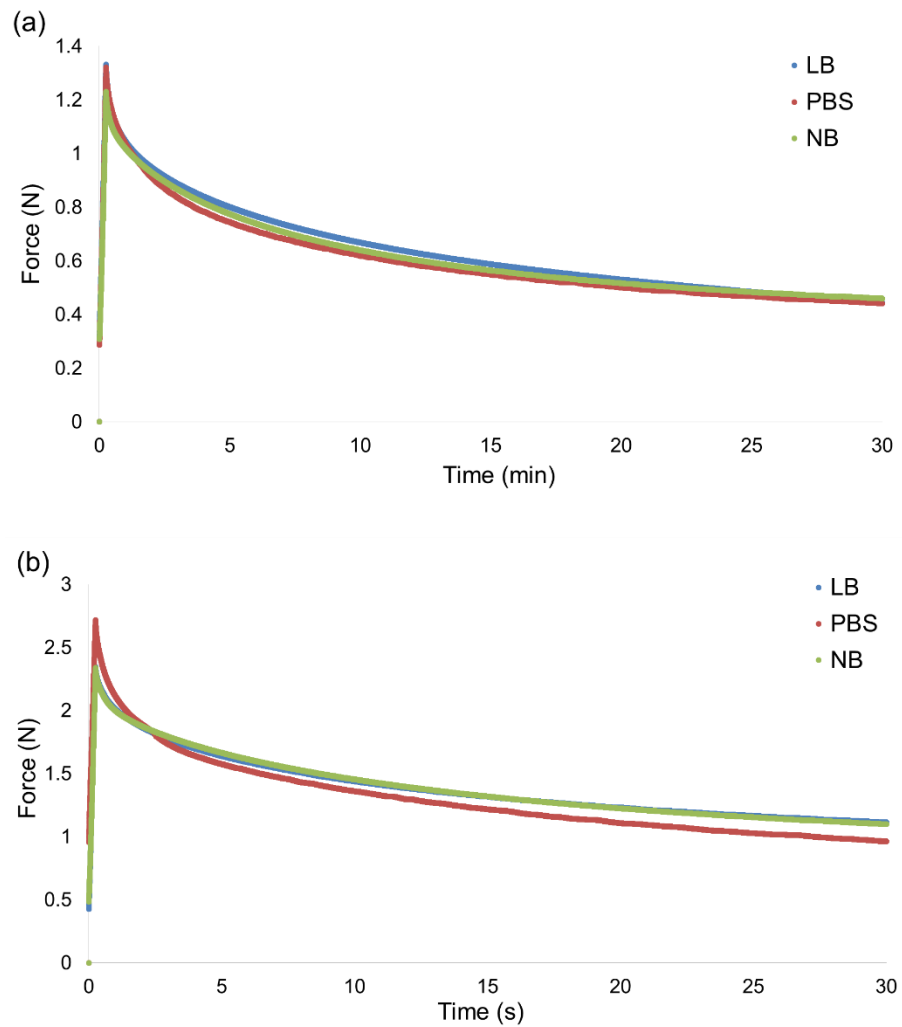
Figure 4.14. Force-time curves of hydrogels without encapsulation at 5% strain for (a) 2% hydrogels and (b) 3% hydrogels. The plotted force curves represent the average force curves value from all tested samples and error bars were removed for better visualisation

	2% hydrogels	
	PBS	NB
LB	0.90	0.79
PBS		0.86
	3% hydrogels	
	PBS	NB
LB	0.50	0.90
PBS		0.43

Table 4.7. p values obtained from Tukey's post hoc test for 2% and 3% hydrogels without encapsulation. The comparisons were made based on the maximum force applied on the hydrogels to reach the strain value

Similar to 1% agarose gels, stiffness values for higher concentration agarose hydrogels were obtained by using Burger's model and Hooke's law summarised in Table 4.8. These Young's modulus values were determined based on the best fit of the model on the force data from the relaxation part after the samples were compressed to 5% strain and only instantaneous elasticity was considered. The element of Burger's model responsible for the initial elastic response is the spring of the Maxwell element (see Figure 2.25). Therefore, this spring coefficient obtained from the model fit (given in Appendix B) was used as the instantaneous stiffness of the hydrogel. In a study, the stiffness of the similar type of agarose (Type VIIA low-gelling temperature agarose powder from Sigma) when the liquid medium was used as deionised water was found to be 76.0 ± 5 kPa and this stiffness value was determined from compression tests within the linear regime of stress and strain curve where the strain values changed from 7% to 15% (Huang *et al.*, 2012a). Taking into consideration that the applied strain in the experiments was similar to the one adapted in this study (5% strain) and that the hydrogels made with different liquid media did not show any significant differences, the calculated stiffness of 2% agarose hydrogels were comparable to the value reported in literature (Chen *et al.*, 2004; Huang *et al.*, 2012a).

For both concentrations tested, gels made with PBS were substantially stiffer than the gels made with growth media (LB and NB) however this difference was not statistically significantly different, unlike the 1% hydrogels. Due to the similarity of the behaviour of higher percentage hydrogels, 2% gels appeared to be the more appropriate than 3% gels for encapsulation process because of their wider range of working temperature (Tuson *et al.*, 2012a).

Concentration of hydrogel (%)	Buffer or media	$E_{gel.0}$ (kPa) (Burger's model)	$E_{gel.0}$ (kPa) (Hooke's law)
2	PBS	71.8 ± 4.6	77.7 ± 5.9
	NB	66.9 ± 5.0	75.0 ± 11.2
	LB	71.1 ± 9.0	78.5 ± 9.2
3	PBS	137.3 ± 18.0	149.3 ± 18.5
	NB	128.7 ± 8.2	138.0 ± 8.7
	LB	130.5 ± 18.9	138.4 ± 19.9

Table 4.8. Instantaneous Young's moduli of 2% and 3% agarose hydrogels without encapsulation obtained from Burger's model (Data represented as mean ± standard deviation, $n \geq 5$)

4.3.6 Stiffness of 2% hydrogels with encapsulated bacterial cells at 5% strain

Having measured the stiffness of hydrogels alone, the next step was to assess whether the encapsulation of bacteria in the gels led to any measurable changes in the stiffness. Therefore, *E. coli* or *S. epidermidis* were encapsulated at a concentration equivalent to 1% of the total hydrogel volume. The stiffness of the gels with encapsulated bacterial cells were characterised and the obtained stiffness values were normalised by the corresponding gel without encapsulation. Since there were no significant differences between the stiffness of the hydrogels made with growth media (NB and LB) and without encapsulation, only LB gels were considered for encapsulation of bacterial cells. PBS gels were also considered since its content was different to that of the growth media.

For both 2% gels made with PBS and LB, an increase in stiffness when bacterial cells were encapsulated was not observed and they showed similar stiffness values as the gels without bacteria (as shown in Figure 4.15). The behaviour observed for 2% PBS gels was similar to that of 1% PBS gels where no significant differences ($p > 0.05$) were observed between gels with and without encapsulation. However, the behaviour of 2% LB gels showed the opposite behaviour compared to 1% LB gels. For 2% LB gels with and without encapsulation, no significant differences ($p > 0.05$) were observed whereas 1% LB gels with encapsulated bacterial cells were significantly stiffer than 1% LB gels without encapsulation (see Figure 4.8c). Therefore, experiments for other LB-based hydrogels (*i.e.* LB-no yeast

extract and LB-no tryptone) were not performed for higher concentration hydrogels.

The stiffness of PBS and LB gels with and without bacteria was calculated and normalised. Similar to the results obtained for 1% gels, both types of bacterial cells (*E. coli* – rod shaped and *S. epidermidis* – spherical shaped) behaved in a similar pattern suggesting that different bacteria types interact similarly with the media and the applied mechanical stimuli.
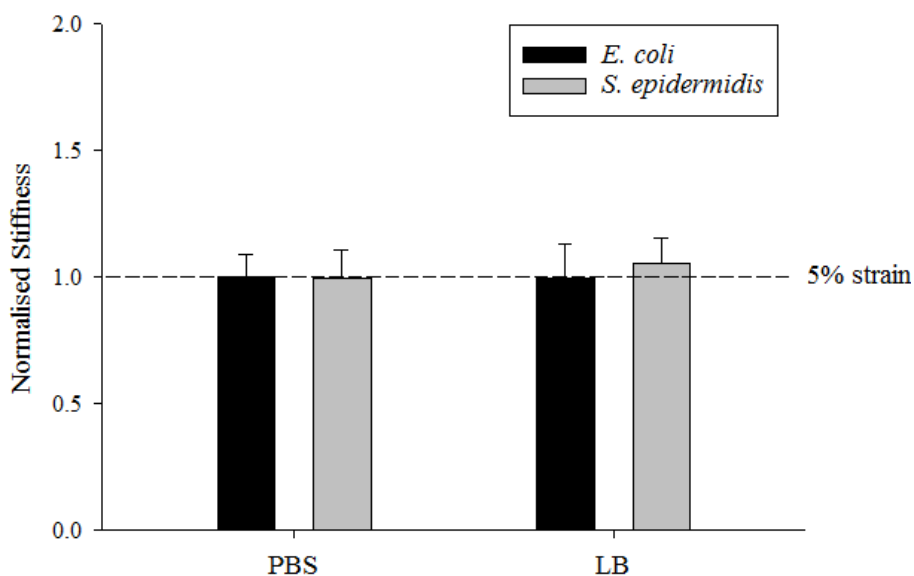
Figure 4.15. Normalised stiffness values of 2% PBS and LB hydrogels when 5% strain was applied (the bars represent the gels with bacteria, the dashed line shows the normalised value for gels without encapsulation and error bars represent standard deviation). This normalisation represents the fold change in the stiffness in hydrogels containing encapsulated cells compared with those without cells, determined from 3 independent experiments. There were no statistically significant differences between the gels of the same growth media/buffer with and without encapsulation ($p > 0.05$)

As the concentration of the hydrogel increases, the porosity of the hydrogel decreased which also indicates that the agarose polymer chains are denser compared to 1% agarose hydrogels (Maaloum *et al.*, 1998; Liang *et al.*, 2006). Therefore, when bacterial cells are encapsulated in higher concentration hydrogels, they do not further crosslink the structure which results in similar stiffness value of the bacterial cell and hydrogel construct compared to hydrogels without encapsulation.

4.4   Summary of the Results and Conclusions

In this chapter, mechanical responses of various hydrogels obtained from compression tests with stress relaxation were presented. Burger's model and Hooke's law were used to determine the instantaneous elastic modulus of the hydrogels without encapsulated bacterial cells. Taking into consideration the applied strain values in the compression tests which were 0.5%, 2% and 5%, a linear relationship was considered between the hydrogels with and without encapsulation (Eq. 50). The instantaneous elastic modulus characterisation revealed that 1% agarose hydrogels presented a strain dependent behaviour. Also, they showed significant differences in mechanical properties among themselves which suggested that the media used could affect the mechanical responses of hydrogels. However, when the same tests were applied to higher concentration agarose hydrogels such a dependence of mechanical properties of hydrogels on the used media was not observed.

When the hydrogels with encapsulated bacterial cells were considered, it was revealed that bacterial cells were significantly stiffer or had stronger interactions with hydrogels when cultured in 1% agarose gels made with LB medium compared to NB medium or PBS. Further studies revealed that the tryptone component of LB was responsible for these observations since similar results were obtained for LB-no yeast extract gels. It was proposed that the pores of the 1% agarose polymer and the bacterial cells interact causing the pores to be compressed and change the structure of the hydrogel (Fig. 4.10), resulting in differences in the overall stiffness. In addition, this behaviour also might be due to changes in the structure of the gel caused by molecules secreted by cells. Since, higher concentration agarose hydrogels were less porous, such a change in the overall stiffness was not observed even for the growth media that altered the 1% gels.

In the next chapter, finite element modelling (FEM) for particle reinforced composites mimicking encapsulation will be presented to assess the composite mechanical response during unconfined compression. Also, the experimental results presented in this chapter and results from FEM will be compared to several mathematical models.

5 Modelling of Compression Responses of Agarose Gels and Bacterial Cell-Hydrogel Constructs

5.1 Introduction

To better understand the bacteria-hydrogel interactions subjected to compression, it is important to apply both analytical and computational modelling because experimental technique cannot reveal the physics of cell-hydrogel interactions. In addition, the computational simulations may also guide the future experimental designs. From the mechanical point of view, the bacteria-hydrogel constructs can be treated as bio-composites and modelling these constructs can reveal more insights of the interactions that cannot be directly observed from the experiments. To simulate the mechanical properties of bio-composites, finite element analysis has been widely used (Ji and Gao, 2004; da Silva *et al.*, 2012; Zlotnikov *et al.*, 2013).

Finite element analysis (FEA) is a numerical technique that is used in many engineering problems to provide approximate solutions using simplified models created to represent these problems (Szabo and BabuÂška, 1991; Bhavikatti, 2005). In a continuum, there can be infinite number of unknowns to the problems. FEA is used to reduce these unknowns to a finite number by distributing them into elements by expressing these unknown variables in terms of shape functions specific to those elements consisting of nodal points. Once these variables are determined, they can be interpolated for any other nodal point. With the contribution of boundary conditions which are used to mimic the problem, the nodal unknowns can be determined by solving simultaneous equations to obtain necessary values such as stresses, strains etc. (Bhavikatti, 2005). Therefore, FEA is a useful tool that can be used to determine the mechanical properties of hydrogels and hydrogels encapsulated with particles. In several studies, it was reported that FEA was used to determine the elastic moduli of particle or fibre reinforced composites (Holzapfel and Gasser, 2001; Yan *et al.*, 2011; Cao and Chen, 2012; Peng *et al.*, 2012).

In this chapter, FEA will be adopted to model compression of agarose hydrogels and bacteria-agarose constructs with a similar setup used in the compression experiments in Chapter 4. Therefore, this characterisation will

also be done for models which represent cases with and without encapsulation of particles. To gain more insights of the compression response of these composites, a parametric study is done. In which case, different variables will be considered for the analysis which includes applied compressive strain, volume fraction of particles, Young's moduli and Poisson's ratios of particle and matrix.

The results obtained from the FEA model will be compared to the corresponding experimental results that were documented in Chapter 4 in addition to several mathematical models from literature that are used to calculate composite stiffness (the details of the adopted models were given at Chapter 2, Section 2.8). Using this technique will be able to confirm if the bacterial cells interact with the environment they are encapsulated in, since the encapsulated particles used in this chapter will represent inert particles and therefore will not interact with the matrix they are encapsulated in.

5.2 Methods

5.2.1 Constructing the model for the finite element modelling

A simple representative model was created using the commercial finite element software ABAQUS CAE 6.14 (Dassault Systèmes Smulia Corp. 2014, Providence, RI, USA) to carry out simulations to find out about the Young's modulus of the bacteria-hydrogel composites. The model used was a representation of the encapsulation with axisymmetric boundary conditions and a uniform static displacement was applied. The boundary conditions were applied in a way that they mimicked the compression tests where the bottom plane was fixed, the movement in the horizontal direction was limited, a vertical compression was applied at the top surface and no boundary conditions were applied to the right plane making it a free surface (see Fig. 5.1). The applied conditions mimicked unconfined compression similar to the experiments carried out as reported in Chapter 4.

This model had two modes: bonded and non-bonded. In bonded simulation mode, the matrix (hydrogel) and the particle (bacteria) were glued together, *i.e.* the separation between the matrix and the particle was not allowed. In contrast, for non-bonded simulation, the bacteria and hydrogel was in

contact where the separation between the matrix and the particle was allowed.

Different mesh sizes were applied on the model and $E_{composite}$ values were obtained until the obtained $E_{composite}$ values were independent of the mesh size used. A finer mesh size was used at the matrix-particle interface and where the boundary conditions were applied, to achieve a more accurate results and to correctly represent the matrix-particle interface and at the symmetry plane. The finer mesh had an element size of 0.05 μm and elsewhere the element size was taken as 0.1 μm. These mesh sizes provided the force response to be independent of mesh size. The mesh structure of the model can be seen from Figure 5.1. The bottom of the construct was fixed at the direction of compression. The compressive displacement was applied on the top surface of the construct. A total number of 2135 and 9823 elements were used for bacteria and hydrogel, respectively for 1% volume fraction of particles. With increasing volume fraction (*i.e.* size of the particle), the number of elements used for the bacterial cell increased up to 26231 and the number of elements used for the gel decreased to 7163. The element type used was CAX8R, which is an 8-node biquadratic axisymmetric quadrilateral with reduced integration. Such high order mesh elements are widely used in two- and three-dimensional problems in engineering applications due to their accuracy in stress analysis and they can accurately capture variations in stress near fillets or holes (Hibbitt *et al.*, 2001; Chandrupatla *et al.*, 2002). Since the matrix and the particle were used as two different phases and they could be separated based on the simulation mode, using such mesh elements were appropriate. In principle, both bacteria and hydrogel are viscoelastic. However, there is a lack of analytical models for the viscoelastic composites. In addition, for experimental analysis in Chapter 4, the elastic moduli were measured. Therefore, for simplicity, a linear elastic model was adopted for both bacteria and hydrogel. Various analytical models are also available for composites with both linear elastic inclusion and elastic matrix.
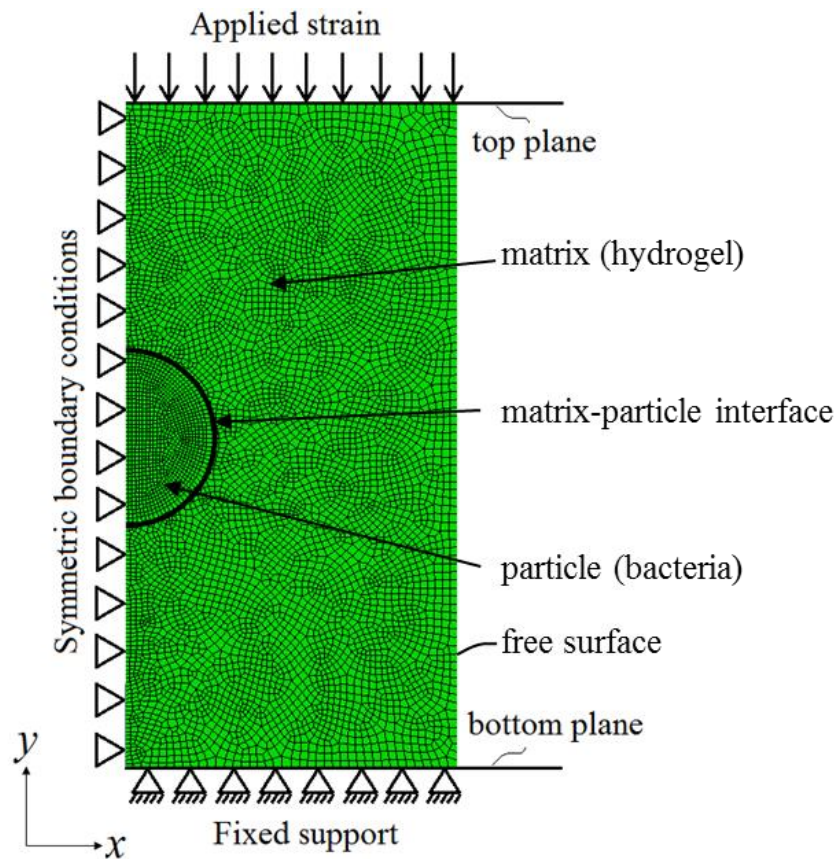
Figure 5.1. Representation of the model for the compression tests. Applied boundary conditions: symmetric boundary conditions on the matrix-particle structure and the planes provided the opportunity to only model half of structure while restraining the linear movement in *x* direction and the rotational movement in *y* and *z* directions, fixed support applied at the bottom plane for the restriction of movement and compressive strain was applied through the top plane

The variables considered in this model were the applied compressive strain, volume fraction of particles, Poisson's ratio and Young's modulus of the particle and the matrix. The tested variables included a wide range of values to model different situations including real-life values obtained from experiments so that the model correctly mimicked the compression experiment conditions.

- For the simulations, two different applied uniform static displacements were chosen, that were 0.5% and 5% (which were the lower and upper limits used for the compression experiments).

- Different volume fractions of cells were tested in both simulation modes. This was done by increasing the particle radius by 0.25 µm at each step from 1 µm to 3.50 µm. This resulted in the volume

fraction to change between 1% (representing the experimental measurements) and 53%.

- For both the matrix and the particle, Poisson's ratio was varied from 0.10 to 0.45 (changed by 0.05 for each of the phases).

- For both of the strain values applied, the Young's modulus of the matrix was chosen as 5 kPa and the Young's modulus of the particle was chosen as 1MPa. The individual matrix and particle stiffness values were chosen so that they had a 200-fold difference between the particle and the matrix. For the higher strain value (*i.e.* 5% strain), the opposite case was tested as well where the Young's modulus of the particle was chosen as 5 kPa and the Young's modulus of the matrix was chosen as 1MPa.

5.2.2 Statistical analysis

Analysis of Variance (ANOVA) with Tukey's post hoc test was applied to the constructs to determine the statistical differences between constructs tested using different Poisson's ratios (both for the matrix and the particle) and also for different volume fraction of particles within the matrix. The significance level (α) was taken as 0.05. The statistical analysis was carried out using Minitab 17.1.0.

5.2.3 Mathematical models to determine composite stiffness

The results obtained from simulations and experiments were compared to several mathematical models used to determine composite stiffness: the Voigt model, Reuss model, and Hashin and Strikman (HS) model with upper and lower bounds (Watt and Peselnick, 1980; Jones, 1998; Lakes and Drugan, 2002). The equations for the mathematical models used are summarised in Table 5.1. For HS model, when the subscripts of volume fraction, bulk and shear modulus indices were reversed, lower bound equations were obtained. The individual matrix and particle stiffness values were chosen so that they had a 200-fold difference between the particle and the matrix, similar to the adapted values in simulations. For the mathematical models and the computational model, the particle volume fraction was chosen as 1% (similar to the volume fraction in experiments).

To compare the simulation results, Poisson's ratio for the particle and matrix was taken as 0.45.

Model	Equation	
Voigt	$E_{Voigt} = E_1V_1 + E_2V_2$	
Reuss	$E_{Reuss} = \dfrac{E_1E_2}{E_1V_2 + E_2V_1}$	$V_1 + V_2 = 1$
HS – shear moduli	$G_{HS-upper} = G_2 + \dfrac{V_1}{\dfrac{1}{G_1 - G_2} + 6(B_2 + 2G_2)V_2/[5(3B_2 + 4G_2)G_2]}$	$G = \dfrac{E}{2(1+v)}$
HS – bulk moduli	$B_{HS-upper} = B_2 + \dfrac{V_1(B_1 - B_2)(3B_2 + 4G_2)}{(3B_2 + 4G_2) + 3(B_1 - B_2)V_2]}$	$B = \dfrac{E}{3(1-2v)}$

Table 5.1. Mathematical model equations. In the equations, subscript 1 refers to the properties of matrix and subscript 2 refers to the properties of particle. *E*, *G, B, V* and v refer to Young's modulus, shear modulus, bulk modulus, volume fraction and Poisson's ratio, respectively

5.3 Results and Discussion

A computational model was created to represent the compression tests for the case where the encapsulated particles do not interact with their environment (*i.e.* inert particles). Several variables were considered in this model, namely the applied compressive strain, the volume fraction of particles, Young's modulus and Poisson's ratio of the particle and the matrix, so that the model correctly mimicked the compression test conditions. It was reported in a previous study (Cerf *et al.*, 2009), that the whole and live *E. coli* cells have a Young's modulus of 2-3 MPa. This stiffness value was approximately 200 times that of the hydrogel Young's modulus (Guegan *et al.*, 2014). The individual matrix and particle stiffness values were chosen so that they represented the same fold difference between the particle (bacteria) and the matrix (hydrogel). The same fold difference was also employed for the mathematical models. Young's modulus was calculated based on the force value applied to the composite when the applied strain value reached either 0.5% or 5%.

5.3.1 Effect of volume fraction on $E_{composite}$

The effect of volume fraction on $E_{composite}$ was tested when the applied strain was 0.5% and 5%. Under the same applied strain, similar volume fraction of particles and Poisson's ratios for both phases, the difference in

von Mises stress responses of non-bonded and bonded simulation for when the applied strain were 5% were presented in Figure 5.2 and Figure 5.3, respectively. Similar behaviour in terms of separation was observed for different strain values tested for both non-bonded and bonded simulations.

The Young's modulus was calculated based on the maximum force value applied on the composite when the strain value was reached. The same approach of normalisation of the force values as in experimental results was used for simulation results as well.

$$E_{composite} = \frac{F_{composite}}{F_{gel}} E_{gel} \tag{51}$$

Here, the E_{gel} value was taken as 5 kPa. The corresponding $E_{composite}$ values are given in Table 5.2 and Table 5.3 for 0.5% applied strain and 5% applied strain, respectively. The Poisson ratio used to obtain the values for both the gel and the cell is 0.45.
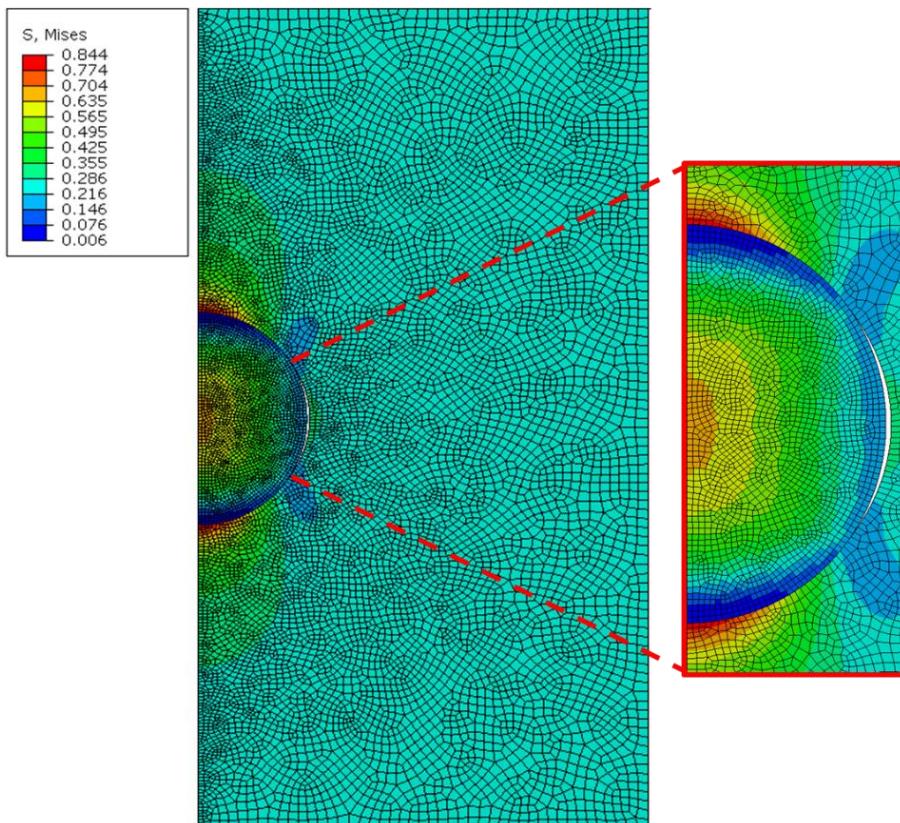
Figure 5.2. Sample von Mises stress outcome for non-bonded simulations when the applied strain is 5%. The volume fraction of particles was 1%.With the applied strain, the separation between the matrix and the particle was allowed in non-bonded simulation. The Poisson's ratio for both phases were 0.45
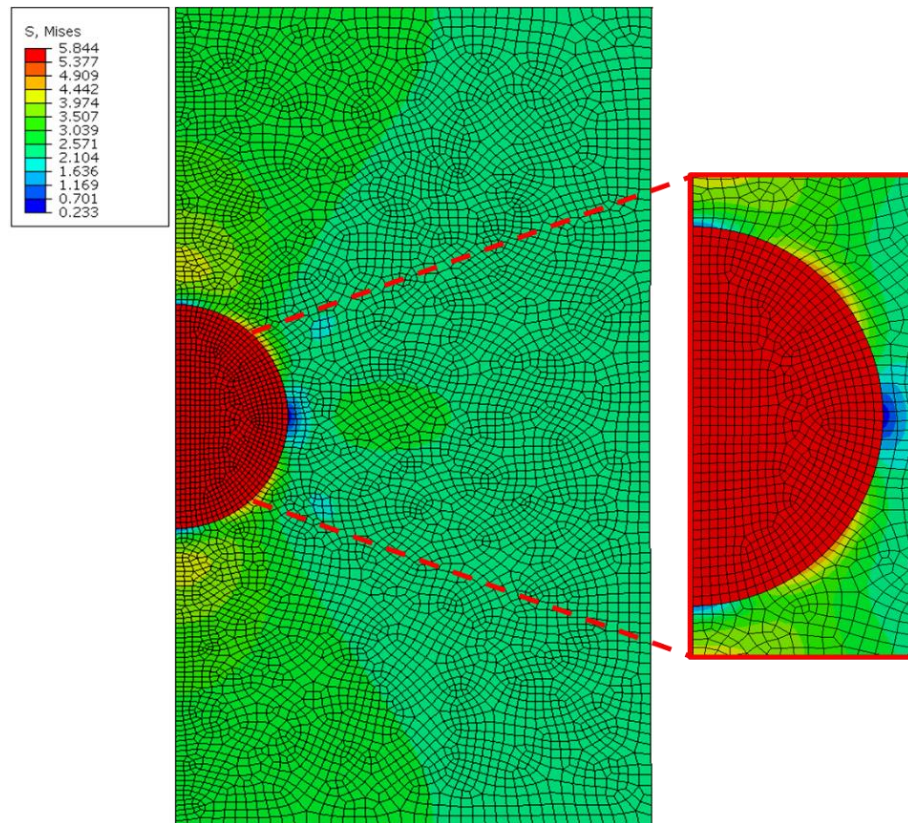
Figure 5.3. Sample von Mises stress outcome for bonded simulations when the applied strain is 5%. The volume fraction of particles was 1%. With the applied strain, the separation between the matrix and the particle was not allowed in bonded simulation. The Poisson's ratio for both phases were 0.45

Volume fraction of particles	$E_{composite}$ (bonded) (kPa)	$E_{composite}$ (non-bonded) (kPa)
0.01	5.11	5.06
0.02	5.22	5.11
0.03	5.39	5.19
0.05	5.62	5.31
0.08	5.95	5.48
0.11	6.40	5.70
0.16	7.04	6.00
0.21	7.96	6.40
0.27	9.37	6.95
0.34	11.66	7.74
0.43	15.80	8.96

Table 5.2. $E_{composite}$ values for different simulation cases at volume fractions of 1% to 43% when the applied strain was 0.5%. The values presented were for when the Poisson's ratio was 0.45 for both phases

Volume fraction of particles	$E_{composite}$ (bonded) (kPa)	$E_{composite}$ (non-bonded) (kPa)
0.01	5.11	5.06
0.02	5.22	5.11
0.03	5.39	5.20
0.05	5.62	5.32
0.08	5.95	5.49
0.11	6.40	5.72
0.16	7.04	6.02
0.21	7.96	6.44
0.27	9.36	7.03
0.34	11.66	7.91
0.43	15.82	9.39

Table 5.3. $E_{composite}$ values for different simulation cases at volume fractions of 1% to 43% when the applied strain was 5%. The values presented were for when the Poisson's ratio was 0.45 for both phases

From the tables, it can be said that the $E_{composite}$ values increased with the increasing volume fraction of particles for both simulation cases and for both applied strains. When the $E_{composite}$ values were compared, there was approximately 0.13% difference between the values for bonded simulation at different applied strains for all tested volume fraction of particles. For non-bonded simulation, this difference increased up to approximately 4.8% as the volume fraction of particles increased. Since the separation of the matrix and the particle was allowed in non-bonded simulations, a gap was observed between these phases (as shown in Figure 5.2) resulting in lower composite stiffness values which suggested that non-bonded composites were softer than the bonded composites.

To observe how the Young's modulus of the composite changes between bonded and non-bonded cases, graphs were plotted for both applied strain values (Fig 5.4). Since the bonded composites were stiffer than the non-bonded composites, the normalisation was done as $E_{bonded}/E_{non-bonded}$.
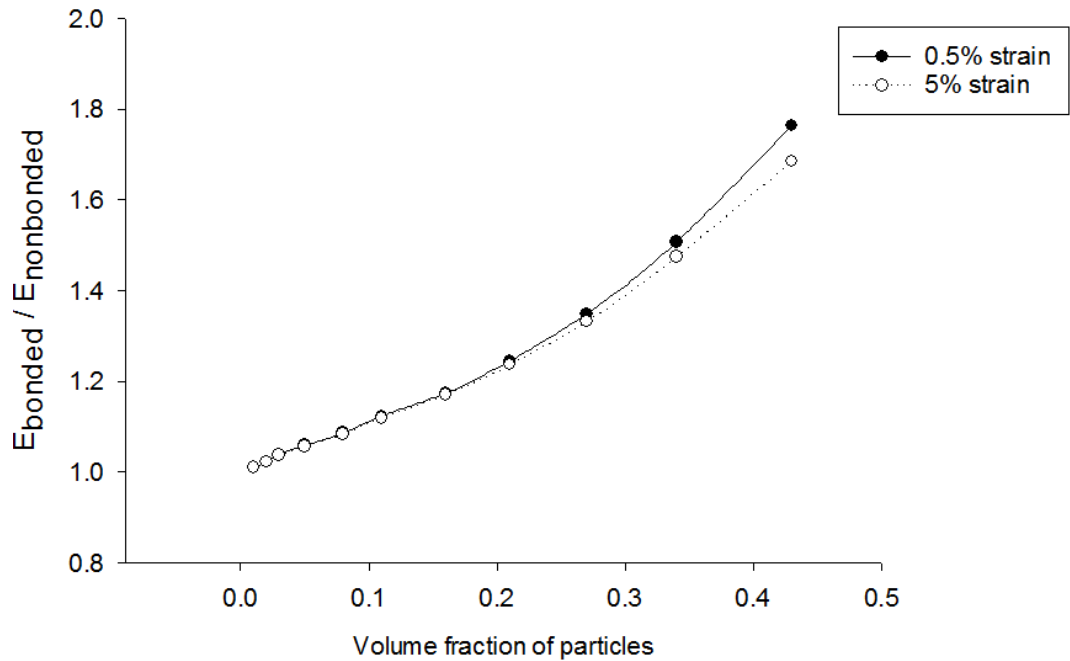
Figure 5.4. Change of the difference between E_{bonded} and $E_{nonbonded}$ when the applied strain was (a) 0.5% and (b) 5% for different volume fraction of particles

As can be seen from Figure 5.4, the relationship between bonded and non-bonded simulation became non-linear as the encapsulated particles in the matrix go from lower volume fraction to higher volume fraction.

5.3.2 Effect of Poisson Ratio on $E_{composite}$

To find out about Poisson's ratio effect on $E_{composite}$, Poisson's ratio values for both the gel and the particle were increased from 0.1 to 0.45 by 0.05 and tested against each other for both simulation modes at two different strain values. For the higher applied strain, two different cases were considered. The first case involved when the encapsulated particles were stiffer than the gel ($E_{particle} > E_{gel}$) and the second case involved when the gel was stiffer than the encapsulated particles ($E_{particle} < E_{gel}$). In both cases, the stiffer material's Young modulus was taken as 1 MPa and the softer material's Young modulus was taken as 5 kPa. For the 0.5% strain, only the first case was considered where the particles were stiffer than the gel.

For instance when $v_{gel} = v_{particle} = 0.45$, $E_{composite}$ values were found as 5.1 kPa, 5.9 kPa, 9.37 kPa and 15.8 kPa for 1% - 43% volume fractions when the particles were stiffer than the gel in bonded simulation at both applied strain values (see Table 5.2 and 5.3). For the opposite case at 5%

applied strain, $E_{composite}$ values for the same volume fractions were found to be 980.4 kPa, 852 kPa, 565.7 kPa, 364.4 kPa, respectively. Similarly, $E_{composite}$ values were obtained using the other Poisson's ratios for the particle and the gel. From the results, it can be said that $E_{composite}$ values increased with increasing volume fraction of particles for the case of softer gel and they decreased with the increasing volume fraction of particles for the case of stiffer gel.

To be able to compare the effect of encapsulated particles on the overall stiffness, an additional condition was also tested for all the different cases to mimic the gels without encapsulation, *i.e.* when both stiffness values for the matrix and the particle were taken as the same value (either 5 kPa or 1 MPa, depending on the type of the case). The data obtained for $E_{composite}$ for the structures with particles were normalised by the data obtained from the case which mimicked the gels without encapsulation.

Figure 5.5-5.7 show the changes in normalised $E_{composite}$ values obtained from bonded simulation using 0.5% and 5% strain values when $v_{particle}$ was changed from 0.10 to 0.45 by 0.05 at each step and for the same range of v_{gel} values, at four different volume fractions, namely 1%, 8%, 27% and 43%. For the lower strain value (see Figure 5.5), it can be seen that the gel Poisson ratio did not affect the stiffness of the overall composite, since all of the curves obtained for different v_{gel} values coincided and there was no statistically significant difference between the normalised $E_{composite}$ values at the same $v_{particle}$ ($p > 0.05$). The stiffness value presented a decreasing trend for $v_{particle}$ values between 0.10-0.20 and then showed and increasing trend for $v_{particle}$ values between 0.25-0.45 for all tested volume fraction of particles. Although the decrease in the first part of the curve for the gels containing high volume fraction of particles (43%) appeared relatively small compared to the gels containing less volume fraction of particles, there was a significant decrease ($p < 0.01$) in the stiffness for all tested volume fractions (the difference in appearance was due to the range of normalised $E_{composite}$). At 0.5% applied strain, when the particle stiffness was higher compared to the gel stiffness, the overall change in normalised stiffness varied between 1.020 - 1.023 for when the volume fraction of

particles was 1%, 1.17 - 1.19 for when the volume fraction of particles was 8%, 1.75 - 1.87 for when the volume fraction of particles was 27% and 2.62 – 3.17 for when the volume fraction of particles was 43%. Normalised $E_{composite}$ values increased with the volume fraction of particles due to the increase in stiffer phase.

For 5% applied strain for when the particle stiffness was higher than the gel stiffness (see Figure 5.6), normalised $E_{composite}$ values were independent of v_{cell} and a linear pattern was observed at all tested volume fractions (the non-linear appearance of the curves for 1% and 8% volume fraction of particles was due to the range of normalised $E_{composite}$). The data obtained for $v_{gel} < 0.25$ at the range of v_{cell} values tested were not significantly different ($p > 0.05$) however there were statistical significant differences for the data obtained for $v_{gel} \geq 0.25$ ($p < 0.01$). At 5% applied strain, when the particle stiffness was higher compared to the gel stiffness, the overall change in normalised stiffness varied between 1.018 - 1.025 for when the volume fraction of particles was 1%, 1.17 - 1.19 for when the volume fraction of particles was 8%, 1.75 - 1.88 for when the volume fraction of particles was 27% and 2.62 – 3.17 for when the volume fraction of particles was 43%. Only for high volume fraction, the Poison's ratio of particle and matrix has significant effect on the normalised stiffness. Normalised $E_{composite}$ values increased with the volume fraction of particles due to the increase in stiffer phase. Although, the range of normalised $E_{composite}$ values were almost exactly the same for both applied strains, the dependence of these values on the Poison's ratio of the phases was the opposite, where at 0.5% applied strain the values were independent of v_{gel} and at 5% applied strain the values were independent of $v_{particle}$.

A similar trend was observed at 5% strain for when the gel stiffness was higher than the particle stiffness (see Figure 5.7), compared to the opposite case where when the particle stiffness was higher than the gel stiffness at the same applied strain. Normalised $E_{composite}$ values were independent of $v_{particle}$ and a linear pattern was observed at all tested volume fractions (the non-linear appearance of the curves for 1% and 8% volume fraction of particles was due to the range of normalised $E_{composite}$). For 1% volume

fraction of particles, only the data obtained for $v_{gel} = 0.45$ among the range of $v_{particle}$ values were significantly different than the rest of the v_{gel} values tested however as the volume fraction of particles increased no statistical differences were observed between the different v_{gel} curves. As the volume fraction of particles increased within the matrix, the order of the curves having different v_{gel} values reversed. For this case, the overall change in normalised stiffness varied between 0.979 – 0.982 for when the volume fraction of particles was 1%, 0.850 – 0.855 for when the volume fraction of particles was 8%, 0.563 – 0.572 for when the volume fraction of particles was 27% and 0.360 – 0.374 for when the volume fraction of particles was 43%. Similarly, for high volume fraction, the Poison's ratio of particle and matrix has significant effect on the normalised stiffness. As expected, the normalised $E_{composite}$ values decreased with the volume fraction of particles due to the increase in softer phase. Similar to the previous case, $E_{composite}$ values were independent of $v_{particle}$ at 5% applied strain.

The results revealed that the dependency of composite stiffness on Poisson's ratio varied under different strain values and it showed significant differences for the higher volume fraction of particles (above 8%) for all tested cases (i.e. stiffer particles and stiffer gel). The change in $E_{composite}$ values were independent of v_{gel} at lower applied strain. On the other hand, although a similar trend was observed for all tested v_{gel} values, $E_{composite}$ values changed with changing v_{gel}.
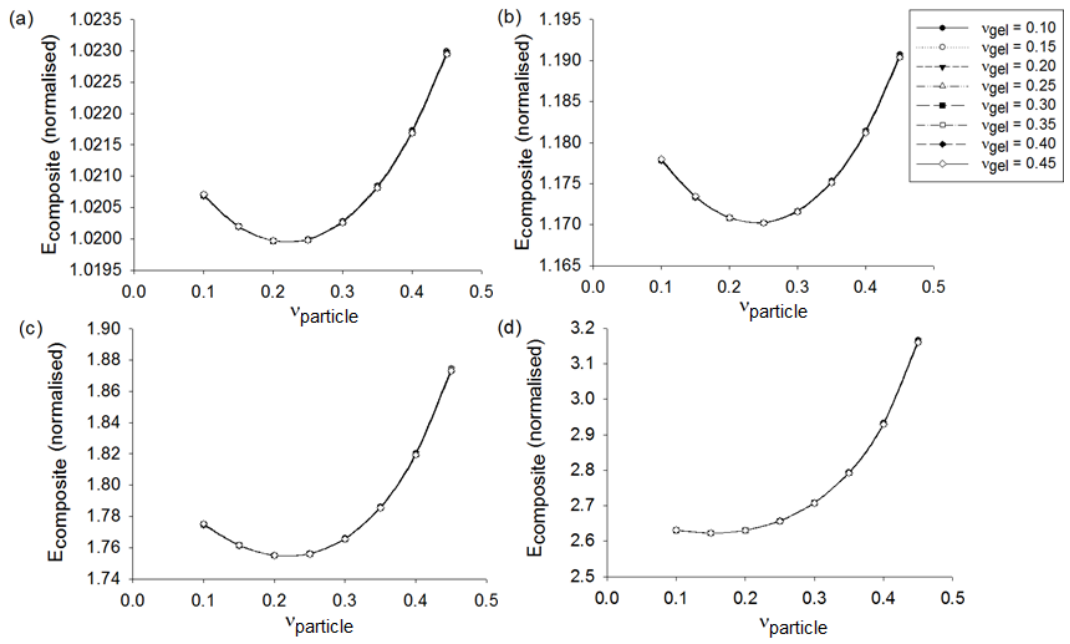
Figure 5.5. The change in normalised stiffness of composites for when the stiffer particles (*i.e.* 1 MPa) were encapsulated in soft gels (*i.e.* 5 kPa) for bonded simulations when the applied strain was 0.5% at different particle and matrix Poisson's ratios for (a) 1% volume fraction, (b) 8% volume fraction, (c) 27% volume fraction and (d) 43% volume fraction of encapsulated particles
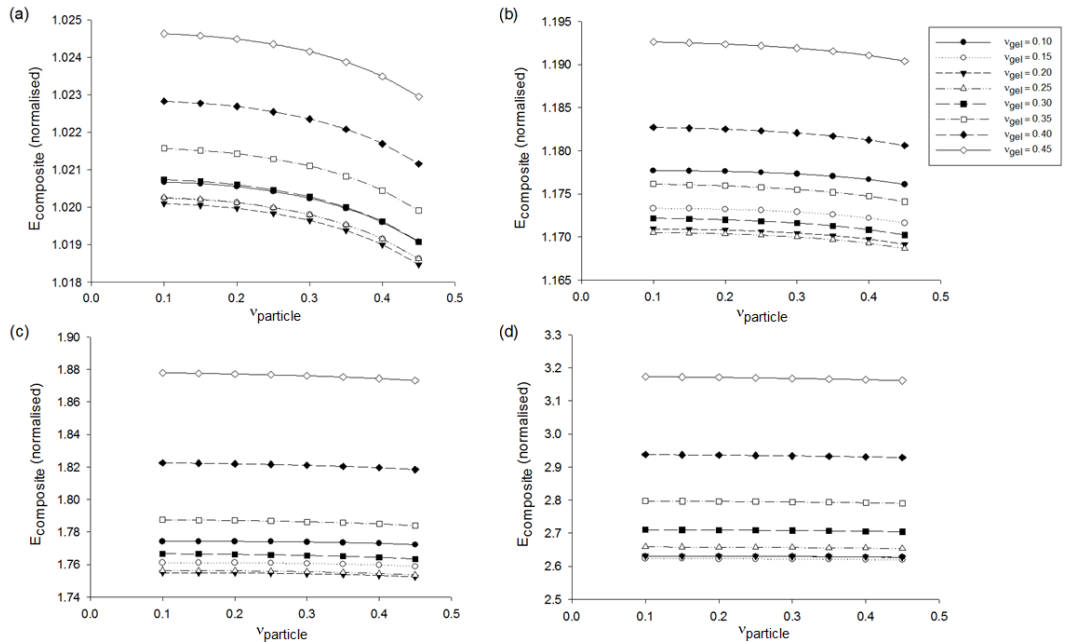
Figure 5.6. The change in normalised stiffness of composites for when the stiffer particles (*i.e.* 1 MPa) were encapsulated in soft gels (*i.e.* 5 kPa) for bonded simulations when the applied strain was 5% at different particle and matrix Poisson's ratios for (a) 1% volume fraction, (b) 8% volume fraction, (c) 27% volume fraction and (d) 43% volume fraction of encapsulated particles
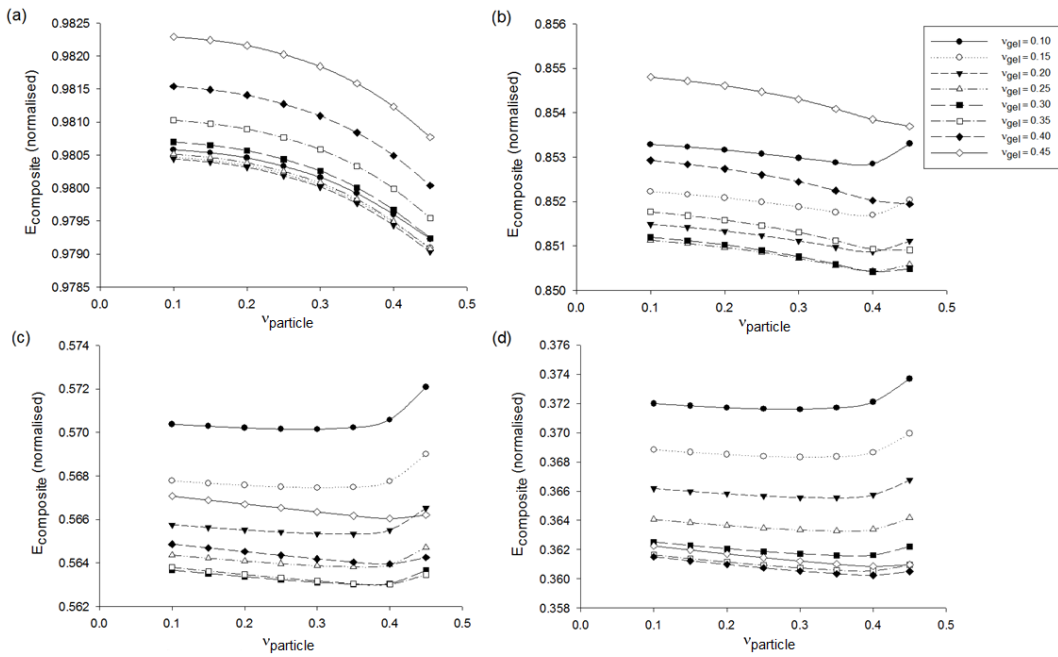
Figure 5.7. The change in normalised stiffness of composites for when the softer particles (*i.e.* 5 kPa) were encapsulated in stiffer gels (*i.e.* 1 MPa) for bonded simulations when the applied strain was 5% at different particle and matrix Poisson's ratios for (a) 1% volume fraction, (b) 8% volume fraction, (c) 27% volume fraction and (d) 43% volume fraction of encapsulated particle

After comparing normalised $E_{composite}$ values obtained from the tested Poisson's ratio range for both gel and particle in terms of Poisson's ratio, a similar comparison was carried out for the different volume fraction of particles for both cases where the gel and the particle had the same Poisson's ratio. When $\nu_{particle}$ and ν_{gel} values were different from each other, the curves obtained were coincident for 0.5% applied strain and they were parallel to each other for all volume fractions and a similar pattern is observed. The difference between the normalised $E_{composite}$ values with phases having the same Poisson's ratio was between 0.2%, 1.1%, 5.3% and 16.8% for volume fractions of 1% - 43% for when the particles were considered stiffer at both applied strains (Fig. 5.8-5.9). When the volume fraction was smaller, the curves were almost coincident, especially at the smaller volume fractions (1% and 8%). The effect of Poisson's ratio became evident when the particle volume fraction is above 25%.

For the case where the gel was considered stiffer, this difference were calculated as 0.02%, 0.05%, 0.74% and 3.06% for volume fractions of 1% - 43%. The Poisson's ratios of the particle and matrix do not have any distinguishable effect on the composite stiffness (see Fig. 5.10).
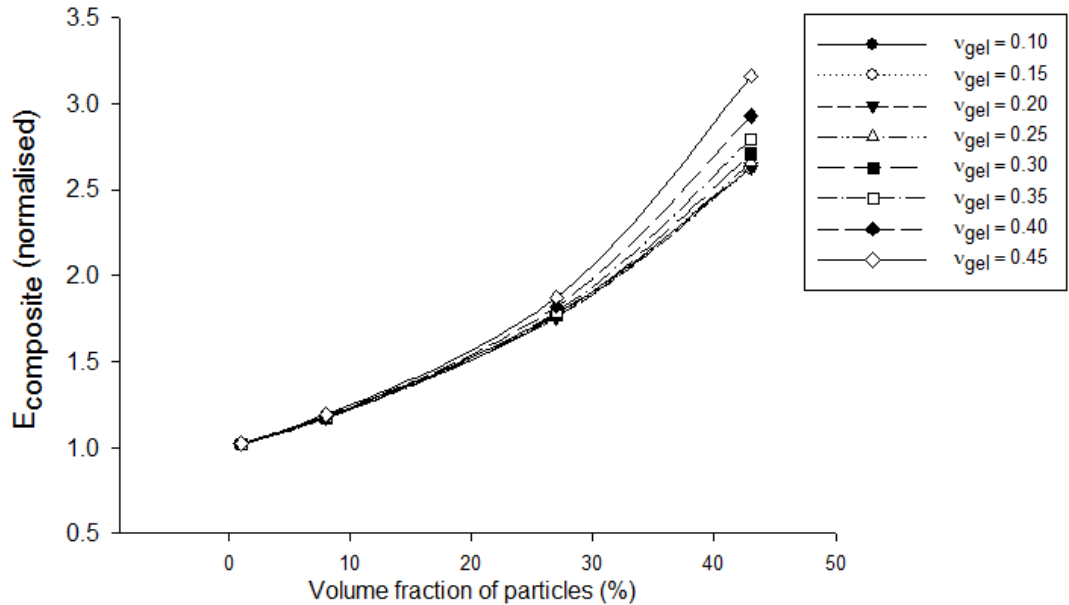
Figure 5.8. Change in $E_{composite}$ with volume fraction for when the stiffer particles (*i.e.* 1 MPa) were encapsulated in softer gels (*i.e.* 5 kPa) where both phases have the same Poisson's ratio ($v_{particle} = v_{gel}$) for bonded simulations when the applied strain was 0.5%
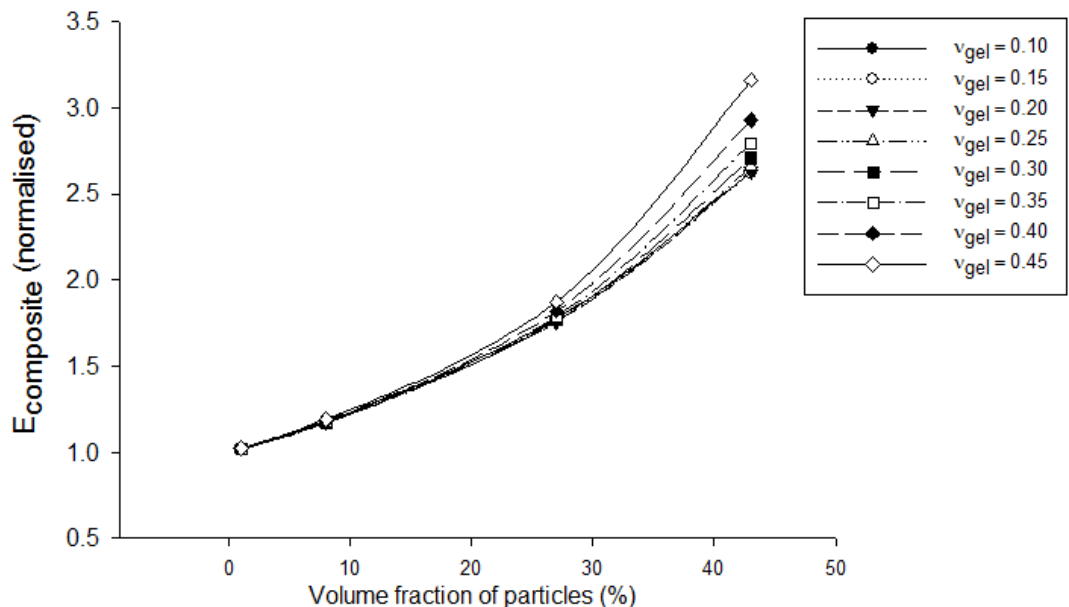
Figure 5.9. Change in $E_{composite}$ with volume fraction for when the stiffer particles (*i.e.* 1 MPa) were encapsulated in softer gels (*i.e.* 5 kPa) where both phases have the same Poisson's ratio ($v_{particle} = v_{gel}$) for bonded simulations when the applied strain was 5%
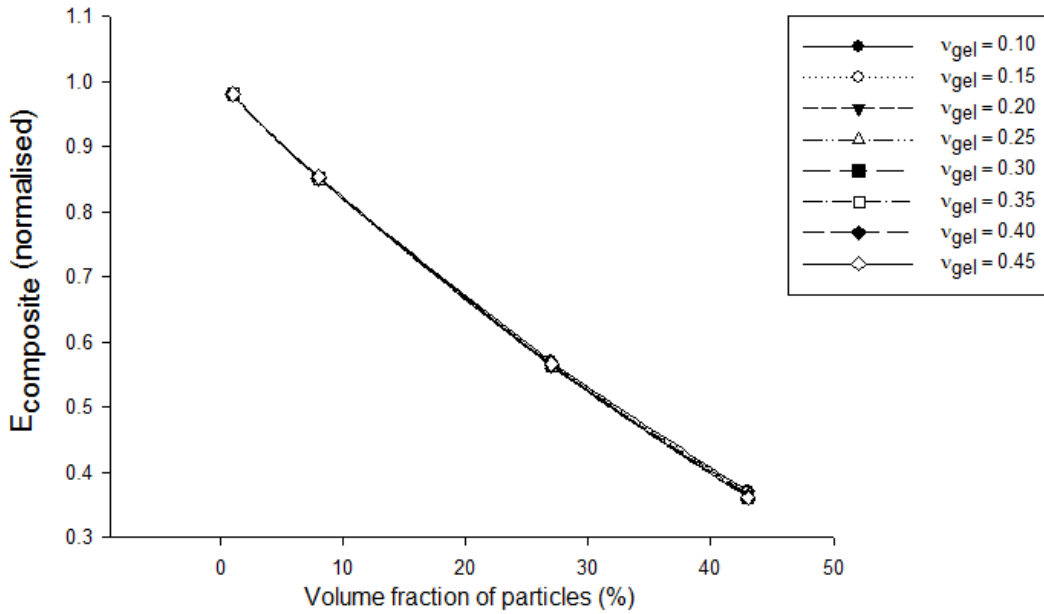
Figure 5.10. Change in $E_{composite}$ with volume fraction for when the softer particles (*i.e.* 5 kPa) were encapsulated in stiffer gels (*i.e.* 1 MPa) where both phases have the same Poisson's ratio ($v_{particle} = v_{gel}$) for bonded simulations when the applied strain was 5%

Similar characterisation and comparisons were carried out for the non-bonded simulations. For instance when $v_{gel} = v_{particle} = 0.45$, $E_{composite}$ values were found as 5.06 kPa, 5.48 kPa, 6.95 kPa and 8.96 kPa for 0.5% applied strain and as 5.06 kPa, 5.49 kPa, 7.03 kPa and 9.39 kPa for 5% applied strain at 1% - 43% volume fractions when the particles were stiffer than the gel in bonded simulation (see Table 5.2 and 5.3). For the opposite case at 5% applied strain, $E_{composite}$ values for the same volume fractions were found to be 197.12 kPa, 177.84 kPa, 130.38 kPa and 89.08 kPa, respectively. Similarly, $E_{composite}$ values were obtained using the other Poisson's ratios for the particle and the gel. From the results, it can be said that $E_{composite}$ values increased with increasing volume fraction of particles for the case of softer gel and they decreased with the increasing volume fraction of particles for the case of stiffer gel.

To be able to compare the effect of encapsulated particles on the overall stiffness, an additional condition was also tested for all the different cases to mimic the gels without encapsulation, *i.e.* when both stiffness values for the matrix and the particle were taken as the same value (either 5 kPa or 1 MPa, depending on the type of the case). The data obtained for $E_{composite}$

for the structures with particles were normalised by the data obtained from the case which mimicked the gels without encapsulation.

Figure 5.11-5.13 shows the changes in normalised $E_{composite}$ values obtained from bonded simulation using 0.5% and 5% strain values when $v_{particle}$ was changed from 0.10 to 0.45 by 0.05 at each step and for the same range of v_{gel} values, at four different volume fractions, namely 1%, 8%, 27% and 43%.

For the lower strain value (see Figure 5.11), it can be seen that the gel Poisson ratio did not affect the overall stiffness of the composite, since all of the curves obtained for different v_{gel} values coincided and there was no statistically significant difference between the normalised $E_{composite}$ values at the same $v_{particle}$ ($p > 0.05$). For an overall trend, normalised $E_{composite}$ values decreased when v_{cell} was increased from 0.1 to 0.45 for all v_{gel} values tested. At 0.5% applied strain, when the particle stiffness was higher compared to the gel stiffness, the overall change in normalised stiffness varied between 1.01 - 1.02 for when the volume fraction of particles was 1%, 1.10 - 1.16 for when the volume fraction of particles was 8%, 1.39 - 1.66 for when the volume fraction of particles was 27% and 1.79 – 2.29 for when the volume fraction of particles was 43%. Normalised $E_{composite}$ values increased with the volume fraction of particles due to the increase in stiffer phase.

For 5% applied strain for when the particle stiffness was higher than the gel stiffness (see Figure 5.12), normalised $E_{composite}$ values decreased when v_{cell} was increased from 0.1 to 0.45 for all v_{gel} values tested. The data obtained for $v_{gel} < 0.40$ at the range of $v_{particle}$ values tested were not significantly different ($p > 0.05$) however there were statistical significant differences for the data obtained for $v_{gel} \geq 0.40$ ($p < 0.05$). However as the volume fraction of particles increased, the difference in v_{gel} values showed statistically significant differences ($p < 0.01$). With the increasing volume fraction of particles within the matrix (8% - 43%), the order of the curves having different v_{gel} values reversed. At 5% applied strain, when the particle stiffness was higher compared to the gel stiffness, the overall change in

normalised stiffness varied between 0.98 - 1.05 for when the volume fraction of particles was 1%, 1.10 - 1.17 for when the volume fraction of particles was 8%, 1.41 - 1.69 for when the volume fraction of particles was 27% and 1.88 – 2.41 for when the volume fraction of particles was 43%. The normalised $E_{composite}$ values were independent of ν_{gel} at 0.5% applied strain and unlike the bonded simulation they depended on both ν_{gel} and ν_{cell} at 5% applied strain. Normalised $E_{composite}$ values increased with the volume fraction of particles due to the increase in stiffer phase.

A similar trend was observed at 5% strain for when the gel stiffness was higher than the particle stiffness (see Figure 5.13), compared to the opposite case where when the particle stiffness was higher than the gel stiffness at the same applied strain. For non-bonded case, normalised $E_{composite}$ values were not independent of $\nu_{particle}$ and a linear pattern was observed at all tested volume fractions (the non-linear appearance of the curves for 1% and 8% volume fraction of particles was due to the range of normalised $E_{composite}$). For 1% volume fraction of particles, only the data obtained for $\nu_{gel} = 0.45$ among the range of ν_{cell} values were significantly different ($p < 0.01$) than the rest of the ν_{gel} values tested, the data obtained for $\nu_{gel} = 0.10$ were also significantly different than the data obtained for $\nu_{gel} = 0.35$ and $\nu_{gel} = 0.30$. With the increasing volume fraction of particles within the matrix (at 43%), the order of the curves having different ν_{gel} values reversed. For this case, the overall change in normalised stiffness varied between 0.95 – 1.02 for when the volume fraction of particles was 1%, 0.86 – 0.93 for when the volume fraction of particles was 8%, 0.64 – 0.69 for when the volume fraction of particles was 27% and 0.44 – 0.49 for when the volume fraction of particles was 43%. Similar to the previous case, normalised $E_{composite}$ values depended both on ν_{gel} and $\nu_{particle}$ at 5% applied strain. For the case where the particles were stiffer, the overall trend was changed when the volume fraction was changed from 1% to 8% and stayed the same for the higher volume fraction of particles. For the opposite case where the gel was stiffer, the trend obtained at 1% was only changed as the volume fraction was increased to 43%.

Similar to the bonded simulations, the results revealed that the dependency of composite stiffness on Poisson's ratio varied under different strain values and it showed significant differences for the higher volume fraction of particles (above 8%) for all tested cases (i.e. stiffer particles and stiffer gel). The change in $E_{composite}$ values were independent of v_{gel} at lower applied strain. On the other hand, although a similar trend was observed for all tested v_{gel} values, $E_{composite}$ values changed with changing v_{gel}.
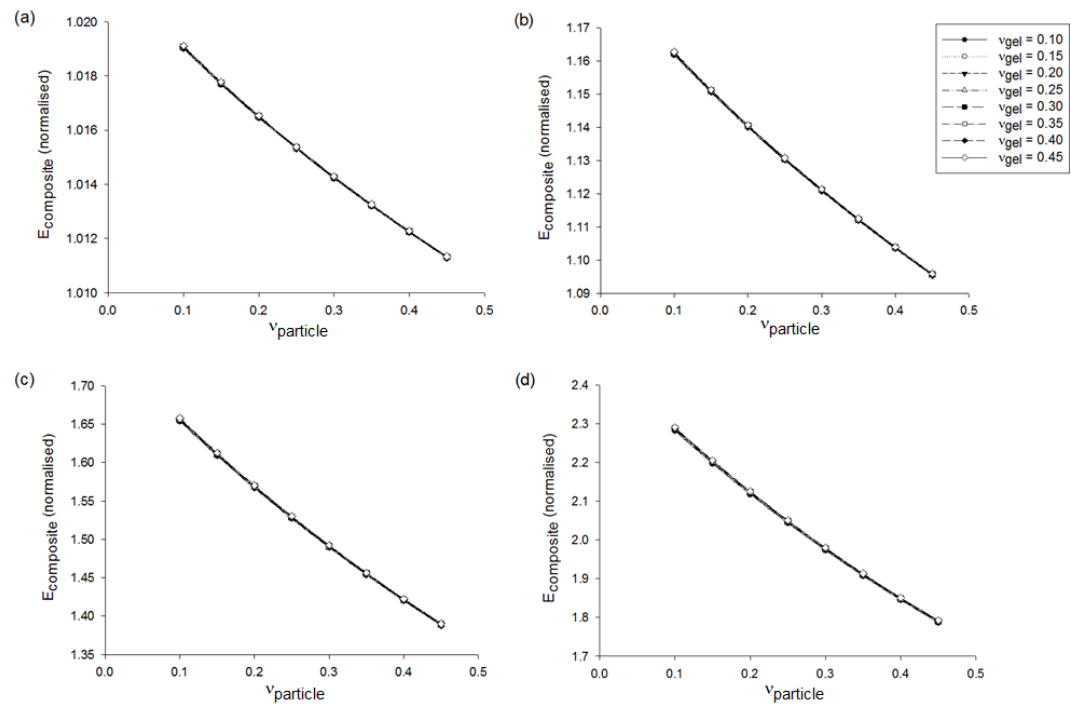
Figure 5.11. The change in normalised stiffness of composites for when the stiffer particles (*i.e.* 1 MPa) were encapsulated in soft gels (*i.e.* 5 kPa) for non-bonded simulations when the applied strain was 0.5% at different particle and matrix Poisson's ratios for (a) 1% volume fraction, (b) 8% volume fraction, (c) 27% volume fraction and (d) 43% volume fraction of encapsulated particles
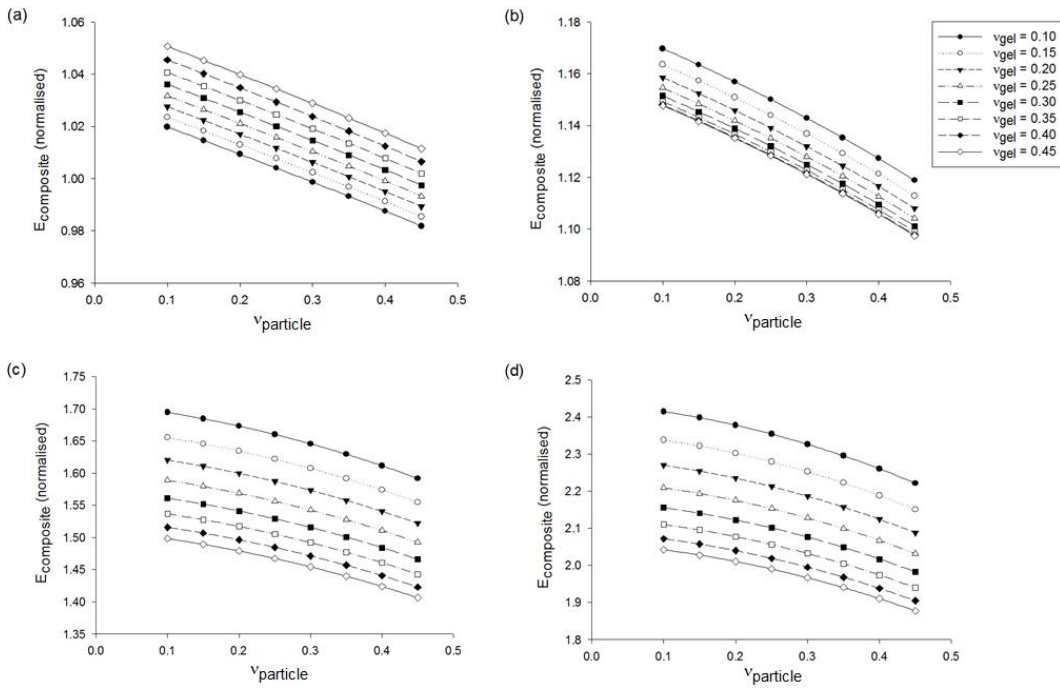
Figure 5.12. The change in normalised stiffness of composites for when the stiffer particles (*i.e.* 1 MPa) were encapsulated in soft gels (*i.e.* 5 kPa) for non-bonded simulations when the applied strain was 5% at different particle and matrix Poisson's ratios for (a) 1% volume fraction, (b) 8% volume fraction, (c) 27% volume fraction and (d) 43% volume fraction of encapsulated particles
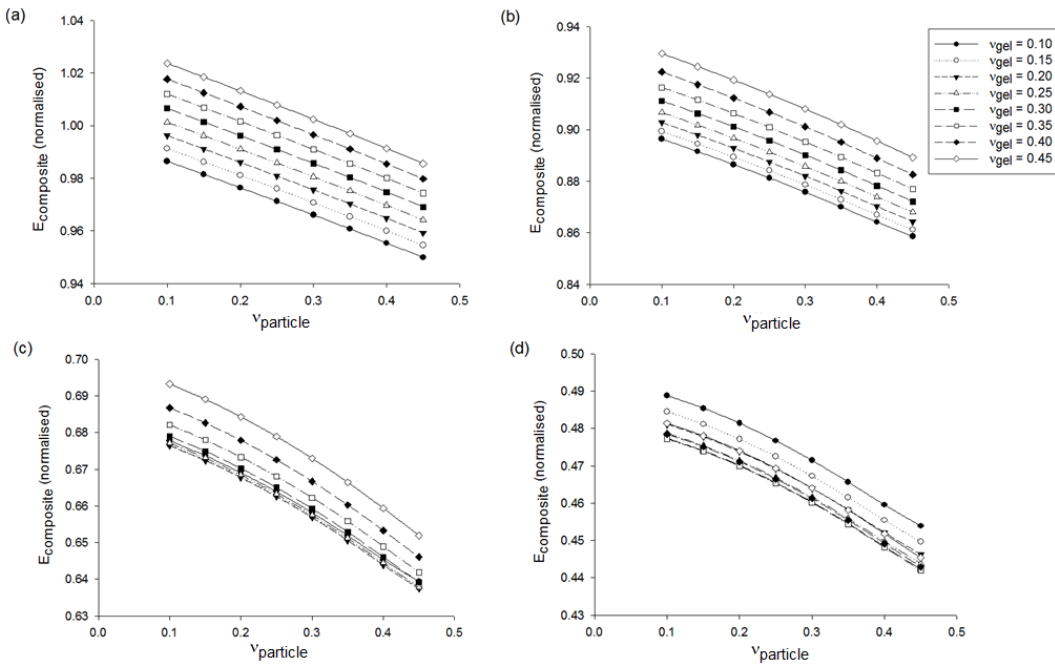
Figure 5.13. The change in normalised stiffness of composites for when the softer particles (*i.e.* 5 kPa) were encapsulated in stiffer gels (*i.e.* 1 MPa) for non-bonded simulations when the applied strain was 5% at different particle and matrix Poisson's ratios for (a) 1% volume fraction, (b) 8% volume fraction, (c) 27% volume fraction and (d) 43% volume fraction of encapsulated particles

After comparing normalised $E_{composite}$ values obtained from the tested Poisson's ratio range for both gel and particle in terms of Poisson's ratio, a similar comparison was carried out for the different volume fraction of particles for both cases where the gel and the particle had the same Poisson's ratio. When $\nu_{particle}$ and ν_{gel} values were different from each other, the curves obtained were coincident for 0.5% applied strain, they were coincident for all volume fractions and a similar pattern is observed. The difference between the normalised $E_{composite}$ values with phases having the same Poisson's ratio was between 0.9%, 6.4%, 18.7% and 27.4% for 0.5% applied strain and 0.8%, 6.6%, 20.5% and 28.6% for 5% applied strain for volume fractions of 1% - 43% for when the particles were considered stiffer (Fig. 5.14-5.15). For both strain values tested, when the volume fraction was small, the curves were almost coincident, especially at the smallest volume fraction (1%).

For the case where the gel was considered stiffer, this difference were calculated as 0.09%, 0.8%, 4.0% and 9.7% for volume fractions of 1% - 43%.The curves obtained for different Poisson's ratios almost completely coincided with each other at small volume fractions (see Fig. 5.16).
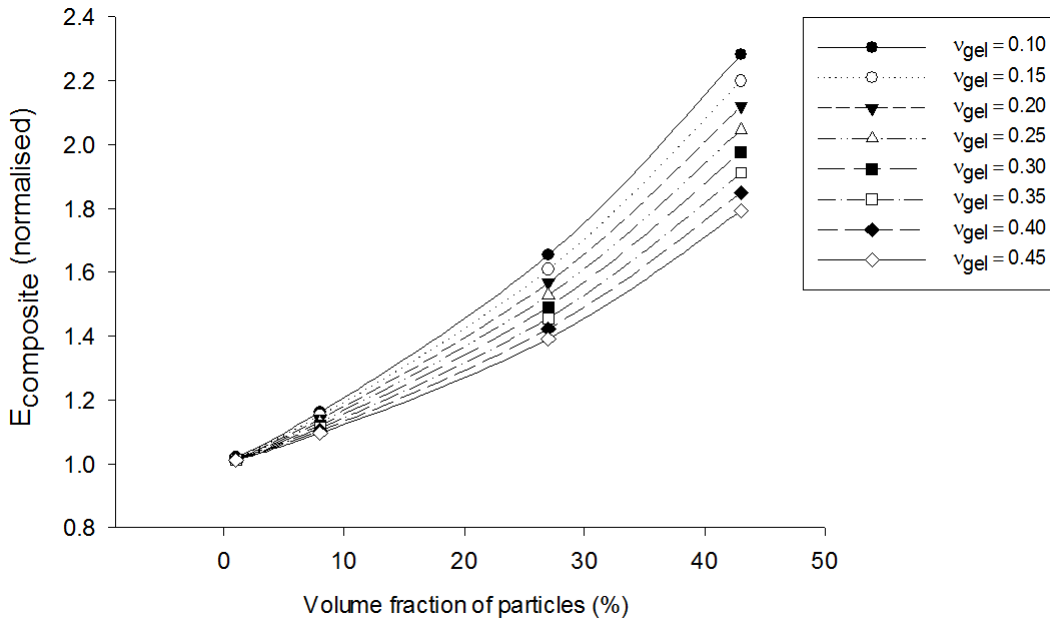
Figure 5.14. Change in $E_{composite}$ with volume fraction for when the stiffer particles (*i.e.* 1 MPa) were encapsulated in softer gels (*i.e.* 5 kPa) where both phases have the same Poisson's ratio ($\nu_{particle} = \nu_{gel}$) for non-bonded simulations when the applied strain was 0.5%
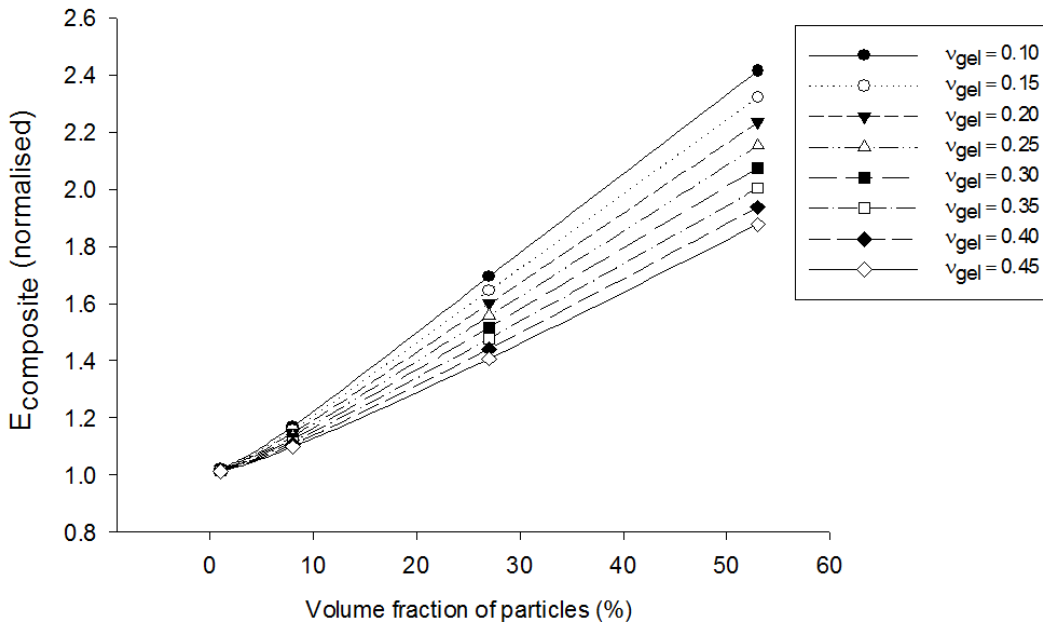
Figure 5.15. Change in $E_{composite}$ with volume fraction for when the stiffer particles (*i.e.* 1 MPa) were encapsulated in softer gels (*i.e.* 5 kPa) where both phases have the same Poisson's ratio ($\nu_{particle} = \nu_{gel}$) for non-bonded simulations when the applied strain was 5%
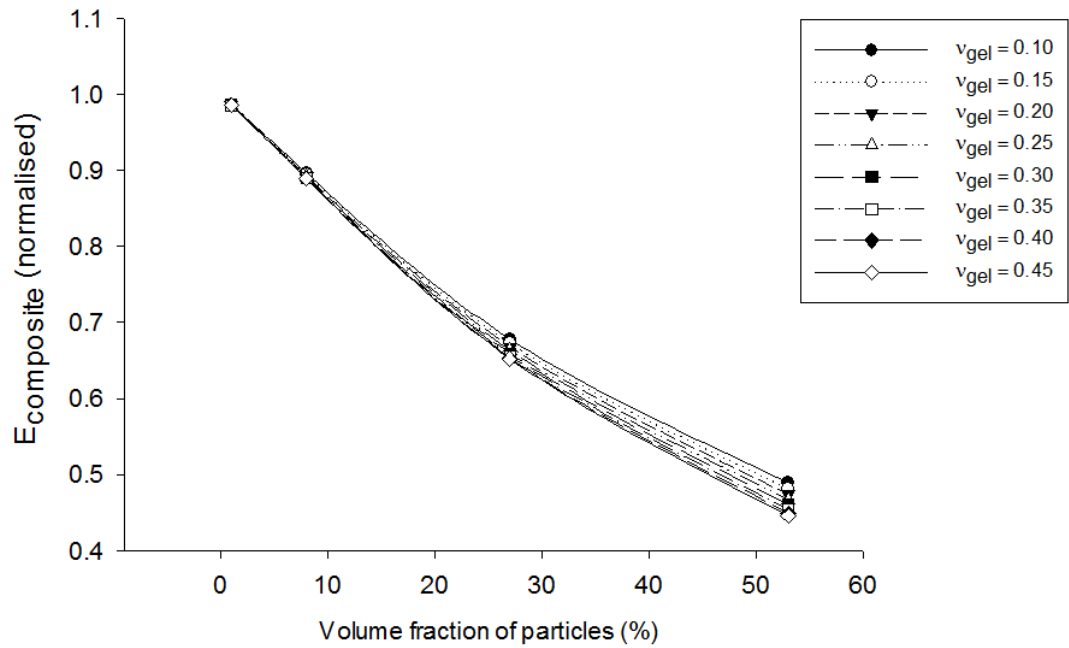
Figure 5.16. Change in $E_{composite}$ with volume fraction for when the softer particles (*i.e.* 5 kPa) were encapsulated in stiffer gels (*i.e.* 1 MPa) where both phases have the same Poisson's ratio ($\nu_{particle} = \nu_{gel}$) for non-bonded simulations when the applied strain was 5%

An incompressible material has a Poisson's ratio of 0.5 (Sokolnikoff, 1956). When hydrogels are fully swollen their properties resemble rubber like materials (Anseth *et al.*, 1996) which are highly incompressible and have a Poisson's ratio close to 0.5. Similarly, bacterial cells are rigid structures featuring viscoelastic properties (Tuson *et al.*, 2012a) and their adapted Poisson's ratio were documented between 0.4-0.5 in several studies (Touhami *et al.*, 2003; Tsang *et al.*, 2006; Limbert *et al.*, 2013). Therefore, in the mathematical models, both the matrix and the particle Poisson's ratios were selected as 0.45. For comparisons with the simulation results, the data used had the Poisson's ratio of 0.45 for both phases.

5.3.3 *Composite stiffness from mathematical models*

Hydrogels with encapsulated cells or particles were considered as composites since they were made by combining two materials having different properties. The gel and the particle were combined so that they did not dissolve in each other and a new material with its unique properties was created. To determine composite stiffness Voigt model, Reuss model, Hashin and Strikman model with upper and lower bounds were used (equations for these mathematical models were given in Table 5.1).

Stiffness values of composites obtained from mathematical models for different volume fraction of particles were summarised in Table 5.4 and plotted in Figure 5.17. To obtain these values, both the matrix and the particle Poisson's ratios were selected as 0.45. Similar to the simulations, the matrix and the particle stiffness were taken as 5kPa and 1MPa, respectively, providing the 200-fold difference.

Volume fraction of particles	Voigt Model (kPa)	Reuss Model (kPa)	HS Model – lower bound (kPa)	HS Model – upper bound (kPa)
0.01	14.95	5.05	3.72	20.87
0.02	24.40	5.10	5.62	24.93
0.03	38.63	5.17	8.52	31.18
0.05	58.33	5.28	12.60	40.09
0.08	84.60	5.43	18.14	52.50
0.11	118.33	5.64	25.45	69.37
0.16	160.51	5.92	34.90	92.09
0.21	211.96	6.30	46.93	122.58
0.27	273.65	6.84	62.14	163.91
0.34	346.58	7.59	81.33	221.03
0.43	431.66	8.72	105.53	302.46
0.53	529.66	10.52	136.21	424.27

Table 5.4. Stiffness values of composites obtained from mathematical models at different volume fraction of particles. To obtain these values, both the matrix and the particle Poisson's ratios were selected as 0.45. Matrix and particle stiffness values were taken as 5kPa and 1MPa, respectively (HS indicates Hashin and Strikman)
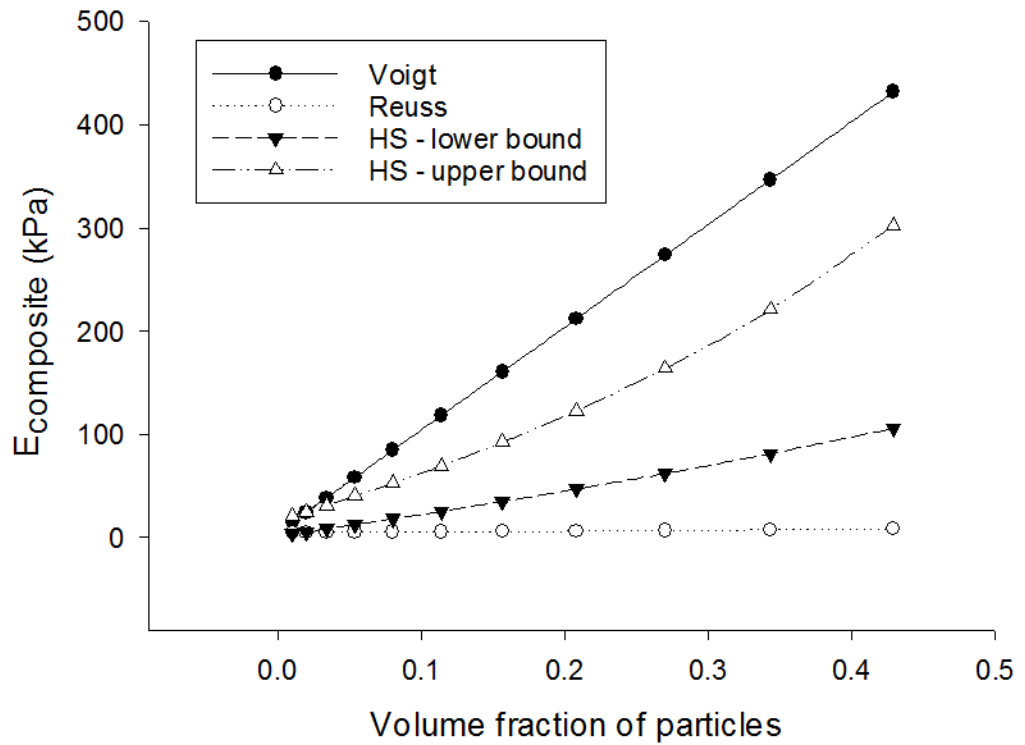
Figure 5.17. Change in $E_{composite}$ with the volume fraction of particles for different mathematical models where both the matrix and the particle Poisson's ratios were selected as 0.45 and their stiffness values were taken as 5kPa and 1MPa, respectively (HS indicates Hashin and Strikman)

Since the Poisson's ratio effects were tested for FEA simulations, the same range that was adopted in the simulations (0.1 - 0.45) were also tested using the lower and upper Hashin-Shtrikman bounds, for the test cases of stiffer particle and stiffer gel. 3D graphs were plotted to demonstrate the relationship between $E_{composite}$, volume fraction and v_{cell}. The data used to obtain these plots were when v_{gel} value was fixed at 0.1 and the $v_{particle}$ was changing between 0.1 - 0.45 so that $v_{particle} \geq v_{gel}$ behaviour of the bounds can be observed. The lower and upper HS bounds for the mentioned cases are given in Figure 5.18 and Figure 5.19.

(a)

(b)
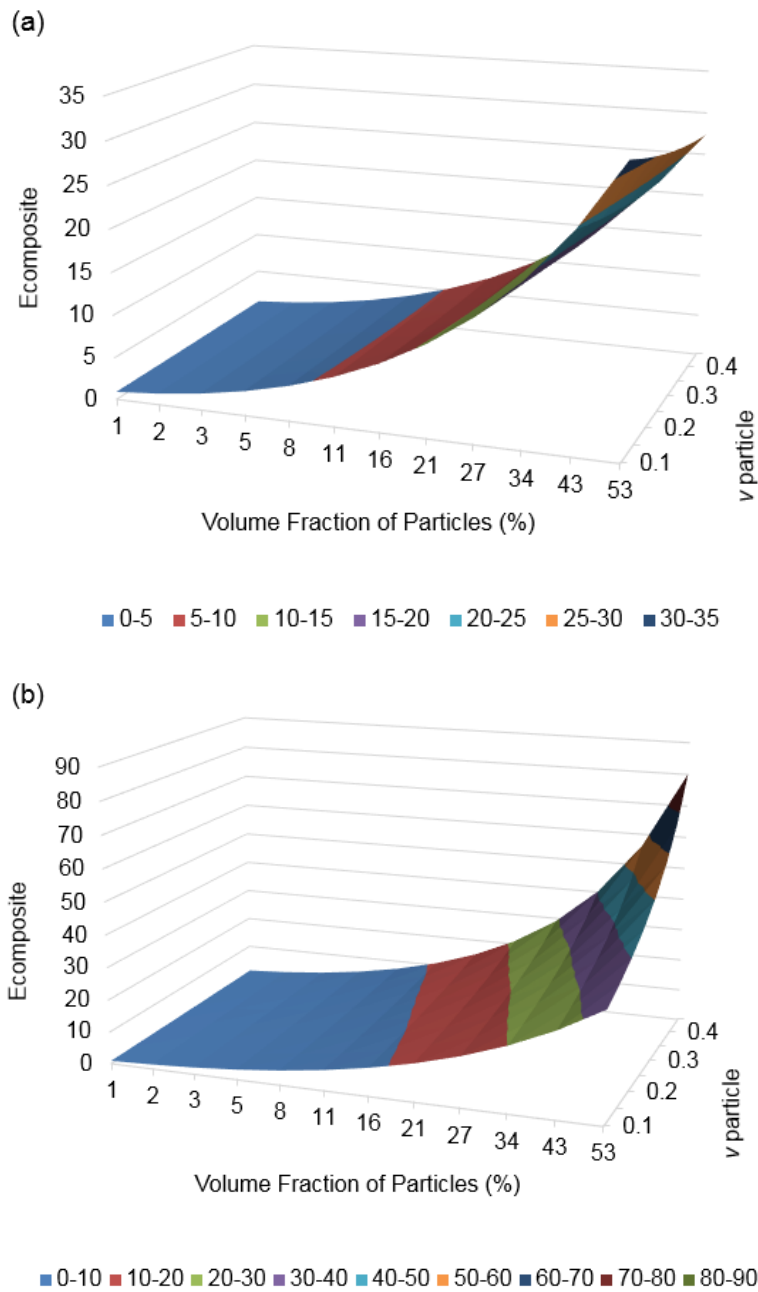
Figure 5.18. Change of $E_{composite}$ with different $v_{particle}$ values and volume fraction of particles for (a) HS lower bound and (b) HS upper bound for the case of stiffer particle

For the case of stiffer particle, the normalised $E_{composite}$ value increased with increasing volume fraction of particles for both HS lower bound and HS upper bound. The Poisson's ratio of particles did not change the stiffness value for HS lower bound where the stiffness value increased with increasing Poisson's ratio of particles for HS upper bound.
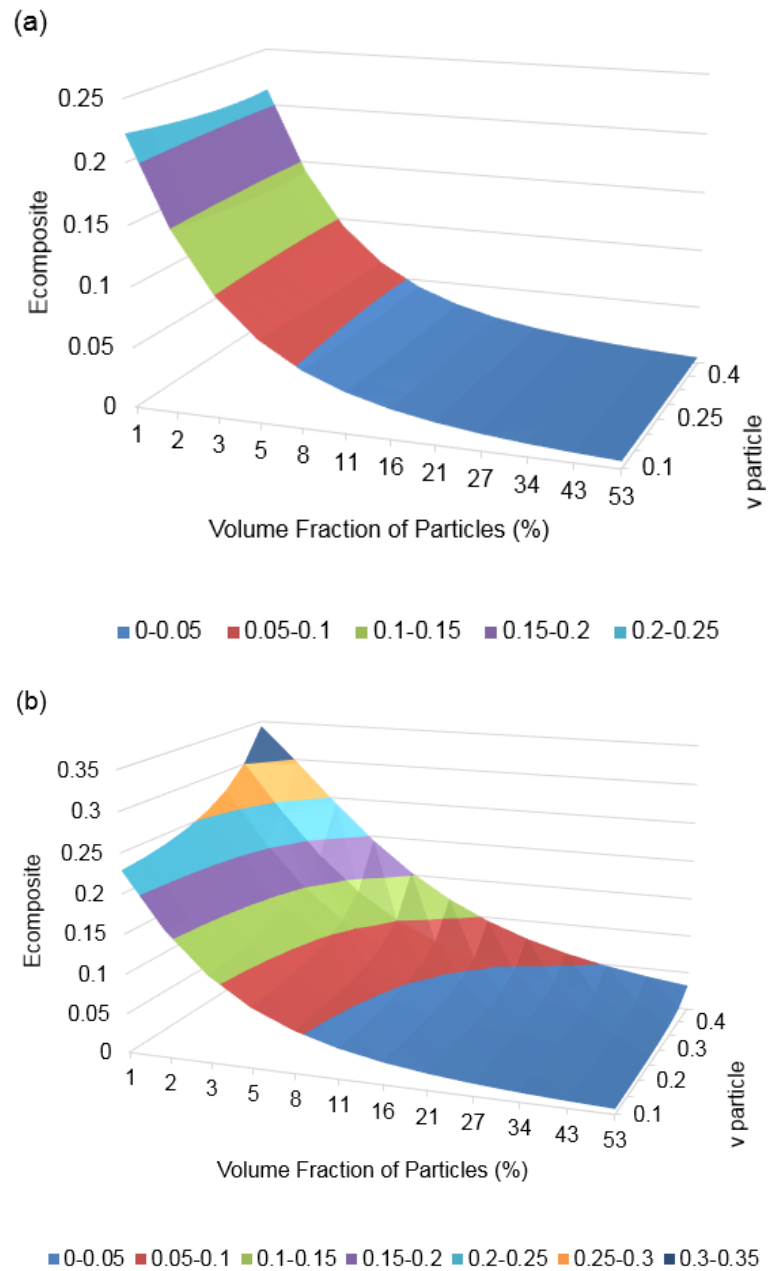
Figure 5.19. Change of $E_{composite}$ with different $v_{particle}$ values and volume fraction of particles for (a) HS lower bound and (b) HS upper bound for the case of stiffer gel

For the case of stiffer gel, the normalised $E_{composite}$ value decreased with increasing volume fraction of particles for both HS lower bound and HS upper bound. The Poisson's ratio of particles did not change the stiffness value for HS lower bound where a slight increase in stiffness was observed with increasing Poisson's ratio of particles for HS upper bound.

5.3.4 Comparisons between the mathematical models, simulation results and experimental results

$E_{composite}$ values obtained from mathematical model values were normalised by the adopted gel stiffness. Normalised mathematical model values, simulation values and the experimental data obtained from compression tests were plotted together for comparison (Fig. 5.20).

The results obtained from both bonded and non-bonded simulation were almost completely coincident with the Reuss model/HS-lower bound. There were two different groups of experimental data at 1% volume fraction: the first group was located between Voigt model/HS-upper bound and Reuss model which consisted of data points from LB and LB-no yeast extract gels (where significant differences were observed between the gels with and without encapsulation) and the second group was closer to Reuss model/HS-lower bound which consisted of data points belonging to 1% gels made with PBS, NB and LB-no tryptone (where no significant differences were observed between the gels with and without encapsulation).

The data obtained from the simulations represented the case for inert particles, where they were not affected by different media or possible structure irregularities of the gel. However, the experimental data suggested that the interactions between the bacterial cells and their environment caused the data to agree with different mathematical models which represent different alignment of the particles. All the simulated results and most of the experimental data agreed with Reuss model, except for the experimental data for bacteria encapsulated hydrogels made with LB or LB-no yeast extract.
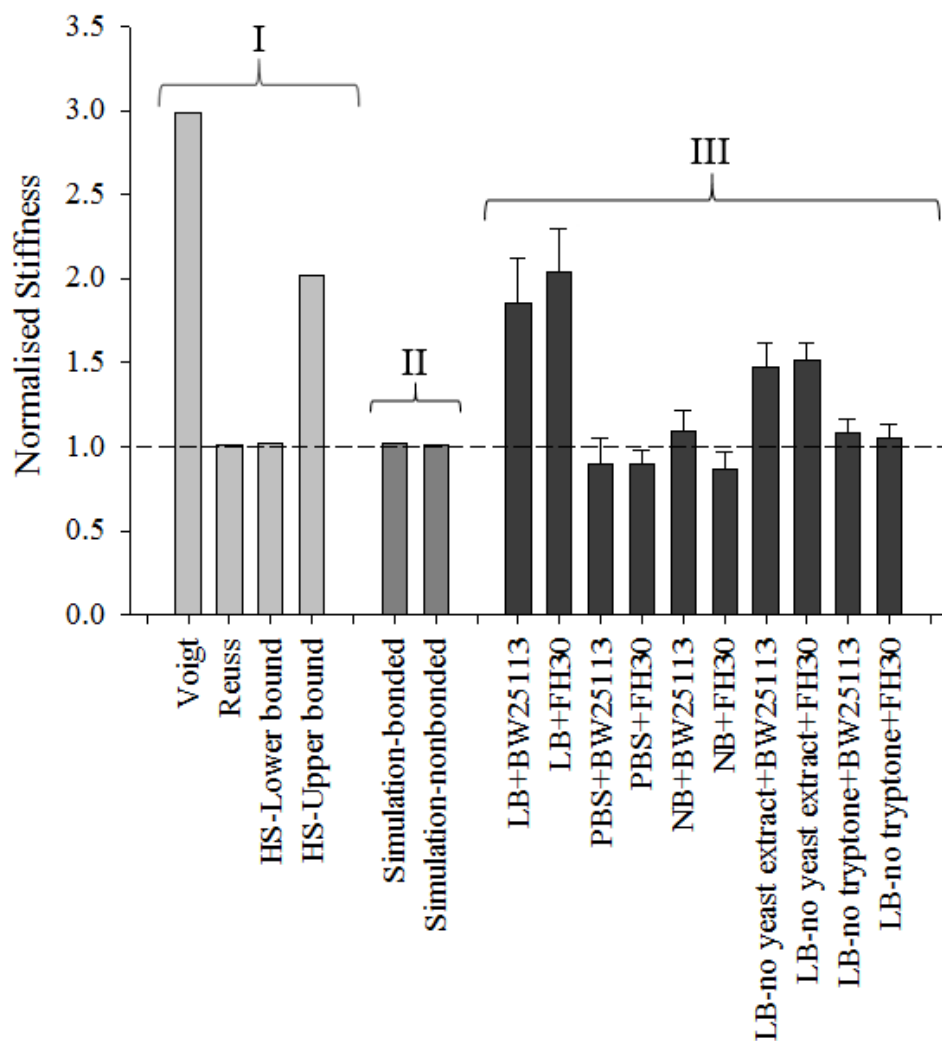
Figure 5.20. Normalised stiffness values obtained from mathematical models (group I - Voigt model, Reuss model, and Hashin and Strikman model with upper and lower bounds), simulations (group II) and experiments (group III) respectively for 5% applied strain. All the data were normalised by either the adapted gel stiffness, *i.e.* matrix without particles and separation (for simulations), or the corresponding 1% agarose gel stiffness with the same media/buffer (for experimental data). The dashed line represents the case without particles/encapsulated cells and the volume fraction of particles is 1%

5.4   Summary of Results and Conclusions

In this chapter, mechanical responses of hydrogels with encapsulated particles were modelled. Using finite element modelling, a parametric study was carried out, allowing many different variables that could affect the stiffness of the composites to be tested. Also, involving inert particles with constant properties provided an indication that the interactions were not limited to the interactions between the hydrogels and their liquid media, but showed that the encapsulated bacterial cells also played a role.

In the simulations, the effects of different variables on stiffness were tested including volume fraction of particles, Poisson's ratio of both phases and the applied strain. It was seen that as the volume fraction of particles increased, the effective stiffness of the composites also increased for both simulation cases (bonded or non-bonded). However, the change in effective stiffness of bonded composites were significantly higher than non-bonded composites, due to the allowed separation of the phases when a strain was applied. It was also shown that although the overall normalised stiffness values were similar in both simulation modes, the dependency on Poisson's ratio varied under different strain values and it showed significant differences for the higher volume fraction of particles (above 8%) for all tested cases (i.e. stiffer particles and stiffer gel).

Simulation results which were summarised in this chapter and experimental results which were documented in Chapter 4 were compared to several mathematical models. It was shown that non-bonded simulation results agreed with the Reuss model at every tested volume fraction. However, bonded simulation diverges from the Reuss model with increasing volume fraction. Also, different experimental data groups were compatible with different mathematical models.

The data obtained from the simulations represented the case for inert particles, where they were not affected by different media or possible structure irregularities of the gel. However, the experimental data suggested that the interactions between the bacterial cells and their environment caused the data to agree with different mathematical models which represent different alignment of the particles.

Previously, it was shown that topological interactions between DNA molecules and the agarose gels with flexible dangling ends caused a difference in the mobility of the DNA knots, i.e. making the characteristic electrophoresis arc bands into a straight line in the case of low dangling end density (Michieletto *et al.*, 2015). This can suggest that the interactions between the bacterial cells and the agarose gels polymer chains could also affect the alignment of the bacterial cells in the hydrogels when they are encapsulated, causing stiffness differences (see Figure 4.8). It also

suggested that more complicated computational model is required for such cases.

In the next chapter, rheological characterisation of agarose hydrogels with encapsulated bacterial cells under different conditions will be presented.

6 Rheological Responses of Agarose Gels and Bacterial Cell-Hydrogel Constructs

6.1 Introduction

The dynamic mechanical analysis is used for understanding the formation mechanism of the hydrogels and to provide information on the rheological properties of these materials by measuring the mechanical response of the samples when they are deformed under a periodic oscillation strain (Van Den Bulcke *et al.*, 2000; Tang *et al.*, 2007; Barbucci, 2009). This characterisation technique is widely used in material science (especially polymer science) due to its compatibility with viscoelastic liquids as well as viscoelastic solids (Kavanagh and Ross-Murphy, 1998), such as hydrogels. In addition to polymers, rheology is also widely used in human biology (Baskurt and Meiselman, 2003; Bhuanantanondh *et al.*, 2018), food science (Ahmed *et al.*, 2016) and pharmaceutics (Edsman *et al.*, 1996; Gaspar and Campos, 2003) to determine material properties with complex flow characteristics.

Due to accessibility and the versatility of the equipment, rheological tests are commonly applied to materials to characterise their viscoelastic properties (Yan and Pochan, 2010). There are various types of rheometers which can have different shearing geometries based on the type of material being tested. A rotational strain controlled rheometer can be used to measure flow properties (*i.e.* shear viscosity from flow tests) and dynamic material properties (*i.e.* shear moduli and phase angle from oscillation tests) which is done by measuring the applied torque under the test conditions. Using this apparatus, time dependent mechanical behaviour of viscoelastic materials can be determined as well, including creep or stress relaxation behaviour.

In Chapter 4, the observed mechanical response was in time domain, which was obtained from stress relaxation tests. Characterising hydrogels using rheology will extend the characterisation to a frequency domain which can reveal different mechanical phenomena. Therefore, in this chapter, rheological responses of agarose hydrogels will be characterised in terms of different variables including frequency, time and temperature. Also, the

effect of physical (*i.e.* stiffness) and chemical (*i.e.* chemical composition of the growth environment) factors on the mechanical interactions between bacterial cells and hydrogels, and bacteria cell mechanics when they are encapsulated in a 3D micro-environment will be explained when they are exposed to shear forces.

6.2 Methods

6.2.1 Sample preparation

The bacterial strains used for compression tests were *E. coli* BW25113 and *S. epidermidis* FH30 and they were grown as explained in Section 3.1.3. Based on the estimated volume of individual stationary phase bacterial cells (1.3µm^3 for *E. coli* (Phillips *et al.*, 2012) and 0.5µm^3 for *S. epidermidis (Foster, 1996))* and the final concentration of cells in the hydrogel, the volume of cells was estimated to occupy approximately 1% of the total volume of hydrogel. Based on the bacterial cell volume and the overall colony forming units within the overnight culture, approximately 20 ml of the *E. coli* overnight culture or 40 ml of *S. epidermidis* overnight culture was centrifuged at 4000 rpm for 10 min at 10°C. The supernatant was removed and the bacterial cells were re-suspended in the growth media or the buffer as the same used for the hydrogel. The hydrogels to be tested and the encapsulation process were prepared as explained in Section 3.2.2.

6.2.2 Rheometer setup and test conditions

In order to obtain the rheological properties of agarose, several rheological tests were applied using a rheometer (Kinexus pro+, Malvern Instruments, Malvern, UK) shown in Figure 6.1. The applied tests to observe the mechanical behaviour of the hydrogels were amplitude sweep test in order to determine the linear viscoelastic region, frequency sweep test to measure viscoelastic response at a frequency range, shear strain rate sweep tests to determine the flow characteristics, oscillation single frequency tests to measure viscoelastic response at a specific frequency and temperature sweep tests to measure viscoelastic response at a temperature range. All the tests (except for the temperature sweep tests) were carried out at two different temperatures: 20°C to provide room temperature conditions and 37°C as this temperature is the physiological condition. The parallel plates used in the rheometer were serrated (Figure 6.2) in order to avoid slippage

during loading and testing (when the samples were under shear). The serrated part of the bottom plate geometry also helped with accurate positioning of the sample and avoid sample slippage. Solvent trap cover (Figure 6.3) and the liquid reservoir were used during the tests and the appropriate liquid medium or buffer was spread around the hydrogels to prevent the samples from drying, as the dried samples would have different mechanical properties because of the change in the water content.
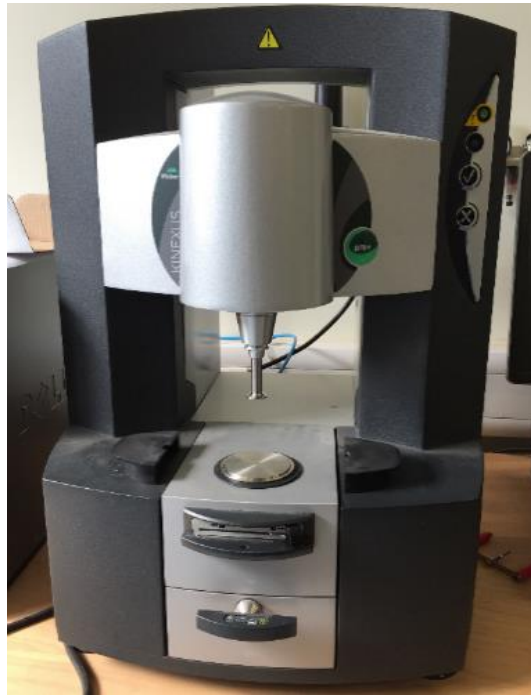
Figure 6.1. Rheometer setup used for rheological tests. This setup involves a fixed bottom plate and a moving top plate
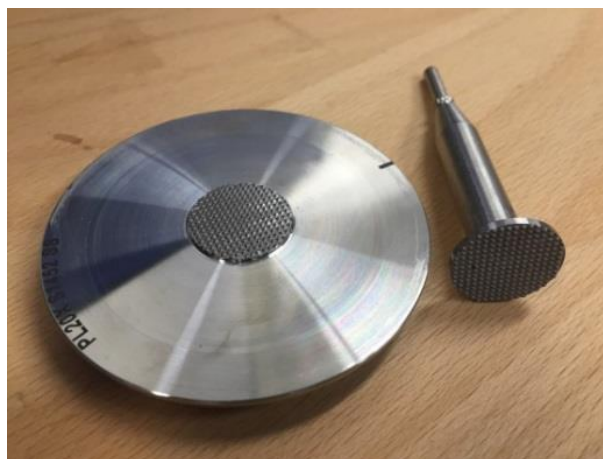
Figure 6.2. Serrated parallel plates to prevent slippage during loading and testing. The diameter of the serrated part of the bottom plate and the top plate were both 20 mm, matching the hydrogel sample diameter

Figure 6.3. Solvent trap system used during testing to prevent drying of the samples

Prior to testing, the system was calibrated to ensure accurate gap sensitivity and the temperature of the system was adjusted to the test temperature to avoid any changes in mechanical properties during temperature stabilisation process. When the temperature of the plates stabilised, the gap between the hydrogel samples and the top plate was adjusted. For this, each sample was placed on the serrated part of the bottom plate. The top plate approached the hydrogel sample so that first of all it was not in contact with the sample and there was approximately 2 mm between the top plate and the hydrogel. By doing this, the movement of the top plate while approaching and finding the sample surface and the initial force applied to the sample by the top plate could be controlled. The control criteria involved two main considerations: the surfaces of both the bottom and the top plates were completely in contact with the hydrogel surfaces and the obtained gap remained the same throughout the test. The initial normal force applied to the sample was chosen as 0.1 N. This applied normal force was sufficient for the plates to be completely in contact with the sample and the gap obtained after applying the initial force was maintained during testing.

6.2.3 Amplitude sweep tests

Amplitude Sweep tests were used to determine the linear viscoelastic region (LVER) of the hydrogels. In the LVER, the stress/strain ratio remains constant which indicates that the elastic modulus remains constant too. A drop in complex modulus indicates a breakdown of material structure and after this region, the response cannot be considered elastic. In order to avoid structure breakdown and ensure that the obtained stress response

was elastic, the LVER was determined using the complex modulus and shear strain curve (Figure 6.4). This curve was plotted in a log-log scale to better identify the LVER. The shear strain value corresponding to the limit of LVER or any other strain value below that can be chosen as a strain value as an input for the following tests. The strain range for this test was chosen as 0.01% - 100%. This test was applied at both 20°C and 37°C to hydrogels with and without encapsulation since the presence of encapsulated particles might change the limit of LVER. To check the effect of applied frequency on the LVER, various frequency values were tested, namely 0.1 Hz or 1 Hz. The analysed samples for this test were 1-5% LB gels without encapsulation, 1% PBS gels without encapsulation, 1% NB gels without encapsulation, 1% LB, 5% LB and 1% PBS gels with encapsulated *E. coli* BW25113 cells and 1% NB gels with encapsulated *S. epidermidis* FH30 cells.
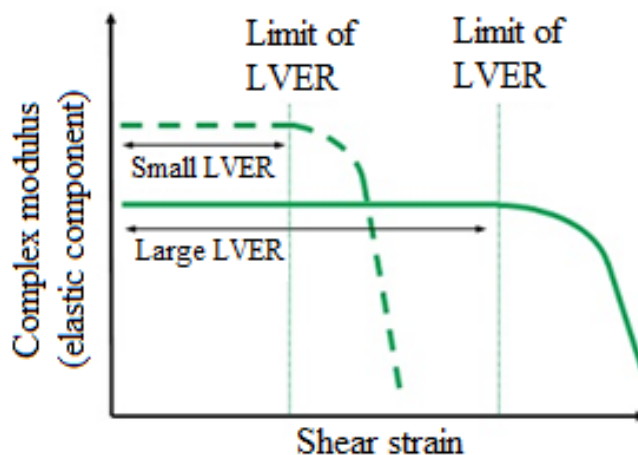
Figure 6.4. The curve showing the change of elastic component of complex modulus with shear strain. This curve was plotted in a log-log scale to better identify the LVER (Kinexus rSpace, version 1.30, Malvern Instruments Ltd., MA, USA)

6.2.4 Frequency sweep tests

Frequency sweep tests involved oscillating the sample at a fixed strain (within LVER that was identified by amplitude sweep tests) while varying the frequency. Depending on the type of the material, the responses vary. The responses for viscoelastic solid, gel like and viscoelastic liquid behaviours are shown in Figure 6.5. From frequency sweep tests, information about complex shear modulus, elastic and viscous shear modulus components, shear viscosity and phase angle were obtained. This test was applied at

both 20°C and 37°C to hydrogels with and without encapsulation at a frequency range of 0.1 Hz – 10 Hz. The duration of each test was 30 min. The analysed samples for this test were 1% and 5% LB gels with and without encapsulated *E. coli* BW25113 cells. These tests were also carried out for two additional strain values of 1% and 5% (which represented values outside of LVER) to show the effect of applied strain on the sample mechanical properties. The tests were repeated at least 3 times for all different sample groups.
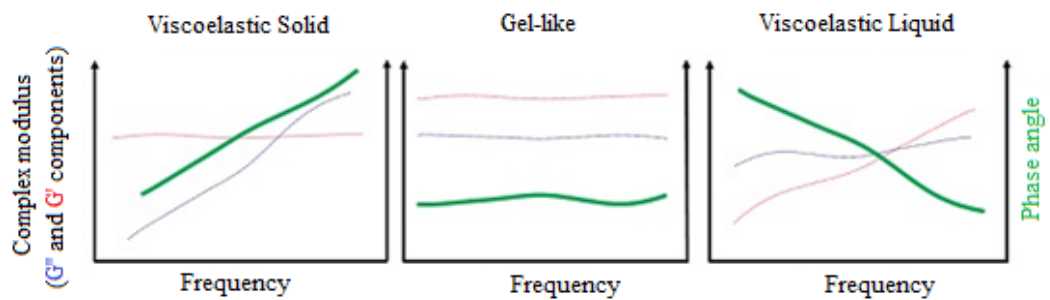
Figure 6.5. Responses of viscoelastic solid, gel like and viscoelastic liquid materials. The blue line represents the change in the viscous component of the complex modulus, the red line represents the change in the elastic component of the complex modulus and the green line represents the change in phase angle for viscoelastic solids, gel like materials and viscoelastic liquids (Kinexus rSpace, version 1.30, Malvern Instruments Ltd., MA, USA)

6.2.5 Single frequency tests

Similar to frequency sweep tests, single frequency tests also involved oscillating the hydrogel sample at a fixed strain (within LVER that was identified by amplitude sweep tests). As the name of the test indicates, these tests were carried out at a specific frequency value of 1 Hz. From single frequency tests, information about complex shear modulus, elastic and viscous shear modulus components, shear viscosity and phase angle were obtained with respect to time which also indicated time dependent shear properties. The samples were oscillated at 1 Hz at a constant temperature (either 20°C or 37°C) for 30 min. The analysed samples for this test were 1% LB gels with and without encapsulated *E. coli* BW25113 cells, 1% PBS gels with and without encapsulated *E. coli* BW25113 cells and 1% NB gels with and without encapsulated *S. epidermidis* FH30 cells. The tests were repeated at least 3 times for all different sample groups.

6.2.6 Temperature sweep tests

In temperature sweep tests, the temperature range tested was between 20°C and 40°C, while the temperature was increased 1°C every 20 sec. These tests involved oscillating the hydrogel sample at a fixed strain (within LVER that was identified by amplitude sweep tests) and at a specific frequency value of 1 Hz. The reason for carrying out the temperature sweep tests at this specified temperature range was to observe the effect of temperature on the rheological properties of the samples in more detail, rather than concentrating only on two specific temperature values that were considered in other rheological tests. From temperature sweep tests, information about complex shear modulus, elastic and viscous shear modulus components, shear viscosity and phase angle were obtained with respect to temperature. The analysed samples for this test were 1% LB gels with and without encapsulated *E. coli* BW25113 cells. The tests were repeated at least 3 times for all different sample groups.

6.2.7 Shear strain rate sweep tests

In these tests, the shear rate applied was increased and the corresponding viscosity values were recorded. Using these values, flow curves were obtained which showed the change in viscosity with shear strain rate. This test was applied at both 20°C and 37°C to hydrogels with and without encapsulation at a fixed frequency of 1 Hz. The shear strain rate range was taken as 0.01 to 100 s^{-1}. The analysed samples for this test were 1% LB gels with and without encapsulated *E. coli* BW25113 cells. The tests were repeated at least 3 times for all different sample groups.

6.2.8 Statistical analysis

Analysis of Variance (ANOVA) with Tukey's post hoc test was applied to determine the statistical differences between hydrogels with and without encapsulation and of gels made with different growth media or buffer for the data acquired from the rheological tests. The significance level (α) was taken as 0.05. The statistical analysis was carried out using Minitab 17.1.0.

6.3 Results and Discussion

6.3.1 Determining linear viscoelastic region (LVER) by amplitude sweep tests

Amplitude sweep tests were applied to agarose hydrogels having different concentrations that were made with different growth media or buffer, and with different encapsulation status. Sample outcomes from the amplitude sweep tests for 2% LB hydrogels without encapsulation and 1% LB hydrogels with encapsulated *E. coli* BW25113 cells are presented in Figure 6.6. In this figure, the change in elastic modulus, viscous modulus and phase angle with shear strain is presented and the areas indicated show the linear viscoelastic region (LVER). These areas were selected based on the criteria where the change in the elastic modulus between the two consecutive data points were less than 5% and the overall trend was constant.

For all tested concentrations of hydrogels, different growth media used and different encapsulation status, the upper limit strain value for LVER was determined as 0.1%. Any value taken between 0.01 and 0.1 would still be in LVER, so the hydrogel structure was not deformed if the shear strain value was chosen according to this range for the following tests. Therefore, they can be considered as small amplitude oscillatory shear (SAOS) tests. However, if the shear strain value was chosen outside of LVER, the structure of the material could start to break down and the tests with such applied strain values are considered as large amplitude oscillatory shear (LAOS) tests.

As can be seen from Figure 6.6, a similar LVER range was observed for the hydrogels with encapsulated bacterial cells as well. This range was found to be independent of test temperature (20°C and 37°C) and the applied frequency (0.1 Hz and 1 Hz). For all the tested samples, to keep this variable constant, the shear strain from LVER was selected as 0.01% for the following tests.
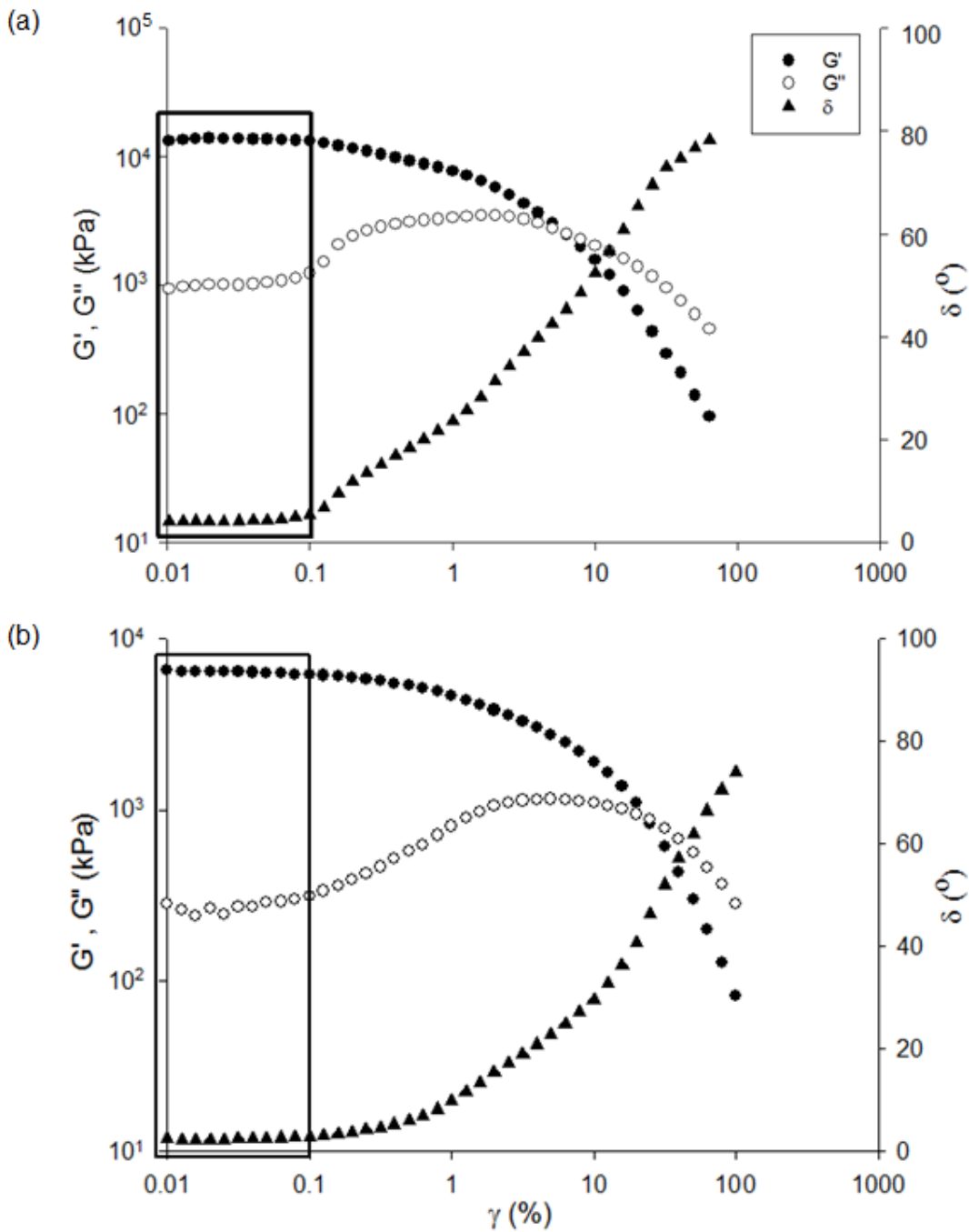
Figure 6.6. Change of elastic modulus, viscous modulus and phase angle with shear strain for (a) 2% agarose hydrogels made with LB when the frequency was 0.1 Hz and (b) 1% LB hydrogels with encapsulated *E. coli* BW25113 cells when the frequency was 1 Hz. The indicated areas represent where the change in the shear moduli is negligible and the corresponding shear strain range indicates the LVER. Shear moduli and shear strain values are plotted in a log-log scale, error bars are removed for better visualisation

6.3.2 Determining mechanical properties of hydrogels from frequency sweep tests and the effect of shear strain

After figuring out the appropriate shear strain value, frequency sweep tests were applied to 1% and 5% agarose gels made with LB to study the dependence of shear moduli, shear viscosity and phase angle on frequency. In order to check the effect of shear strain, three different values were chosen, one value within the LVER and two values out of this region.

Firstly, while carrying out these tests, the shear strain was chosen within the LVER so that the structure of the material was not changed and only the effect of frequency on the mechanical properties was observed. For this reason, the shear strain value was chosen as 0.01%.

Sample outcomes showing the change of elastic and viscous shear moduli and phase angle with frequency for 1% LB gels with and without encapsulated cells are given in Figure 6.7. The start and end frequency values for the given figure was 10 Hz and 0.1 Hz, respectively. The complex shear modulus, elastic modulus, viscous modulus and phase angle values were independent of frequency so that for the given frequency range the material was gel-like (see Figure 6.5). When the storage modulus is greater than the loss modulus and the phase angle is less than 45°, the material shows more of solid characteristics and when the loss modulus is greater than the storage modulus and the phase angle is greater than 45°, the material shows more of liquid characteristics (Barnes, 2000; Zuidema *et al.*, 2014). From the data collected for the different concentration hydrogels with and without encapsulation at both tested temperatures, it can be said that when the applied shear strain value was selected from LVER, all hydrogels showed solid characteristics. A similar frequency independent trend was observed for all samples having different concentrations tested at both 20ºC and 37ºC.
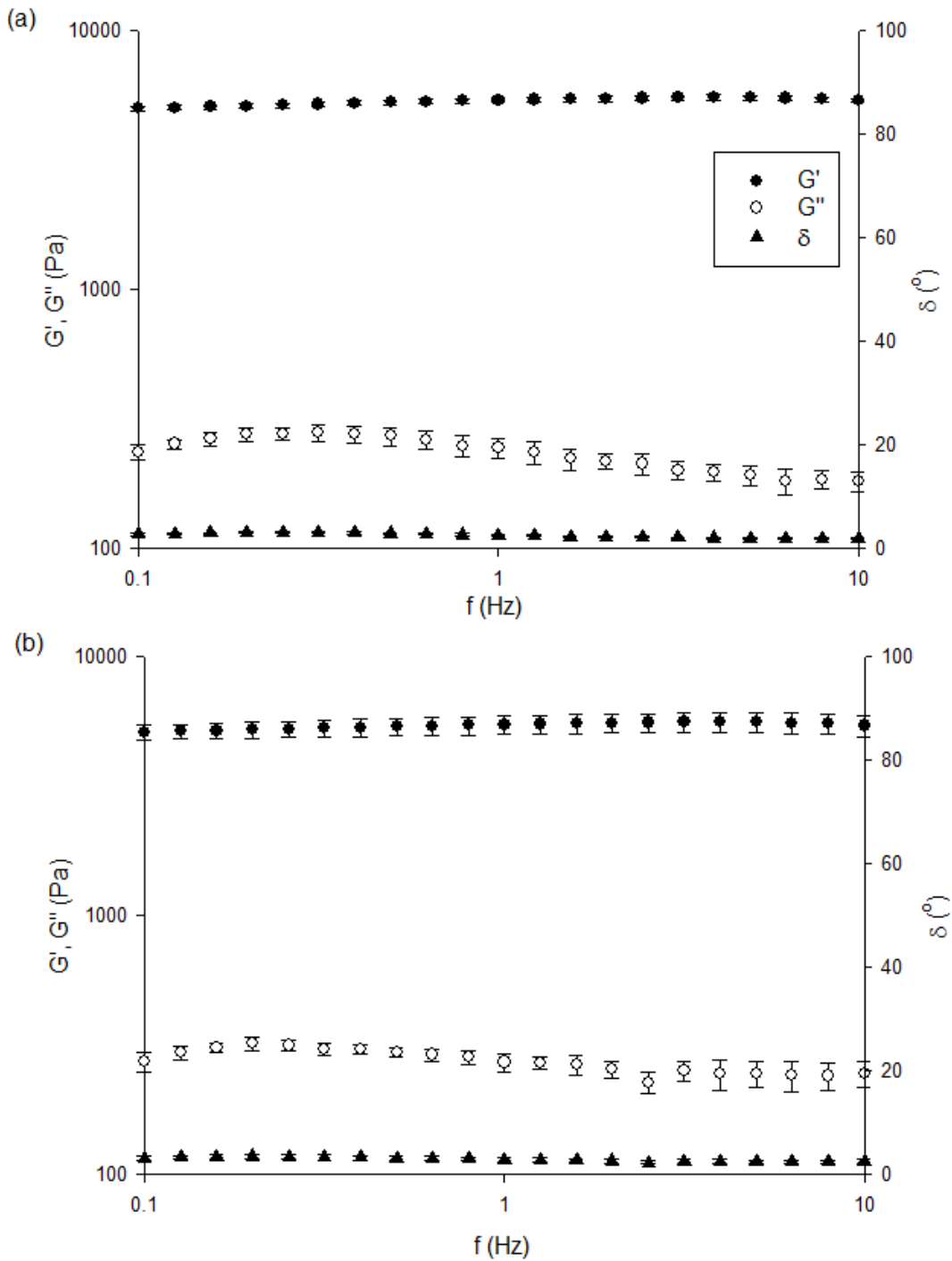
Figure 6.7. Dependence of elastic and viscous shear moduli and phase angle on frequency for (a) 1% LB agarose gel without encapsulation and (b) 1% LB agarose gel with encapsulated *E. coli* BW25113 cells, when the applied strain was 0.01% and the temperature was 20ºC. Shear moduli and frequency values are plotted in a log-log scale

At the shear strain of 0.01%, complex shear modulus, elastic and viscous components of shear modulus of hydrogels without encapsulation are summarised in Table 6.1. As can be seen from the table, the shear moduli increased with concentration at both tested temperatures. For both

126

concentrations, the elastic shear modulus values were significantly higher than the viscous modulus values ($p \leq 0.01$), so the gels had solid characteristics. Also, when the complex shear modulus and the elastic shear modulus values were compared, no significant differences were observed ($p > 0.05$) for all the groups tested. Therefore the gels were elastically dominated. A similar pattern was obtained for gels with encapsulated bacterial cells. Although the documented mechanical properties of the agarose hydrogels varied in literature due to the liquid media used to make the gels and the type of agarose, the dependence of agarose hydrogel shear properties on frequency were found to be similar to the behaviour observed in this study within the frequency range tested (Balgude *et al.*, 2001; Ulrich *et al.*, 2010; Zuidema *et al.*, 2014). Different types of hydrogels also presented frequency independent behaviour at a similar frequency range (He *et al.*, 2011; Head *et al.*, 2016).

Stiffness of 1% gels decreased as the temperature increased from 20°C to 37°C however an opposite behaviour was observed for 5% gels. The reason behind this behaviour can be explained by the different density of cross-links of the hydrogel structures. 5% gels have significantly more cross-links compared to that of 1% gels and an increase in temperature can change the structure of the gels resulting in opposite behaviour of the observed stiffness.

Gel percentage (%)	Temperature (^{o}C)	Complex shear modulus (kPa)	Elastic shear modulus (kPa)	Viscous shear modulus (kPa)
1	20	5.33 ± 0.11	5.32 ± 0.11	0.23 ± 0.02
5		16.21 ± 1.62	15.55 ± 1.57	4.56 ± 0.39
1	37	3.77 ± 0.63	3.76 ± 0.63	0.23 ± 0.02
5		27.95 ± 7.22	25.98 ± 6.26	9.58 ± 5.88

Table 6.1. Complex shear modulus, elastic shear modulus and viscous shear modulus over the frequency range of 10 Hz and 0.01 Hz at a shear strain of 0.1% for 1% and 5% LB agarose gels without encapsulation (data represented as mean ± standard deviation, $n \geq 3$)

Complex shear modulus, elastic shear modulus and viscous shear modulus values of 1% and 5% hydrogels with and without encapsulation were normalised and they are plotted in Figure 6.8 and Figure 6.9 respectively. At 20°C, there were no significant differences between the complex shear moduli of gels with and without encapsulated bacterial cells ($p > 0.05$) however at 37°C complex shear moduli of gels with encapsulation were significantly less ($p \leq 0.01$) compared to gels without encapsulation. *E. coli* cells grow and double quicker at 37°C and an increase in the number of bacterial cells or a change in bacterial cell size may have resulted in the destruction of the gel structure for the lower concentration of agarose, causing the shear moduli values to reduce at higher temperatures. However, for 5% agarose hydrogels, a similar amount of decrease was not observed which can be attributed the denser polymer chain structure which can restrict bacterial growth. For 1% LB gel, the moduli of cell – hydrogel construct decreased by about 50%. Whilst, the moduli of cell – hydrogel construct dropped by approximately 30%, compared to its 5% LB gel counterpart.
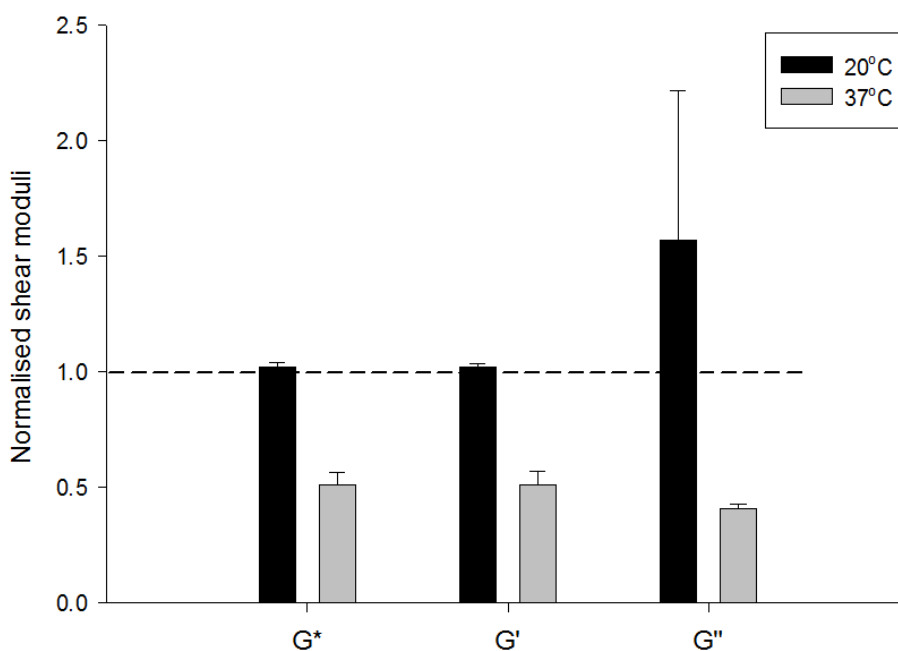
Figure 6.8. Normalised complex shear modulus, elastic shear modulus and viscous shear modulus of 1% LB gels with and without encapsulated *E. coli* BW25113 obtained from frequency sweep tests at 0.01% strain and at 20°C and 37°C. The dashed line shows the normalised value for gels without encapsulation and error bars represent standard deviation
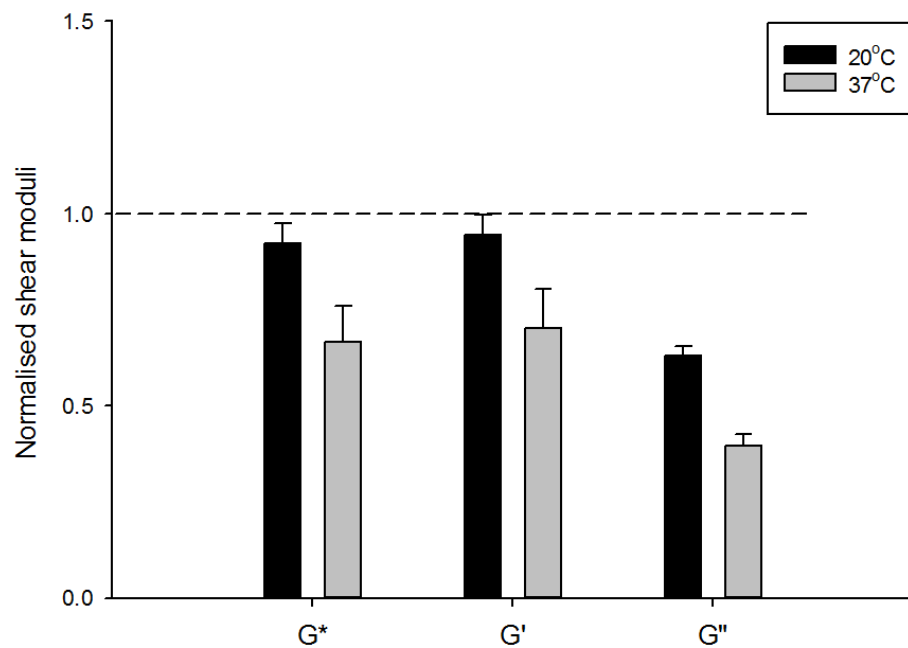
Figure 6.9. Normalised complex shear modulus, elastic shear modulus and viscous shear modulus of 5% LB gels with and without encapsulated *E. coli* BW25113 obtained from frequency sweep tests at 0.01% strain and at 20ºC and 37ºC. The dashed line shows the normalised value for gels without encapsulation and error bars represent standard deviation

6.3.2.1 Determining mechanical properties of hydrogels from frequency sweep tests using a shear strain value out of LVER

For the frequency sweep tests with a shear strain rate value out of LVER, the shear strain values were chosen as 1% and 5%. A sample outcome of elastic and viscous shear moduli and phase angle for 1% agarose made with LB is given in Figure 6.10. The start and end frequency values for the given figure were 10 Hz and 0.01 Hz, respectively. The complex shear modulus, elastic modulus, viscous modulus and phase angle values were independent of frequency so that for the given frequency range the material was gel-like over the test duration of 30 min. From the data collected for the different concentration hydrogels with and without encapsulation at both tested temperatures, it can be said that at the adopted temperatures when the applied shear strain value was selected out of LVER, the hydrogels showed solid characteristics.
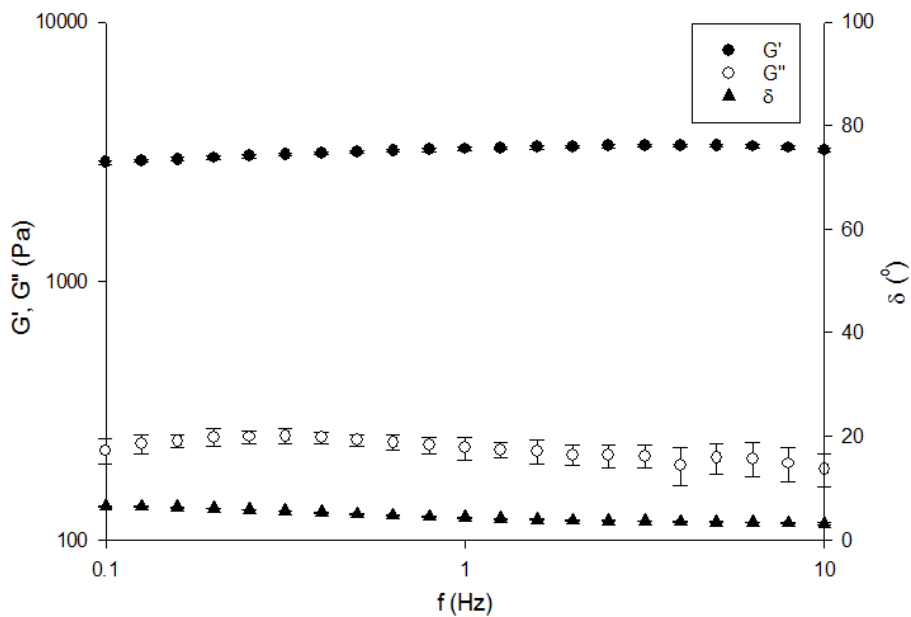
Figure 6.10. Dependence of elastic and viscous shear moduli and phase angle on frequency for 1% LB agarose gel without encapsulation when the applied strain was 1% and the temperature was 20°C. Shear moduli and frequency values are plotted in a log-log scale

At the shear strains of 1% and 5%, complex shear modulus, elastic and viscous components of shear modulus of hydrogels without encapsulation are summarised in Table 6.2. For both concentrations and both tested temperatures, the elastic shear modulus values were significantly higher than the viscous modulus values ($p \leq 0.01$), which confirmed the solid characteristics of the hydrogels. Also, when the complex shear modulus and the elastic shear modulus values were compared, no significant differences were observed ($p > 0.05$) for all the groups tested.

For 1% gels, a decrease in stiffness was observed for both when the temperature was increased to 20°C to 37°C and when the applied strain was increased from 1% to 5%. For 5% gels, an increase in stiffness was observed when the temperature was increased to 20°C to 37°C and a decrease was observed when the applied strain was increased from 1% to 5%. For the case of temperature, a similar behaviour was observed for both 1% and 5% gels when they were compared among the same group of applied strain (either 1% applied strain or 5% applied strain), which was similar to the behaviour observed for the strain value within LVER. This behaviour can be attributed to the different cross-linking densities of the gels which result in different stiffness response. However, when the applied

130

strain was increased from 1% to 5% (where both values were out of LVER), all groups showed a decrease in stiffness, possibly due to the collapse of the structure of the hydrogels.

When the stiffness values of 1% and 5% gels summarised in Tables 6.1 and 6.2 were analysed together, it can be seen that the stiffness of the gels among individual groups (*i.e.* group of same concentration gels tested at the same temperature) decreased as the applied strain increased, similar to the strain softening behaviour observed in Chapter 4.

Gel percentage (%)	Temperature (°C)	Applied strain (%)	Complex shear modulus (kPa)	Elastic shear modulus (kPa)	Viscous shear modulus (kPa)
1	20	1	4.93 ± 0.36	4.89 ± 0.37	0.60 ± 0.08
5	20		7.53 ± 0.09	6.85 ± 0.10	3.13 ± 0.01
1	37		3.25 ± 0.05	3.24 ± 0.05	0.24 ± 0.001
5	37		19.54 ± 5.78	13.72 ± 1.68	13.69 ± 6.56
1	20	5	4.10 ± 0.12	3.98 ± 0.12	0.98 ± 0.007
5	20		2.13 ± 0.31	1.09 ± 0.24	1.82 ± 0.22
1	37		2.10 ± 0.16	2.01 ± 0.14	0.62 ± 0.08
5	37		3.63 ± 1.35	2.39 ± 0.77	2.65 ± 1.36

Table 6.2. Complex shear modulus, elastic shear modulus and viscous shear modulus over the frequency range of 10 Hz and 0.01 Hz at the shear strains 1% and 5% for 1% and 5% LB agarose gels without encapsulation (data represented as mean ± standard deviation, $n \geq 3$)

Complex shear modulus, elastic shear modulus and viscous shear modulus values of 1% and 5% hydrogels with and without encapsulation were normalised and they are plotted in Figure 6.11 and Figure 6.12 respectively for 20°C and 37°C. For 1% gels at 20°C, there were no significant differences between the complex shear moduli of gels with and without encapsulated bacterial cells ($p > 0.05$) when the applied shear strain was 1%, however a significant decrease ($p \leq 0.01$) was observed between the

same group of gels when the applied strain was 5%. This was possibly due to the increased fracture of the gel structure with the higher applied strain. At 37ºC, there were no significant differences between the complex shear moduli of gels with and without encapsulated bacterial cells ($p > 0.05$) for both of the applied shear strains.
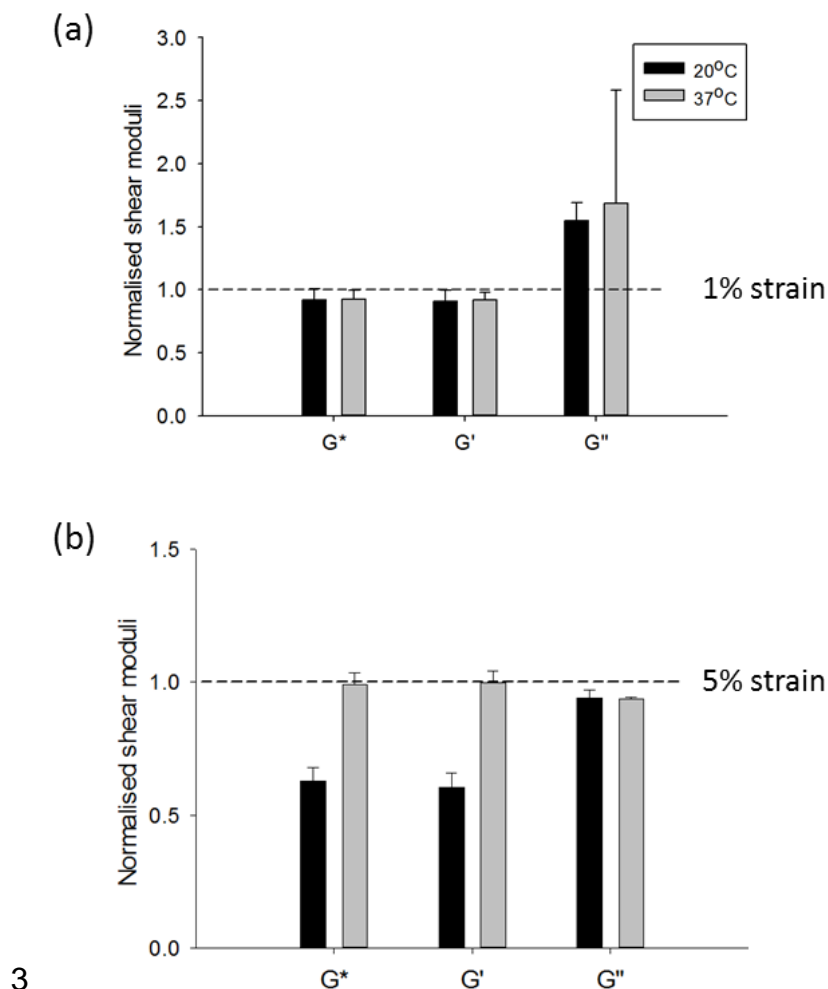
Figure 6.11. Normalised complex shear modulus, elastic shear modulus and viscous shear modulus of 1% LB gels with and without encapsulated *E. coli* BW25113 obtained from frequency sweep tests at (a) 1% and (b) 5% strain, at 20ºC and 37ºC. The dashed line shows the normalised value for gels without encapsulation and error bars represent standard deviation

For 5% gels at 20ºC, there was significant differences between the complex shear moduli of gels with and without encapsulated bacterial cells ($p \leq 0.05$) when the applied shear strain was 1%, however no significant differences were observed ($p > 0.05$) between the same group of gels when the applied strain was 5%. At 37ºC, there were no significant differences between the

complex shear moduli of gels with and without encapsulated bacterial cells ($p > 0.05$) for both of the applied shear strains. These results can be attributed to two different factors: first one is due to the complex interactions between hydrogel properties and bacterial cells at different temperatures and the second one is due to the constructs being subjected to LAOS which involves large and rapid material deformations where the rheological responses depend on the applied strain (Hyun *et al.*, 2011; Sathaye *et al.*, 2015).
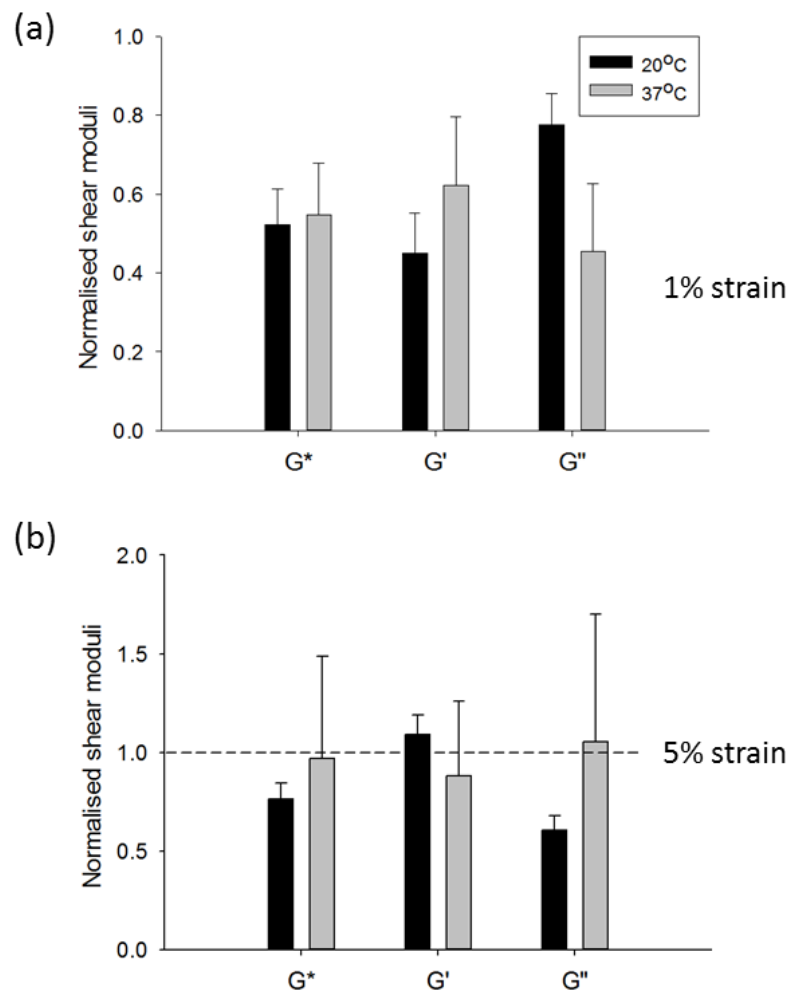
Figure 6.12. Normalised complex shear modulus, elastic shear modulus and viscous shear modulus of 5% LB gels with and without encapsulated *E. coli* BW25113 obtained from frequency sweep tests at (a) 1% strain and (b) 5% strain, at 20ºC and 37ºC. The dashed line shows the normalised value for gels without encapsulation and error bars represent standard deviation

For the case of strain values within LVER, due to the similar responses of 1% and 5% hydrogels, only 1% hydrogels with and without encapsulation were considered for the following tests (single frequency, temperature sweep and shear strain rate sweep tests).

6.3.3 Determining mechanical properties of hydrogels from single frequency tests

Single frequency tests were used to determine the change in shear properties of the hydrogels in time at a constant frequency. In these tests, the adopted frequency value was 1 Hz. This particular frequency value was chosen since it was used in other studies characterising the rheological properties of different types of hydrogels (Huang *et al.*, 2012b; Khyati, 2012; Huang *et al.*, 2013; Russ *et al.*, 2014). As determined previously, the shear strain value was used as 0.01% to stay within LVER. These tests were also applied at temperatures 20°C and 37°C. Sample outcomes of the change in elastic and viscous shear moduli and phase angle with time for 1% LB agarose gels with and without encapsulated bacterial cells are given in Figure 6.13. A similar behaviour was obtained for gels tested at 37°C and also with encapsulation. The reason to have a time independent behaviour was using agarose hydrogels that already reached their complete gel phase (Nordqvist and Vilgis, 2011; Huang *et al.*, 2013; Zuidema *et al.*, 2014).
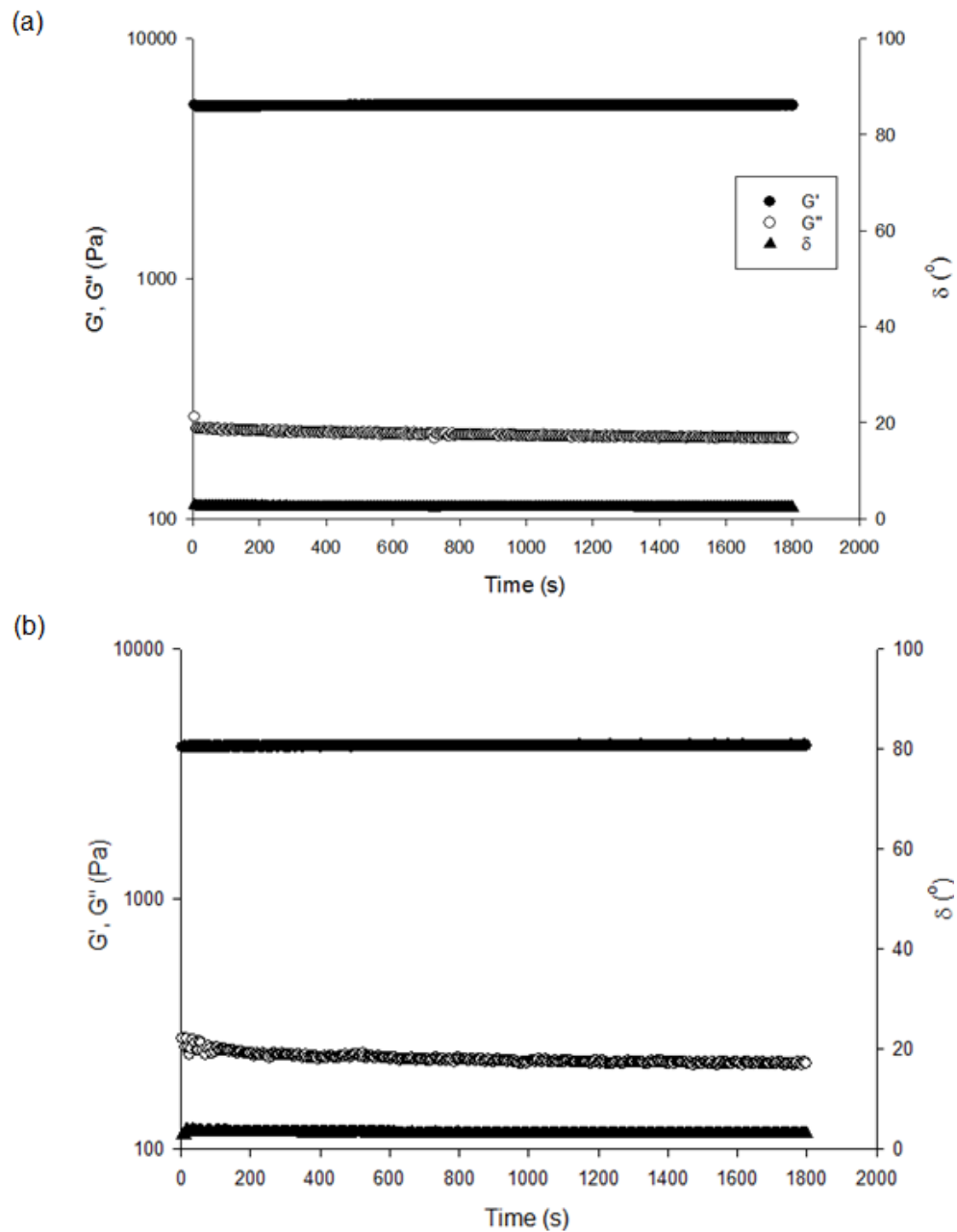
Figure 6.13. Dependence of elastic and viscous shear moduli and phase angle on time for 1% LB agarose gel (a) without encapsulation and (b) with encapsulated *E. coli* BW25113 cells, when the applied strain was 0.01% and the temperature was 20°C. Shear moduli values are plotted in a log-log scale and error bars are removed for better visualisation

At the shear strain of 0.01%, complex shear modulus, elastic and viscous components of shear modulus of 1% LB, PBS and NB hydrogels without encapsulation are summarised in Table 6.5. As can be seen from the table, the shear moduli values decreased when the temperature was increased from 20°C to 37°C. For all of the different hydrogels tested, the elastic shear modulus values were significantly higher than the viscous modulus values ($p \leq 0.01$), so the gels had solid characteristics. Also, when the complex

135

shear modulus and the elastic shear modulus values were compared, no significant differences were observed ($p > 0.05$).

When the gels made with different media were compared, at both 20°C and 37°C, there were no significant differences between the complex shear moduli of LB gels and PBS gels or LB gels and NB gels without encapsulated bacterial cells ($p > 0.05$) however for both temperatures significant differences were observed between PBS and NB gels ($p \leq 0.05$). Such differences can be attributed to the salt concentration within the liquid media used. It has been shown for various types of hydrogels that salt concentration affected the overall hydrogel mechanical properties (LeRoux *et al.*, 1999; Ozbas *et al.*, 2004). A similar phenomenon may take place causing differences in interactions between the solutions and the agarose polymer network.

Temperature (°C)	Media or Buffer	Complex shear modulus (kPa)	Elastic shear modulus (kPa)	Viscous shear modulus (kPa)
	PBS	5.97 ± 0.85	5.96 ± 0.85	0.25 ± 0.04
20	NB	4.68 ± 0.27	4.68 ± 0.27	0.18 ± 0.02
	LB	5.26 ± 0.19	5.25 ± 0.19	0.22 ± 0.03
	PBS	4.55 ± 0.43	4.54 ± 0.43	0.21 ± 0.05
37	NB	3.83 ± 0.17	3.82 ± 0.17	0.18 ± 0.02
	LB	4.10 ± 0.46	4.09 ± 0.46	0.18 ± 0.03

Table 6.3. Complex shear modulus, elastic shear modulus and viscous shear modulus of 1% LB, PBS and NB agarose gels without encapsulation (data represented as mean ± standard deviation, $n \geq 5$)

Complex shear modulus, elastic shear modulus and viscous shear modulus values of 1% LB, PBS and NB hydrogels with and without encapsulation were normalised and they are plotted in Figure 6.14, Figure 6.15 and Figure 6.16 respectively for both tested temperatures.

For the gels with encapsulation at 20°C, there were no significant differences observed between the gels made with the same media or buffer ($p > 0.05$) for all shear moduli. For 37°C, the same behaviour was observed for LB and PBS gels with encapsulated *E. coli* BW25113 cells however there were significant differences between NB gels without encapsulation and NB

gels with encapsulated *S. epidermidis* FH30 cells ($p \leq 0.01$ for G*, G' and G").
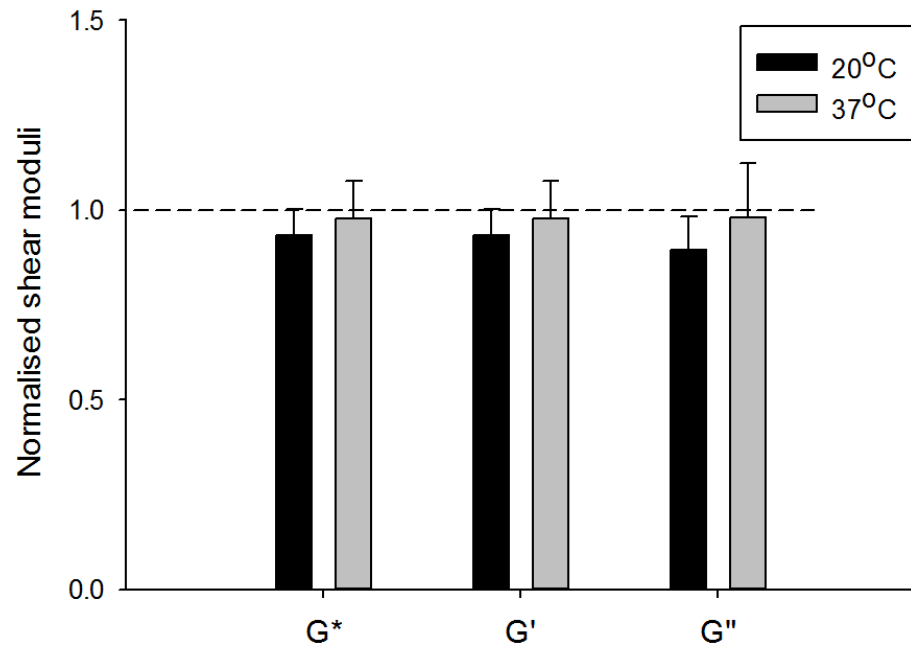
Figure 6.14. Normalised complex shear modulus, elastic shear modulus and viscous shear modulus of 1% LB gels with and without encapsulated *E. coli* BW25113 obtained from single frequency tests at 0.01% strain and 1 Hz, at 20°C and 37°C. The dashed line shows the normalised value for gels without encapsulation and error bars represent standard deviation
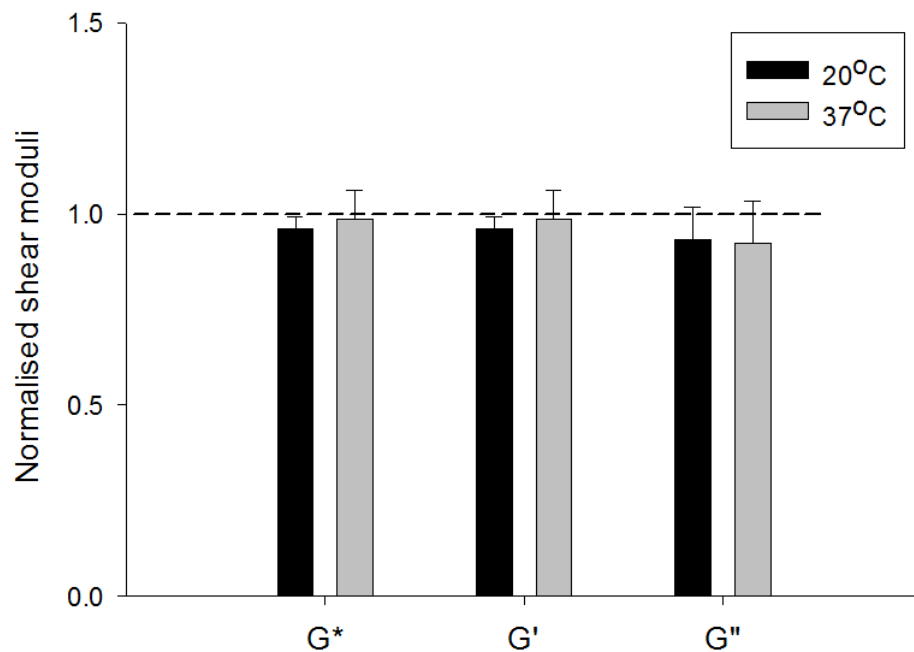
Figure 6.15. Normalised complex shear modulus, elastic shear modulus and viscous shear modulus of 1% PBS gels with and without encapsulated *E. coli* BW25113 obtained from single frequency tests at 0.01% strain and 1 Hz, at 20°C and 37°C. The dashed line shows the normalised value for gels without encapsulation and error bars represent standard deviation
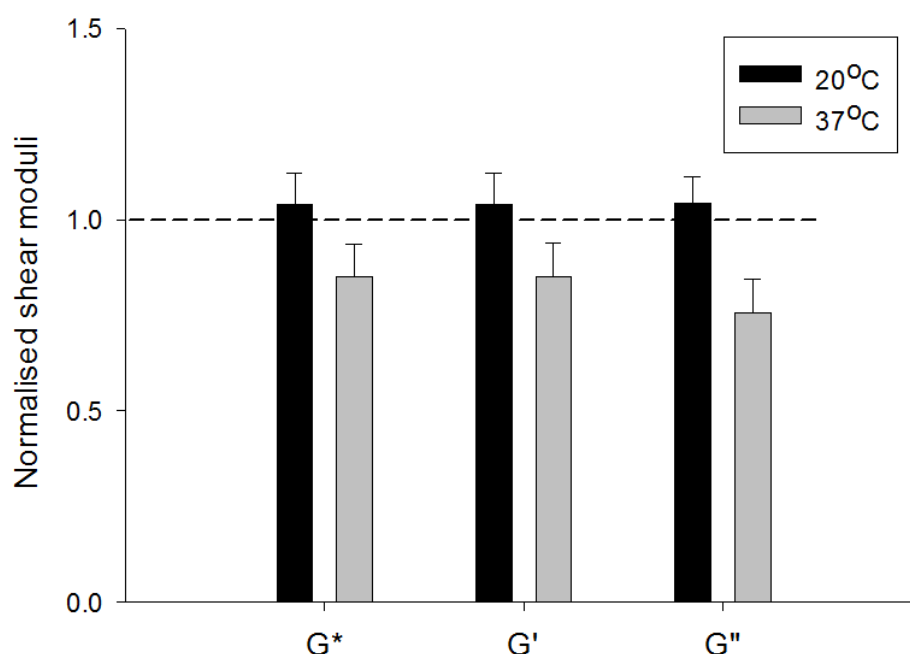
Figure 6.16. Normalised complex shear modulus, elastic shear modulus and viscous shear modulus of 1% NB gels with and without encapsulated *S. epidermidis* FH30 obtained from single frequency tests at 0.01% strain and 1 Hz, at 20°C and 37°C. The dashed line shows the normalised value for gels without encapsulation and error bars represent standard deviation

6.3.4 Determining mechanical properties of hydrogels from temperature sweep tests

Temperature sweep tests were used to determine the change in shear properties of the hydrogels with temperature at a constant frequency. In these tests, the adopted frequency value was 1 Hz. As determined from amplitude sweep tests, the shear strain value was used as 0.01% to stay within LVER. The tested temperature range was from 20°C to 40°C. Sample outcomes for the change of elastic and viscous shear moduli and phase angle with changing temperature for 1% LB agarose gels with and without encapsulation are given in Figure 6.17. The complex shear modulus and elastic modulus slightly decreased with increasing temperature and viscous modulus slightly increased with increasing temperature. However, the amount of change in these values could still be considered negligible since it did not affect the behaviour of the hydrogels and for the tested temperature range the material was gel-like. From the data collected for the hydrogels with and without encapsulation, it can be said that when the applied shear strain value was selected from LVER, hydrogels showed solid characteristics. Similar behaviour for agarose hydrogels was reported in

literature for similar tested temperatures (Landers *et al.*, 2002; Nordqvist and Vilgis, 2011).
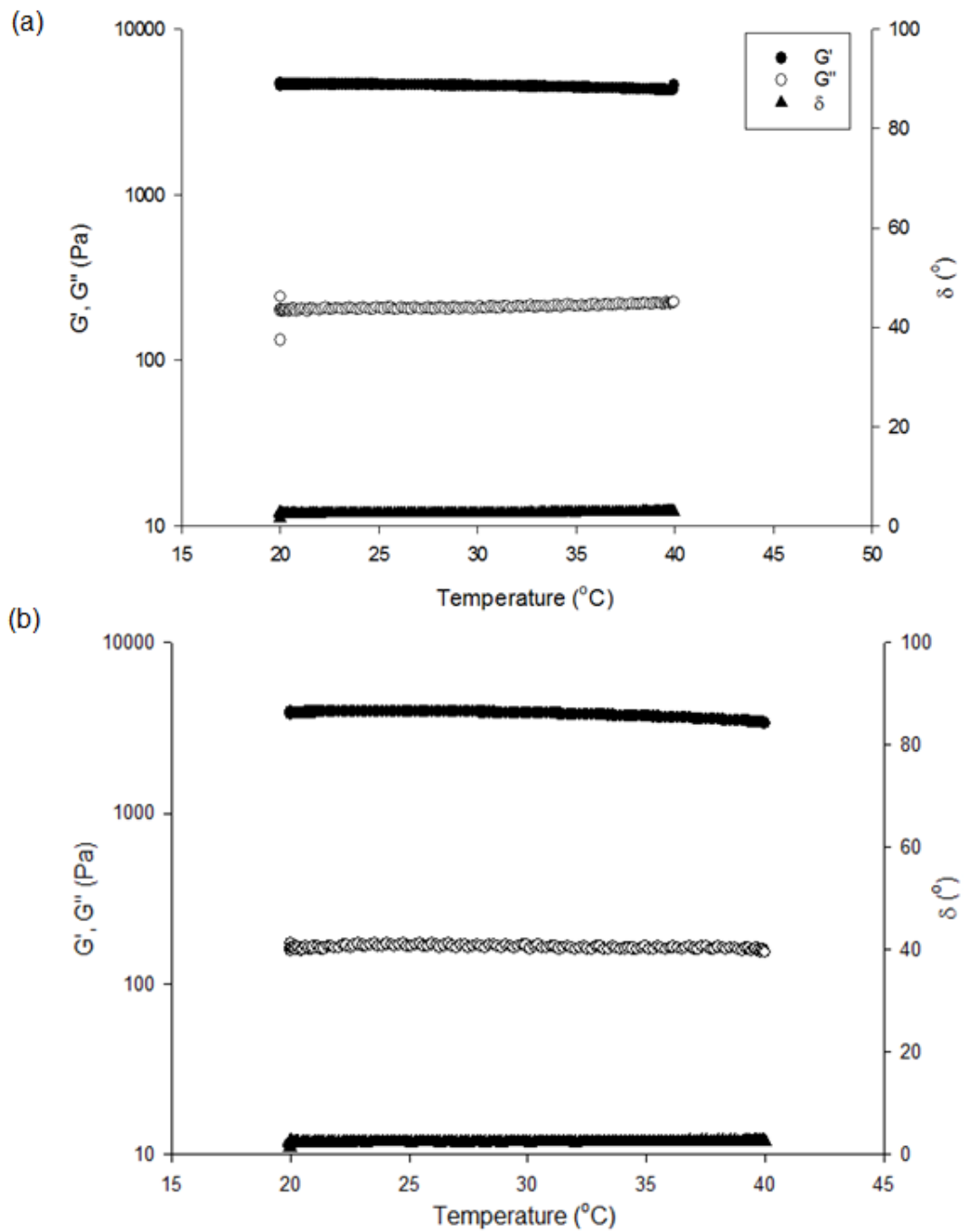
Figure 6.17. Dependence of elastic and viscous shear moduli and phase angle on temperature for 1% LB agarose gel without encapsulation when the applied strain was 0.01%. Shear moduli values are plotted in a log-log scale and error bars are removed for better visualisation

At the shear strain of 0.01%, complex shear modulus, elastic and viscous components of shear modulus of 1% LB hydrogels without encapsulation are summarised in Table 6.4, where mean values were presented for all shear moduli since the change in shear moduli from 20°C and 40°C was negligible.

For both cases, the elastic shear modulus values were significantly higher than the viscous modulus values ($p \leq 0.01$), so the gels had solid characteristics. Also, when the complex shear modulus and the elastic shear modulus values were compared, no significant differences were observed ($p > 0.05$).

Complex shear modulus (kPa)	Elastic shear modulus (kPa)	Viscous shear modulus (kPa)
4.54 ± 0.11	4.53 ± 0.11	0.21 ± 0.01

Table 6.4. Complex shear modulus, elastic shear modulus and viscous shear modulus of 1% LB agarose gels without encapsulation (data represented as mean ± standard deviation, $n \geq 3$)

Complex shear modulus, elastic shear modulus and viscous shear modulus values of 1% hydrogels with and without encapsulation were normalised and they are plotted in Figure 6.18. For the tested temperature range, the complex shear moduli of gels with encapsulation showed no significant differences ($p > 0.05$) when compared to gels without encapsulation.
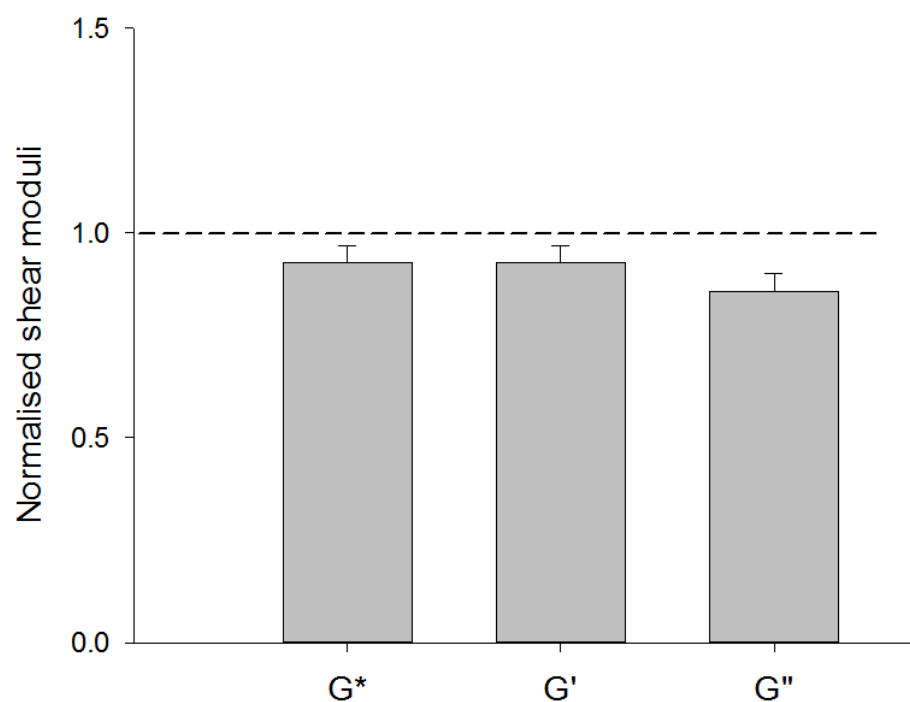
Figure 6.18. Normalised complex shear modulus, elastic shear modulus and viscous shear modulus of 1% LB gels with and without encapsulated *E. coli* BW25113 obtained from temperature tests at 0.01% shear strain. The dashed line shows the normalised value for gels without encapsulation and error bars represent standard deviation

6.3.5 Determining mechanical properties of hydrogels from shear strain rate sweep tests

Shear strain rate sweep tests were applied to the hydrogels to observe their flow characteristics (since they carry both the viscous and elastic properties) and to determine the type of behaviour the samples follow (such as Newtonian liquid, shear thinning, shear thickening or Bingham plastic) which can be linked to injectibility of the hydrogels. Shear rate dependent behaviour of 1% LB agarose gels with and without encapsulation are shown in Figure 6.19. When shear rate increased from 0.1 s^{-1} to 100 s^{-1} at a frequency of 1 Hz, the viscosity of the gels decreased so that the amplitude was varied generating a non-linear response. This type of behaviour, i.e. when viscosity significantly decreases with increasing shear rate, is referred as shear thinning behaviour which suggests that agarose hydrogels can be injected by applying high shear rate during injection and also they show self-heal characteristics shortly after removing shear stress (Guvendiren *et al.*, 2012). The change of viscosity with shear rate was not significantly different ($p > 0.05$) among the gels. The trend of the viscosity change with shear rate

was the same for 1% LB gels with and without encapsulation which can be attributed to the hindrance and friction among the different polymer chains which was also observed in different type of hydrogel mixtures reported in the literature (Kuo and Ma, 2001; Fernandez *et al.*, 2008; Duan *et al.*, 2017; Kandemir *et al.*, 2018).

(a)

(b)
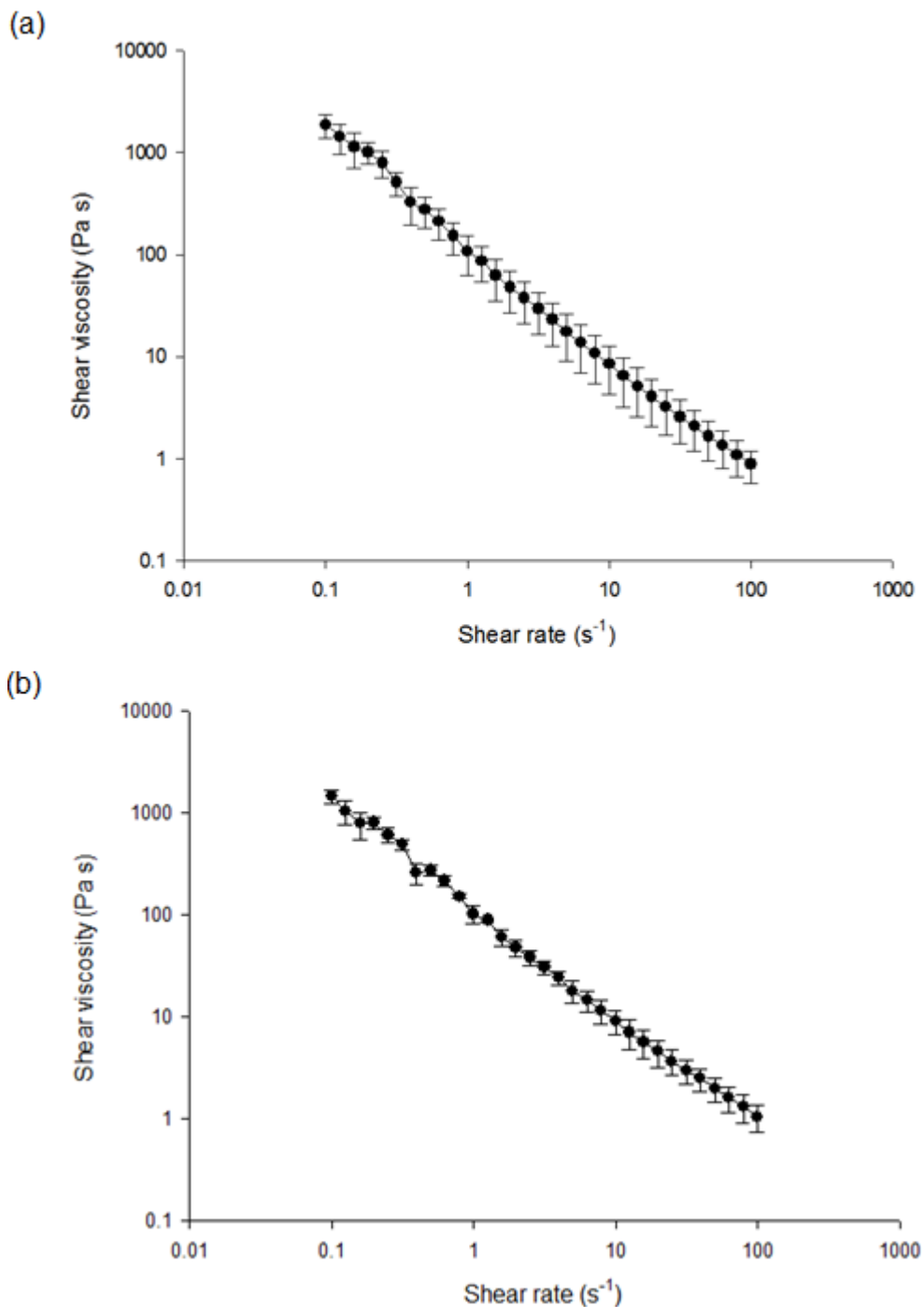
Figure 6.19. The change of shear viscosity of 1% LB gels (a) without encapsulation and (b) with encapsulated *E. coli* BW25113 cells, with increasing shear rate. The gels showed shear thinning behaviour

6.3.6 *Viability Check after Rheology Testing*

The viability of bacterial cells was determined after single frequency tests. For this purpose, 1% LB and 1% PBS hydrogel samples with encapsulated *E. coli* BW25113 cells were melted slightly right after the rheological testing and then plated on LB agar plates which were then grown overnight at 37°C. The melting of the samples took place in a 50°C water bath since a higher temperature could kill the bacterial cells. Table 6.5 summarises the colony counts obtained from the plating of hydrogel samples with encapsulation for PBS and LB gels.

Dilution series	Colony count for PBS	Colony count for LB
10^{-8}	2	3
10^{-7}	9	11
10^{-6}	48	52
10^{-5}	330	381

Table 6.5. Colony count values from gels made with PBS and LB after single frequency test (1 Hz) with an applied strain of 0.01% at 20°C

The dilution series were calculated backwards to find the colony forming units per ml. It was found that there are 9.3×10^8 cfu/ml from PBS samples and 1.3×10^9 cfu /ml for LB samples. A reason for the difference in colony counts might be because of the medium, since in PBS the bacterial cells do not grow whereas in LB medium colonies grow. However it could just be random variation since the difference was very small, and overall the viable count procedure focuses on an estimate of the colony count.

When the overnight culture of *E. coli* BW25113 was plated on LB agar plates, the total viable counts revealed that these cultures contained ~ 1.3×10^{11} cfu/ml. Although there were differences between the values obtained after the rheological tests and from the liquid medium, it should be noted that the samples used could not be melted completely and therefore might not be revealing the actual colony count within the hydrogels.

Due to the limitations of this method, these viability tests were not repeated for other tests and it was assumed that a similar viability was maintained in the rheological tests carried out at a strain value within LVER and an appropriate temperature.

6.4   Summary of Results and Conclusions

In this chapter, the shear properties of various hydrogels with and without encapsulation obtained from rheological characterisation were presented. Amplitude sweep tests were applied to agarose hydrogels having different concentrations to determine the LVER and for all the samples tested, the suitable shear strain value was determined as 0.01%. Using this value, the dependence of shear properties of hydrogels (including complex shear modulus, elastic and viscous shear moduli, phase angle and shear viscosity) with frequency, time, temperature and shear strain rate were determined.

For all of the tests considered for rheological characterisation, the elastic shear modulus values were significantly higher than the viscous modulus values and there were no significant differences between complex shear modulus values and elastic shear modulus values so the gels had solid characteristics. Therefore, it can be concluded that agarose hydrogels were elastically dominated.

The shear properties of agarose hydrogels with and without encapsulation having different concentrations were found to be independent of frequency when the applied frequency range was 0.01 Hz to 10 Hz. Within LVER, it was shown that the magnitude of the shear moduli increased with the increasing concentration for gels with and without encapsulation. However for strain values taken outside of LVER (*i.e.* for the case of LAOS), complex interactions were observed between hydrogel shear properties and bacterial cells at different temperatures. Therefore, it was shown that the applied strain has an important role on the mechanical properties of the hydrogels as well as bacterial cell – hydrogel interactions. In addition to testing the hydrogels within a range of frequency, a single frequency value from this range was chosen and the shear properties of various agarose hydrogels were obtained in time. Since the tested gels all reached their complete gel phase, a time independent behaviour was observed.

The hydrogels were also tested through a range of temperature values to examine the effect of temperature in more detail. The temperature range for the tests were chosen such that the results could be comparable to the other rheological tests and the bacterial cells that were encapsulated in the

hydrogels were not harmed. Overall, the results presented an almost independent trend. When the hydrogel flow characteristics were analysed, it was determined that all tested hydrogels showed shear thinning behaviour similar to other types of hydrogels documented in literature.

Overall, when the hydrogels with and without encapsulation were compared, a specific alteration of shear properties was not observed similar to the case in compression tests. Therefore, it can be speculated that the type of forces applied on the hydrogels may also affect the bacterial cell and hydrogel interactions.

In the next chapter, bacterial cell elongation in 1% agarose hydrogels made with different growth media will be presented. The data acquired will be used to explain possible interactions between hydrogels, the growth media and bacterial cells.

7   Bacterial Cell Elongation in Agarose Hydrogels

7.1   Introduction

In the previous chapters, mechanical characterisation techniques were applied to the key materials of this study, which are hydrogels and hydrogels with encapsulated bacterial cells, to explain the interactions between them. The results obtained from these techniques revealed differences in mechanical behaviour for the different conditions tested which involved either physical or chemical variables, such as stiffness of the hydrogels, chemical composition of the hydrogels and the types of testing where the applied loading was different. Although finite element modelling technique, which involved inert particles, was adopted to reveal the effect of bacterial cells on the experimental results, they were not sufficient enough to visualise how the bacterial cells behave when they are encapsulated in a 3D microenvironment.

In this chapter, bacterial cell behaviour when they are encapsulated in hydrogels will be characterised. This will be done by imaging the elongation behaviour of the bacterial cells in different 1% agarose hydrogels. Also, the elongation behaviour will be modelled to gain more insights of the bacterial cell behaviour when they are encapsulated. A parametric study will be done where different variables are considered for the analysis which include bacterial cell and hydrogel stiffness and different mechanical responses of both phases (either elastic or viscoelastic).

7.2   Methods

7.2.1   Sample preparation for batch growth curves and elongation analysis

E. coli MC1061 and *S. epidermidis* FH30 cells were grown in the growth media used to make the hydrogels which included LB, NB, LB-no yeast extract and LB-no tryptone to obtain batch growth curves. 25 ml of a growth medium was used to start the test culture with the addition of 1% v/v of overnight culture of either *E. coli* MC1061 or *S. epidermidis* FH30. OD_{600} readings were recorded every 20 min for 7 hours. The experiments were performed in triplicate.

The bacterial strain used for elongation analysis was *E. coli* MC1061 pEGFP containing GFP plasmid and they were grown as explained in Section 3.1.3. The antibiotic used to maintain the plasmid for fluorescence expression was ampicillin. Stationary phase fluorescent *E. coli* MC1061 cells with pEGFP were encapsulated in the 1% agarose hydrogel made with different growth media including LB media, LB-no yeast extract, LB-no tryptone and NB media. The encapsulation of bacterial cells were done at a volume of 2:1. The sterile hydrogels were prepared at a higher concentration so that the overall concentration was 1% when the culture was added to the hydrogel. Here, the bacterial cell culture was not pelleted as it was for previous experimental techniques and cells were directly added from the overnight culture to avoid overcrowding the hydrogel for imaging. The resulting hydrogel and bacterial cell mixture was thoroughly mixed using a vortex mixer and then injected in an isolated PDMS chamber. The different types of chambers used for imaging are shown in Figure 7.1. To avoid drying of the gel, the chamber was filled completely with the mixture and after injection the inlets were isolated as well.
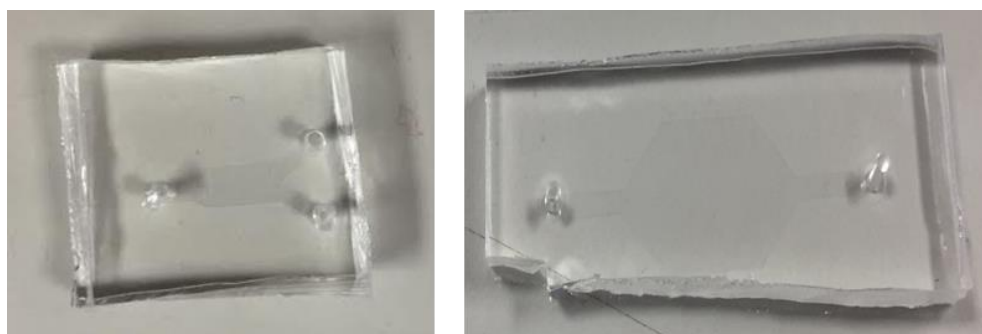
Figure 7.1. Various shapes of PDMS microfluidic chambers used in the study

7.2.2 Modification of E. coli MC1061 DNA for division inhibition

PeqGold Plasmid Miniprep Kit I (VWR International, Leicestershire, UK) was used to extract pure plasmid DNA. The plasmid to inhibit bacterial division is chloramphenicol resistant pPZV56 which has the *sul*A gene related to the inhibition (Bi and Lutkenhaus, 1993).

To extract the DNA which contained the specific gene inhibiting division, first of all, *E.coli* cells that carry pPZV56 plasmid were grown overnight at 37 °C

with shaking. The overnight culture was pelleted by centrifugation for 10 min at 5,000g in a 15 ml centrifuge tube. The supernatant was discarded. 250 µl of Solution I/RNase A was added to the pellet and the bacterial cells were completely suspended by vortexing. This step was followed by adding 250 µl of Solution II to the new solution which was gently mixed by rotating to obtain a cleared lysate. For the neutralisation of the lysate, 350 µl of Solution III was added and gently mixed by inverting the tube until a flocculent white precipitate was formed. The solution was centrifuged at 10,000g for 10 minutes at room temperature.

For the binding of the plasmid, the supernatant was transferred to a PerfectBind DNA Column which was placed in a 2 ml collection tube. During the transfer step, the pellet disturbance was avoided. The collection tube with the DNA column was centrifuged for 1 min at 10,000g at room temperature. This step was applied to completely pass the lysate through the membrane. This solution was washed with 750 µl of DNA wash buffer completed with ethanol, it was centrifuged for 1 min at 10,000g and the supernatant was discarded. To remove the ethanol from the column with the plasmid, it was centrifuged for 2 min at 10,000g. The column was then transferred to a fresh 1.5 ml micro-centrifuge tube. Depending on the desired final concentration 50 - 100 µl elution buffer was added directly to the binding matrix in the PerfectBind DNA column. For elution of the DNA, the column was centrifuged for 1 min at 5,000g.

To grow the modified *E. coli* MC1061 cells, a single colony that was taken from an LB agar plate containing both ampicillin and chloramphenicol and grown overnight at 37°C in LB media containing the same antibiotics with shaking. The overnight solution was inoculated at a ratio of 1:50 in fresh LB medium with ampicillin and chloramphenicol until the bacterial cells reached log phase (OD of ~ 0.6). Before imaging the bacterial cells, sodium salicylate was added to block the division.

7.2.3 Imaging encapsulated bacterial cells and single cell elongation analysis

Using a confocal microscope equipped with perfect focus system (Nikon A1R with PFS) (see Figure 7.2 for the setup), cell elongation was imaged for approximately two hours at 37°C and at a magnification of 60× among

an identified range in z-direction. This 20 µm range, which was divided in 0.4 µm layers, was selected so that it was located at the middle of the chamber and away from chamber boundaries, and contained enough cells to be analysed.

Figure 7.2. Confocal microscope with a PFS and environmental chamber

After obtaining the time lapse images, first of all they were analysed using NIS elements software (Nikon UK Limited, Surrey, UK) to determine the appropriate z-planes to be analysed among the collected data. Approximately 3 different z-planes were projected on top of each other to get an accurate measure of the dimensions of the individual bacterial cells. The individual z-layer thickness of 0.4 µm was suitable for the projection, *i.e.* with this thickness value no other cells contributed to the dimensions of the individual bacterial cell.

The extent of cell elongation in gels with different growth media was found using an in-house MATLAB code (details of this code are given in Appendix D). From the grey-scale images of one of the z planes, a single bacterium was identified which was not in contact with the other neighbouring bacteria and its coordinates were determined by using the MATLAB figure axes. The images were cropped (this was done by using `imcrop` command) so that a new set of images were obtained and they were saved within a new directory containing only the images of the single bacterium. The edges of that single bacterium were detected, an ellipse was fitted around the identified edges, and the length of the major axis which specified the length of the bacteria was determined as shown in Figure 7.3. To do this, the

cropped set of images containing the single bacterium were converted in black and white images (this was done by using `im2bw` command) with the gel represented by the colour black and the bacterial cell represented by the colour white, for all the time steps of the same plane and all holes within the black or white area were filled by the same colour pixels to provide continuity of the image (this was done by using `imfill` command). The grey-scale pixels were converted to either black or white based on their intensity. The boundaries of the bacterium (the black-white interface) were determined and they were shown with circles where their centres represented the identified edges (this was done by using `bwboundaries` command). An ellipse was fitted to the identified edges by using `fit_ellipse` and the length of major and minor axes were determined by using the ellipse parameters which were saved and used for elongation analysis.

This procedure was applied for all the images taken at 2 min intervals for 2 h for the same bacterial cell. A total number of 30, 26, 21 and 19 individual cells were analysed from LB, NB, LB-no yeast extract and LB-no tryptone gels, respectively.
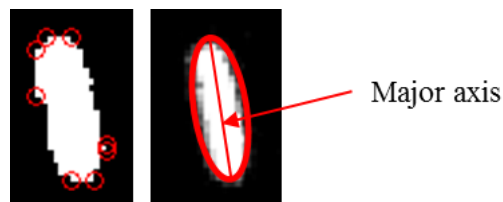
Figure 7.3. The images illustrate how the bacteria elongation was determined: an ellipse was fitted around the identified edges of the bacteria and the major axis of the ellipse indicated the length of the bacteria. The difference in the length of major axes indicated the bacteria growth at a particular time interval

7.2.4 Constructing a computational model for bacterial cell elongation

A simple representative model was created using the commercial finite element software ABAQUS CAE 6.14 (Dassault Systèmes Smulia Corp. 2014, Providence, RI, USA) to carry out simulations to find out about bacterial cell elongation when encapsulated in hydrogels. The model used was a representation of the encapsulation with axisymmetric boundary conditions. The boundary conditions were applied in a way that they

mimicked the elongation tests: the bottom plane of the gel, where no bacterial cells were present, was fixed, a limited movement of the top plane of the gel and the bacterial cell was allowed in the horizontal direction to monitor any changes in shape and the top of the construct was fixed at the direction of elongation for these planes (see Fig. 7.4). The bacteria elongation was determined from the displacement of the edge of the bacterial cell inside the gel. In the model, the elongation of the bacterial cell was provided by expansion and the expansion coefficient was determined by the image analyses of single bacterial cells. Expansion was not considered for the gel part of the construct. In terms of elastic properties, both materials were considered isotropic but in terms of elongation, bacterial cells were considered to be orthotropic. The set-up of the model was created based on CLAMP model given in literature (Tuson *et al.*, 2012a).

Different mesh sizes were applied on the model and elongation of the bacterial cells was obtained until it was independent of the mesh size used. A finer mesh size was used at the gel – bacterial cell interface and where the boundary conditions were applied, to achieve more accurate results and to correctly represent the gel – bacterial cell interface and at the symmetry plane. The mesh was controlled by number and more elements were used resulting in a finer mesh structure where a more sensitive analysis was needed. These mesh sizes provided the displacement response to be independent of mesh size. The mesh structure of the model can be seen from Figure 7.3. A total number of 1080 and 17222 two-dimensional 4-node linear quadrilateral elements of type CAX4R were used for bacterial cell and hydrogel, respectively. Similar to the elements used in the compression modelling, these were also reduced-integration elements. For the hydrogel, an additional 311 3-node linear triangular elements of type CAX3 were also used to provide the connectivity between the refined and unrefined regions.
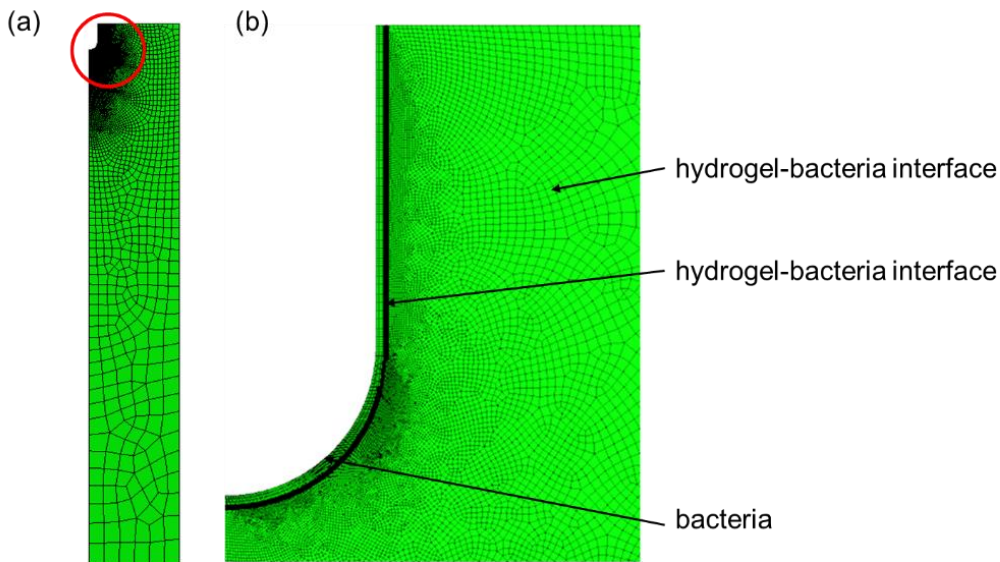
Figure 7.4. Representation of the model for the elongation tests. Applied boundary conditions: symmetric boundary conditions on the hydrogel-bacteria construct and the planes provided the opportunity to only model half of structure while restraining the linear movement in *x* direction and the rotational movement in *y* and *z* directions, fixed support applied at the bottom plane for the restriction of movement and compressive strain was applied through the top plane

In the model, material properties of the hydrogel and the bacterial cell were characterised by two different ways, either elastic or viscoelastic. For the elastic mode, various *E. coli* elastic cell properties were obtained from literature (Abu-Lail and Camesano, 2006; Cerf *et al.*, 2009) and a range of 2-15 MPa were tested. As the hydrogel material properties, the elastic moduli were taken as 15 kPa, 25 kPa and 80 kPa, representing the LB gel stiffness values at different strain values (see Table 4.2 in Chapter 4). Since the bacterial cell elastic properties had a range of values reported, the tested values were increased by involving the intermediate values. For the viscoelastic part, the hydrogel material properties were found using Prony series (since this was the time dependent viscoelastic model used in ABAQUS) and similar to the elastic properties various *E. coli* viscoelastic cell properties were obtained from literature. In the model created to mimic the elongation of bacterial cells, there were some variables considered, namely elastic or viscoelastic properties and the Poisson's ratio of both phases, and the expansion coefficient of the bacterial cells in the direction of elongation. Similar to the value used in compression model and the mathematical models in Chapter 5, the Poisson's ratio for both phases were

152

taken as 0.45. The expansion coefficient was chosen based on the growth rate determined from imaging experiments. No turgor pressure was considered in the present model.

7.2.5 Statistical analysis

Analysis of Variance (ANOVA) with Tukey's post hoc test was applied to determine the statistical differences between the rates of elongation of bacterial cells in different hydrogels. The significance level (α) was taken as 0.05. The statistical analysis was carried out using Minitab 17.1.0.

7.3 Results and Discussions

7.3.1 Growth of bacterial cells in liquid media

Batch growth curves were obtained for *E. coli* MC1061 pEFGP and *S. epidermidis* FH30 in the growth media used to make the hydrogels (LB, NB, LB-no yeast extract and LB-no tryptone, respectively) to obtain their growth behaviour in an environment where no hydrogel forces were acting on them (Fig 7.5). During exponential phase there were no significant differences ($p > 0.05$) between growth rates when different growth media were used for both *E. coli* and *S. epidermidis* cells. However, the lag phase of *S. epidermidis* cells was longer compared to that of *E. coli* cells for all the growth media considered. Bacteria growth in liquid media did not affect the overall growth behaviour of the bacterial cells when the growth took place without any forces acting on them by the hydrogels (*i.e.* when they were not encapsulated). The doubling time for *E. coli* cells was measured as 20 min and the doubling time for *S. epidermidis* cells was measured as 40 min during exponential phase.

S. epidermidis FH30 cells were only used for the batch growth experiments to observe differences of growth behaviour within liquid media and they were not used for elongation experiments due to their cocci shape, since the detection of changes in bacterial size is difficult for such bacteria.
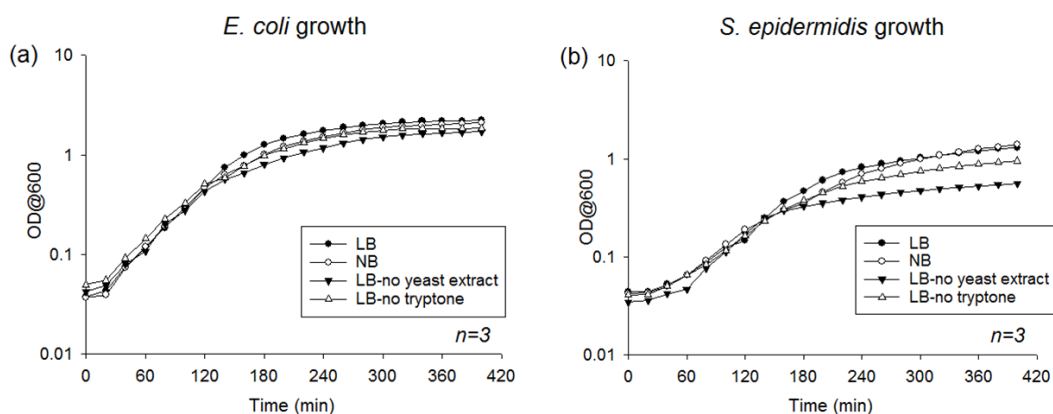
Figure 7.5. (a) *E. coli* and (b) *S. epidermidis* cell growth in different liquid growth media

7.3.2 E. coli MC1061 pEFGP growth in 1% agarose gels made with different growth media

To determine how bacterial cells interacted with the hydrogels, to demonstrate their viability when encapsulated and to examine the medium effect, their growth in hydrogels was measured. For this reason, from an overall image of a z plane a single bacterium was identified. An example of a z plane, where single bacterial cells were identified, is shown in Figure 7.6. Due to the NIS Elements software, the cells appear in white however normally they have GFP which expressed a bright green colour.

After obtaining individual images of the identified single bacterial cells, the edges of each single bacterium were determined, an ellipse was fitted around the identified edges, and the length of the major axis was determined. The change in length of the bacterial cells were normalised by their initial length to account for variability of the initial bacterial cell size. The length of the bacterial cells at each time point was represented by the length of the major axis of an ellipse fitted around the edges of the bacteria. The same approach was used for all of the images captured at different times and the differences between the axis lengths indicated the bacteria growth at a particular time interval. The initial and final states of a single bacterium was shown in Figure 7.7 as an example.
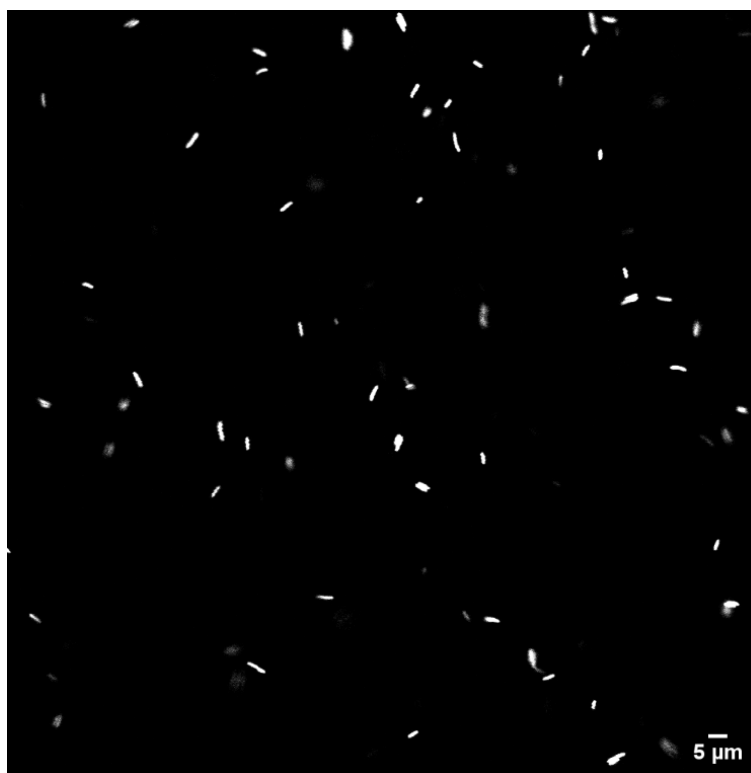
Figure 7.6. *E. coli* MC1061 pEGFP cells encapsulated in 1% LB gel. This representative image from a representative z-plane shows the distribution of the cells within the gel at one of the time points
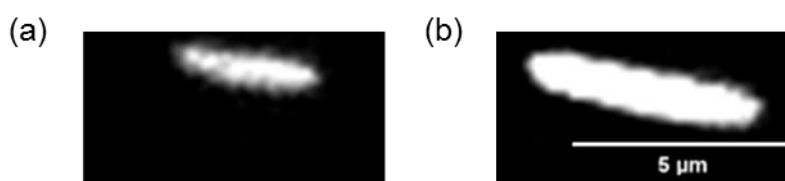
Figure 7.7. (a) Initial and (b) final length of a single *E. coli* MC1061 pEGFP cell that was encapsulated in 1% LB agarose hydrogel

Stationary phase bacteria elongation in different growth media was shown in Figure 7.8. After the imaging period of two hours, *E. coli* cells had elongated approximately 12.8% ± 1.1% in LB gels, 4.3% ± 0.58% in NB gels, 4.8% ± 0.96% in LB-no yeast extract gels and 5.5% ± 1.8% in LB-no tryptone gels (data given as mean ± standard error). There were no significant differences in the rate of elongation for NB, LB-no yeast extract and LB-no tryptone gels. However, the rate of elongation in LB gels were significantly higher than the rate obtained from other hydrogels ($p < 0.05$). This may be due to LB medium being a nutritionally richer medium compared to the other growth media. In the mechanical compression tests, it was evident that the presence of tryptone weakened the hydrogel as

measured at different applied strains. It is interesting to note that the stiffness decreased by 76-78% when the applied strain increased from 0.5 to 5%, for hydrogels made with LB, LB-no tryptone or LB-no yeast extract. For PBS and NB gels, the stiffness decreased only by 66% when the applied strain increased from 0.5 to 5%.
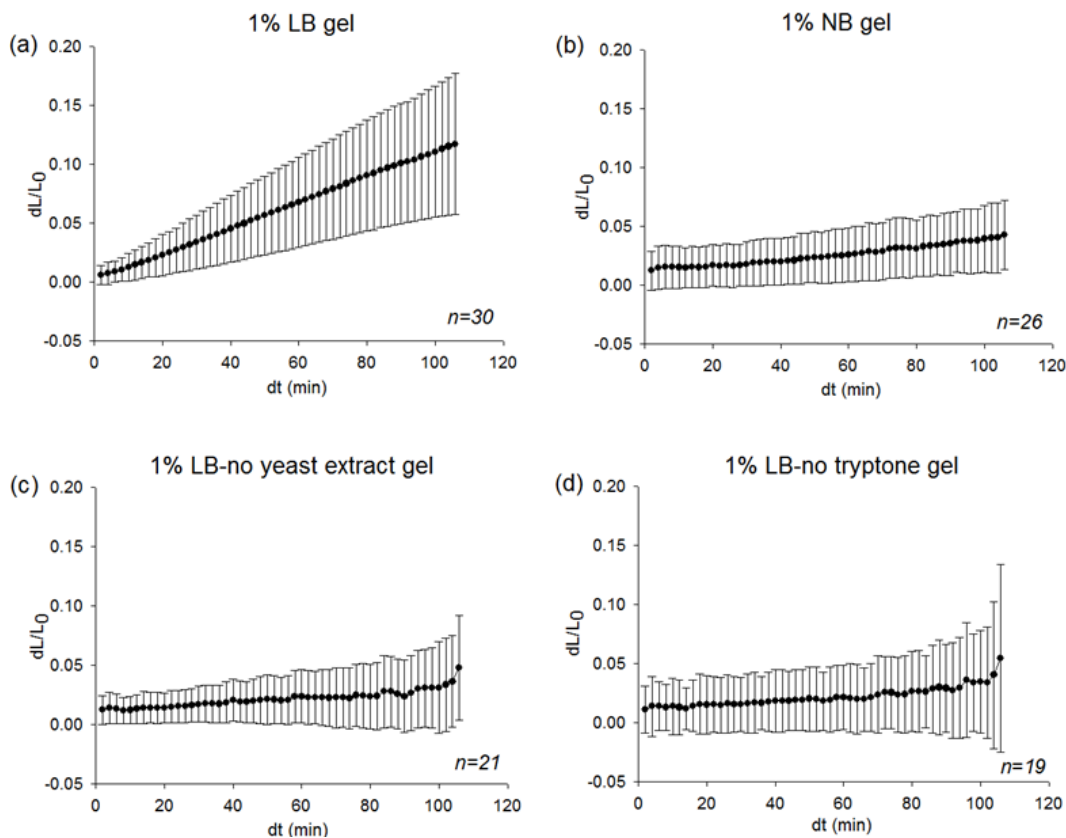
Figure 7.8. Stationary phase *E. coli* cell elongation in 1% agarose hydrogels made with (a) LB, (b) NB, (c) LB-no yeast extract and (d) LB-no tryptone. Data points and error bars represent mean values and standard deviation, respectively. Number of replicates for each experiment is indicated at their individual sections

In addition, the doubling time of the encapsulated cells were calculated by fitting a curve to the data. From the fit, doubling time of *E. coli* cells in LB gels, NB gels, LB-no yeast extract gels and LB-no tryptone gels were calculated as 15.2 h, 60.5 h, 80.3 h and 69.4 h respectively. The reason for the long doubling time may be due to the bacterial cells either not being able to reach exponential phase or grow at all due to the forces acting on them from their 3D micro-environment, especially when certain growth media were used. However, it is important to point out that bacterial cell lysis was not observed.

To obtain the doubling times, first of all, a linear line (*i.e.* $y = mx + c$) was fitted to the normalised elongation data where the equation coefficients m and c were identified. The doubling time x was determined by taking y as 2 (to indicate doubling in length since the vertical axis was normalised by the initial length). Due to the obtained normalised elongation, the trend was assumed to continue linearly, however, this may not be the case if bacterial cells adopt completely to their 3D environment similar to that of liquid media.

The cell elongation may also be limited by nutrient diffusion, which presumably will be much slower in a hydrogel than in broth. As the bacterial cells have such slow growth rates in hydrogels made with different media, it is unlikely that volume changes caused by growth in media could have led to significant increases in the stiffness of the bacteria/gel constructs with the timeframe of the compression tests with stress relaxation (as documented in Chapter 4). The computational simulations presented at Chapter 5 also confirmed this since the modelled encapsulated particles did not change their volume in time and the difference between the gel with particles and without particles did not show any significant differences for both bonded and non-bonded cases (see Fig. 5.20). Therefore, the key mechanisms to answer for the hydrogel stiffening effect is likely due to changes in cell mechanical properties and/or cell-materials interactions when cells are in contact with the hydrogels with different physical/chemical properties.

It is known that bacterial cells change surface characteristics to adapt to nutrient availability (Ni et al., 2016) which would affect how they interact with their environments. In addition, different sources of tryptone can affect physiological state of bacterial cells even in liquid medium (De Spiegeleer et al., 2004). Although no cell lysis was observed in the experiments, this factor might have played a role in the differences in the elongation rates. Different cell-materials interactions affected the cell membrane, cell phenotype and other physiological conditions of bacteria when bacterial cells are in contact with two-dimensional materials surfaces (Tuson and Weibel, 2013). All these may also happen when bacterial cells are in contact with three-dimensional materials.

Since stationary phase *E. coli* MC1061 pEFGP cells showed such slow growth rates (especially for certain growth media), log-phase ($OD_{600} \sim 0.5$)

bacterial cells, which showed much faster growth rate and also shorter doubling time in liquid media, were also encapsulated in 1% LB hydrogels. The reason for this was to determine the different behaviour of various phases of bacterial cells. Even though the cell mixture was thoroughly mixed before encapsulation and since the cells were elongating and doubling at a faster rate even within the hydrogel, they formed clusters (as shown in Figure 7.9) where single bacteria elongation analysis could not be performed. Early log-phase bacterial cells (OD_{600} ~ 0.2) were also encapsulated and imaged within hydrogels where the growth behaviour was similar to that of stationary phase cells. Therefore, the experiments for early-log phase and log-phase cells were not repeated for hydrogels made with other growth media.

Figure 7.9. Clustering of log-phase *E. coli* MC1061 pEFGP cells when encapsulated in 1% LB agarose hydrogels

7.3.3 Growth of modified E. coli MC1061 cells in 1% LB agarose gel

To overcome the clustering issue, modified *E. coli* MC1061 cells with both pEGFP and pPZV56 plasmids were considered. After the modification of the bacterial cells, first of all, they were grown to log-phase (OD_{600} ~ 0.6) and imaged to see if the modification was successful. Figure 7.10 and Figure 7.11 show the phase contrast and fluorescent images of modified *E. coli* MC1061 cells placed on an agarose pads, respectively. As can be seen from these images, the bacterial cells either carried the pPZV56 plasmid which blocked division or pEFGP plasmid which expressed fluorescence. The DNA modification was repeated twice but a similar result was observed for both trials where only one of the plasmids was effective. Therefore, the modification of the DNA to carry both of the plasmids was not considered successful.
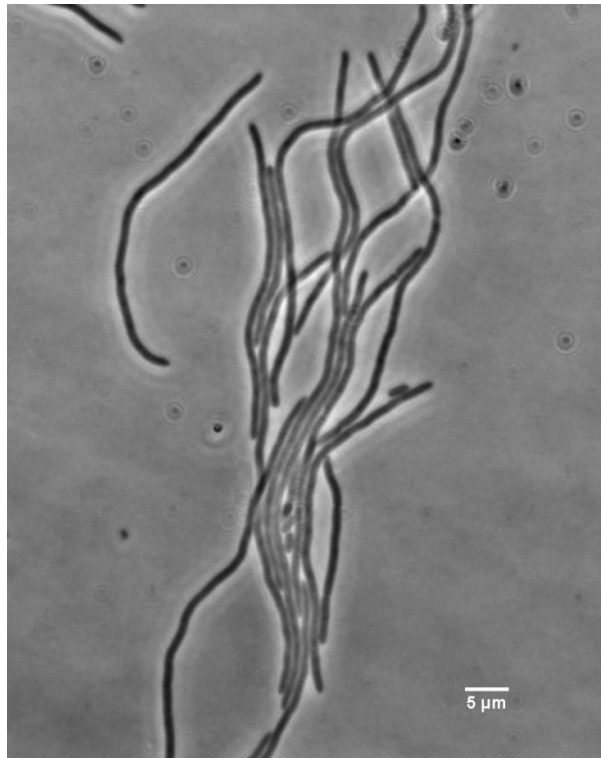
Figure 7.10. The phase contrast image of modified *E. coli* MC1061 cells with pEGFP and pPZV56 plasmids on an agarose pad. Here the OD_{600} of the bacterial cells was 0.6
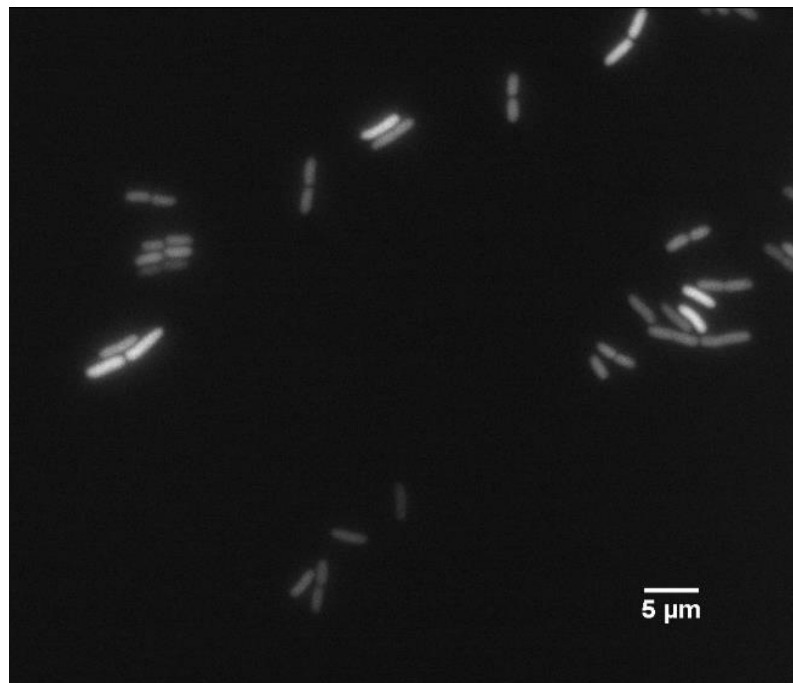
Figure 7.11. The fluorescent image of modified *E. coli* MC1061 cells with pEGFP and pPZV56 plasmids on an agarose pad. Here the OD_{600} of the bacterial cells was 0.6

Since the modified *E. coli* MC1061 cells expressed either the division inhibitor plasmid or the fluorescence plasmid, the bacteria elongation analysis was carried out for cells with only pPZV56 plasmid that inhibited bacterial division. A similar imaging technique was adopted using a phase contrast microscopy with PFS to determine the elongation of log-phase modified *E. coli* MC1061 cells. The cells were encapsulated in 1% LB agarose gels and they were imaged for 2 h. A representative z-plane is shown in Figure 7.12.

Since the overall size of the modified bacterial cells were notably longer than the *E. coli* MC1061 cells without modification, they occupied a bigger area in the hydrogel which created larger irregularities in the overall hydrogel structure. For this reason, while imaging, as the bacterial cells elongated, they moved to different focal planes causing the image set to follow an incompatible pattern making the PFS obsolete. Therefore, information about elongation for modified *E. coli* MC1061 cells with division inhibitor could not be acquired.

5 µm
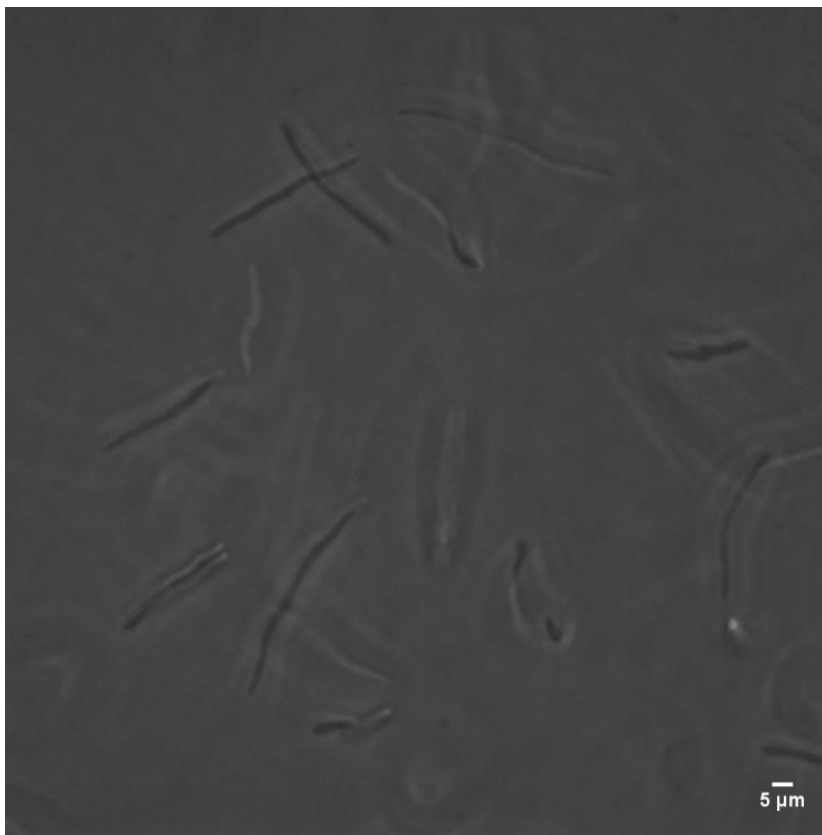
Figure 7.12. *E. coli* MC1061 cells with modification encapsulated in 1% LB gel. This representative image from a representative z-plane shows the distribution of the cells within the gel at one of the time points

7.3.4 Results from bacterial cell elongation model

When the elastic model was considered, as the stiffness of the bacterial cells increased, the total elongation of the cells also increased for all tested hydrogel stiffness values (see Tables 7.1-7.4). For LB gel properties (Table 7.1), for the lower values of the tested cell stiffness range, *i.e.* when the cell stiffness was taken as 2 MPa and 3 MPa, wrinkling behaviour of the cell and gel interface was observed especially when the higher gel stiffness was considered. The wrinkling behaviour of this interface with increasing cell stiffness is shown in Figure 7.13 and the wrinkling behaviour of the interface with increasing gel stiffness is shown in Figure 7.14.

The wrinkling behaviour observed in the model could not be verified experimentally due to the imaging capabilities which was only at micron scale. However, this behaviour obtained from the model was not ignored due to the fact that bacterial elongation might have been affected by the wrinkling behaviour which can result in physiological consequences that could affect bacteria division or even viability.

For the changing bacterial cells stiffness, it can be seen from Figure 7.13 that the number of wrinkles decreased as the adopted bacteria stiffness increased. For the elastic model, the threshold of bacterial stiffness was 11 MPa where a slight wrinkling behaviour was observed. Any stiffness above this value did not result in wrinkling. For the changing bacterial cells stiffness, it can be seen from Figure 7.14 that the number of wrinkles increased as the adopted gel stiffness increased. In general, a smaller difference of stiffness between the gel and the bacterial cell resulted in more wrinkles on the bacterial cell wall. Overall, if the fold difference between the bacterial cell and the LB gels was more than 160, wrinkling behaviour was not observed.

The wrinkle amplitude range was also given in Table 7.1. The measurements were taken from the peak values of all the wrinkles that were observed for the same construct. When these amplitude measurements from similar groups were compared (such as for the groups when the gel stiffness was 80 kPa and the cell stiffness values were changing), no significant differences ($p > 0.05$) were observed.

The overall elongation was analysed in 20 steps for the given expansion coefficient. The wrinkling behaviour did not initiate exactly when the elongation started but after approximately 70% of cell elongation took place for when the cell stiffness was taken as 2 MPa. As the stiffness value increased, the initialisation of the wrinkling behaviour appeared after 95% of cell elongation took place and this behaviour was only observed for the latest stage of the tested range.
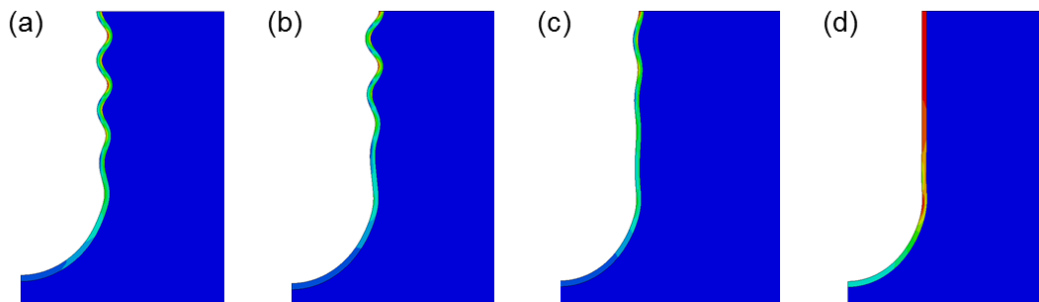
Figure 7.13. Elongation behaviour of encapsulated bacterial cells when both phases were considered to have elastic properties. Here, the bacterial cell stiffness was (a) 2 MPa, (b) 5 MPa, c) 11 MPa and (d) 15 MPa, and the gel stiffness was 80 kPa (The elongation shown here is not to scale and the total displacement values corresponding to the images are given in Table 7.1)
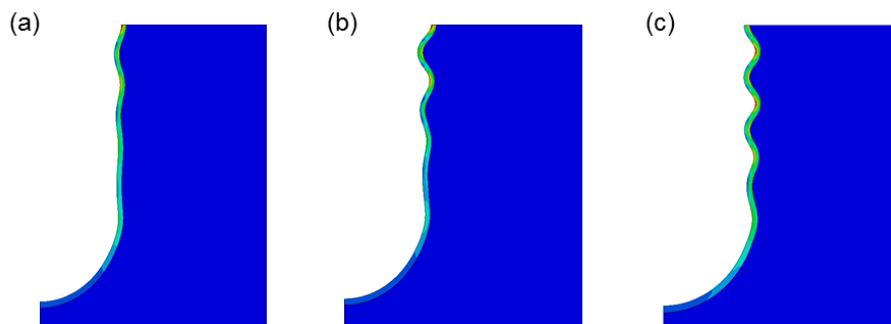
Figure 7.14. Elongation behaviour of encapsulated bacterial cells when both phases were considered to have elastic properties. Here, the bacterial hydrogel stiffness was (a) 15 kPa, (b) 25 kPa and c) 80 kPa, and the bacterial cell stiffness was 2 MPa (The elongation shown here is not to scale and the total displacement values corresponding to the images are given in Table 7.1)

For the cases presented in Figure 7.13 and 7.14, the time of initial wrinkling occurrence and the elongation at that time point were determined. For a gel stiffness of 80 kPa, when the bacterial cell stiffness was 2 MPa, 5 MPa and 11 MPa, wrinkling started at 84th minute, 90th minute and 120th minute

respectively and the elongation at those time points were 0.080 μm, 0.136 μm and 0.243 μm, following the same order.

For a bacterial cell stiffness of 2 MPa, when the gel stiffness was 15 kPa and 25 kPa, wrinkling started at 114th minute and 96th minute respectively and the elongation at those time points were 0.233 μm and 0.161 μm, following the same order.

Stiffness of cell (MPa)	Stiffness of gel (kPa)	Total elongation (μm)	Wrinkling behaviour (Number of wrinkles)	Wrinkle amplitude range (nm)
2	80	0.097	Yes (6)	19 – 43
	25	0.179	Yes (5)	15 – 51
	15	0.238	Yes (3)	13 – 32
3	80	0.118	Yes (6)	19 – 46
	25	0.223	Yes (3)	19 – 41
	15	0.270	No	
4	80	0.140	Yes (5)	24 – 48
	25	0.259	No	
	15	0.284	No	
5	80	0.157	Yes (5)	20 – 50
	25	0.270	No	
	15	0.292	No	
6	80	0.173	Yes (5)	17 – 51
	25	0.279	No	
	15	0.300	No	
10	80	0.229	Yes (3)	17 – 35
	25	0.300	No	
	15	0.311	No	
11	80	0.243	Yes (2)	10 – 28
	25	0.301	No	
	15	0.312	No	
12	80	0.243	No	
	25	0.301	No	
	15	0.312	No	
15	80	0.255	No	
	25	0.303	No	
	15	0.314	No	

Table 7.1. Elongation of a rod shaped bacterial cell in hydrogels with mechanical properties like1% LB gels obtained at different applied strains. Here, only elastic properties were considered

The wrinkling behaviour observed in 1% LB gels was attributed to the elastic instability of the encapsulated cells in a softer environment similar to the trend as Euler buckling in an elastic medium (Landau and Lifshitz, 1986).

For NB, LB-no yeast extract and LB-no tryptone gel properties (Tables 7.2-7.4, respectively), a wrinkling behaviour was not observed even for the smaller range of tested cell stiffness values. Therefore, the whole range of cell stiffness values as adopted in LB gels were not considered for these gel properties. The reason why no wrinkling behaviour was observed for these gels was due to their small elongation rates. As mentioned for LB gels, such a behaviour occurred after approximately 70% cell elongation, which was higher than the measured values for these gels (where the elongation rate changed between 4.3%-5.5%). There were no significant differences ($p > 0.05$) between the measured displacement of the cells when NB, LB-no yeast extract and LB-no tryptone gels were considered.

Stiffness of cell (MPa)	Stiffness of gel (kPa)	Total elongation (µm)	Wrinkling behaviour (Number of wrinkles)
2	70	0.024	No
	27	0.038	No
	25	0.039	No
3	70	0.030	No
	27	0.043	No
	25	0.044	No

Table 7.2. Elongation of a single rod shaped bacterial cell in hydrogels with mechanical properties like1% NB gels obtained at different applied strains. Here, only elastic properties were considered

Stiffness of cell (MPa)	Stiffness of gel (kPa)	Total elongation (µm)	Wrinkling behaviour (Number of wrinkles)
2	71	0.029	No
	26	0.046	No
	16	0.054	No
3	71	0.036	No
	26	0.053	No
	16	0.059	No

Table 7.3. Elongation of a single rod shaped bacterial cell in hydrogels with mechanical properties like1% LB-no yeast extract gels obtained at different applied strains. Here, only elastic properties were considered

Stiffness of cell (MPa)	Stiffness of gel (kPa)	Total elongation (µm)	Wrinkling behaviour (Number of wrinkles)
	86	0.029	No
2	31	0.050	No
	20	0.058	No
	86	0.037	No
3	31	0.058	No
	20	0.065	No

Table 7.4. Elongation of a single rod shaped bacterial cell in hydrogels with mechanical properties like1% LB-no tryptone gels obtained at different applied strains. Here, only elastic properties were considered

For the viscoelastic part, the hydrogel material properties were found by fitting Prony series model on the relaxation data obtained from compression tests with stress relaxation and the parameters were summarised in Table 7.5. Prony series model was used since this was the time dependent viscoelastic model used in the finite element software ABAQUS. Similar to the elastic properties, viscoelastic parameters of *E. coli* cells were obtained from literature (Vadillo-Rodriguez *et al.*, 2009). For comparison, the elastic behaviour of both phases were taken similar to the ones that were used in the elastic model.

Applied strain (%)	Media of the hydrogel	g_∞	$\tau\ (s)$
	LB	0.18	647.41
0.5	LB – no yeast extract	0.21	667.42
	LB – no tryptone	0.19	773.62
	NB	0.17	657.16
	LB	0.28	752.34
2	LB – no yeast extract	0.23	628.85
	LB – no tryptone	0.25	660.09
	NB	0.20	734.21
	LB	0.33	433.56
5	LB – no yeast extract	0.31	599.12
	LB – no tryptone	0.29	544.42
	NB	0.33	264.60

Table 7.5. Prony series fit parameters for 1% agarose hydrogels made with various growth media for different tested strains

Similar to the elastic model, when the viscoelastic elastic model was considered, as the stiffness of the bacterial cells increased, the total elongation/displacement of the cells also increased for all tested hydrogel stiffness values representing the different kind of gels tested.

For viscoelastic LB gel properties (Table 7.6), for the lower values of the tested cell stiffness range, *i.e.* when the cell stiffness was taken as 2 MPa and 3 MPa, wrinkling behaviour of the cell and gel interface was observed especially when the higher gel stiffness was considered. When both phases were considered viscoelastic, the wrinkling behaviour of this interface with increasing cell stiffness is shown in Figure 7.15 and the wrinkling behaviour of the interface with increasing gel stiffness is shown in Figure 7.16. As can be seen, the number of wrinkles decreased as the adopted bacteria stiffness increased. This behaviour was similar to the one observed in elastic model. However, unlike the elastic model, the threshold of bacterial stiffness was 12 MPa where only a slight wrinkling behaviour was observed. Any stiffness value adopted for the cells above this value did not result in wrinkling. Overall, when both phases were considered viscoelastic, if the fold difference between the bacterial cell and the LB gels was more than 200, wrinkling behaviour was not observed.

The wrinkle amplitude range obtained from the viscoelastic model was also given in Table 7.6. The measurements were taken from the peak values of all the wrinkles that were observed for the same construct. When these amplitude measurements from similar groups were compared (such as for the groups when the gel stiffness was 80 kPa and the cell stiffness values were changing), no significant differences ($p > 0.05$) were observed.

The overall elongation was analysed in 20 steps for the given expansion coefficient. A similar behaviour to that of the elastic model was observed and the wrinkling behaviour did not initiate exactly when the elongation started but after either 70% of cell elongation took place for when the cell stiffness was taken as 2 MPa or 95% of cell elongation took place for when the cell stiffness was taken as 12 MPa.

Therefore, having viscoelastic properties of both materials did not change the overall elongation behaviour but it changed the amount of the total displacement of bacterial cells where the bacterial cells showed less displacement in the gels when both phases were considered viscoelastic for a cell stiffness value up to 12 MPa.
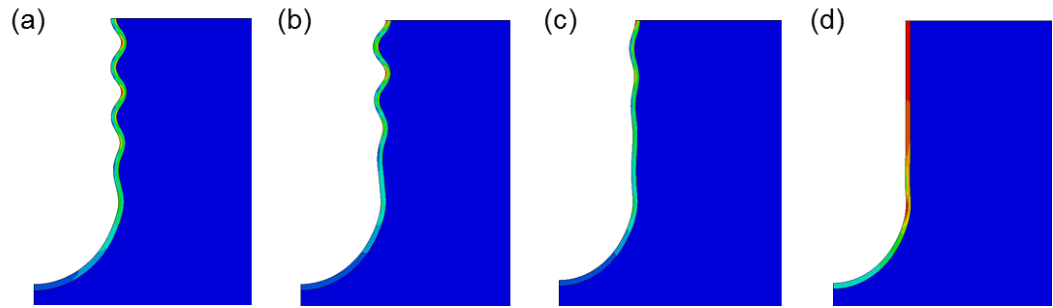
Figure 7.15. Elongation behaviour of encapsulated bacterial cells when both phases were considered to have viscoelastic properties. Here, the bacterial cell stiffness was (a) 2 MPa, (b) 5 MPa, c) 12 MPa and (d) 15 MPa, and the gel stiffness was 80 kPa (The elongation shown here is not to scale and the total displacement values corresponding to the images are given in Table 7.6)
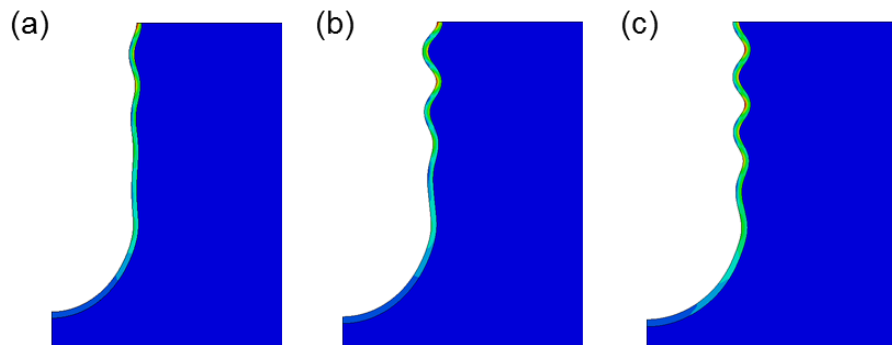
Figure 7.16. Elongation behaviour of encapsulated bacterial cells when both phases were considered to have viscoelastic properties. Here, the bacterial hydrogel stiffness was (a) 15 kPa, (b) 25 kPa and c) 80 kPa, and v the bacterial cell stiffness was 2 MPa (The elongation shown here is not to scale and the total displacement values corresponding to the images are given in Table 7.6)

For the cases presented in Figure 7.15 and 7.16, the time of initial wrinkling occurrence and the elongation at that time point were determined. For a gel stiffness of 80 kPa, when the bacterial cell stiffness was 2 MPa, 5 MPa and 12 MPa, wrinkling started at 84th minute, 84th minute and 120th minute respectively and the elongation at those time points were 0.076 µm, 0.125 µm and 0.242 µm, following the same order.

For a bacterial cell stiffness of 2 MPa, when the gel stiffness was 15 kPa and 25 kPa, wrinkling started at 102th minute and 90th minute respectively and the elongation at those time points were 0.189 µm and 0.139 µm, following the same order. When these values, for both when the gel stiffness and the cell stiffness were kept constant, were compared with the values

167

obtained from the elastic model, no significant differences were observed ($p > 0.05$).

Stiffness of cell (MPa)	Stiffness of gel (kPa)	Total elongation (µm)	Wrinkling behaviour (Number of wrinkles)	Wrinkle amplitude range (nm)
2	80	0.093	Yes (6)	18 – 42
	25	0.160	Yes (5)	20 – 51
	15	0.202	Yes (5)	10 – 48
3	80	0.113	Yes (6)	19 – 46
	25	0.198	Yes (5)	11 – 49
	15	0.255	No	
4	80	0.131	Yes (6)	19 – 46
	25	0.233	Yes (3)	16 – 35
	15	0.271	No	
5	80	0.150	Yes (5)	22 – 50
	25	0.259	No	
	15	0.281	No	
6	80	0.164	Yes (4)	25 – 48
	25	0.269	No	
	15	0.288	No	
10	80	0.217	Yes (3)	22 – 43
	25	0.291	No	
	15	0.304	No	
12	80	0.242	Yes (3)	10 - 29
	25	0.297	No	
	15	0.309	No	
13	80	0.254	No	
	25	0.299	No	
	15	0.310	No	
15	80	0.263	No	
	25	0.303	No	
	15	0.313	No	

Table 7.6. Elongation of a rod shaped bacterial cell in hydrogels with mechanical properties like1% LB gels obtained at different applied strains. Here, viscoelastic properties were considered

Euler buckling was also observed in viscoelastic columns (Dost and Glockner, 1982; Vinogradov, 1987). Therefore, the wrinkling behaviour observed in 1% LB gels when both phases (gel and the bacterial cells) had viscoelastic properties can be attributed to this phenomena.

Due to the small expansion rate, the viscoelastic properties did not change the cell displacement or the overall expansion behaviour when NB, LB-no

yeast extract and LB-no tryptone gels were considered. Therefore, the results were not presented again.

7.4   Summary of Results and Conclusions

In this chapter, bacterial cell elongation behaviour when they were encapsulated in hydrogels was characterised both by experimental and finite element modelling techniques.

Encapsulated bacterial cells were imaged for a period of 2 h in 1% hydrogels made with different growth media and it was determined that *E. coli* MC1061 cells which expressed fluorescence elongated in LB gels significantly more than in hydrogels made with other growth media. However, a similar elongation behaviour was not observed for LB-no yeast extract gel. This difference may be attributed to LB medium being a nutritionally richer medium compared to the other growth media. It was previously shown that, mechanical forces applied on the bacterial cells influenced bacterial growth dynamics and the geometry of the cell wall (Kumar and Libchaber, 2013; Si *et al.*, 2015). From the elongation experiments, it can be concluded that since different forces were applied to the encapsulated bacterial cells from the hydrogels that were made with different media, this may have also contributed to the different growth rates obtained which adds to the previously proposed mechanism where a complex interaction mechanism was suggested.

The elongation of bacterial cells were also modelled using the some of the results attained from the experimental setup, such as the growth rate. For both elastic and viscoelastic models, an increase in the elongation of the cells was observed when the stiffness of the bacterial cells increased for all tested gel properties. Also, a wrinkling behaviour of the cell and gel interface was observed especially when the LB gel mechanical properties were considered for the lower values of the tested cell stiffness range. For both cases, the number of wrinkles decreased as the adopted bacteria stiffness increased with a slight difference in the threshold bacteria stiffness where only a slight wrinkling behaviour was observed. Therefore, considering viscoelastic properties for both materials did not change the overall elongation behaviour, but it changed the amount of the total displacement

of bacterial cells where the bacterial cells showed less displacement in the gels for a cell stiffness up to 12 MPa.

A wrinkling behaviour as seen from the modelling results was not revealed in the experiments. The reason for this may be because the wrinkles were found to be at nanoscale (up to 50 nm) where the resolution of the equipment was not sufficient to capture such differences. Therefore, the morphology of the *E. coli* MC1061 cells that were presented in several images throughout this chapter should not be interpreted as wrinkles.

The results obtained from the created model suggested that a more complicated computational model is required which involves turgor pressure and multiple expansion directions to better represent the bacterial elongation behaviour when they are encapsulated in 3D microenvironments. Also, the experiments can be further developed for the modified *E. coli* MC1061 cells with the division inhibitor and then combined with the finite element model to also take into account various cell lengths. If wrinkling of bacterial cell wall takes place, it might affect the bacteria division or viability. To prevent this from happening, bacteria might become stiffer which may be correlated with turgor pressure where turgor pressure can be affected by both the osmolarity of the cytoplasm and the osmolarity of the extracellular medium (Deng *et al.*, 2011; Rojas *et al.*, 2014). More advanced techniques such as super-resolution imaging may be used to further examine this hypothesis.

8   Conclusions and Future Work

8.1   Conclusions

An array of experimental, computational and theoretical approaches have been employed to explore the interactions between typical bacteria (*E. coli* and *S. epidermidis*) and the three-dimensional biomaterials like agarose gel.

Agarose hydrogels made with PBS, NB, LB and LB based media with and without encapsulated bacterial cells were analysed using different characterisation techniques which resulted in different responses. Similar test conditions were modelled as well to take into account the effect of the bacterial cells.

Based on the main findings of this research project, the following conclusions can be drawn:

- The instantaneous elastic modulus characterisation of 1% agarose hydrogels presented a strain dependent behaviour.
- 1% agarose hydrogels made with different growth media showed significant differences in mechanical properties among themselves suggesting that the media used could affect the mechanical responses of hydrogels.
- When the same tests were applied to higher concentration agarose hydrogels (2% and higher) such a dependence of mechanical properties of hydrogels on the used media was not observed. Therefore, this is related to the stiffness of the fabricated hydrogels.
- Bacterial cells became significantly stiffer or had stronger interactions with hydrogels when cultured in 1% agarose gels made with LB medium compared to NB medium or PBS. Furthermore, it was revealed that the tryptone component of LB was responsible for such a behaviour. Previously, it has been shown that mechanical properties of agarose gels were affected by the presence and amount of sugars (such as glucose and sucrose), urea and guanidine hydrochloride (Watase *et al.*, 1990; Deszczynski *et al.*, 2003). Although the peptide-based tryptone has an unclear chemical

composition, the different peptides within tryptone could be affecting agarose gel mechanical properties in a similar manner.

- The FEA model results also confirmed that bacterial cells had a contribution in the change of mechanical properties of hydrogels since there were no differences observed between the simulated hydrogels with and without encapsulated particles at similar test conditions when the bacterial cells were treated as inert particles.

- A change in mechanical properties of hydrogels with encapsulated bacterial cells was not observed when higher concentration hydrogels were considered. It can be concluded that the changes in mechanical properties of hydrogels are also related to the stiffness of the fabricated hydrogels and bacterial cells could not have similar interactions with the hydrogels having stiffer structures. The reason for this can be attributed to the higher density of the agarose polymer chains, which does not allow the bacterial cells to interact in a similar way as in 1% gels.

- The tryptone present in LB did not affect the growth of bacterial cells in planktonic culture or in 3D microenvironments when the elongation rate was considered.

- The dependence of the mechanical properties on the chemical composition and the encapsulated bacterial cells is also related to the type of loading applied since a concentration or encapsulation dependent mechanical property difference was not observed when rheological characterisation was carried out which can be related to the rheological tests being carried out as SAOS tests.

Overall, this research project demonstrated that, subtle differences in physical/chemical properties of the 3D microenvironment regulate cell mechanics and mechanical interactions with hydrogels. Thus, changes in extracellular polymer matrix caused by factors, such as drugs, may regulate bacteria mechanics, which potentially may lead to changes in cell structure and metabolic functions.

8.2 Future work

The findings of this study complemented those of previous researchers, and contributed to extend the knowledge on the interactions with bacterial cells and hydrogels considered in a 3D microenvironment. Especially, a specific variable was identified that has an effect on the hydrogel mechanical properties. Nevertheless, some suggestions are listed below that will be valuable for future research.

- Further improvement of FEA models for compression tests:

In this study, the constructed FEA models, which took into account many variables, represented the basic experimental setup for the compression tests. The model can be further developed to take into consideration the particle shape. Also, the relaxation behaviour can be involved as well to compare with the experimental data.

- Experimental design to investigate the response observed in FEA elongation model:

The FEA model for the elongation revealed a wrinkling behaviour at certain bacterial cell and hydrogel stiffness values. The experimental setup can be further improved to observe such behaviour. Furthermore, modified *E. coli* MC1061 cells with pEGFP and pPZV56 plasmids can be utilised for such experiments. Turgor pressure will also be implemented to FEA.

- Develop FEA models for rheological characterisation:

In the rheological experiments, a difference was not observed between hydrogels with and without encapsulation when different conditions were tested which included various gel concentrations and test temperatures. Similar to the compression tests, this lack of difference can be attributed to the complex interactions between hydrogels, bacterial cells (which vary under different conditions) and the type of applied force. Therefore, it will be beneficial to construct a FEA model to represent the rheological experiments for the case of inert particles.

- Expand the variety of liquid medium:

Other media having a high protein content (such as bovine serum (Cistola *et al.*, 1987)) should also be used to fabricate the hydrogels to observe the media effect.

- Further microbiological tests:

The impact of different 3D microenvironments on transcription and protein expression by bacteria can be tested, to suggest a potential for the control of biofilms by modulation of the extracellular matrix.

Appendix A – Viability of Encapsulated Bacterial Cells

A1.1 Viability of encapsulated cells from plating method

After finding the melting temperature of agarose hydrogels, suitable concentrations for encapsulation of bacteria were decided to be 1-5%. The hydrogel concentrations were divided into three groups: 1% and 3% hydrogels, 2% and 4% hydrogels, 5% hydrogels and for the three different experiment groups, overnight cultures were produced separately. The bacterial density of the overnight culture used for the experimental groups were 2.6×10^9 cfu/ml, 3.7×10^9 cfu/ml and 2.0×10^9 cfu/ml, respectively. The encapsulated bacterial cells were plated on LB plates at three different times: as soon as they were encapsulated, after 2 h and after 4h.

After the bacteria inside the encapsulation solution were grown on the LB plates overnight, they were counted from different dilution series. The images for one of the trials of 1% hydrogel at 10^{-5} and 10^{-6} dilutions are given in Figures A1.1 - A1.3.
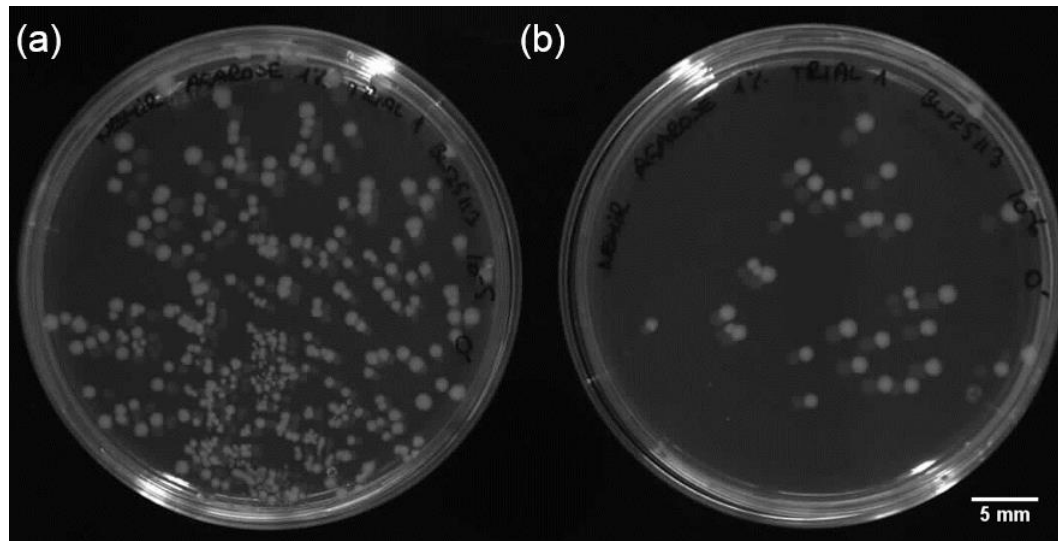
Figure A1.1. Encapsulated *E. coli* BW25113 in 1% agarose (a) 10^{-5} and (b) 10^{-6} spread at minute 0
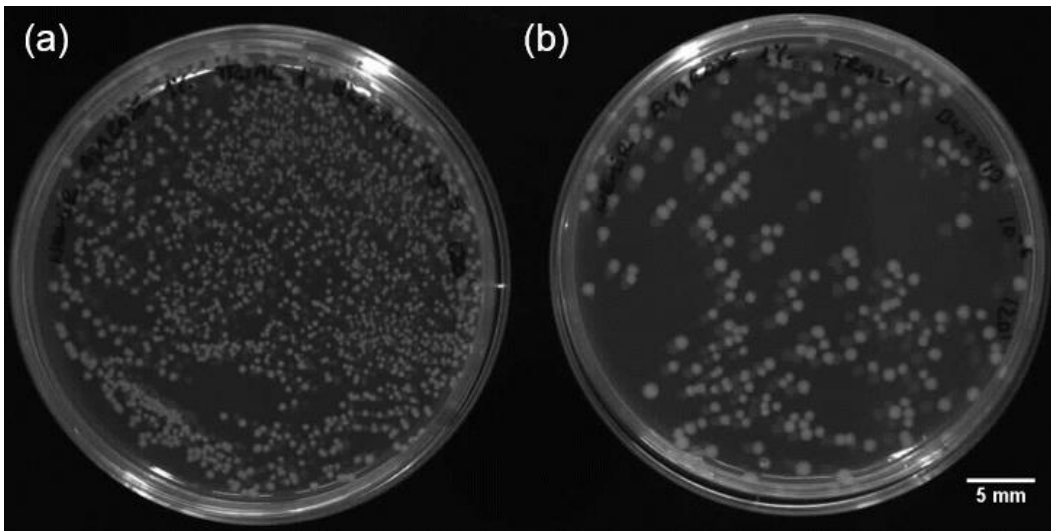
Figure A1.2. Encapsulated *E. coli* BW25113 in 1% agarose (a) 10^{-5} and (b) 10^{-6} spread at minute 120
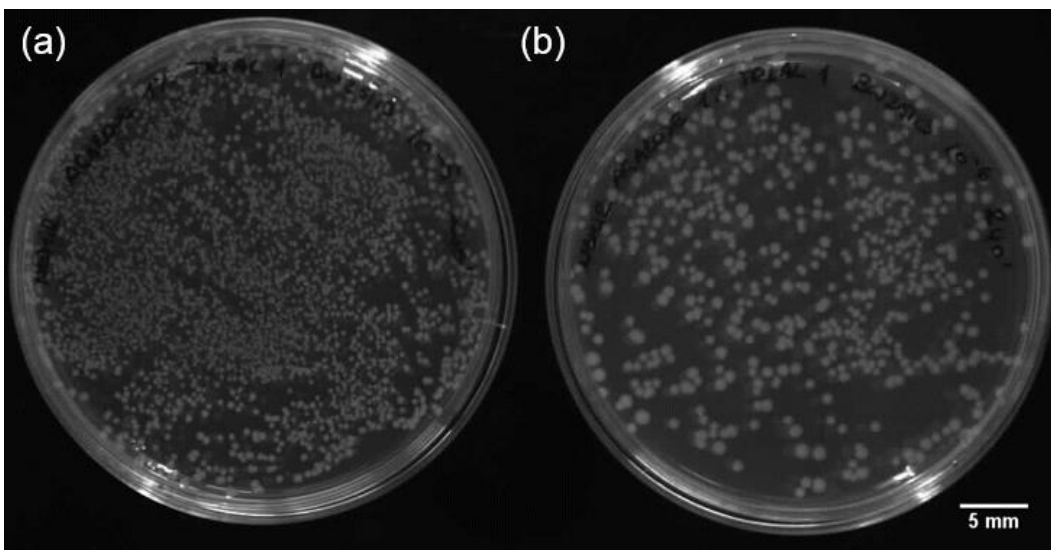
Figure A1.3. Encapsulated *E. coli* BW25113 in 1% agarose (a) 10^{-5} and (b) 10^{-6} spread at minute 240

The viability of the encapsulated bacteria was assessed based on the bacterial density information. From the colony counts on each plate, the bacterial density of the encapsulation solution was calculated for all the time intervals and given in Table A1.1.

Gel concentration (%)	Minute 0 Mean (cfu/ml) ($\times 10^6$)	Minute 120 Mean (cfu/ml) ($\times 10^6$)	Minute 240 Mean (cfu/ml) ($\times 10^6$)
1	28.3 ± 12.9	317 ± 47.3	690 ± 43.6
2	2.57 ± 0.61	11.8 ± 2.93	109 ± 21.0
3	1.07 ± 0.57	13.0 ± 2.65	277 ± 10.7
4	1.73 ± 0.46	2.80 ± 0.62	197 ± 20.8
5	N/A	9.70 ± 7.55	68.3 ± 10.0

Table A1.1. Bacterial density values for different time intervals (Data presented as mean ± standard deviation, $n = 3$)

A1.2   Viability of encapsulated cells from imaging

The viability of the encapsulated bacteria cells inside agarose hydrogels was also shown by imaging of the cells stained with LIVE/DEAD BacLight Bacterial Viability Kit, using a confocal microscope at x63 magnification. 1% agarose hydrogels with *E. coli* BW25113 and *S. epidermidis* FH30 cells with bacterial cells encapsulated at 1% and 3% volume fractions were imaged. The images obtained from the confocal microscope is given in Figures A1.4 and A1.5. The green colour indicates the live cells and the red colour indicates the dead cells. Based on this information, it can be said that the bacteria cells remain alive when encapsulated in 1% agarose hydrogels.
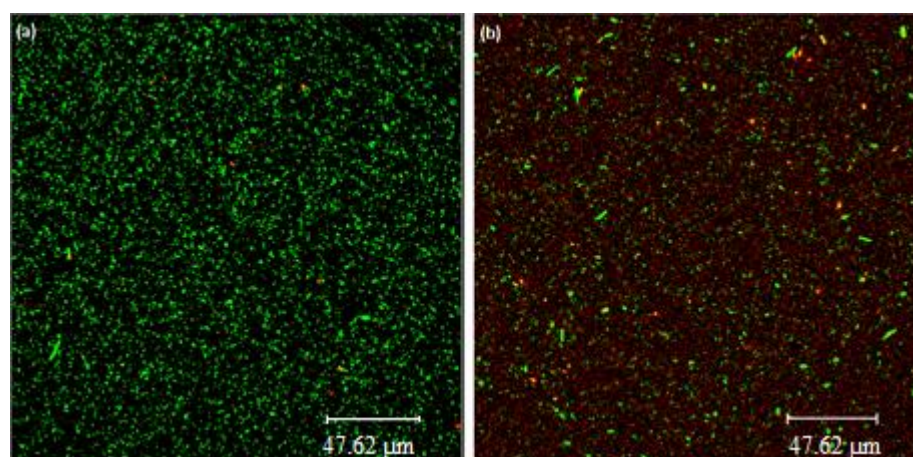
Figure A1.4. Encapsulated *E. coli* BW25113 in 1% agarose (a) at 1% volume fraction and (b) at 3% volume fraction
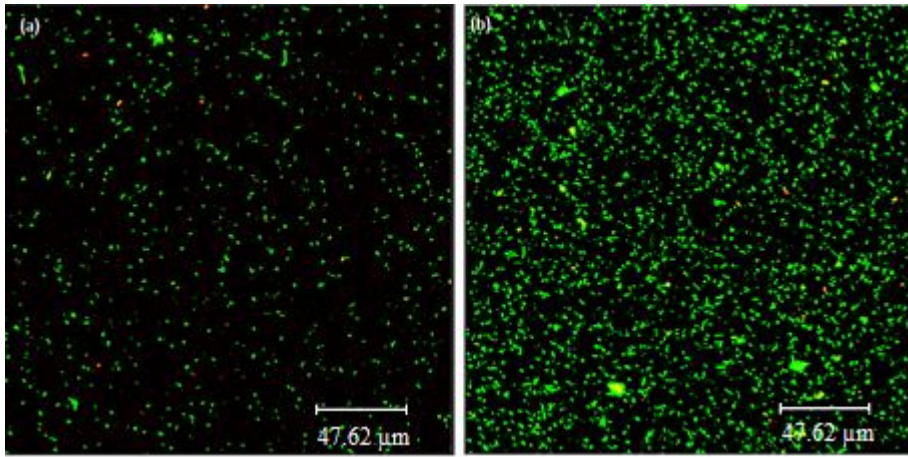
Figure A1.5 Encapsulated *S. epidermidis* FH30 in 1% agarose (a) at 1% volume fraction and (b) at 3% volume fraction

S. epidermidis FH30 cells with encapsulated cells at 3% volume fraction were also encapsulated in 5% agarose hydrogel to check the viability in higher percentage hydrogels (Figure A1.6). The imaging was done at x63 magnification.
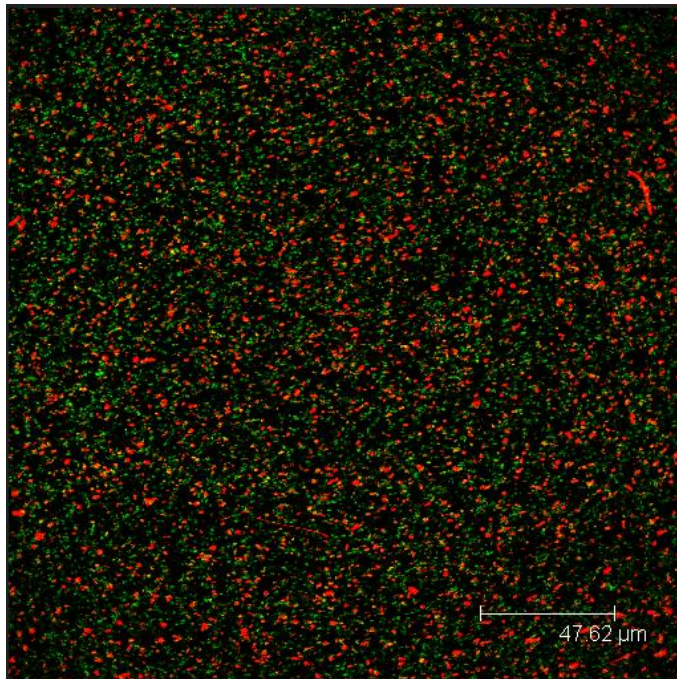
Figure A1.6. Encapsulated *S. epidermidis* FH30 in 5% agarose gel at 3% volume fraction

A1.3 Conclusions from viability of bacterial cells encapsulated in hydrogels

From both experiments about the viability of encapsulated bacteria cells, similar conclusions were reached. For the results obtained from plating, as can be seen from the bacterial density values in Table A1.1, there is a ~10-fold increase at the end of the second hour for the hydrogel concentrations of 1-3% which indicates that the bacteria cells were not dying and they were viable. For 4% hydrogels, the increase was ~1.5 fold for the same period of growth which suggests that the bacteria cells were still viable but due to the concentration effect, they did not grow as freely as in lower concentrations. For 5% agarose hydrogel at minute 0, there was a possible error at the dilution series since no colonies grew on the agar plates. From the data collection for all concentration hydrogels at the end of 240 minutes, it was also found out that the colony counts increased supporting cell viability.

The images obtained from confocal imaging were preliminary, this technique was only applied once to the specified hydrogels at an empirical diffusion time of the fluorescent dyes. From the images obtained, the encapsulation done for 1% hydrogels, the cells are viable both at lower and higher volume fractions of cells, especially for *S. epidermidis*. There seems to be several clusters of live cells for both *E. coli* and *S. epidermidis* cells at higher volume fractions which might be due to the population of cells. The encapsulation of the *S. epidermidis* cells in 5% agarose hydrogel suggests that there are more dead cells compared to the ones obtained for 1% agarose hydrogel. From the images obtained for 5% hydrogels with encapsulation, the live and dead cell ratio was ~1:1.

Appendix B – Burger's Model Fit for 1% Agarose Gels Tested at Different Strain Values
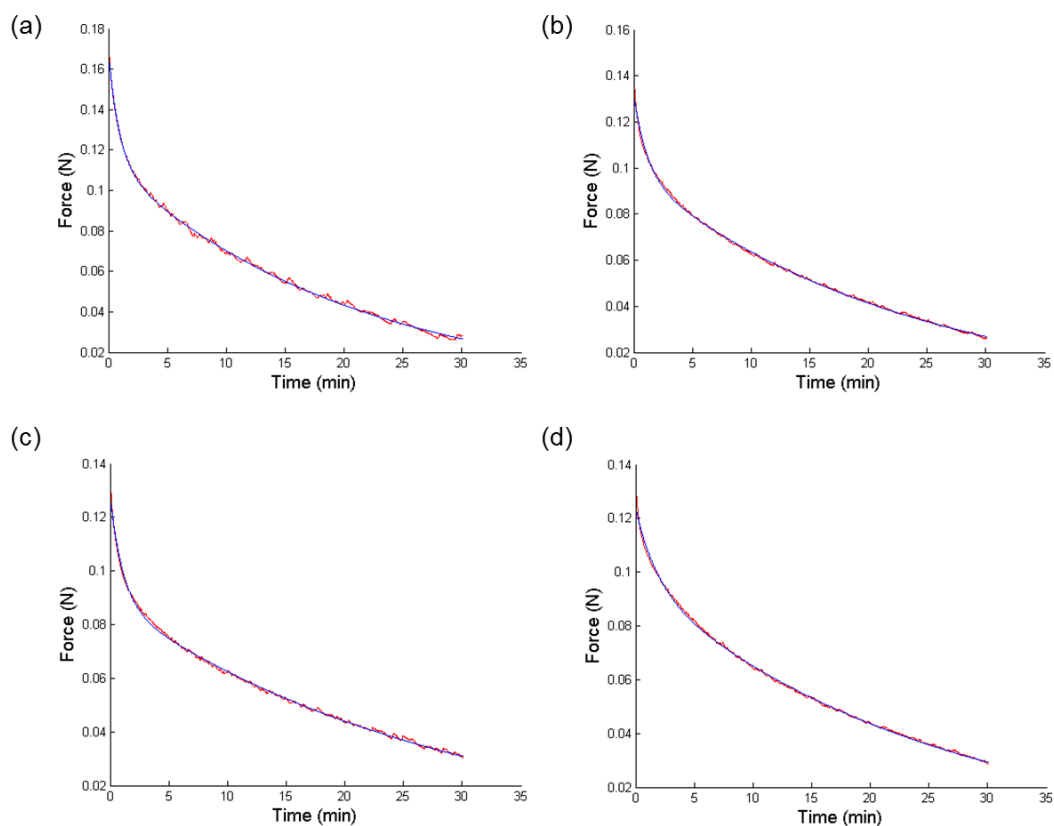
Figure B.1. Burger's model fit for 1% agarose hydrogels without encapsulation made with (a) PBS, (b) NB, (c) LB-no yeast extract and (d) LB-no tryptone, when the applied strain was 0.5%
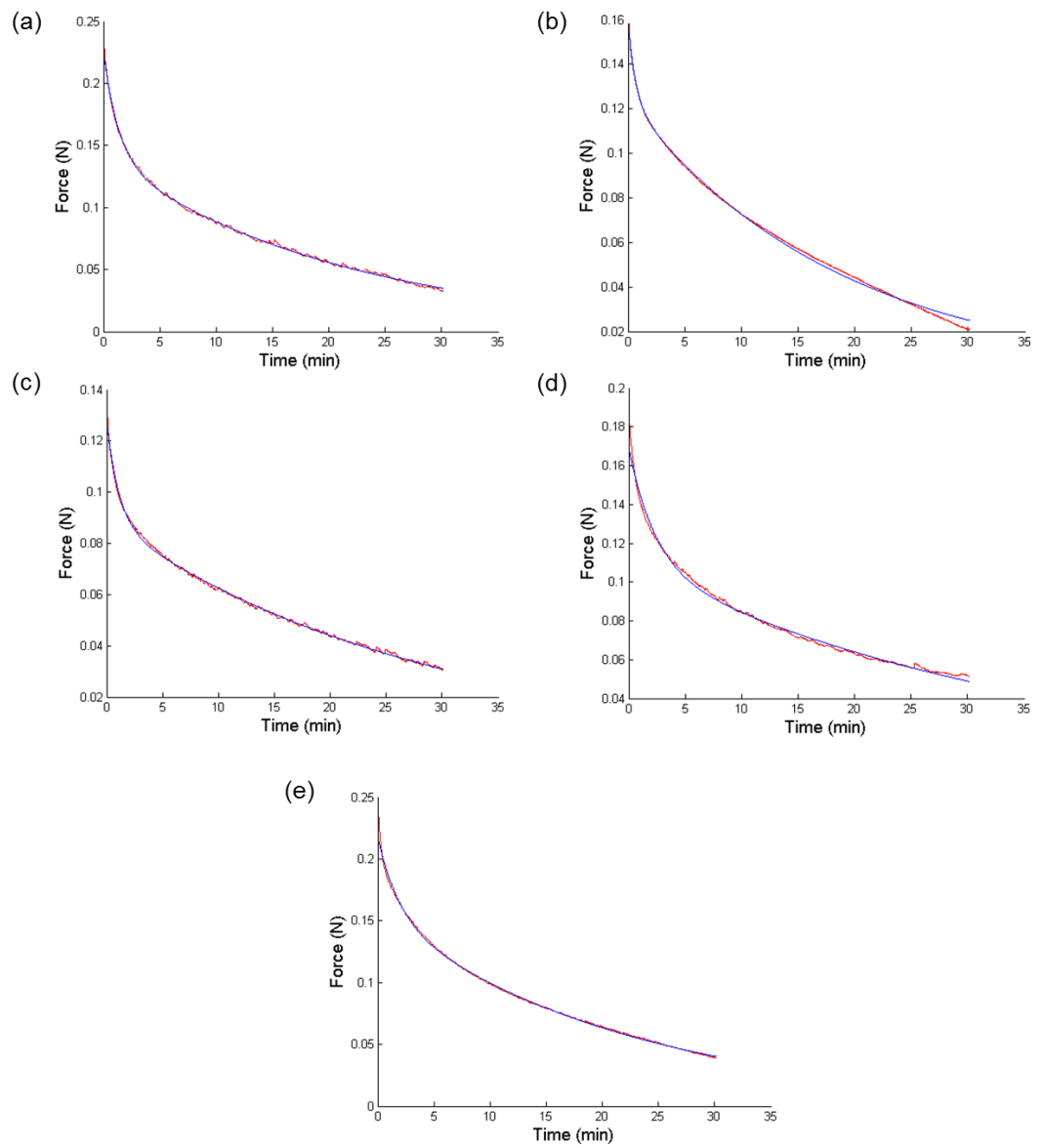
Figure B.2. Burger's model fit for 1% agarose hydrogels without encapsulation made with (a) PBS, (b) NB, (c) LB, (d) LB-no yeast extract and (e) LB-no tryptone, when the applied strain was 2%
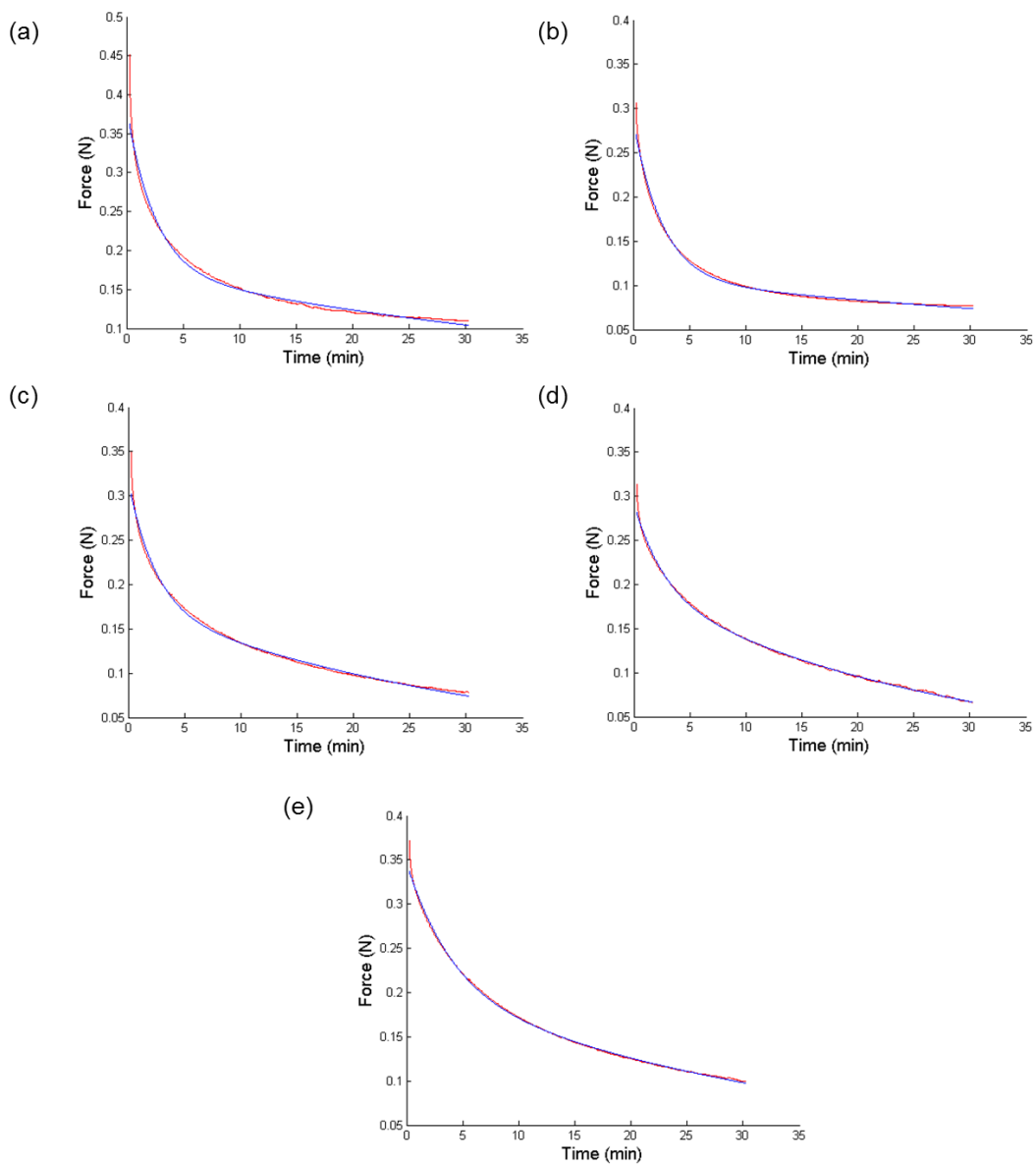
Figure B.3. Burger's model fit for 1% agarose hydrogels without encapsulation made with (a) PBS, (b) NB, (c) LB, (d) LB-no yeast extract and (e) LB-no tryptone, when the applied strain was 5%
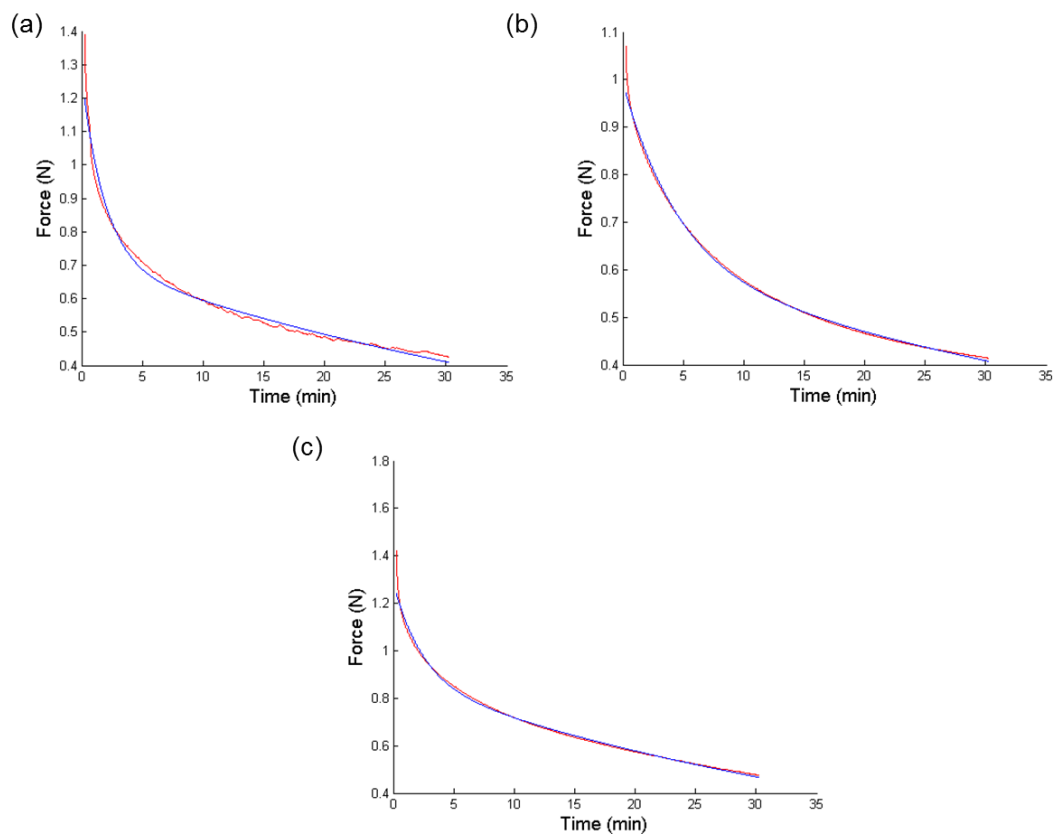
Figure B.4. Burger's model fit for 2% agarose hydrogels without encapsulation made with (a) PBS, (b) NB, (c) LB, when the applied strain was 5%
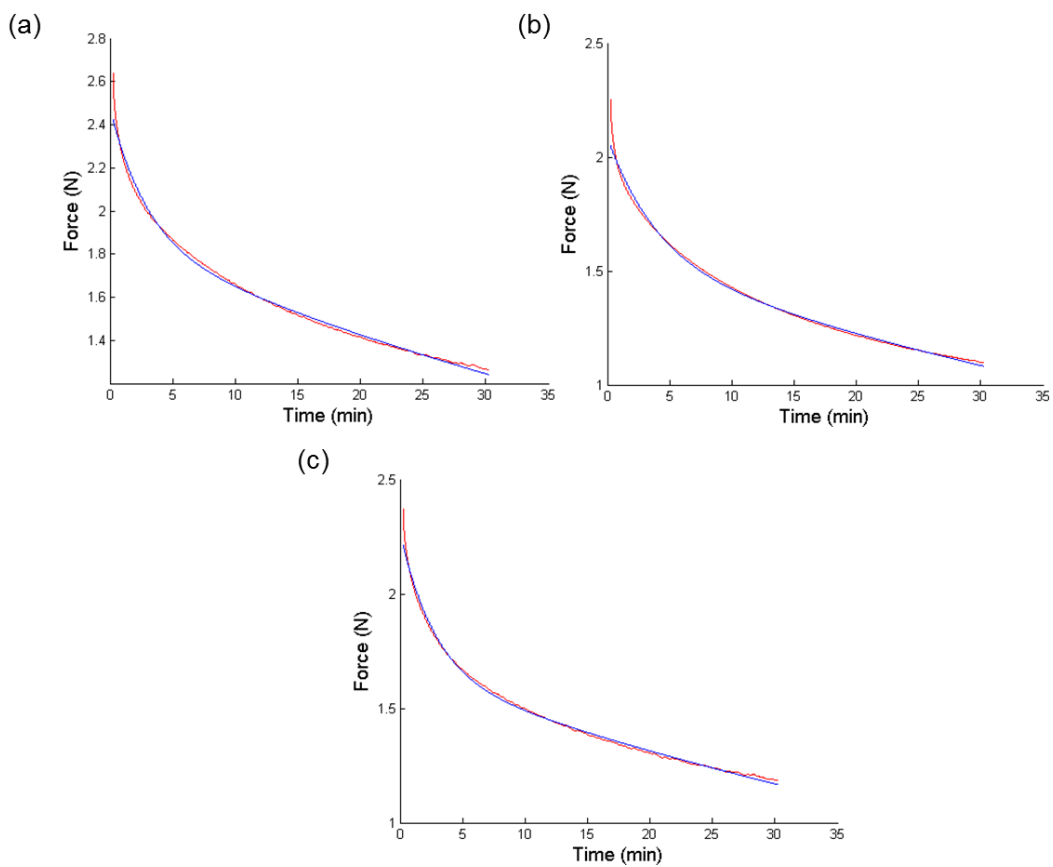
Figure B.5 Burger's model fit for 3% agarose hydrogels without encapsulation made with (a) PBS, (b) NB, (c) LB, when the applied strain was 5%

Appendix C – Frequency Sweep Response of 1% Hydrogels for Wider Frequency Range
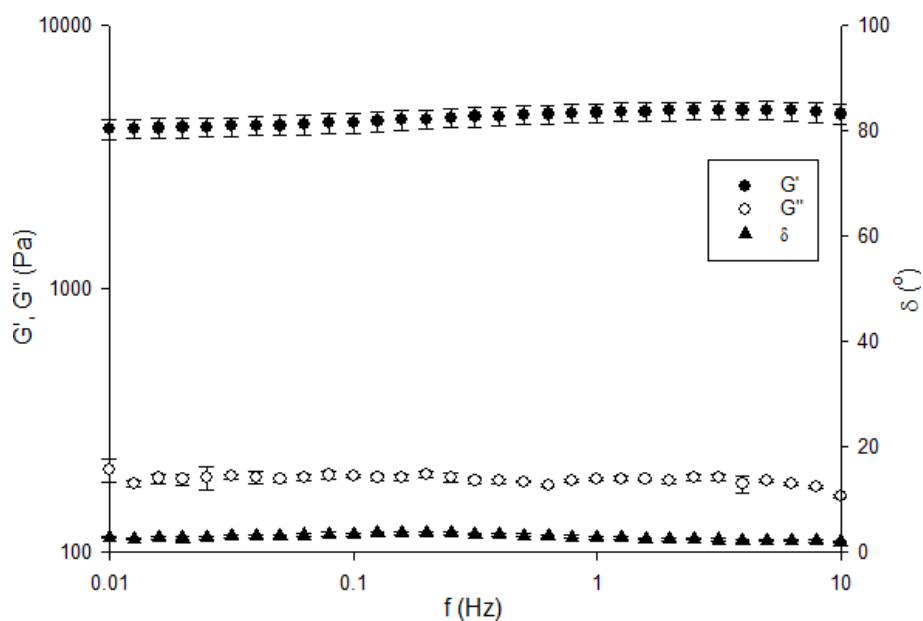
Figure C.1. Dependence of elastic and viscous shear moduli and phase angle on frequency for 1% LB agarose gel without encapsulation when the applied strain was 0.01% and the temperature was 37°C. Shear moduli and frequency values are plotted in a log-log scale
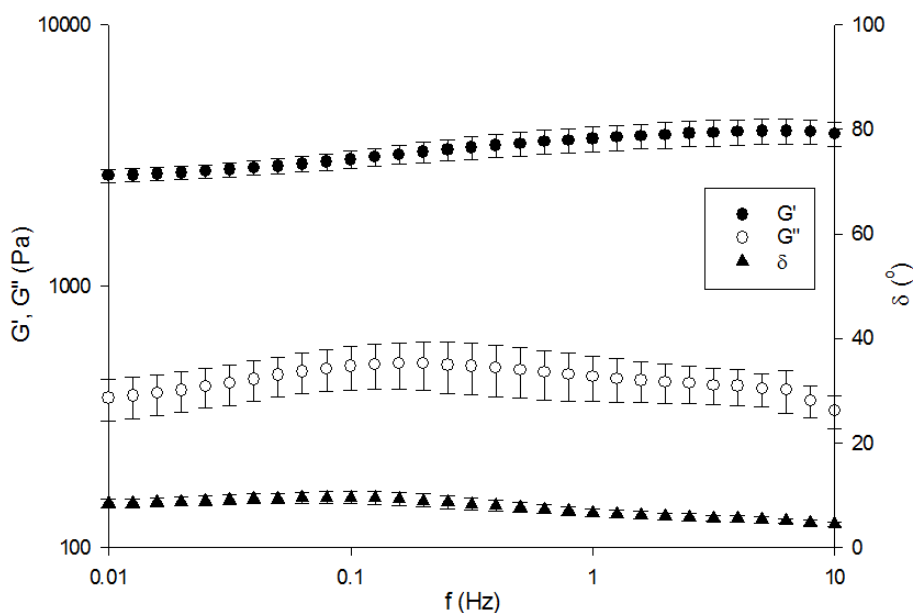
Figure C.2. Dependence of elastic and viscous shear moduli and phase angle on frequency for 1% LB agarose gel without encapsulation when the applied strain was 1% and the temperature was 37°C. Shear moduli and frequency values are plotted in a log-log scale

Appendix D – Bacterial Length and Elongation Determination

Codes for cropping the overall z-plane images to obtain single bacteria image directory, steps for fitting an ellipse to the edges of single bacteria and obtaining ellipse parameters are presented in this Appendix.

- Cropping the overall z-plane images: this code involves reading the images to be analysed, identifying the coordinates of single bacterium within the overall z-plane and cropping the images to obtain a new directory of image files containing only the bacterial cell to be analysed.

```matlab
for z=12    % Read all images taken at each time step for a plane
        for t=1:59
            if t<10 & z<10
                imgname = ['081216t0' int2str(t) 'xy1z0'
int2str(z) '.tif']
                filename =['bacteria3_' int2str(t) '.tif']
            elseif t<10 & z<100
                imgname = ['081216t0' int2str(t) 'xy1z'
int2str(z) '.tif']
                filename =['bacteria3_' int2str(t) '.tif']
            elseif t>=10 & z<10
                imgname = ['081216t' int2str(t) 'xy1z0'
int2str(z) '.tif']
                filename =['bacteria3_' int2str(t) '.tif']
            elseif t>=10 & z<100
                imgname = ['081216t' int2str(t) 'xy1z'
int2str(z) '.tif']
                filename =['bacteria3_' int2str(t) '.tif']
            end
            x=imread(imgname);
            figure(1)          ⎤
            imshow(x)          ⎥
            axis on            ⎥  I
            grid on            ⎦

%           y=imcrop(x,[380,410,30,40]);  ⎤
%           figure(2)                     ⎥
%           imshow(y)                     ⎥
%           pause(0.001)                  ⎥
%           mkdir('bact1')                ⎥  II
%           cd('bact1')                   ⎥
%           imwrite(y,filename)           ⎥
%           cd ..                         ⎦
        end
    end
```

After reading the files and deciding on the coordinates of single bacteria to be analysed, part I should be held and part II should be released.

- Identifying the edges of the bacteria cells and fitting an ellipse to obtain ellipse parameters and these parameters were saved under param_bact file to be used to calculate the bacterial elongation.

```matlab
fol_no =1;
folname = ['F:\imaging\08122016_1pc_stationary\images\bact'
int2str(fol_no)];
savename = ['param_bact' int2str(fol_no) '.mat'];
cd(folname)
fileno =[1];
counter=0;
for fi =1:59
    counter = counter+1;
    clear  filename X Y Y1 BW2 BW3 x y STATS
    if fi<100
        filename = ['bacteria1_' int2str(fi) '.tif'];
    end

   X=imread(filename);    % image reading
    figure(1)
    imshow(X)
    Y = im2bw(X,0.05); % turn image to black and white
    Y1 =bwareaopen(Y,20);  % removes all connected objects that
have fewer than P pixels from the binary image, producing another
binary image
    BW2 = imfill(Y1,'holes'); % fills the holes in either the
black or white region
    BW3 = imdilate( BW2, strel('disk', 1) );
    BW4 = bwboundaries(BW3); % traces the exterior boundaries of
binary (BW) image
    x = BW4{1,1}(:,2);
    y = BW4{1,1}(:,1);
    STATS =
regionprops(Y1,'MajorAxisLength','MinorAxisLength','Extrema','Peri
meter'); %Measure properties of image regions
    maj_ax(counter)=STATS.MajorAxisLength;
    min_ax(counter)=STATS.MinorAxisLength;
    perimeter(counter)=STATS.Perimeter;
    figure(2)
    imshow(Y1)
    hold on
    plot(STATS.Extrema(:,1),STATS.Extrema(:,2),'ro')
    figure(3)
    imshow(Y1)
    hold on
    plot(x,y,'ro')
    param_ellipse = fit_ellipse( x,y,3)
    ax_maj(counter) = 2*param_ellipse.a;
    ax_min(counter) = 2*param_ellipse.b;
    pause(0.001)

end

figure(11)
plot(maj_ax,'b-')
hold on
plot(ax_maj,'r-')

figure(12)
plot(min_ax,'b-')
```

```matlab
hold on
plot(ax_min,'r-')

for j=1:length(ax_min)-1
    for i=1:j
        dl_ax_maj(i,j)=(ax_maj(j+1)-ax_maj(j));
    end
end


for k=1:length(ax_min)-1
    for l=1:k
        dl_ax_min(l,k)=(ax_min(k+1)-ax_min(k));
    end
end


for m=1:length(maj_ax)-1
    for n=1:m
        dl_maj_ax(n,m)=(maj_ax(m+1)-maj_ax(m));
    end
end


for p=1:length(min_ax)-1
    for q=1:p
        dl_min_ax(q,p)=(min_ax(p+1)-min_ax(p));
    end
end

save(savename,'maj_ax','min_ax','ax_maj','ax_min','dl_maj_ax','dl_
min_ax','dl_ax_maj','dl_ax_min')
```

- <u>Calculating the elongation</u>: after saving the ellipse parameters, they were used to calculate the growth

```matlab
for folno=1:30
    folname = ['1_bact' int2str(folno)];
    filename = ['param_bact' int2str(folno) '.mat'];
    savename = ['growth_bact_' int2str(folno) '.mat'];
    cd(folname)
    clear maj_ax min_ax Bac
    Bac = struct('dL',{},'dT',{});
    load(filename)
    time = (0:length(maj_ax)-1)*120;
    len = length(maj_ax);

    for step =1:len-1
        dL =[]; dT = [];
        for ele=1:step
            dl =diff(maj_ax(ele:step:len));
            dt =diff(time(ele:step:len));
            dL=[dL dl];
            dT=[dT dt];
        end
        dL=dL/maj_ax(1);
        Bac(step).dL = dL;
        Bac(step).dT = dT;
    end
    save (savename,'Bac')
    cd ..

end
```

- **<u>Plotting the elongation</u>**: using the saved parameters from growth_bact, a normalised elongation plot was created.

```matlab
um_pix=0.2;
m_dbl_1=[];s_dbl_1=[];
for time=1:58
    diff_len_1=[];diff_time1=0;
    for folno=1:30
        folname = ['1_bact' int2str(folno)];
        filename = ['growth_bact_' int2str(folno) '.mat'];
        cd(folname)
        clear Bac
        load(filename)
        diff_len_1=[diff_len_1 [Bac(time).dL]];
        diff_time1 = [diff_time1 [Bac(time).dT]];
        cd ..
    end
    clear p q
    [p,q] = find(diff_len_1<0);
    diff_len_1(q)=[];
    m_dbl_1(time)= mean(diff_len_1);
    s_dbl_1(time)=std(diff_len_1);
end

m_dbl_1=um_pix*(m_dbl_1);
s_dbl_1=um_pix*(s_dbl_1);
dt = (1:58)*120;

figure(1)
errorbar(dt,m_dbl_1,s_dbl_1)
hold on
plot(dt,m_dbl_1,'ro','markersize',3,'MarkerFaceColor','r')
set(gca,'Fontsize',25)
xlabel('dt (s)','Fontsize',25)
ylabel('dL/L0','Fontsize',25)
title('1% LB gel')
axis([0 8000 -0.05 0.30])
print('-dtiff','-r1000','lb')
```

References

Absolom, D.R., Lamberti, F.V., Policova, Z., Zingg, W., van Oss, C.J. and Neumann, A.W. (1983) 'Surface thermodynamics of bacterial adhesion', *Applied and Environmental Microbiology*, 46(1), pp. 90-97.

Abu-Lail, N.I. and Camesano, T.A. (2006) 'The effect of solvent polarity on the molecular surface properties and adhesion of *Escherichia coli*', *Colloids and Surfaces B: Biointerfaces*, 51(1), pp. 62-70.

Ahearne, M. (2014) 'Introduction to cell–hydrogel mechanosensing', *Interface Focus*, 4(2), p. 20130038.

Ahearne, M., Yang, Y., El Haj, A.J., Then, K.Y. and Liu, K.-K. (2005) 'Characterizing the viscoelastic properties of thin hydrogel-based constructs for tissue engineering applications', *Journal of The Royal Society Interface*, 2(5), pp. 455-463.

Ahmed, E.M. (2015) 'Hydrogel: Preparation, characterization, and applications: A review', *Journal of Advanced Research*, 6(2), pp. 105-121.

Ahmed, J., Ptaszek, P. and Basu, S. (2016) *Advances in Food Rheology and Its Applications*. Woodhead Publishing.

Alam, S.Y. and Hammoum, F. (2015) 'Viscoelastic properties of asphalt concrete using micromechanical self-consistent model', *Archives of Civil and Mechanical Engineering*, 15(1), pp. 272-285.

An, Y.H. and Friedman, R.J. (1998) 'Concise review of mechanisms of bacterial adhesion to biomaterial surfaces', *Journal of Biomedical Materials Research Part A*, 43(3), pp. 338-348.

Angert, E.R. (2005) 'Alternatives to binary fission in bacteria', *Nature Reviews Microbiology*, 3(3), p. 214.

Anseth, K.S., Bowman, C.N. and Brannon-Peppas, L. (1996) 'Mechanical properties of hydrogels and their experimental determination', *Biomaterials*, 17(17), pp. 1647-1657.

Antoine, E.E., Vlachos, P.P. and Rylander, M.N. (2014) 'Review of collagen I hydrogels for bioengineered tissue microenvironments: characterization of mechanics, structure, and transport', *Tissue Engineering Part B: Reviews*, 20(6), pp. 683-696.

Atlas, R.M. (2010) *Handbook of Microbiological Media*. 4th edition. CRC Press.

Augst, A.D., Kong, H.J. and Mooney, D.J. (2006) 'Alginate hydrogels as biomaterials', *Macromolecular Bioscience*, 6(8), pp. 623-633.

Baba, T., Ara, T., Hasegawa, M., Takai, Y., Okumura, Y., Baba, M., Datsenko, K.A., Tomita, M., Wanner, B.L. and Mori, H. (2006) 'Construction of *Escherichia coli* K-12 in-frame, single-gene knockout mutants: the Keio collection', *Molecular Systems Biology*, 2(1), pp. 2006.0008.

Baker, B.M. and Chen, C.S. (2012) 'Deconstructing the third dimension–how 3D culture microenvironments alter cellular cues', *J Cell Sci*, 125(13), pp. 3015-3024.

Baker, E.L., Lu, J., Yu, D., Bonnecaze, R.T. and Zaman, M.H. (2010) 'Cancer cell stiffness: integrated roles of three-dimensional matrix stiffness and transforming potential', *Biophysical Journal*, 99(7), pp. 2048-2057.

Balgude, A.P., Yu, X., Szymanski, A. and Bellamkonda, R.V. (2001) 'Agarose gel stiffness determines rate of DRG neurite extension in 3D cultures', *Biomaterials*, 22(10), pp. 1077-1084.

Barbucci, R. (2009) *Hydrogels: Biological Properties and Applications*. Springer.

Barnes, H.A. (2000) *A handbook of elementary rheology*. Wales: The University of Wales Institute of Non-Newtonian Fluid Mechanics.

Barnes, H.A., Hutton, J.F. and Walters, K. (1989) *An introduction to rheology (Vol. 3)*. Elsevier.

Bartholomew, J.W. and Mittwer, T. (1952) 'The gram stain', *Bacteriological Reviews*, 16(1), p. 1.

Baskurt, O.K. and Meiselman, H.J. (2003) *Seminars in thrombosis and hemostasis*. Thieme Medical Publishers, Inc.

Bausch, A.R., Ziemann, F., Boulbitch, A.A., Jacobson, K. and Sackmann, E. (1998) 'Local measurements of viscoelastic parameters of adherent cell surfaces by magnetic bead microrheometry', *Biophysical Journal*, 75(4), pp. 2038-2049.

Beveridge, T.J. (1999) 'Structures of gram-negative cell walls and their derived membrane vesicles', *Journal of Bacteriology*, 181(16), pp. 4725-4733.

Beveridge, T.J. and Davies, J.A. (1983) 'Cellular responses of *Bacillus subtilis* and *Escherichia coli* to the Gram stain', *Journal of Bacteriology*, 156(2), pp. 846-858.

Bhattarai, N., Gunn, J. and Zhang, M. (2010) 'Chitosan-based hydrogels for controlled, localized drug delivery', *Advanced Drug Delivery Reviews*, 62(1), pp. 83-99.

Bhavikatti, S. (2005) *Finite element analysis*. New Age International, pp. 4-7.

Bhuanantanondh, P., Grecov, D. and Kwok, E. (2018) 'Rheological study of viscosupplements and synovial fluid in patients with osteoarthritis', *CMBES Proceedings*, 33(1).

Bi, E. and Lutkenhaus, J. (1993) 'Cell division inhibitors *SulA* and *MinCD* prevent formation of the FtsZ ring', *Journal of Bacteriology*, 175(4), pp. 1118-1125.

Boresi, A.P., Schmidt, R.J. and Sidebottom, O.M. (1993) *Advanced mechanics of materials*. 6 edn. Wiley New York.

Bowman, K.J. (2004) *Mechanical Behavior of Materials*. Wiley.

Bray, D. (2000) 'Critical point drying of biological specimens for scanning electron microscopy', in *Supercritical Fluid Methods and Protocols*. Springer, pp. 235-243.

Brock, T.D. and Finley, S. (1985) 'Life at high temperatures', *Science*, 230(4722), pp. 132-138.

Brockel, U., Meier, W. and Wagner, G. (2013) 'Product Design and Engineering: Formulation of Gels and Pastes'. Germany: Wiley-VCH. Available at: http://wiley-vch.e-bookshelf.de/products/reading-epub/product-id/3937491/title/Product%2BDesign%2Band%2BEngineering.html?lang=dt (Accessed: May/08/2015).

Brown, R.C. and Hopps, H.C. (1973) 'Staining of bacteria in tissue sections: a reliable Gram stain method', *American Journal of Clinical Pathology*, 60(2), pp. 234-240.

Buwalda, S.J., Boere, K.W.M., Dijkstra, P.J., Feijen, J., Vermonden, T. and Hennink, W.E. (2014) 'Hydrogels in a historical perspective: From simple networks to smart materials', *Journal of Controlled Release*, 190, pp. 254-273.

Caló, E. and Khutoryanskiy, V.V. (2015) 'Biomedical applications of hydrogels: A review of patents and commercial products', *European Polymer Journal*, 65, pp. 252-267.

Cao, Y.-P. and Chen, K.-L. (2012) 'Theoretical and computational modelling of instrumented indentation of viscoelastic composites', *Mechanics of Time-Dependent Materials*, 16(1), pp. 1-18.

Casadaban, M.J. and Cohen, S.N. (1980) 'Analysis of gene control signals by DNA fusion and cloning in *Escherichia coli*', *Journal of Molecular Biology*, 138(2), pp. 179-207.

Cerf, A., Cau, J.-C., Vieu, C. and Dague, E. (2009) 'Nanomechanical properties of dead or alive single-patterned bacteria', *Langmuir*, 25(10), pp. 5731-5736.

Chai, Q., Jiao, Y. and Yu, X. (2017) 'Hydrogels for biomedical applications: Their characteristics and the mechanisms behind them', *Gels*, 3(1), p. 6.

Chandrupatla, T.R., Belegundu, A.D., Ramesh, T. and Ray, C. (2002) *Introduction to finite elements in engineering*. 3 edn. Prentice Hall Upper Saddle River, NJ.

Chaudhuri, O., Gu, L., Darnell, M., Klumpers, D., Bencherif, S.A., Weaver, J.C., Huebsch, N. and Mooney, D.J. (2015) 'Substrate stress relaxation regulates cell spreading', *Nature Communications*, 6, p. 6365.

Chaudhuri, O., Gu, L., Klumpers, D., Darnell, M., Bencherif, S.A., Weaver, J.C., Huebsch, N., Lee, H.-P., Lippens, E. and Duda, G.N. (2016) 'Hydrogels with tunable stress relaxation regulate stem cell fate and activity', *Nature Materials*, 15(3), p. 326.

Chawla, K.K. and Meyers, M. (1999) *Mechanical behavior of materials*. Prentice Hall.

Chen, D.T., Wen, Q., Janmey, P.A., Crocker, J.C. and Yodh, A.G. (2010a) 'Rheology of soft materials', *Condensed Matter Physics*, 1.

Chen, J. (2014a) 'Nanobiomechanics of living cells: a review', *Interface Focus*, 4(2), p. 20130055.

Chen, J. (2014b) 'Rheometer and Rheology - Private Communication '.

Chen, J., Bader, D.L., Lee, D.A. and Knight, M.M. (2015) 'Finite Element Analysis of Mechanical Deformation of Chondrocyte to 2D Substrate and 3D Scaffold', *Journal of Mechanics in Medicine and Biology*, 15(05), p. 1550077.

Chen, J., Birch, M.A. and Bull, S.J. (2010b) 'Nanomechanical characterization of tissue engineered bone grown on titanium alloy in vitro', *Journal of Materials Science: Materials in Medicine*, 21(1), pp. 277-282.

Chen, J., Irianto, J., Inamdar, S., Pravincumar, P., Lee, D.A., Bader, D.L. and Knight, M.M. (2012) 'Cell mechanics, structure, and function are regulated by the stiffness of the three-dimensional microenvironment', *Biophysical Journal*, 103(6), pp. 1188-1197.

Chen, J., Wright, K. and Birch, M. (2014) 'Nanoscale viscoelastic properties and adhesion of polydimethylsiloxane for tissue engineering', *Acta Mechanica Sinica*, 30(1), pp. 2-6.

Chen, Q., Suki, B. and An, K.-N. (2004) 'Dynamic mechanical properties of agarose gels modeled by a fractional derivative model', *Journal of Biomechanical Engineering*, 126(5), pp. 666-671.

Chen, X. and Stewart, P.S. (1996) 'Chlorine penetration into artificial biofilm is limited by a reaction− diffusion interaction', *Environmental Science & Technology*, 30(6), pp. 2078-2083.

Cheng, G., Zhang, Z., Chen, S., Bryers, J.D. and Jiang, S. (2007) 'Inhibition of bacterial adhesion and biofilm formation on zwitterionic surfaces', *Biomaterials*, 28(29), pp. 4192-4199.

Christensen, R. (2012a) *Theory of viscoelasticity: an introduction*. Elsevier.

Christensen, R.M. (2012b) *Mechanics of composite materials*. Courier Corporation.

Cistola, D.P., Small, D. and Hamilton, J. (1987) 'Carbon 13 NMR studies of saturated fatty acids bound to bovine serum albumin. I. The filling of individual fatty acid binding sites', *Journal of Biological Chemistry*, 262(23), pp. 10971-10979.

Cloyd, J.M., Malhotra, N.R., Weng, L., Chen, W., Mauck, R.L. and Elliott, D.M. (2007) 'Material properties in unconfined compression of human nucleus pulposus, injectable hyaluronic acid-based hydrogels and tissue engineering scaffolds', *European Spine Journal*, 16(11), pp. 1892-1898.

Connell, J.L., Ritschdorff, E.T., Whiteley, M. and Shear, J.B. (2013) '3D printing of microscopic bacterial communities', *Proceedings of the National Academy of Sciences*, 110(46), pp. 18380-18385.

Copeland, M.F. and Weibel, D.B. (2009) 'Bacterial swarming: a model system for studying dynamic self-assembly', *Soft Matter*, 5(6), pp. 1174-1187.

Corkhill, P.H., Hamilton, C.J. and Tighe, B.J. (1989) 'Synthetic hydrogels VI. Hydrogel composites as wound dressings and implant materials', *Biomaterials*, 10(1), pp. 3-10.

Cowie, J.M.G. and Arrighi, V. (2007) *Polymers: chemistry and physics of modern materials*. CRC press.

Croisier, F. and Jérôme, C. (2013) 'Chitosan-based biomaterials for tissue engineering', *European Polymer Journal*, 49(4), pp. 780-792.

Csonka, L.N. (1989) 'Physiological and genetic responses of bacteria to osmotic stress', *Microbiological Reviews*, 53(1), pp. 121-147.

D'Amico, S., Collins, T., Marx, J.C., Feller, G. and Gerday, C. (2006) 'Psychrophilic microorganisms: challenges for life', *EMBO Reports*, 7(4), pp. 385-389.

da Silva, L.J., Panzera, T.H., Christoforo, A.L., Durão, L.M.P. and Lahr, F.A.R. (2012) 'Numerical and experimental analyses of biocomposites reinforced with natural fibres', *International Journal of Materials Engineering*, 2(4), pp. 43-49.

De Spiegeleer, P., Sermon, J., Lietaert, A., Aertsen, A. and Michiels, C. (2004) 'Source of tryptone in growth medium affects oxidative stress resistance in *Escherichia coli*', *Journal of Applied Microbiology*, 97(1), pp. 124-133.

Deng, Y., Sun, M. and Shaevitz, J.W. (2011) 'Direct measurement of cell wall stress stiffening and turgor pressure in live bacterial cells', *Physical Review Letters*, 107(15), p. 158101.

Deszczynski, M., Kasapis, S., MacNaughton, W. and Mitchell, J.R. (2003) 'Effect of sugars on the mechanical and thermal properties of agarose gels', *Food Hydrocolloids*, 17(6), pp. 793-799.

Donachie, W.D. (1968) 'Relationship between cell size and time of initiation of DNA replication', *Nature*, 219(5158), p. 1077.

Dost, S. and Glockner, P. (1982) 'On the dynamic stability of viscoelastic perfect columns', *International Journal of Solids and Structures*, 18(7), pp. 587-596.

Duan, P., Kandemir, N., Wang, J. and Chen, J. (2017) 'Rheological Characterization of Alginate Based Hydrogels for Tissue Engineering', *MRS Advances*, 2(24), pp. 1309-1314.

Eaton, P. and West, P. (2010) *Atomic force microscopy*. Oxford University Press.

Edmondson, R., Broglie, J.J., Adcock, A.F. and Yang, L. (2014) 'Three-dimensional cell culture systems and their applications in drug discovery and cell-based biosensors', *Assay and Drug Development Technologies*, 12(4), pp. 207-218.

Edsman, K., Carlfors, J. and Harju, K. (1996) 'Rheological evaluation and ocular contact time of some carbomer gels for ophthalmic use', *International Journal of Pharmaceutics*, 137(2), pp. 233-241.

Ellison, C. and Brun, Y.V. (2015) 'Mechanosensing: a regulation sensation', *Current Biology*, 25(3), pp. R113-R115.

Eshelby, J.D. (1957) 'The determination of the elastic field of an ellipsoidal inclusion, and related problems', *Proceedings of the Royal Society of*

London. Series A. Mathematical and Physical Sciences, 241(1226), pp. 376-396.

Eun, Y.-J., Utada, A.S., Copeland, M.F., Takeuchi, S. and Weibel, D.B. (2010) 'Encapsulating bacteria in agarose microparticles using microfluidics for high-throughput cell analysis and isolation', *ACS Chemical Biology*, 6(3), pp. 260-266.

Even, C., Marlière, C., Ghigo, J.-M., Allain, J.-M., Marcellan, A. and Raspaud, E. (2017) 'Recent advances in studying single bacteria and biofilm mechanics', *Advances in Colloid and Interface S n cience*, 247, pp. 573-588.

Fernandez, E., Lopez, D., Mijangos, C., Duskova-Smrckova, M., Ilavsky, M. and Dusek, K. (2008) 'Rheological and thermal properties of agarose aqueous solutions and hydrogels', *Journal of Polymer Science Part B: Polymer Physics*, 46(3), pp. 322-328.

Findley, W.N., Davis, F.A. and Onaran, K. (1989) *Creep and relaxation of nonlinear viscoelastic materials*. New York: Dover Publications.

Fischer, M., Vahdatzadeh, M., Konradi, R., Friedrichs, J., Maitz, M.F., Freudenberg, U. and Werner, C. (2015) 'Multilayer hydrogel coatings to combine hemocompatibility and antimicrobial activity', *Biomaterials*, 56, pp. 198-205.

Fitzgerald, M.M., Bootsma, K., Berberich, J.A. and Sparks, J.L. (2015) 'Tunable Stress Relaxation Behavior of an Alginate-Polyacrylamide Hydrogel: Comparison with Muscle Tissue', *Biomacromolecules*, 16(5), pp. 1497-1505.

Foster, T. (1996) '*Staphylococcus*', in Baron, S. (ed.) *Epidemiology-Medical Microbiology*. Galveston (TX): University of Texas Medical Branch at Galveston.

François, D., Pineau, A. and Zaoui, A. (1998) *Mechanical behaviour of materials*. Springer.

Garrett, T.R., Bhakoo, M. and Zhang, Z. (2008) 'Bacterial adhesion and biofilms on surfaces', *Progress in Natural Science*, 18(9), pp. 1049-1056.

Gasik, M., Gantar, A. and Novak, S. (2017) 'Viscoelastic behaviour of hydrogel-based composites for tissue engineering under mechanical load', *Biomedical Materials*, 12(2), p. 025004.

Gaspar, L. and Campos, P.M. (2003) 'Rheological behavior and the SPF of sunscreens', *International Journal of Pharmaceutics*, 250(1), pp. 35-44.

Gay, D., Hoa, S.V. and Tsai, S.W. (2003) *Composite materials: design and applications*. CRC Press.

Gong, S., Li, Z. and Zhao, Y.Y. (2011) 'An extended Mori–Tanaka model for the elastic moduli of porous materials of finite size', *Acta Materialia*, 59(17), pp. 6820-6830.

Griepentrog, M., Krämer, G. and Cappella, B. (2013) 'Comparison of nanoindentation and AFM methods for the determination of mechanical properties of polymers', *Polymer Testing*, 32(3), pp. 455-460.

Gu, H. and Ren, D. (2014) 'Materials and surface engineering to control bacterial adhesion and biofilm formation: A review of recent advances', *Frontiers of Chemical Science and Engineering*, 8(1), pp. 20-33.

Guegan, C., Garderes, J., Le Pennec, G., Gaillard, F., Fay, F., Linossier, I., Herry, J.M., Fontaine, M.N.B. and Réhel, K.V. (2014) 'Alteration of bacterial adhesion induced by the substrate stiffness', *Colloids and Surfaces B: Biointerfaces*, 114, pp. 193-200.

Gulrez, S.K.H., Al-Assaf, S. and Phillips, G.O. (2011) 'Hydrogels: Methods of Preparation, Characterisation and Applications', in Carpi, A. (ed.) *Progress in Molecular and Environmental Bioengineering - From Analysis and Modeling to Technology Applications*. Rijeka: InTech, p. Ch. 05.

Gutiérrez, M.C., García-Carvajal, Z.Y., Jobbágy, M., Yuste, L., Rojo, F., Abrusci, C. and Ferrer, M.L. (2007) 'Hydrogel scaffolds with immobilized bacteria for 3D cultures', *Chemistry of Materials*, 19(8), pp. 1968-1973.

Guvendiren, M., Lu, H.D. and Burdick, J.A. (2012) 'Shear-thinning hydrogels for biomedical applications', *Soft Matter*, 8(2), pp. 260-272.

Hall, D., Skerrett, E. and Thomas, W. (1978) 'Critical point drying for scanning electron microscopy: a semi-automatic method of preparing biological specimens', *Journal of Microscopy*, 113(3), pp. 277-290.

Hanke, L.D. (2001) 'Handbook of analytical methods for materials', *Materials Evaluation and Engineering Inc., Plymouth*, pp. 35-38.

Harapanahalli, A.K., Younes, J.A., Allan, E., van der Mei, H.C. and Busscher, H.J. (2015) 'Chemical signals and mechanosensing in bacterial responses to their environment', *PLoS Pathogens*, 11(8), p. e1005057.

Harkes, G., Feijen, J. and Dankert, J. (1991) 'Adhesion of *Escherichia coli* on to a series of poly (methacrylates) differing in charge and hydrophobicity', *Biomaterials*, 12(9), pp. 853-860.

Harrison Jr, A.P. (1984) 'The acidophilic thiobacilli and other acidophilic bacteria that share their habitat', *Annual Reviews in Microbiology*, 38(1), pp. 265-292.

Hashin, Z. (1962) 'The elastic moduli of heterogeneous materials', *Journal of Applied Mechanics*, 29(1), pp. 143-150.

Hashin, Z. and Shtrikman, S. (1963) 'A variational approach to the theory of the elastic behaviour of multiphase materials', *Journal of the Mechanics and Physics of Solids*, 11(2), pp. 127-140.

He, L., Fullenkamp, D.E., Rivera, J.G. and Messersmith, P.B. (2011) 'pH responsive self-healing hydrogels formed by boronate–catechol complexation', *Chemical Communications*, 47(26), pp. 7497-7499.

Head, D.A., Tronci, G., Russell, S.J. and Wood, D.J. (2016) 'In Silico Modeling of the Rheological Properties of Covalently Cross-Linked Collagen Triple Helices', *ACS Biomaterials Science & Engineering*, 2(8), pp. 1224-1233.

Hesse, E., Hefferan, T.E., Tarara, J.E., Haasper, C., Meller, R., Krettek, C., Lu, L. and Yaszemski, M.J. (2010) 'Collagen type I hydrogel allows migration, proliferation, and osteogenic differentiation of rat bone marrow stromal cells', *Journal of Biomedical Materials Research Part A*, 94(2), pp. 442-449.

Hibbitt, Karlsson and Sorensen (2001) *ABAQUS/Explicit: user's manual*. Hibbitt, Karlsson and Sorenson Incorporated.

Hill, R. (1965) 'Theory of mechanical properties of fibre-strengthened materials—III. self-consistent model', *Journal of the Mechanics and Physics of Solids*, 13(4), pp. 189-198.

Ho, P.-L., Ho, L.-Y., Yau, C.-Y., Tong, M.-K. and Chow, K.-H. (2017) 'A novel selective medium for isolation of *Bacteroides fragilis* from clinical specimens', *Journal of Clinical Microbiology*, 55(2), pp. 384-390.

Hoffman, A.S. (2012) 'Hydrogels for biomedical applications', *Advanced Drug Delivery Reviews*, 64, pp. 18-23.

Hogg, S. (2013) *Essential microbiology*. John Wiley & Sons.

Holback, H., Yeo, Y. and Park, K. (2011) 'Hydrogel swelling behavior and its biomedical applications', in *Biomedical Hydrogels*. Elsevier, pp. 3-24.

Holzapfel, G.A. and Gasser, T.C. (2001) 'A viscoelastic model for fiber-reinforced composites at finite strains: Continuum basis, computational aspects and applications', *Computer Methods in Applied Mechanics and Engineering*, 190(34), pp. 4379-4403.

Hooton, T.M., Bradley, S.F., Cardenas, D.D., Colgan, R., Geerlings, S.E., Rice, J.C., Saint, S., Schaeffer, A.J., Tambayh, P.A. and Tenke, P. (2010) 'Diagnosis, prevention, and treatment of catheter-associated urinary tract infection in adults: 2009 International Clinical Practice Guidelines from the Infectious Diseases Society of America', *Clinical Infectious Diseases*, 50(5), pp. 625-663.

Hosford, W.F. (2010) *Mechanical behavior of materials*. Cambridge University Press.

Hu, M., Kurisawa, M., Deng, R., Teo, C.-M., Schumacher, A., Thong, Y.-X., Wang, L., Schumacher, K.M. and Ying, J.Y. (2009) 'Cell immobilization in gelatin–hydroxyphenylpropionic acid hydrogel fibers', *Biomaterials*, 30(21), pp. 3523-3531.

Hu, Y., Zhao, X., Vlassak, J.J. and Suo, Z. (2010) 'Using indentation to characterize the poroelasticity of gels', *Applied Physics Letters*, 96(12), p. 121904.

Huang, G., Zhang, X., Xiao, Z., Zhang, Q., Zhou, J., Xu, F. and Lu, T.J. (2012a) 'Cell-encapsulating microfluidic hydrogels with enhanced mechanical stability', *Soft Matter*, 8(41), pp. 10687-10694.

Huang, H., Ding, Y., Sun, X.S. and Nguyen, T.A. (2013) 'Peptide hydrogelation and cell encapsulation for 3D culture of MCF-7 breast cancer cells', *PloS One*, 8(3), p. e59482.

Huang, H., Herrera, Alvaro I., Luo, Z., Prakash, O. and Sun, Xiuzhi S. (2012b) 'Structural Transformation and Physical Properties of a Hydrogel-Forming Peptide Studied by NMR, Transmission Electron Microscopy, and Dynamic Rheometer', *Biophysical Journal*, 103(5), pp. 979-988.

Huang, K.C., Mukhopadhyay, R., Wen, B., Gitai, Z. and Wingreen, N.S. (2008) 'Cell shape and cell-wall organization in Gram-negative bacteria', *Proceedings of the National Academy of Sciences*, 105(49), pp. 19282-19287.

Hunt, N.C., Hallam, D., Karimi, A., Mellough, C.B., Chen, J., Steel, D.H.W. and Lako, M. (2017) '3D culture of human pluripotent stem cells in RGD-alginate hydrogel improves retinal tissue development', *Acta Biomaterialia*, 49, pp. 329-343.

Hur, S.S., Del Alamo, J.C., Park, J.S., Li, Y.-S., Nguyen, H.A., Teng, D., Wang, K.-C., Flores, L., Alonso-Latorre, B. and Lasheras, J.C. (2012) 'Roles of cell confluency and fluid shear in 3-dimensional intracellular forces in endothelial cells', *Proceedings of the National Academy of Sciences*, 109(28), pp. 11110-11115.

Hyun, K., Wilhelm, M., Klein, C.O., Cho, K.S., Nam, J.G., Ahn, K.H., Lee, S.J., Ewoldt, R.H. and McKinley, G.H. (2011) 'A review of nonlinear oscillatory shear tests: Analysis and application of large amplitude oscillatory shear (LAOS)', *Progress in Polymer Science*, 36(12), pp. 1697-1753.

Ingraham, J.L. (1958) 'Growth of psychrophilic bacteria', *Journal of bacteriology*, 76(1), p. 75.

Jasuja, N. and Sehgal, P. 'Gram-negative Bacteria vs Gram-positive Bacteria'. Diffen.com. Diffen LLC, n.d. Web. Available at:

http://www.diffen.com/difference/Gram-negative_Bacteria_vs_Gram-positive_Bacteria (Accessed: December/30/2014).

Jen, A.C., Wake, M.C. and Mikos, A.G. (1996) 'Hydrogels for cell immobilization', *Biotechnology and Bioengineering*, 50(4), pp. 357-364.

Ji, B. and Gao, H. (2004) 'Mechanical properties of nanostructure of biological materials', *Journal of the Mechanics and Physics of Solids*, 52(9), pp. 1963-1990.

Jiang, L., Sun, Z., Chen, X., Li, J., Xu, Y., Zu, Y., Hu, J., Han, D. and Yang, C. (2015) 'Cells Sensing Mechanical Cues: Stiffness Influences the Lifetime of Cell–Extracellular Matrix Interactions by Affecting the Loading Rate', *ACS Nano*, 10(1), pp. 207-217.

Joanne, M.W., Linda, M.S. and Christopher, J.W. (2008) *Prescott, Harley and Klein's microbiology*. New York: McGraw Hill.

Johnson, J.R., Kuskowski, M.A. and Wilt, T.J. (2006) 'Systematic Review: Antimicrobial Urinary Catheters To Prevent Catheter-Associated Urinary Tract Infection in Hospitalized Patients Antimicrobial Urinary Catheters', *Annals of Internal Medicine*, 144(2), pp. 116-126.

Jones, R.M. (1998) *Mechanics of composite materials*. CRC press.

Kandemir, N., Xia, Y., Duan, P., Yang, W. and Chen, J. (2018) 'Rheological Characterization of Agarose and Poloxamer 407 (P407) Based Hydrogels', *MRS Advances*, 3(30), pp. 1719-1724.

Kang, H.-W., Lee, S.J., Ko, I.K., Kengla, C., Yoo, J.J. and Atala, A. (2016) 'A 3D bioprinting system to produce human-scale tissue constructs with structural integrity', *Nature Biotechnology*, 34(3), p. 312.

Katsikogianni, M. and Missirlis, Y.F. (2004) 'Concise review of mechanisms of bacterial adhesion to biomaterials and of techniques used in estimating bacteria-material interactions', *Eur Cell Mater*, 8(3), pp. 37-57.

Kavanagh, G.M. and Ross-Murphy, S.B. (1998) 'Rheological characterisation of polymer gels', *Progress in Polymer Science*, 23(3), pp. 533-562.

Kelly, P. (2013) 'Solid mechanics part I: An introduction to solid mechanics', *Solid Mechanics Lecture Notes*, pp. 283-337.

Khyati, D. (2012) *Characterization of Rheological Properties and Degradation of Genipin Crosslinked Fibrin Hydrogel For Annulus Repair*. Master's thesis. City College of New York.

Knight, M.M., Van de Breevaart Bravenboer, J., Lee, D.A., Van Osch, G., Weinans, H. and Bader, D.L. (2002) 'Cell and nucleus deformation in compressed chondrocyte–alginate constructs: temporal changes and calculation of cell modulus', *Biochimica et Biophysica Acta (BBA)-General Subjects*, 1570(1), pp. 1-8.

Kobayashi, H. and Ikada, Y. (1991) 'Covalent immobilization of proteins on to the surface of poly (vinyl alcohol) hydrogel', *Biomaterials*, 12(8), pp. 747-751.

Koh, W.-G., Revzin, A., Simonian, A., Reeves, T. and Pishko, M. (2003) 'Control of mammalian cell and bacteria adhesion on substrates micropatterned with poly (ethylene glycol) hydrogels', *Biomedical Microdevices*, 5(1), pp. 11-19.

Kolewe, K.W., Peyton, S.R. and Schiffman, J.D. (2015) 'Fewer bacteria adhere to softer hydrogels', *ACS Applied Materials & Interfaces*, 7(35), pp. 19562-19569.

Kolewe, K.W., Zhu, J., Mako, N.R., Nonnenmann, S.S. and Schiffman, J.D. (2017) 'Bacterial adhesion is effected by the thickness and stiffness of poly (ethylene glycol) hydrogels', *ACS Applied Materials & Interfaces*, 10(3), pp.2275-2281.

Kolter, R., Siegele, D.A. and Tormo, A. (1993) 'The stationary phase of the bacterial life cycle', *Annual Reviews in Microbiology*, 47(1), pp. 855-874.

Kong, H.J., Smith, M.K. and Mooney, D.J. (2003) 'Designing alginate hydrogels to maintain viability of immobilized cells', *Biomaterials*, 24(22), pp. 4023-4029.

Kuhn, H. and Medlin, D. (2000) 'ASM Handbook. Volume 8: Mechanical Testing and Evaluation', *ASM International, Member/Customer Service Center, Materials Park, OH 44073-0002, USA, 2000. 998*.

Kumar, P. and Libchaber, A. (2013) 'Pressure and Temperature Dependence of Growth and Morphology of *Escherichia coli*: Experiments and Stochastic Model', *Biophysical Journal*, 105(3), pp. 783-793.

Kuo, C.K. and Ma, P.X. (2001) 'Ionically crosslinked alginate hydrogels as scaffolds for tissue engineering: part 1. Structure, gelation rate and mechanical properties', *Biomaterials*, 22(6), pp. 511-521.

Kurland, N.E., Drira, Z. and Yadavalli, V.K. (2012) 'Measurement of nanomechanical properties of biomolecules using atomic force microscopy', *Micron*, 43(2), pp. 116-128.

Lakes, R. and Lakes, R.S. (2009) *Viscoelastic materials*. Cambridge university press.

Lakes, R.S. and Drugan, W.J. (2002) 'Dramatically stiffer elastic composite materials due to a negative stiffness phase?', *Journal of the Mechanics and Physics of Solids*, 50(5), pp. 979-1009.

Landau, L. and Lifshitz, E. (1986) 'Theory of Elasticity' 3. Oxford: Butterworth-Heinemann.

Landers, R., Hübner, U., Schmelzeisen, R. and Mülhaupt, R. (2002) 'Rapid prototyping of scaffolds derived from thermoreversible hydrogels and tailored for applications in tissue engineering', *Biomaterials*, 23(23), pp. 4437-4447.

Lee, K.Y., Rowley, J.A., Eiselt, P., Moy, E.M., Bouhadir, K.H. and Mooney, D.J. (2000) 'Controlling mechanical and swelling properties of alginate hydrogels independently by cross-linker type and cross-linking density', *Macromolecules*, 33(11), pp. 4291-4294.

LeRoux, M.A., Guilak, F. and Setton, L.A. (1999) 'Compressive and shear properties of alginate gel: effects of sodium ions and alginate concentration', *Journal of Biomedical Materials Research: An Official Journal of The Society for Biomaterials, The Japanese Society for Biomaterials, and The Australian Society for Biomaterials and the Korean Society for Biomaterials*, 47(1), pp. 46-53.

Li, B. and Logan, B.E. (2004) 'Bacterial adhesion to glass and metal-oxide surfaces', *Colloids and Surfaces B: Biointerfaces*, 36(2), pp. 81-90.

Li, H.-X., Zare, Y. and Rhee, K.Y. (2017) 'Mathematical Simplification of the Tandon–Weng Approach to the Mori–Tanaka Model for Estimating the Young's Modulus of Clay/Polymer Nanocomposites', *The Journal of The Minerals, Metals & Materials Society*, 69(12), pp. 2819-2824.

Li, J., Suo, Z. and Vlassak, J.J. (2014) 'Stiff, strong, and tough hydrogels with good chemical stability', *Journal of Materials Chemistry B*, 2(39), pp. 6708-6713.

Liang, S., Xu, J., Weng, L., Dai, H., Zhang, X. and Zhang, L. (2006) 'Protein diffusion in agarose hydrogel in situ measured by improved refractive index method', *Journal of Controlled Release*, 115(2), pp. 189-196.

Lichter, J.A., Thompson, M.T., Delgadillo, M., Nishikawa, T., Rubner, M.F. and Van Vliet, K.J. (2008) 'Substrata mechanical stiffness can regulate adhesion of viable bacteria', *Biomacromolecules*, 9(6), pp. 1571-1578.

Lim, F. and Sun, A.M. (1980) 'Microencapsulated islets as bioartificial endocrine pancreas', *Science*, 210(4472), pp. 908-910.

Limbert, G., Bryan, R., Cotton, R., Young, P., Hall-Stoodley, L., Kathju, S. and Stoodley, P. (2013) 'On the mechanics of bacterial biofilms on non-dissolvable surgical sutures: A laser scanning confocal microscopy-based finite element study', *Acta Biomaterialia*, 9(5), pp. 6641-6652.

Liu, J. (2004) 'Stability of viscoplastic flow', *2003 Program of Study Non-Newtonian Geophysical Fluid Dynamics*, pp. 232-252.

Lu, H., Fu, B., Daphalapurkar, N., Hanan, J., Leventis, N. and Sotiriou-Leventis, L. (2008) 'Simulation of the evolution of the nanostructure of crosslinked silica-aerogels under compression', *Polymer Preprints*, 49(2), 564.

Lu, Y.-C., Song, W., An, D., Kim, B.J., Schwartz, R., Wu, M. and Ma, M. (2015) 'Designing compartmentalized hydrogel microparticles for cell encapsulation and scalable 3D cell culture', *Journal of Materials Chemistry B*, 3(3), pp. 353-360.

Maaloum, M., Pernodet, N. and Tinland, B. (1998) 'Agarose gel structure using atomic force microscopy: gel concentration and ionic strength effects', *Electrophoresis*, 19(10), pp. 1606-1610.

Mahaffy, R.E., Park, S., Gerde, E., Käs, J.A.C.K. and Shih, C.K. (2004) 'Quantitative analysis of the viscoelastic properties of thin regions of fibroblasts using atomic force microscopy', *Biophysical Journal*, 86(3), pp. 1777-1793.

Mainardi, F. and Spada, G. (2011) 'Creep, relaxation and viscosity properties for basic fractional models in rheology', *The European Physical Journal Special Topics*, 193(1), pp. 133-160.

Maitra, J. and Shukla, V.K. (2014) 'Cross-linking in hydrogels-a review', *American Journal of Polymer Science*, 4(2), pp. 25-31.

Makris, N., Dargush, G. and Constantinou, M. (1993) 'Dynamic analysis of generalized viscoelastic fluids', *Journal of Engineering Mechanics*, 119(8), pp. 1663-1679.

Malkin, A.Y. and Isayev, A.I. (2017) *Rheology: concepts, methods, and applications*. 3 edn. Toronto: ChemTec Publishing.

Mansfeld, F. (2007) 'The interaction of bacteria and metal surfaces', *Electrochimica Acta*, 52(27), pp. 7670-7680.

Mao, A.S., Shin, J.-W., Utech, S., Wang, H., Uzun, O., Li, W., Cooper, M., Hu, Y., Zhang, L. and Weitz, D.A. (2017) 'Deterministic encapsulation of single cells in thin tunable microgels for niche modelling and therapeutic delivery', *Nature Materials*, 16(2), pp. 236-243.

Martinsen, A., Skjåk-Bræk, G. and Smidsrød, O. (1989) 'Alginate as immobilization material: I. Correlation between chemical and physical properties of alginate gel beads', *Biotechnology and Bioengineering*, 33(1), pp. 79-89.

Mauck, R.L., Soltz, M.A., Wang, C.C., Wong, D.D., Chao, P.H.G., Valhmu, W.B. and Ateshian, G.A. (2000) 'Functional tissue engineering of articular cartilage through dynamic loading of chondrocyte-seeded agarose gels', *Journal of biomechanical engineering*, 122(3), pp. 252-260.

McCrum, N.G., Buckley, C. and Bucknall, C.B. (1997) *Principles of polymer engineering*. Oxford University Press, USA.

Michieletto, D., Marenduzzo, D. and Orlandini, E. (2015) 'Topological patterns in two-dimensional gel electrophoresis of DNA knots', *Proceedings of the National Academy of Sciences*, 112(40), pp. E5471-E5477.

Miller, K. (2005) 'Method of testing very soft biological tissues in compression', *Journal of Biomechanics*, 38(1), pp. 153-158.

Miyoshi, E., Takaya, T. and Nishinari, K. (1996) 'Rheological and thermal studies of gel-sol transition in gellan gum aqueous solutions', *Carbohydrate Polymers*, 30(2-3), pp. 109-119.

Monod, J. (1949) 'The growth of bacterial cultures', *Annual Reviews in Microbiology*, 3(1), pp. 371-394.

Moran, B. and Knauss, W.G. (1992) 'Crack-tip stress and deformation fields in strain-softening nonlinearly viscoelastic materials', *Journal of Applied Mechanics*, 59(1), pp. 95-101.

Moreno-Arotzena, O., Meier, J.G., del Amo, C. and García-Aznar, J.M. (2015) 'Characterization of fibrin and collagen gels for engineering wound healing models', *Materials*, 8(4), pp. 1636-1651.

Morishita, T., Deguchi, Y., Yajima, M., Sakurai, T. and Yura, T. (1981) 'Multiple nutritional requirements of lactobacilli: genetic lesions affecting amino acid biosynthetic pathways', *Journal of Bacteriology*, 148(1), pp. 64-71.

Morita, R.Y. (1975) 'Psychrophilic bacteria', *Bacteriological Reviews*, 39(2), p. 144.

Ni, L., Yang, S., Zhang, R., Jin, Z., Chen, H., Conrad, J.C. and Jin, F. (2016) 'Bacteria differently deploy type-IV pili on surfaces to adapt to nutrient availability', *NPJ Biofilms and Microbiomes*, 2, p. 15029.

Nordqvist, D. and Vilgis, T.A. (2011) 'Rheological study of the gelation process of agarose-based solutions', *Food Biophysics*, 6(4), p. 450.

Normand, V., Lootens, D.L., Amici, E., Plucknett, K.P. and Aymard, P. (2000) 'New insight into agarose gel mechanical properties', *Biomacromolecules*, 1(4), pp. 730-738.

Osswald, T.A. (2015) *Understanding polymer processing: processes and governing equations*. Carl Hanser Verlag GmbH Co KG.

Oyen, M.L. (2014) 'Mechanical characterisation of hydrogel materials', *International Materials Reviews*, 59(1), pp. 44-59.

Ozbas, B., Kretsinger, J., Rajagopal, K., Schneider, J.P. and Pochan, D.J. (2004) 'Salt-triggered peptide folding and consequent self-assembly into hydrogels with tunable modulus', *Macromolecules*, 37(19), pp. 7331-7337.

Ozel, C.A., Khawar, K.M. and Arslan, O. (2008) 'A comparison of the gelling of isubgol, agar and gelrite on in vitro shoot regeneration and rooting of variety Samsun of tobacco (Nicotiana tabacum L.)', *Scientia Horticulturae*, 117(2), pp. 174-181.

Pabst, B., Pitts, B., Lauchnor, E. and Stewart, P.S. (2016) 'Gel-entrapped *Staphylococcus aureus* bacteria as models of biofilm infection exhibit growth in dense aggregates, oxygen limitation, antibiotic tolerance, and heterogeneous gene expression', *Antimicrobial Agents and Chemotherapy*, 60(10), pp. 6294-6301.

Papanicolaou, G.C. and Zaoutsos, S.P. (2011) '1 - Viscoelastic constitutive modeling of creep and stress relaxation in polymers and polymer matrix composites A2 - Guedes, Rui Miranda', in *Creep and Fatigue in Polymer Matrix Composites*. Woodhead Publishing, pp. 3-47.

Park, S.W. (2001) 'Analytical modeling of viscoelastic dampers for structural and vibration control', *International Journal of Solids and Structures*, 38(44), pp. 8065-8092.

Park, S.W. and Schapery, R.A. (1999) 'Methods of interconversion between linear viscoelastic material functions. Part I—a numerical method based on Prony series', *International Journal of Solids and Structures*, 36(11), pp. 1653-1675.

Paul, B. (1959) *Prediction of elastic constants of multiphase materials*. Providence RI: Brown University

Peng, R., Zhou, H., Wang, H. and Mishnaevsky Jr, L. (2012) 'Modeling of nano-reinforced polymer composites: Microstructure effect on Young's modulus', *Computational Materials Science*, 60, pp. 19-31.

Peppas, N., Huang, Y., Torres-Lugo, M., Ward, J. and Zhang, J. (2000) 'Physicochemical foundations and structural design of hydrogels in

medicine and biology', *Annual Review of Biomedical Engineering*, 2(1), pp. 9-29.

Peppas, N.A., Hilt, J.Z., Khademhosseini, A. and Langer, R. (2006) 'Hydrogels in biology and medicine: from molecular principles to bionanotechnology', *Advanced Materials*, 18(11), pp. 1345-1360.

Persat, A., Nadell, C.D., Kim, M.K., Ingremeau, F., Siryaporn, A., Drescher, K., Wingreen, N.S., Bassler, B.L., Gitai, Z. and Stone, H.A. (2015) 'The mechanical world of bacteria', *Cell*, 161(5), pp. 988-997.

Phillips, R., Kondev, J., Theriot, J. and Garcia, H. (2012) *Physical biology of the cell*. Garland Science.

Pitigraisorn, P., Srichaisupakit, K., Wongpadungkiat, N. and Wongsasulak, S. (2017) 'Encapsulation of *Lactobacillus acidophilus* in moist-heat-resistant multilayered microcapsules', *Journal of Food Engineering*, 192, pp. 11-18.

Portoles, J.F. and Cumpson, P.J. (2013) 'A compact torsional reference device for easy, accurate and traceable AFM piconewton calibration', *Nanotechnology*, 24(33), p. 335706.

Preiss, L., Hicks, D.B., Suzuki, S., Meier, T. and Krulwich, T.A. (2015) 'Alkaliphilic bacteria with impact on industrial applications, concepts of early life forms, and bioenergetics of ATP synthesis', *Frontiers in Bioengineering and Biotechnology*, 3, p. 75.

Rao, A. (1997) *Introduction to microbiology*. PHI Learning Pvt. Ltd.

Rasmussen, K. and Østgaard, K. (2003) 'Adhesion of the marine bacterium Pseudomonas sp. NCIMB 2021 to different hydrogel surfaces', *Water Research*, 37(3), pp. 519-524.

Ratkowsky, D.A., Olley, J., McMeekin, T.A. and Ball, A. (1982) 'Relationship between temperature and growth rate of bacterial cultures', *Journal of Bacteriology*, 149(1), pp. 1-5.

Record Jr, M.T., Courtenay, E.S., Cayley, D.S. and Guttman, H.J. (1998) 'Responses of *E. coli* to osmotic stress: large changes in amounts of cytoplasmic solutes and water', *Trends in Biochemical Sciences*, 23(4), pp. 143-148.

Reimer, L. (1998) *Scanning electron microscopy: physics of image formation and microanalysis*. 2 edn. Springer.

Rietschel, E.T., Kirikae, T., Schade, F.U., Mamat, U., Schmidt, G., Loppnow, H., Ulmer, A.J., Zähringer, U., Seydel, U. and Di Padova, F. (1994) 'Bacterial endotoxin: molecular relationships of structure to activity and function', *The FASEB Journal*, 8(2), pp. 217-225.

Rodriguez, F., Cohen, C., Ober, C.K. and Archer, L. (2014) *Principles of polymer systems*. CRC Press.

Rojas, E., Theriot, J.A. and Huang, K.C. (2014) 'Response of *Escherichia coli* growth rate to osmotic shock', *Proceedings of the National Academy of Sciences*, 111(21), pp. 7807-7812.

Romanò, C.L., Malizos, K., Capuano, N., Mezzoprete, R., D'Arienzo, M., Van Der Straeten, C., Scarponi, S. and Drago, L. (2016) 'Does an antibiotic-loaded hydrogel coating reduce early post-surgical infection after joint arthroplasty?', *Journal of Bone and Joint Infection*, 1, p. 34.

Ronken, S., Wirz, D., Daniels, A., Kurokawa, T., Gong, J. and Arnold, M. (2013) 'Double-network acrylamide hydrogel compositions adapted to achieve cartilage-like dynamic stiffness', *Biomechanics and modeling in mechanobiology*, 12(2), pp. 243-248.

Rose, S.V., Dizeux, A., Narita, T., Hourdet, D. and Marcellan, A. (2013) 'Time dependence of dissipative and recovery processes in nanohybrid hydrogels', *Macromolecules*, 46(10), pp. 4095-4104.

Rosso, L., Lobry, J.R., Bajard, S. and Flandrois, J.P. (1995) 'Convenient model to describe the combined effects of temperature and pH on microbial growth', *Applied and Environmental Microbiology*, 61(2), pp. 610-616.

Roylance, D. (2001) 'Engineering viscoelasticity', in *Mechanics of Materials*. Cambridge MA: Department of Materials Science and Engineering–Massachusetts Institute of Technology, pp. 1-37.

Ruedinger, F., Lavrentieva, A., Blume, C., Pepelanova, I. and Scheper, T. (2015) 'Hydrogels for 3D mammalian cell culture: a starting guide for laboratory practice', *Applied Microbiology and Biotechnology*, 99(2), pp. 623-636.

Russ, N., Zielbauer, B.I. and Vilgis, T.A. (2014) 'Impact of sucrose and trehalose on different agarose-hydrocolloid systems', *Food Hydrocolloids*, 41, pp. 44-52.

Russell, J.B. and Dombrowski, D.B. (1980) 'Effect of pH on the efficiency of growth by pure cultures of rumen bacteria in continuous culture', *Applied and Environmental Microbiology*, 39(3), pp. 604-610.

Saha, N., Monge, C., Dulong, V., Picart, C. and Glinel, K. (2013) 'Influence of polyelectrolyte film stiffness on bacterial growth', *Biomacromolecules*, 14(2), pp. 520-528.

Sakai, T., Matsunaga, T., Yamamoto, Y., Ito, C., Yoshida, R., Suzuki, S., Sasaki, N., Shibayama, M. and Chung, U.-i. (2008) 'Design and fabrication of a high-strength hydrogel with ideally homogeneous network structure from tetrahedron-like macromonomers', *Macromolecules*, 41(14), pp. 5379-5384.

Salalha, W., Kuhn, J., Dror, Y. and Zussman, E. (2006) 'Encapsulation of bacteria and viruses in electrospun nanofibres', *Nanotechnology*, 17(18), p. 4675.

Salton, M.R.J. and Kim, K.-S. (1996) 'Structure in Bacteriology', in Baron, S. (ed.) *Medical Microbiology*. 4th edn. Galveston (TX): University of Texas Medical Branch at Galveston.

Sathaye, S., Mbi, A., Sonmez, C., Chen, Y., Blair, D.L., Schneider, J.P. and Pochan, D.J. (2015) 'Rheology of peptide-and protein-based physical hydrogels: Are everyday measurements just scratching the surface?', *Wiley Interdisciplinary Reviews: Nanomedicine and Nanobiotechnology*, 7(1), pp. 34-68.

Schaffner, M., Rühs, P.A., Coulter, F., Kilcher, S. and Studart, A.R. (2017) '3D printing of bacteria into functional complex materials', *Science Advances*, 3(12), p. eaao6804.

Scharfenberger, A., Clark, M., Lavoie, G., O'Connor, G., Masson, E. and Beaupre, L. (2007) 'Treatment of an infected total hip replacement with the PROSTALAC system: Part 1: Infection resolution', *Canadian Journal of Surgery*, 50(1), p. 24.

Schiessel, H., Metzler, R., Blumen, A. and Nonnenmacher, T. (1995) 'Generalized viscoelastic models: their fractional equations with solutions', *Journal of physics A: Mathematical and General*, 28(23), p. 6567.

Shapiro, J.M. and Oyen, M.L. (2014) 'Viscoelastic analysis of single-component and composite PEG and alginate hydrogels', *Acta Mechanica Sinica*, 30(1), pp. 7-14.

Shen, H., Li, H. and Brinson, L. (2008) 'Effect of microstructural configurations on the mechanical responses of porous titanium: a numerical design of experiment analysis for orthopedic applications', *Mechanics of Materials*, 40(9), pp. 708-720.

Shields, R.C., Mokhtar, N., Ford, M., Hall, M.J., Burgess, J.G., ElBadawey, M.R. and Jakubovics, N.S. (2013) 'Efficacy of a marine bacterial nuclease against biofilm forming microorganisms isolated from chronic rhinosinusitis', *PLoS One*, 8(2), p. e55339.

Shih, Y.R.V., Tseng, K.F., Lai, H.Y., Lin, C.H. and Lee, O.K. (2011) 'Matrix stiffness regulation of integrin-mediated mechanotransduction during osteogenic differentiation of human mesenchymal stem cells', *Journal of Bone and Mineral Research*, 26(4), pp. 730-738.

Shlomo, Y.B., Blom, A., Clark, E., Deere, K., Gregson, C., Hunt, L., Judge, A., Mouchti, S., Price, A., Sayers, A. and Whitehouse, M. (2017) *NJR 14th Annual Report 2017* (14). National Joint Registry.

Si, F., Li, B., Margolin, W. and Sun, S.X. (2015) 'Bacterial growth and form under mechanical compression', *Scientific Reports*, 5, p. 11367.

Sigma-Aldrich 'Agar CAS Number: 9002-18-0 Product Information'. Sigma-Aldrich. Available at: http://www.sigmaaldrich.com/content/dam/sigma-aldrich/docs/Sigma-Aldrich/Product_Information_Sheet/a5306pis.pdf (Accessed: May/04/2015).

Sigma-Aldrich 'Agarose CAS Number: 9012-36-6, Product Information Sheet'. Sigma-Aldrich. Available at: http://www.sigmaaldrich.com/content/dam/sigma-aldrich/docs/Sigma/Product_Information_Sheet/a0701pis.pdf (Accessed: May/04/2015).

Silhavy, T.J., Kahne, D. and Walker, S. (2010) 'The bacterial cell envelope', *Cold Spring Harbor Perspectives in Biology*, 2(5), p. a000414.

Smith, K. and Oatley, C. (1955) 'The scanning electron microscope and its fields of application', *British Journal of Applied Physics*, 6(11), p. 391.

Sokolnikoff, I.S. (1956) *Mathematical theory of elasticity*. 2 edn. McGraw-Hill book company.

Song, F., Brasch, M.E., Wang, H., Henderson, J.H., Sauer, K. and Ren, D. (2017) 'How bacteria respond to material stiffness during attachment: a role of *Escherichia coli* flagellar motility', *ACS Applied Materials & Interfaces*, 9(27), pp. 22176-22184.

Song, F. and Ren, D. (2014) 'Stiffness of cross-linked poly (dimethylsiloxane) affects bacterial adhesion and antibiotic susceptibility of attached cells', *Langmuir*, 30(34), pp. 10354-10362.

Spetz, G. (1999) *Stress Relaxation Tests*. Sweeden: Elastacon AB.

Stammen, J.A., Williams, S., Ku, D.N. and Guldberg, R.E. (2001) 'Mechanical properties of a novel PVA hydrogel in shear and unconfined compression', *Biomaterials*, 22(8), pp. 799-806.

Stewart, E.J., Ganesan, M., Younger, J.G. and Solomon, M.J. (2015) 'Artificial biofilms establish the role of matrix interactions in staphylococcal biofilm assembly and disassembly', *Scientific Reports*, 5, p. 13081.

Strange, D.G., Fletcher, T.L., Tonsomboon, K., Brawn, H., Zhao, X. and Oyen, M.L. (2013) 'Separating poroviscoelastic deformation mechanisms in hydrogels', *Applied Physics Letters*, 102(3), p. 031913.

Strathmann, M., Griebe, T. and Flemming, H.-C. (2000) 'Artificial biofilm model–a useful tool for biofilm research', *Applied Microbiology and Biotechnology*, 54(2), pp. 231-237.

Sutton, S. (2006) *Pharmaceutical Microbiology Forum Newsletter*.

Szabo, B.A. and Babuška, I. (1991) *Finite element analysis*. John Wiley & Sons.

Tamplenizza, M., Tocchio, A., Gerges, I., Martello, F., Martelli, C., Ottobrini, L., Lucignani, G., Milani, P. and Lenardi, C. (2015) 'In vivo imaging study of

angiogenesis in a channelized porous scaffold', *Molecular Imaging*, 14(6), p. 7290.2015. 00011.

Tang, Y.-F., Du, Y.-M., Hu, X.-W., Shi, X.-W. and Kennedy, J.F. (2007) 'Rheological characterisation of a novel thermosensitive chitosan/poly(vinyl alcohol) blend hydrogel', *Carbohydrate Polymers*, 67(4), pp. 491-499.

Tibbitt, M.W. and Anseth, K.S. (2009) 'Hydrogels as extracellular matrix mimics for 3D cell culture', *Biotechnology and Bioengineering*, 103(4), pp. 655-663.

Touhami, A., Nysten, B. and Dufrêne, Y.F. (2003) 'Nanoscale mapping of the elasticity of microbial cells by atomic force microscopy', *Langmuir*, 19(11), pp. 4539-4543.

Townsend-Nicholson, A. and Jayasinghe, S.N. (2006) 'Cell electrospinning: a unique biotechnique for encapsulating living organisms for generating active biological microthreads/scaffolds', *Biomacromolecules*, 7(12), pp. 3364-3369.

Trieu, H.H. and Qutubuddin, S. (1994) 'Polyvinyl alcohol hydrogels I. Microscopic structure by freeze-etching and critical point drying techniques', *Colloid and Polymer Science*, 272(3), pp. 301-309.

Tsang, P.H., Li, G., Brun, Y.V., Freund, L.B. and Tang, J.X. (2006) 'Adhesion of single bacterial cells in the micronewton range', *Proceedings of the National Academy of Sciences*, 103(15), pp. 5764-5768.

Tsotsas, E. and Mujumdar, A.S. (2011) *Modern Drying Technology, Volume 3: Product Quality and Formulation*. John Wiley & Sons.

Tuson, H.H., Auer, G.K., Renner, L.D., Hasebe, M., Tropini, C., Salick, M., Crone, W.C., Gopinathan, A., Huang, K.C. and Weibel, D.B. (2012a) 'Measuring the stiffness of bacterial cells from growth rates in hydrogels of tunable elasticity', *Molecular Microbiology*, 84(5), pp. 874-891.

Tuson, H.H., Renner, L.D. and Weibel, D.B. (2012b) 'Polyacrylamide hydrogels as substrates for studying bacteria', *Chemical Communications*, 48(10), pp. 1595-1597.

Tuson, H.H. and Weibel, D.B. (2013) 'Bacteria–surface interactions', *Soft Matter*, 9(17), pp. 4368-4380.

Tzikang, C. (2000) *Determining a Prony series for a viscoelastic material from time varying strain data*. NASA Center for AeroSpace Information.

Ulrich, T.A., Jain, A., Tanner, K., MacKay, J.L. and Kumar, S. (2010) 'Probing cellular mechanobiology in three-dimensional culture with collagen–agarose matrices', *Biomaterials*, 31(7), pp. 1875-1884.

Vadillo-Rodriguez, V., Schooling, S.R. and Dutcher, J.R. (2009) 'In situ characterization of differences in the viscoelastic response of individual gram-negative and gram-positive bacterial cells', *Journal of Bacteriology*, 191(17), pp. 5518-5525.

Van Breemen, L.C.A., Engels, T.A.P., Klompen, E.T.J., Senden, D.J.A. and Govaert, L.E. (2012) 'Rate-and temperature-dependent strain softening in solid polymers', *Journal of Polymer Science Part B: Polymer Physics*, 50(24), pp. 1757-1771.

Van Den Bulcke, A.I., Bogdanov, B., De Rooze, N., Schacht, E.H., Cornelissen, M. and Berghmans, H. (2000) 'Structural and rheological properties of methacrylamide modified gelatin hydrogels', *Biomacromolecules*, 1(1), pp. 31-38.

Vinogradov, A. (1987) 'Buckling of viscoelastic beam columns', *AIAA Journal*, 25(3), pp. 479-483.

Wang, S. and Tarbell, J.M. (2000) 'Effect of fluid flow on smooth muscle cells in a 3-dimensional collagen gel model', *Arteriosclerosis, Thrombosis, and Vascular Biology*, 20(10), pp. 2220-2225.

Wang, X.D., Meier, R.J. and Wolfbeis, O.S. (2013) 'Fluorescent pH-Sensitive Nanoparticles in an Agarose Matrix for Imaging of Bacterial Growth and Metabolism', *Angewandte Chemie International Edition*, 52(1), pp. 406-409.

Watase, M. and Arakawa, K. (1968) 'Rheological properties of hydrogels of agar-agar. III. Stress relaxation of agarose gels', *Bulletin of the Chemical Society of Japan*, 41(8), pp. 1830-1834.

Watase, M. and Nishinari, K. (1980) 'Rheological properties of agarose-gelatin gels', *Rheologica Acta*, 19(2), pp. 220-225.

Watase, M., Nishinari, K., Williams, P.A. and Phillips, G.O. (1990) 'Agarose gels: effect of sucrose, glucose, urea, and guanidine hydrochloride on the rheological and thermal properties', *Journal of Agricultural and Food Chemistry*, 38(5), pp. 1181-1187.

Watt, J.P. and Peselnick, L. (1980) 'Clarification of the Hashin-Shtrikman bounds on the effective elastic moduli of polycrystals with hexagonal, trigonal, and tetragonal symmetries', *Journal of Applied Physics*, 51(3), pp. 1525-1531.

Weinstein, R.A. and Darouiche, R.O. (2001) 'Device-associated infections: a macroproblem that starts with microadherence', *Clinical Infectious Diseases*, 33(9), pp. 1567-1572.

White, J.L. (1990) *Principles of polymer engineering rheology*. John Wiley & Sons.

Wilson, H.J. 'Polymeric Fluids (Part I-II) and Linear Viscoelasticity (Part III) Lecture GM05 Notes'. UCL. Available at: http://www.ucl.ac.uk/~ucahhwi/GM05/ (Accessed: May/08/2015).

Wood, J.M. (2015) 'Bacterial responses to osmotic challenges', *The Journal of General Physiology*, 145(5), pp. 381-388.

Wozniak, M.A. and Keely, P.J. (2005) 'Use of three-dimensional collagen gels to study mechanotransduction in T47D breast epithelial cells', *Biological Procedures Online*, 7(1), pp. 144-161.

Wrzeszcz, A., Steffens, M., Balster, S., Warnecke, A., Dittrich, B., Lenarz, T. and Reuter, G. (2015) 'Hydrogel coated and dexamethasone releasing cochlear implants: Quantification of fibrosis in guinea pigs and evaluation of insertion forces in a human cochlea model', *Journal of Biomedical Materials Research Part B: Applied Biomaterials*, 103(1), pp. 169-178.

Wu, S., Liu, X., Yeung, K.W., Liu, C. and Yang, X. (2014) 'Biomimetic porous scaffolds for bone tissue engineering', *Materials Science and Engineering: R: Reports*, 80, pp. 1-36.

Xu, D., Liu, C.Y. and Craig, S.L. (2011) 'Divergent shear thinning and shear thickening behavior of supramolecular polymer networks in semidilute entangled polymer solutions', *Macromolecules*, 44(7), pp. 2343-2353.

Xu, T., Jin, J., Gregory, C., Hickman, J.J. and Boland, T. (2005) 'Inkjet printing of viable mammalian cells', *Biomaterials*, 26(1), pp. 93-99.

Yan, C. and Pochan, D.J. (2010) 'Rheological properties of peptide-based hydrogels for biomedical and other applications', *Chemical Society Reviews*, 39(9), pp. 3528-3540.

Yan, W., Pun, C.L., Wu, Z. and Simon, G.P. (2011) 'Some issues on nanoindentation method to measure the elastic modulus of particles in composites', *Composites Part B: Engineering*, 42(8), pp. 2093-2097.

Yeung, T., Georges, P.C., Flanagan, L.A., Marg, B., Ortiz, M., Funaki, M., Zahir, N., Ming, W., Weaver, V. and Janmey, P.A. (2005) 'Effects of substrate stiffness on cell morphology, cytoskeletal structure, and adhesion', *Cytoskeleton*, 60(1), pp. 24-34.

Younes, R., Hallal, A., Fardoun, F. and Chehade, F.H. (2012) 'Comparative review study on elastic properties modeling for unidirectional composite materials', in Hu, N. (ed) *Composites and their properties*. IntechOpen, pp. 391-408.

Zeikus, J.G. (1979) 'Thermophilic bacteria: ecology, physiology and technology', *Enzyme and Microbial Technology*, 1(4), pp. 243-252.

Zhang, J. and Peppas, N. (2002) 'Morphology of poly (methacrylic acid)/poly (N-isopropyl acrylamide) interpenetrating polymeric networks', *Journal of Biomaterials Science, Polymer Edition*, 13(5), pp. 511-525.

Zhao, S., Agarwal, P., Rao, W., Huang, H., Zhang, R., Liu, Z., Yu, J., Weisleder, N., Zhang, W. and He, X. (2014) 'Coaxial electrospray of liquid core–hydrogel shell microcapsules for encapsulation and miniaturized 3D culture of pluripotent stem cells', *Integrative Biology*, 6(9), pp. 874-884.

Zhao, X., Huebsch, N., Mooney, D.J. and Suo, Z. (2010) 'Stress-relaxation behavior in gels with ionic and covalent crosslinks', *Journal of Applied Physics*, 107(6), p. 063509.

Zhu, H.X., Fan, T.X. and Zhang, D. (2015) 'Composite materials with enhanced dimensionless Young's modulus and desired Poisson's ratio', *Scientific Reports*, 5, p.14103.

Zignego, D.L., Jutila, A.A., Gelbke, M.K., Gannon, D.M. and June, R.K. (2014) 'The mechanical microenvironment of high concentration agarose for applying deformation to primary chondrocytes', *Journal of Biomechanics*, 47(9), pp. 2143-2148.

Zlotnikov, I., Shilo, D., Dauphin, Y., Blumtritt, H., Werner, P., Zolotoyabko, E. and Fratzl, P. (2013) 'In situ elastic modulus measurements of ultrathin protein-rich organic layers in biosilica: towards deeper understanding of superior resistance to fracture of biocomposites', *RSC Advances*, 3(17), pp. 5798-5802.

Zuidema, J.M., Rivet, C.J., Gilbert, R.J. and Morrison, F.A. (2014) 'A protocol for rheological characterization of hydrogels for tissue engineering strategies', *Journal of Biomedical Materials Research Part B: Applied Biomaterials*, 102(5), pp. 1063-1073.

Zussman, E. (2011) 'Encapsulation of cells within electrospun fibers', *Polymers for Advanced Technologies*, 22(3), pp. 366-371.